UNIVERSIDADE FEDERAL DO RIO DE JANEIRO

ALEXANDRE MENDONÇA TEIXEIRA

RECOVERY OF THERMODYNAMIC HYDRATE INHIBITORS METHANOL, ETHANOL, AND MEG IN OFFSHORE NATURAL GAS PRODUCTION: Exergy, Economic, and Environmental Analyses

RIO DE JANEIRO

2019

Alexandre Mendonça Teixeira

RECOVERY OF THERMODYNAMIC HYDRATE INHIBITORS METHANOL, ETHANOL, AND MEG IN OFFSHORE NATURAL GAS PRODUCTION: Exergy, Economic, and Environmental Analyses

Tese de Doutorado apresentada ao Programa de Pós-Graduação em Engenharia de Processos Químicos e Bioquímicos, Escola de Química, Universidade Federal do Rio de Janeiro, como parte dos requisitos necessários à obtenção do título de Doutor em Ciências.

Orientadores:

Prof. José Luiz de Medeiros, D.Sc.

Prof. Ofelia de Queiroz Fernandes Araújo, Ph.D

RIO DE JANEIRO

2019

FICHA CATALOGRÁFICA

T266r

Teixeira, Alexandre Mendonça
Recovery of thermodynamic hydrate inhibitors methanol, ethanol, and MEG in offshore natural gas production: exergy, economic, and environmental analyses / Alexandre Mendonça Teixeira. -- Rio de Janeiro, 2019.
249 f.

Orientador: José Luiz de Medeiros.
Coorientadora: Ofélia de Queiroz Fernandes Araújo.
Tese (doutorado) - Universidade Federal do Rio de Janeiro, Escola de Química, Programa de Pós Graduação em Engenharia de Processos Químicos e Bioquímicos, 2019.

1. Análise Exergética. 2. Inibidor de Hidrato Termodinâmico. 3. Hidratos. 4. Garantia de Escoamento. 5. Separador Supersônico. I. de Medeiros, José Luiz, orient. II. Araújo, Ofélia de Queiroz Fernandes, coorient. III. Título.

RECOVERY OF THERMODYNAMIC HYDRATE INHIBITORS METHANOL, ETHANOL, AND MEG IN OFFSHORE NATURAL GAS PRODUCTION: Exergy, Economic, and Environmental Analyses

ALEXANDRE MENDONÇA TEIXEIRA

Tese de Doutorado apresentada ao Programa de Pós-Graduação em Engenharia de Processos Químicos e Bioquímicos, Escola de Química, Universidade Federal do Rio de Janeiro, como parte dos requisitos necessários à obtenção do título de Doutor em Ciências.

Aprovado por:

José Luiz de Medeiros, D.Sc
(Orientador – Presidente da Banca)

Ofélia de Queiroz Fernandes Araújo, Ph.D
(Orientadora)

Argimiro Resende Secchi, D.Sc

Bettina Susanne Hoffmann, D.Sc

Márcio Luis Lyra Paredes, D.Sc.

Victor Rolando Ruiz Ahón, D.Sc.

Escola de Química
Universidade Federal do Rio de Janeiro
2019

AGRADECIMENTOS

Agradeço aos meus pais, Marisa e Edson, por todo o apoio e incentivo não só durante minha jornada acadêmica, como em toda a minha vida.

À minha namorada Sheila, por estar sempre ao meu lado, me apoiando e me dando forças.

Aos meus orientadores José Luiz de Medeiros e Ofélia Araújo, pelos ensinamentos, compreensão e paciência ao ensinar.

Aos colegas de trabalho pela parceria e troca de conhecimentos.

E a todos que de alguma forma me auxiliaram nessa jornada.

.

RESUMO

TEIXEIRA, Alexandre Mendonça. **Recovery of Thermodynamic Hydrate Inhibitors Methanol, Ethanol, and MEG in Offshore Natural Gas Production: Exergy, Economic, and Environmental Analyses.** Rio de Janeiro, 2019. Tese (Doutorado em Engenharia de Processos Químicos e Bioquímicos) – Escola de Química, Universidade Federal do Rio de Janeiro, 2019.

Na produção offshore de gás natural a formação de hidratos é um problema cuja solução consiste em injetar inibidores termodinâmicos de hidratos nas cabeças de poços para manter a temperatura de equilíbrio gás-hidrato abaixo da temperatura do fluido extinguindo as condições termodinâmicas para tal formação. Na plataforma a corrente de produção chega multifásica com gás, condensado de hidrocarbonetos e fase aquosa com inibidor e sais. O processamento consiste no tratamento destas fases. O gás deve ter seus pontos de orvalho (água/hidrocarbonetos) ajustados para exportação; o condensado de hidrocarbonetos também é exportado e a fase água/inibidor é processada para recuperar inibidor pobre que retorna aos poços. Em plataformas, onde espaço e recursos são limitados, análises energética, exergética, econômica e de emissão de CO_2 são úteis para localizar: (i) uso ineficiente de energia e potência; (ii) perdas de inibidores voláteis (metanol/etanol) para a fase do gás acarretando custos de reposição; e (iii) emissão excessiva de CO_2 devido ao uso ineficiente de potência que implica em maior queima de gás. Este trabalho aborda estes aspectos obtendo soluções para: (i) análise exergética da recuperação de inibidores termodinâmicos de hidratos mediante definição adequada do reservatório ambiental de referência; (ii) desenvolvimento de um novo processo SS-THI-Recovery baseado em separadores supersônicos que reduz drasticamente as perdas de inibidores para o gás simultaneamente ajustando os pontos de orvalho do gás final e gerando receita com o GLP recuperado; e (iii) análise técnico-econômica-ambiental sobre a alavancagem econômica de SS-THI-Recovery em relação à rota tradicional, onde é mostrado que tal alavancagem permite arcar com a captura de 43% do CO_2 gerado mantendo desempenho econômico superior.

Palavras-chave: Análise Exergética; Inibidor de Hidrato Termodinâmico; Hidratos; Garantia de Escoamento; Separador Supersônico.

ABSTRACT

TEIXEIRA, Alexandre Mendonça. **Recovery of Thermodynamic Hydrate Inhibitors Methanol, Ethanol, and MEG in Offshore Natural Gas Production: Exergy, Economic, and Environmental Analyses**. Rio de Janeiro, 2019. Tese (Doutorado em Engenharia de Processos Químicos e Bioquímicos) – Escola de Química, Universidade Federal do Rio de Janeiro, 2019.

In offshore natural gas production, hydrate formation is a problem whose solution consists in injecting thermodynamic hydrate inhibitors in well-heads to keep the gas-hydrate equilibrium temperature below the fluid temperature extinguishing the thermodynamic conditions for such formation. At the platform, the production fluids arrive as a multiphase stream comprising gas, hydrocarbon condensate and the water-inhibitor-salts phase. The processing consists of treating such phases. The gas must have its dew-points (water/hydrocarbons) adjusted for exportation; the hydrocarbon condensate is exported as well; and the water-inhibitor-salts phase is processed to return lean inhibitor to the wells. In offshore rigs, where space and resources are limited, energy, exergy, economic and CO_2 emissions assessments are useful to locate: (i) inefficient use of energy and power; (ii) losses of volatile inhibitors (methanol/ethanol) to the gas phase entailing make-up costs; and (iii) excessive CO_2 emissions due to inefficient usage of power implying greater gas-firing. This work approaches these aspects obtaining solutions for: (i) exergy analysis of the recovery of thermodynamic hydrate inhibitors proportionated by the appropriate choice of the Reference Environmental Reservoir; (ii) development of a new process SS-THI-Recovery prescribing supersonic separators to drastically lower inhibitor losses to the gas phase simultaneously adjusting the dew-points of the final gas and generating extra revenue from the recovered LPG; and (iii) techno-economic-environmental analysis on the economic leverage proportionated by SS-THI-Recovery relatively to the traditional route, where it is shown that such leverage affords capturing 43% of all generated CO_2 mantaining superior economic performance.

Keywords: Exergy analysis; thermodynamic hydrate inhibitor; hydrates; flow assurance; supersonic separator.

CONTENTS

INDEX OF FIGURES

INDEX OF TABLES

CHAPTER I – INTRODUCTION

I.1 – Motivation and Contextualization

In the past few decades, the humanity has crossed natural boundaries in search of energetic resources as occurred in the exploration and production in deep-water offshore environments. Around a third of the oil and gas extracted worldwide comes from offshore sources, and it is likely to continue to rise over the coming decades due to abundant oil and gas deposits deep in the oceans (World Ocean Review 3, 2014). Further, as many oil and gas fields in shallow waters have becoming more or less exhausted, companies tend to penetrate greater depths to access this energy resource.

Offshore exploration of natural gas has increased all over the globe due to the high offer of this energy resource in ocean basins, and along with that a lot of challenges have emerged. Particularly, a major concern is related to flow assurance, i.e. to ensure successful flow in pipelines and processing facilities and guarantee continuous production without flow restriction.

In the context of natural gas production the presence of water in contact with light hydrocarbon species of natural gas – CH_4, C_2H_6, C_3H_8, C_4H_{10} – defines the scenario for the appearance of solid gas hydrates. Gas hydrate formation is considered as the most critical aspect in flow assurance strategies, particularly in deep-water offshore fields. Hydrocarbon gas hydrate formation in flowlines occurs as consequence of favorable thermodynamic conditions, which can be materialized basically by the occurrence of the three first factors next and severely aggravated by the fourth factor (Gupta and Singh, 2012): (i) presence of production liquid water or vapor water saturation along with the gas; (ii) conditions of high pressure in flowlines; (iii) low external pipe temperature close to 0°C due to the high depth involved; (iv) frequent line shutdowns and flow interruptions under exposure to the three above factors.

As the above conditions are typically found in deep-water subsea gas pipelines, measures for prevention, control and abatement of such gas hydrate compounds is mandatory in offshore gas production.

Gas hydrate plugs can mean tremendous safety and economic impacts on gas flowline operation and can stop production completely for several days or months, and even result in pipeline loss in the worst case. Further, the removal and remediation of plugs of gas hydrate, once they are formed, can be a very costly and time-consuming process, which emphasizes the importance of preventive measures like the inhibition of hydrate formation (Nazeri et al., 2012). Hydrates not only act chronically progressively restricting flow and gradually imposing higher compressor costs due to head losses, but they can also form solid plugs that can suddenly cause damages to equipment like automatic valves and heat transfer surfaces. Therefore, the need for avoiding hydrate formation in natural gas flowlines is evident.

In this sense, a common alternative to overcome gas hydrate issues is the continuous injection of hydrate inhibitors in well-heads, so that the inhibitor flows together with production fluids, thus preventing or retarding hydrate formation and consequently avoiding significant safety hazards in production facilities and preventing loss of production.

There are several categories of commercial agents for gas hydrate inhibition, namely: Thermodynamic Hydrate Inhibitors (THI), Kinetic Hydrate Inhibitors (KHI) and Anti-Agglomerating Hydrate Inhibitors (AAHI).

Regarding the recent developments of technologies of gas hydrate inhibition, the achievements in the past decades of new technologies of Kinetic Hydrate Inhibitors (KHI) and Anti-Agglomerating Hydrate Inhibitors (AAHI) are very impressive and worth of note. An appealing factor is that Low Dosage Hydrate Inhibitors, like KHIs and AAHIs, are receiving recent commercial attention due to their more pragmatic and practical way of utilization, since there is no need of recovery of KHIs and AAHIs after use, i.e. there is no need for investments in recovery plants or separation processes. On the other hand, KHIs and AAHIs are in frontal contrast with the category of THIs, which, classically, are the most used in terms of global scale, but depends heavily on recovery technologies.

KHIs have limited application as they are dependent on the *subcooling* (the difference between the hydrate formation temperature and the cooler system operating temperature at a given pressure) and present subcooling limitations. That is, if the subcooling is high, which

represents a situation where the system is experiencing severe conditions and a great driving force for hydrate formation, KHIs are not effective. Further, the effectiveness of AAIHs require the presence of a liquid hydrocarbon phase (oil or condensate) in sufficient quantities and gas to oil ratio below certain limits (Clark et al., 2005). In contrast, THIs are very effective in severe conditions. Hence, in this work, only the THI category is studied.

As natural gas flows in pipeline, its temperature and pressure vary. In most subsea pipelines, after the well-head, the production stream cools and may reach the temperature of seabed before arriving at processing facilities. Thus, natural gas temperature within pipeline should be always higher than local hydrate temperature so as to prevent hydrate formation. In this sense, thermodynamic hydrate inhibitors (THIs) are highlighted by their mechanism of hydrate inhibition: they shift the hydrate formation conditions to lower temperatures and higher pressures, therefore placing the system in a region without the risk of hydrate formation.

Therefore, THIs are continuously injected in wellheads, flowing together with production fluids and avoiding hydrate formation. When reaching the platform, the incoming stream has its three phases separated: (i) a bottom aqueous phase comprised of THI, water and salts; (ii) an intermediate hydrocarbon condensate phase and (iii) an upper gas phase. The THI-H_2O-salts phase is rich in terms of water and it is sent to a recovery unit for THI regeneration (THI-RU), so as to enable its reinjection to production wells.

Concerning THIs, alcohols and glycols are the most common used compounds for injection, particularly methanol, ethanol and Monoethylene Glycol (MEG). In connection with the notion that THIs are High Dosage Hydrate Inhibitors, due to the high cost of replacing the large amounts of hydrate inhibitors used within the natural gas processing system, there is a strong economic drive to recycle and recirculate the THI.

Among them, MEG can be effectively regenerated and recycled with low losses, configuring a cost-effective choice for hydrate inhibition (Haghighi et al., 2009). Moreover, the latest MEG reclamation plant designs are cheaper to build, safer and easy to operate. Up-to-date MEG Recovery Units have simpler equipment and offer substantially better performance,

especially in terms of reliability, high recovery of MEG, low energy consumption, low carbon emission, adequate disposal of salt and water back into the sea with environmentally acceptable levels of contamination, and they also comply with the best Health, Safety & Environment (HSE) standards (Nazzer and Keogh, 2006). All those features are advantageous for offshore environment, rendering MEG as the preferred THI.

Methanol and ethanol can be recovered and recycled as well, however they present significant losses to vapor phase since they are volatile. Also, they are undesirable contaminants in sales gas, and their presence can lead to sales gas depreciation. Furthermore, regarding HSE, MEG represents less risk factors, being much less flammable and toxic, and this could be a decisive factor in offshore environment.

Since THI recovery processes are distillation-based processes, they present high energy consumption. Depending on the adopted THI technology and process conditions, there will be different requirements of heating, cooling and electric energy (EE) for the recovery unit operation. Since only THI Recovery Units (THI-RUs) located on offshore platforms are considered here, it is critical to minimize heating, cooling and EE requirements and also the extent of energy degradation.

A better understanding of a process is attained when a more complete thermodynamic view is taken. In this sense, a comprehensive analysis of a complex thermodynamic processing system includes both energy and exergy analyses. Exergy Analysis (ExA) has been recognized in the field of chemical and thermoelectric plants as a powerful tool to assess degradation of energy quality. ExA quantifies the percentage of destroyed exergy via process irreversibilities, as well as it assesses the primary sinks responsible for exergy destruction due to process inefficiencies (Boroumandjazi et al., 2013). Moreover, ExA might also be used as criteria for optimization of process design in order to minimize energy requirements and energy degradation, as well as it can serve as a tool to evaluate the effectiveness of engineering measures used to improve a process, by comparing the efficiencies values before and after the changes, giving insights on how much better a process became (Moran and Shapiro, 2006).

In recent years, there has been a growing interest in the application of exergy analysis to offshore oil and gas platforms, which is evidenced by the increase of exergy studies in the literature developed to evaluate the performance of offshore facilities (Sanchéz and Oliveira, 2015). Further, the literature shows that it is not possible to anticipate quantitative results with basis on previous studies of exergy analysis of offshore oil and gas platforms, since each platform must be assessed individually in order to pinpoint major sources of exergy destruction on that specific facility (Voldsund, 2014).

Therefore, one objective of this work is to conduct an exergy analysis of offshore THI-RUs in order to identify major sources of exergy destruction and pinpoint process inefficiencies.

In addition, another issue related to hydrate inhibition with THI injection concerns the high make-up requirements when employing volatile THIs, such as methanol or ethanol. They are lost into the sales gas and configure a major operating expense for THI make-up, which represents a comparative disadvantage relatively to MEG (Son and Wallace, 2000) and limits their application. Moreover, all losses of THIs to the gas phase from the high pressure three-phase separator (HPS) are unrecoverable by THI-RU plants, since such plants only recover THI from the bottom phase (THI-water-salts) from the HPS. Therefore, volatile THIs are lost to export gas in conventional natural gas processing and are not recoverable, which represents a major drawback, entailing high economic losses.

Furthermore, in view of the growing concern over the increasing atmospheric concentration of greenhouse gases related to human activity, particularly CO_2, which global concentration in the atmosphere is the main cause of planet climate change contributing to increase the Earth's mean temperature, mitigating CO_2 emissions is also a subject of interest.

Hence, this work also aims to overcome the above mentioned aspects related to volatile THI make-up requirements otherwise not addressed in the literature and also aims to mitigate CO_2 emissions. Keeping in mind a sustainable view of the whole picture, an ideal scenario would consist of mitigating THI losses, therefore enhancing economic performance and simultaneously reducing CO_2 emissions, which constitutes a great challenge.

I.2 – The Present Work and Achievements

As stated in Section I.1, one objective of the present work is to compare the recovery processes of THIs regarding energy consumption and exergy efficiency. This subject is addressed in **CHAPTER II**, wherein MEG Recovery Processes (Traditional Process, Full-Stream and Slip-Stream Process) are compared by implementing and solving mass and energy balances of the respective flowcharts in the professional simulator Aspen HYSYS, obtaining values of energy consumption for the processes, as well as providing the thermodynamic properties of the streams for the Exergy Analysis.

The simulation consisted of only two components – water and MEG – while salts were not included, since MEG Recovery Processes were previously simulated with/withouth NaCl (with the thermodynamic package NRTL-electrolytes for liquid phase coupled to Peng-Robinson for gas phase vs. Glycol Package) and showed that differences in heat duties were always below 2% (Teixeira et al., 2016). Thus, the inclusion of salts in the simulation was not considered, since strong electrolytes at high concentrations would pose problems to the estimation of thermodynamic properties employing common electrolyte models such as NRTL-electrolytes, and estimated thermodynamic properties (*H, S*) for streams with high salts content (e.g. NaCl) would bring inaccuracy for the Exergy Analysis of MEG Recovery Units (including the NaCl chemical potential in the Reference Environmental Reservoir (RER) - μ^{0}_{NaCl}). Therefore, it's reasonable to assume that, since the influence of NaCl on MEG Recovery Processes is not significant in energy terms, the effects on exergy terms would not be significant as well.

A mathematical expression for exergy was developed through the application of conservation equations and the First and Second Laws of Thermodynamics to the systems in question. Since exergy is a property that depends on the definition of a reference environment reservoir (RER), ExA was performed via two RER approaches by means of two distinct criteria for the corresponding states of the THI species.

When the traditional RER approach is used, the results show to be meaningless, providing high and unrealistic exergy efficiencies for all processes. In this work, a novel RER approach

was developed, wherein the magnitude of exergy flows are lower, leading to realistic exergy efficiencies that allow discrimination of processes. RER Approach #1, although consistent and correct, failed to provide discrimination of Exergy Performances and realistic results, whereas the proposed novel RER Approach #2 was able to provide much more realistic and meaningful exergy efficiency values.

The ExA methodology was also presented with a built-in Consistency Cross-Check of exergy values. This check is conducted by calculating the rate of lost exergy via two independent ways which use different kinds of thermodynamic properties generated by the simulation environment. These two ways gave discrepancies always below 1% in all MRU applications of ExA, either with RER Approach #1 or RER Approach #2. This fact validates the presented method and can be applied to other THIs.

In view of the relevance of such results that brought insights to exergy studies and potential application in other fields, in addition to the publication of the content of CHAPTER II in Journal of Natural Gas Science and Engineering (Appendix E.1), this work was also published as a book in an extended version with further detailing and analyses (Appendix E.2). Other related works are presented in Appendix E.3 (proceedings of PSE-2015 Conference, held in Copenhagen, Denmark), Appendix E.4 (Proceedings of OTC-Brazil 2015, held in Rio de Janeiro, Brazil) and Appendix E.5 (Proceedings of Rio Oil and Gas 2016, held in Rio de Janeiro, Brazil).

Next, aiming the mitigation of THI losses, **CHAPTER III** discloses a new and original process employing supersonic separators (SS), liquid water injections and water extraction of THI. This combination of resources can, cost-effectively, dramatically reduce THI losses to the gas, simultaneously executing water dew point adjustment (WDPA) and hydrocarbon dew point adjustment (HCDPA) of the final treated gas, thus making it suitable for direct commercialization. Besides, this new process does not aggregate high costs and can also recover condensed C3+ hydrocarbons (LPG) from HCDPA, which represents a potential tertiary factor of revenues.

This new process is referred as “SS-THI-Recovery” and should not be confused with the conventional THI Recovery Unit (THI-RU) processes that recover THIs from the bottom aqueous phase from the HPS. In other words, SS-THI-Recovery explores a THI recovery niche that was neglected by THI-RU technologies; i.e., it is complementary to THI-RUs and does not compete with them. This process is technically evaluated via process simulations with HYSYS 8.8 by using process flow diagrams (PFDs) where SS-THI-Recovery acts integrated to THI-RU processes.

Such simulations employed thermodynamic modeling appropriate to handle complex polar systems containing water, MEG, methanol, ethanol and hydrocarbons by means of the CPA Equation of State (CPA-EOS). In addition, the supersonic separator (SS) is rigorously thermodynamically modeled via a HYSYS Unit Operation Extension (UOE), namely, SS-UOE developed in another work (Arinelli et al., 2017). SS-UOE rigorously handles multiphase – single-phase, two-phase and three-phase – equilibrium supersonic flow and phase-split in SS and calculates the correct multiphase – single-phase, two-phase or three-phase – equilibrium sound speed (c) with another HYSYS UOE, namely, PEC-UOE also from another work (de Medeiros et al., 2017).

In view of such innovative process with superior results, the content of CHAPTER III was published in Journal of Natural Gas Science and Engineering (Appendix E.6) and several embodiments of SS-THI-Recovery process consolidated a pending patent in Brazilian Patent and Trademark Office (Appendix E.7). Further, this work originated a Chapter of another published book by our group (Appendix E.8). Another related published paper in Materials Science Forum is shown in Appendix E.9.

Since SS-THI-Recovery was shown to reduce costs with THI make-up and power consumption, presenting much higher revenues due to extraction of good-grade LPG in the SS processing in comparison with conventional processing, in **CHAPTER IV** an economic analysis is performed in order to quantify such economic leverage provided by SS-THI-Recovery. Keeping in mind the goal to reduce CO_2 emissions, this work investigated if the economic leverage provided by the new SS gas processing was capable to afford a Carbon Capture and Storage (CCS) unit consisting of a Post-Combustion Carbon Capture plant with

aqueous MEA (PCC-MEA), and a Compression and Dehydration Unit (CDU) also employing supersonic separators for dehydration of the CO_2-rich stream from PCC-MEA. Such contribution was published in Journal of Environmental Management (Appendix E.11).

Therefore, two alternatives were technically and economically compared: (i) Conventional Process without CCS unit; and (ii) SS-THI-Recovery with CCS Unit for post-combustion carbon capture from exhausts. The new SS gas processing was shown to produce sufficient economic benefits which could pay the costs of the proposed CCS unit reducing CO_2 emissions while maintaining economic superiority relative to the conventional gas processing in several scenarios. This work employed methanol as THI for exemplification; hence, SS-MeOH-Recovery was shown to be superior on both economic and environmental grounds, providing a cleaner production of NG and LPG and configuring successful CO_2 management.

Furthermore, additional research performed in parallel with the studies on hydrate inhibition and recovery is presented in **CHAPTER V**. This Chapter describes some unpublished results and some co-authored works regarding the processing of natural gas with high and ultra-high CO_2 content (Appendices E.12-E.16), including the comparison of conventional routes with supersonic separator-based routes, the use of supersonic separators for carbon capture, as well as economic assessments and environmental evaluations.

In view of the above discussed aspects, this Thesis achieved significant results, bringing insights and innovations for the literature and contributing to advance the scientific knowledge in the fields of THI recovery, natural gas processing and CO_2 mitigation.

I.3 – Thesis Structure

The content of this Thesis is divided into six chapters, wherein each chapter from II to V presents one (or more) main contribution of this work published (or to be published) in a recognized Scientific Journal. Consequently, each chapter from I to VI has specific nomenclature, abbreviations, bibliographic review, methods and conclusions.

CHAPTER I introduces the subject of this Thesis, contextualizing and discussing key aspects of this work, evidencing the motivation for the study, the objectives, achievements and the Thesis structure.

CHAPTER II addresses Exergy Analysis for MEG Recovery Units (MRUs). It contributes to a better understanding of hydrate inhibition using MEG injection in offshore fields by discussing relevant features concerning hydrates, hydrate inhibition and MEG recovery processes in offshore rigs, as well as comparatively evaluating three MRU technologies in terms of energy consumption and exergy efficiency. In addition, this Chapter also presented the development of formulae for exergy flow and brought pertinent discussion about reference states for MEG so as to achieve an effective exergy analysis. Finally, after exergy analysis is successfully conducted, wherein the most inefficient components are identified in MEG plants, a sensitivity analysis based on common design criteria was also covered in order to evaluate its impact on overall efficiency.

CHAPTER III presents a novel process ("SS-THI-Recovery") for mitigating THI losses to gas phase, especially when the employed THI is volatile such as methanol or ethanol. This "out-of-the-box" process configuration for recovering thermodynamic hydrate inhibitors (THIs) from gas phase employs supersonic separators (SS) with water injection and was successfully demonstrated to recover any of THIs methanol, ethanol or MEG from the gas phase leaving the high pressure three-phase separator, simultaneously performing HCDPA and WDPA operations and exporting NG and good grade LPG with high commercial value.

CHAPTER IV explores the potentials and advantages disclosed in CHAPTER III for SS-THI-Recovery. An economic analysis is conducted in order to quantify the economic leverage achieved by SS-THI-Recovery in comparison with the conventional natural gas processing,

and such leverage was shown to be capable to afford a post-combustion carbon capture unit and the associated compression and dehydration costs for the CO_2-rich stream. Further, a novel design of a CCS unit employing SS is disclosed, which allows for the dehydration of the CO_2-rich stream with negligible pressure drop, requiring minimum compression power for exportation and also contributing to improve process economics. Finally, an economic sensitivity analysis was conducted and it was shown that the alternative of SS-THI-Recovery with CCS is favored in the scenarios of high crude oil prices and high carbon taxes.

CHAPTER V presents some unpublished results that complement the study done in CHAPTER IV by extending such analyses for the THIs ethanol and MEG. Also, this Chapter presents some additional research publications performed in parallel with the studies on hydrate inhibition and recovery, such as processes for conditioning natural gas with high and ultra-high CO_2 content, wherein supersonic separator-based routes are compared to conventional gas processing, evidencing the particularities of such (supercritical) fluid with high and ultra-high CO_2 content. Also, the use of supersonic separators for carbon capture is addressed, and technical, economic and environmental analyses were conducted as well.

Finally, **CHAPTER VI** brings an overview of this work, with concluding remarks about the achieved results in this Thesis.

By last, Appendices A and B comprehend published Supplementary Materials belonging to the exergy study conducted in CHAPTER II. Analogously, Appendices C and D comprehend published Supplementary Materials belonging to economic analysis and SS-UOE validation discussed in CHAPTER IV. Appendix E gathers the entire production derived from this thesis, encompassing published papers, published proceedings, published books, published book chapters and pending patents, namely:

Appendix E.1 – Exergy Analysis of Monoethylene glycol recovery processes for hydrate inhibition in offshore natural gas fields. Journal of Natural Gas Science and Engineering, Vol. 35, p. 798-813, 2016.

Appendix E.2 – Monoethylene Glycol as Hydrate Inhibitor in Offshore Natural Gas Processing: From Fundamentals to Exergy Analysis. SpringerBriefs in Petroleum Geoscience & Engineering, SPRINGER, 2018.

Appendix E.3 – Exergy Analysis of Monoethylene Glycol (MEG) Recovery Systems. Computer Aided Chemical Engineering. Proceedings of PSE-2015.

Appendix E.4 – Offshore Monoethylene Glycol Recovery Units: The Importance of Choice of MEG State in the Reference Environment for Effective Exergy Analysis. Proceedings of OTC Brasil, 2015.

Appendix E.5 – Exergy Analysis of Offshore Recovery Processes of Thermodynamic Hydrate Inhibitors. Proceedings of Rio Oil and Gas, 2016.

Appendix E.6 – Recovery of thermodynamic hydrate inhibitors methanol, ethanol and MEG with supersonic separators in offshore natural gas processing. Journal of Natural Gas Science and Engineering, Vol. 52, p. 166-186, 2018.

Appendix E.7 – Processo para Recuperar Inibidores Termodinâmicos de Hidratos de Cargas de Gás Natural Utilizando Separador Supersônico Simultaneamente Ajustando Ponto de Orvalho de Hidrocarbonetos e Ponto de Orvalho de Água do Gás Final. Brazilian Patent Application BR 10 2017 015092 5, Filed in 13/07/2017

Appendix E.8 – Offshore Processing of CO_2-Rich Natural Gas with Supersonic Separator. Multiphase Sound Speed, CO_2 Freeze-Out and HYSYS Implementation. SPRINGER, 2019.

Appendix E.9 – Offshore Natural Gas Conditioning and Recovery of Methanol as Hydrate Inhibitor with Supersonic Separators: Increasing Energy Efficiency with Lower CO2 Emissions. Materials Science Forum, Vol. 965, pp 97-105, 2019.

Appendix E.10 – Economic Leverage of Thermodynamic Hydrate Inhibitor Recovery from Raw Natural Gas with Supersonic Separator: Post-combustion capture of 43% of CO2 emissions preserving offshore gas plant profitability. Proceedings of SDEWES-2018.

Appendix E.11 – Economic Leverage Affords Post-Combustion Capture of 43% of Carbon Emissions: Supersonic Separators for Methanol Hydrate Inhibitor Recovery from Raw Natural Gas and CO2 Drying. Journal of Environmental Management, Vol. 236, pp. 534-550, 2019.

Appendix E.12 - Offshore processing of CO2 rich natural gas with supersonic separator versus conventional routes. Journal of Natural Gas Science and Engineering, Vol. 46, p. 199-221, 2017.

Appendix E.13 - Supersonic separator for cleaner offshore processing of natural gas with high carbon dioxide content: Environmental and economic assessments. Journal of Cleaner Production, Vol. 233, p. 510-521, 2019.

Appendix E.14 - CO_2 Rich Natural Gas Processing: Technical, Power Consumption and Emission Comparisons of Conventional and Supersonic Technologies. Materials Science Forum, Vol. 965, pp 79-86, 2019.

Appendix E.15 - Carbon capture and high-capacity supercritical fluid processing with supersonic separator: Natural gas with ultra-high CO2 content. Journal of Natural Gas Science and Engineering, Vol. 66, p. 265-283, 2019.

Appendix E.16 - Supersonic separator for cleaner offshore processing of supercritical fluid with ultra-high carbon dioxide content: Economic and environmental evaluation. Journal of Cleaner Production, Vol. 234, p. 1385-1398, 2019.

I.4 – References

Arinelli L.O., Trotta T.A.F., Teixeira, A.M., de Medeiros, J.L., Araújo O.Q.F., 2017. Offshore Processing of CO2 Rich Natural Gas with Supersonic Separator versus Conventional Routes. Journal of Natural Gas Science and Engineering. Vol. 46, pp. 199-221. http://dx.doi.org/10.1016/j.jngse.2017.07.010

Boroumandjazi, G., Rismanchi, B., Saidur, R. A review on exergy analysis of industrial sector. Renewable and Sustainable Energy Reviews, Volume 27, Nov 2013, pp. 198-203, Elsevier. http://dx.doi.org/10.1016/j.rser.2013.06.054

Clark L W, Frostman L M, Anderson J. Low-Dosage Hydrate Inhibitors (LDHI): Advances in Flow Assurance Technology for Offshore Gas Production Systems. Proceedings of International Petroleum Technology Conference, 2005. IPTC 10562.

de Medeiros, J.L., Arinelli, L.O., Araújo, O.Q.F., 2017. Speed of sound of multiphase and multi-reactive equilibrium streams: a numerical approach for natural gas applications. Journal of Natural Gas Science and Engineering. Vol. 46, pp. 222-241. http://dx.doi.org/10.1016/j.jngse.2017.08.006

Gupta, G., Singh, S. K. Hydrate Inhibition - Optimization in Deep Water Gas Field. SPE Oil and Gas India Conference and Exhibition, 28-30 March, 2012, Mumbai, India. SPE 153504. http://dx.doi.org/10.2118/153504-MS

Haghighi H, Chapoy A, Burgess R, Tohidi B. Experimental and thermodynamic modelling of systems containing water and ethylene glycol: Application to flow assurance and gas processing. Fluid Phase Equilibria, Volume 276(1), 2009, pp. 24–30, Elsevier. http://dx.doi.org/10.1016/j.fluid.2008.10.006

Nazeri, M., Tohidi, B., Chapoy, A. An Evaluation of Risk of Hydrate Formation at the Top of a Pipeline. SPE Asia Pacific Oil & Gas Conference and Exhibition, 22–24 Oct, 2012, Perth, Australia. SPE 160404. http://dx.doi.org/10.2118/160404-MS

Nazzer, C. A., Keogh, J. Advances in Glycol Reclamation Technology. Offshore Technology Conference, 1-4 May, 2006, Houston, USA. OTC 18010. http://dx.doi.org/10.4043/18010-MS

Sánchez, Y.A.C. and de Oliveira Jr., S., Exergy analysis of offshore primary petroleum processing plant with CO2 capture, Energy, 88, 46-56, 2015. doi: 10.1016/j.energy.2015.05.130

Son K.V., Wallace C., 2000. Reclamation/regeneration of glycols used for hydrate inhibition. Deep Offshore Technology. http://reclaim.com/wp-content/uploads/2013/10/reclamation-regeneration-of-glycols-used-for-hydrate-inhibition.pdf [Accessed 14 June 2017]

Voldsunt et al.. “Exergy destruction and losses on four North Sea offshore platforms: A comparative study of the oil and gas processing plants”. Energy. Vol 74, 2014, p.45-78. http://dx.doi.org/10.1016/j.energy.2014.02.080.

World Ocean Review 3, 2014, Maribus gGmbH, Hamburg, Germany. ISBN 978-3-86648-221-0. Available at http://worldoceanreview.com/wp-content/downloads/wor3/WOR3_chapter_1.pdf. Accessed 8 Nov 2016.

CHAPTER II – EXERGY ANALYSIS OF MONOETHYLENE GLYCOL RECOVERY PROCESSES FOR HYDRATE INHIBITION IN OFFSHORE NATURAL GAS FIELDS

This article was published in Journal of Natural Gas Science and Engineering Vol. 35 (2016) pp. 798-813 (doi: 10.1016/j.jngse.2016.09.017)

Exergy Analysis of Monoethylene Glycol Recovery Processes for Hydrate Inhibition in Offshore Natural Gas Fields

Alexandre Mendonça Teixeira*[a], Lara de Oliveira Arinelli[1a], José Luiz de Medeiros[2a] and Ofélia de Queiroz F. Araújo[3a]

[a]Escola de Química, Federal University of Rio de Janeiro. Av. Horacio Macedo, 2030, Bl. E, 21949–900, Rio de Janeiro, RJ, Brazil

*Corresponding author: alexandremtxr@gmail.com

[1]lara.arinelli@gmail.com, [2]jlm@eq.ufrj.br, [3]ofelia@eq.ufrj.br

Abstract

Gas hydrate formation is an issue in natural gas production. In offshore deepwater scenarios the situation is aggravated by the inaccessibility, salinity, low temperatures and high pressures. Monoethylene glycol (MEG) injection in well-heads is one of the used technologies for flow assurance in gas flowlines. Rich MEG is processed in MEG Recovery Units (MRU) to be recovered as Lean MEG returned to well-heads. In offshore rigs, besides determining energy requirements, the assessment of energy degradation is also important, which can be done by Exergy Analysis. In this work, an exergy formulation is developed and three technologies of offshore MRUs are assessed. Since exergy is a property that depends on the definition of a reference environment reservoir (RER), Exergy Analysis is performed via two RER approaches, both presenting consistent results. Approach #1 prescribes the usual standard atmosphere, with the addend that it is saturated by equilibrium with an infinite body of liquid water and MEG is in chemical equilibrium with air species. Since MEG is spontaneously oxidable, this entails very high exergy flows for MRU streams with MEG. As MEG is practically conserved, high exergy efficiencies result for all MRUs hindering their discrimination. Approach #2 prescribes also the standard atmosphere in equilibrium with liquid water containing MEG at infinite dilution, but not in chemical equilibrium with air. The MEG condition in MRU streams is now more akin with the MEG state in this RER, resulting

that MEG streams have lower magnitude of exergy flow, leading to realistic exergy efficiencies that allow MRU discrimination. The underlying reason is that the input exergy flows now have magnitude comparable with exergy losses

Keywords: Exergy, Hydrate Inhibition, MEG Recovery, Exergy Analysis

Abbreviations

ADC	Atmospheric Distillation Column
ChW, CW	Chilled Water (10 ^{o}C) and Cooling Water (25 – 40 ^{o}C)
EE	Electric Energy (kW)
ExA	Exergy Analysis
FLS	Flash-Evaporator
FPSO	Floating Production, Storage and Offloading
FS	Full-Stream Process
HSE	Health, Safety & Environment
HRWH	Heat Recovery Water Heater
LHS	Left Hand Side
MEG	Monoethylene Glycol
MRU	MEG Recovery Unit
NG	Natural Gas
PFD	Process Flow Diagram
PHW	Pressurized Hot Water (200 ^{o}C)
RER	Reference Environmental Reservoir
RHS	Right Hand Side
SDC	Sub-atmospheric (vacuum) Distillation Column
SVLE	Solid-Vapor-Liquid Equilibrium
SS	Slip-Stream Process
SW	Seawater (20 – 35 ^{o}C)
TP	Traditional MEG Recovery Process
TST-EOS	Twu-Sim-Tassone Equation of State
VLE	Vapor-Liquid Equilibrium

Nomenclature

$\dot{B}, \overline{B}_{K_j}, \overline{B}_{F_j}$: *exergy flow rate (kW) and molar exergies of streams K_j and F_j (kJ/mol)*

F_j : *molar flow rate of j^{th} inlet stream (mol/s)*

(g) : *standard state of pure ideal gas at 25 ^oC and 1 atm*

$\overline{G}$, $\overline{H}$: *molar Gibbs free energy (kJ/mol) and molar enthalpy (kJ/mol)*

K_j : *molar flow rate of j^{th} outlet stream (mol/s)*

nc : *number of components*

P : *absolute pressure (kPa)*

$\dot{Q}_0$: *heat transfer rate (System viewpoint) from R_H to the System (kW)*

R : *ideal gas constant ($8.314.10^{-3}$ kJ/mol.K)*

R_H , R_V, R_k : *heat reservoir, volume reservoir and species k reservoir*

RR : *column reflux ratio*

$\overline{S}$: *molar entropy (kJ/K.mol)*

T : *absolute temperature (K)*

TAPP : *thermal approach of heat exchange (^oC)*

$\dot{U}$: *rate of change of internal energy (kW)*

$\overline{V}$: *molar volume (m^3/mol)*

$\dot{W}$, $\dot{W}_V$: *rate of shaft work done by System (kW) and rate of volume work done by System on R_V (kW)*

Y_{kFj} : *mol fraction of species k in stream F_j*

Greek Symbols

$\dot{\Xi}_k$: *energy transfer from reservoir of species k to the System (kW)*

$\dot{\Omega}_k, \dot{\Omega}_V, \dot{\Omega}_S$: *net rate of creation of species k (mol/s), volume (m^3/s), and entropy (kJ/K.s) in the Universe*

μ_k : *chemical potential of species k (kJ/kmol)*

Subscripts

0 = *relative to Reference Environmental Reservoir (RER) or relative to reservoir* R_H *at* T_0

i, k = *related to component*

j = *index of stream*

Superscripts

$^{\infty, H2O}$ = *infinite dilution in water*

0 = *relative to Reference Environmental Reservoir (RER)*

f = *formation at standard conditions (for pure component)*

LOST = *related to work lost by irreversibilities*

nfs = *number of feed streams*

nps = *number of product streams*

nwi = *number of power streams imported by the System*

nwe = *number of power streams exported by the System*

w = *related to exergy flows associated to pure electric (mechanical) energy*

II.1 Introduction

One major concern in offshore natural gas (NG) production, particularly in deepwater fields, is the formation of gas hydrate in subsea pipelines, which is considered as the most critical aspect in flow assurance strategies. Gas hydrate plugs can have tremendous safety and economic impacts on gas flowline operation and can stop production completely for several days or months, and in the worst case, can result in pipeline loss. Furthermore, the removal of plugs of gas hydrate and remediation can be costly and time-consuming, emphasizing the relevancy of inhibition of hydrate formation (Nazeri et al., 2012).

Natural gas hydrates are crystalline water-based solids physically resembling ice, with a crystalline structure comprised of water and light hydrocarbon molecules (mainly CH_4). Hydrate structures are characterized by repetitive crystal units composed of asymmetric, spherical-like “cages” of hydrogen-bonded water molecules, each cage typically containing one (or more) guest molecule(s) held in its interior by dispersion forces. Common hydrate

crystalline structures are cubic structure I (sI), cubic structure II (sII), or hexagonal structure H (sH). Type I cubic structure sI is formed with guest molecules having diameters between 4.2 and 6 Å, such as CH_4, C_2H_6, CO_2, and H_2S, therefore being directly associated to natural gas hydrates, but the other two structures can also occur in the NG context. Cubic structure sII is more common with larger hydrocarbon molecules like C_3H_8 and i-C_4H_{10}, while the hexagonal structure sH is associated with multicomponent cages that encapsulates two hydrocarbon molecules like CH_4 with C_4H_{10}, C_5H_{12} or C_6H_{14} (Sloan and Koh, 2008). Such solids can be formed above the freezing temperature of water and, for this reason, represent a major flow assurance concern. Gas flowline hydrate formation occurs as consequence of favorable thermodynamic conditions, which are defined basically by three factors: (i) presence of production water along with the gas, (ii) high operating pressures in flowlines, and (iii) low temperature close to 0^oC (Gupta and Singh, 2012). Those conditions are typically found in deepwater subsea gas flowlines and therefore the prevention or control of hydrates formation is necessary in order to avoid safety hazards in flowlines and the consequent production losses (Sloan and Koh, 2008).

In this context, the most adopted strategy for gas hydrate inhibition is the continuous injection of a hydrate inhibitor in the well-heads, so as to avoid hydrate formation and consequently ensure unimpeded flow. Regarding thermodynamic inhibitors of hydrates, MEG injection has been widely used because of its relative advantages over other inhibitors, namely: low losses to vapor phase, low solubility in condensate phase, high depression of water freezing point, high depression of hydrate formation temperature and good attenuation of corrosion. Furthermore, MEG can be easily recovered and effectively regenerated and recycled, configuring a cost effective choice for hydrate inhibition (Haghighi et al., 2009). In addition, the latest MEG reclamation plant designs are cheaper to build and to operate, they have simpler equipment and offer substantially better performance, especially in terms of reliability, high recovery of MEG, energy consumption, low carbon emission, adequate disposal of salt and water back in the sea with environmentally acceptable levels of contamination, and they also comply with the best Health, Safety & Environment (HSE) standards (Nazzer and Keogh, 2006).

II.1.1 MEG Recovery Unit: MRU

After injection, MEG flows along with the production fluids towards the platform, where the incoming stream has its three phases separated: (i) an aqueous bottom phase, comprised mainly of MEG, water and salts; (ii) an intermediate hydrocarbon liquid phase (condensate), and (iii) an upper gas phase of NG with low water content. The aqueous phase, after removal of hydrocarbons in a pre-treatment step, is also known as Rich MEG, aqueous MEG containing at least 25% w/w of water and salts (Bikkina et al., 2012). The Rich MEG is sent to the MEG Recovery Unit (MRU) in order to remove water, salts and other impurities. The recovered MEG is known as Lean MEG containing a minimum of 80% w/w MEG. Lean MEG is returned to be re-injected into the well-heads, thereby completing the MEG loop. Currently, there are three main technologies for offshore MRUs, namely: Traditional Process (TP), Full-Stream Process (FS) and Slip-Stream Process (SS).

TP simply processes Rich MEG with an atmospheric distillation column (ADC) to distillate part of the water producing the re-concentrated Lean MEG as bottoms at a temperature near to 140 ^{o}C. TP usually works well when there is no formation water with the produced gas. However, formation water is usually associated with raw NG and therefore the Lean MEG from TP retains inorganics (NaCl, Ca^{+2}, carbonates, oxides and sulfides), which accumulate overtime and deposit as scale on filters, piping and exchanger surfaces, deteriorating MRU capacity and facilitating corrosion and thermal degradation of glycol (Nazzer and Keogh, 2006).

FS treats Rich MEG with three serial steps: (i) ADC again for the first removal of water with bottoms temperature below 140 °C; (ii) Flash-Evaporator (FLS) operating under vacuum (0.2 bar A) at vapor temperatures below 120 ^{o}C, wherein the feed instantaneously vaporizes after mixing with the recycled hot liquor (with MEG above 90% w/w), while salts precipitate as a slurry in the concentrated liquor; and (iii) the vapor stream from the FLS, containing only MEG and water, feeds a sub-atmospheric distillation column (SDC) at 0.2 bar A to be separated into pure water (top) and Lean MEG (Nazzer and Keogh, 2006). FLS operates under vacuum to ensure low operating temperatures in the hot liquor recycle ($T \leq 140$ ^{o}C) preventing thermal degradation of MEG, which starts at 162 ^{o}C. This degradation produces

oxidized species (e.g. acetic and formic acids; Alharooni, 2015) leading to a weakening of hydrate inhibition, which in turn entails make-up of fresh MEG to recompose the inhibitor (Montzaud, 2011). Furthermore, the heater of liquor recycle is a critical item that must reliably heat a high flow rate of salty recycle liquor without exposing it to high skin temperatures that might promote thermal degradation and/or vaporization with salt precipitation, leading to fouling (Nazzer and Keogh, 2006). Since the liquor heater must not allow suspended particulate matter to settle and incrust, a spiral heat exchanger (SHE) is the preferred design, as it avoids solids build up through a high velocity field that prevents stagnant areas (Latta et al., 2016).

SS process is a combination of the aforementioned Traditional and Full-Stream processes, wherein only a fraction (the Slip-Stream) of the ADC bottoms is treated in a FLS+SDC train and then mixed with the untreated MEG from ADC. This arrangement depends on the salt incoming rate. If it is not too high, it is possible to remove a good part of the water in the pre-concentrator ADC and control the salt content in the lean MEG by running the slip-stream through the FLS (reclaimer) followed by the SDC to finish the removal of water from the slip fraction (Seiersten et al., 2010). The final concentration of salts in the Lean MEG should therefore be kept below a precipitation limit that is acceptable for service.

II.1.2 Power, Heating and Cooling Resources Available to Offshore MRUs

Depending on the adopted MRU technology and process conditions, there will be different requirements of heating, cooling and electric energy (EE) for operation. Since only MRUs located on offshore platforms are considered here, it is critical to minimize heating, cooling and EE requirements and also the extent of energy degradation. Moreover, the platform environment molds the available options of cooling, heating and EE resources.

The EE supply on offshore oil and gas rigs is normally provided by gas turbines. Gas turbines are widely used for onsite power generation and as mechanical drives in offshore oil and gas production facilities such as FPSOs (Araújo et al., 2016). The temperature of exhaust from gas turbines with power output rating up to 50 MW (both industrial heavy-duty and aero-

derivatives) range between 400 °C–600 °C (Bianchi et al., 2014; GE Aviation, 2003). In offshore rigs the waste heat from the exhaust gases is partly recovered to increase the temperature of a liquid heating medium, such as mineral oil or pressurized hot water (PHW), which circulates in a closed loop supplying heat to facilities (Nguyen et al., 2013). The most common heating medium in topside facilities is PHW, which is easily produced via Heat Recovery Water Heaters (HRWH) (Araújo et al., 2016) with low safety risk compared to mineral oil or high pressure steam (PARAT Halvorsen AS, 2008). Although it is not uncommon to utilize direct EE for heat supply on offshore rigs (Myhre, 2001), up-to-date systems adopt PHW as a low cost heating solution for reboilers and heaters operating below 180 ^{o}C (Araújo et al., 2016). In this work all considered MRU heating duties are supplied by PHW supposed available at 200 ^{o}C. FPSO gas turbine power stations are designed with capacity near to 100 MW of EE at full service, not counting the spare machines. At 100 MW of EE, most vendors guarantee a minimum heat recovery of 75 MW in the HRWH (Araújo et al., 2016). Thus, it is reasonable to assume that the PHW circuit has a maximum capacity of 75 MW of heat supply in typical scenarios, which is perfectly suitable to MRU requirements.

The main cooling resource available in offshore rigs is seawater (SW). Again there is a sealed secondary circuit of cooling water (CW) removing heat from process units and discharging it at the coils of the open primary SW circuit (Nguyen et al, 2013). The SW primary circuit is also used to cool the condenser of a refrigeration machine that produces chilled water (ChW) at 10 ^{o}C. ChW is necessary in the sub-cooler at the top of the SDC in order to kill the flow of steam to the vacuum pump in FS and SS processes. To design the cooling systems of CW and ChW, the inlet temperature of SW is a critical factor, which depends on the climatic zone and the depth where SW is collected. In general, SW is collected at low depths and flows to cool the secondary CW and ChW circuits, being returned to the sea afterwards. This work assumes a tropical or subtropical marine scenario where SW is admitted at 20 ^{o}C, returning at a temperature of 35 ^{o}C to avoid environmental issues.

II.1.3 Exergy Analysis of Offshore MRUs versus Reference Environmental Reservoir (RER)

Exergy Analysis (ExA) has been recognized as a tool to assess energy degradation in chemical and thermoelectric plants. ExA quantifies the percentage of destroyed exergy by irreversibilities and assesses the primary sinks of exergy destruction due to inefficiencies (Boroumandjazi et al., 2013). ExA may also be used for design optimization in order to minimize energy requirements and degradation. This work addresses the performance of MRU technologies in terms of ExA. A complete picture of the thermodynamic performance of a process can be achieved via ExA complementing conventional energy analysis. ExA clearly indicates the blocks which destroy exergy the most, i.e., the most thermodynamically inefficient units. This is done by drawing a map of how the rate of exergy destruction is distributed over the process. Therefore, ExA pinpoints the plant components that can be improved and reveals whether or not, and by how much, it is possible to design a more efficient use of energy (Dincer and Zamfirescu, 2011).

The flow of exergy is a concept derived by combining the 1^{st} and 2^{nd} Laws of Thermodynamics for open systems. It corresponds to the maximum power obtainable when a stream is brought into equilibrium with its surroundings, i.e. a Reference Environmental Reservoir (RER). Therefore, exergy depends not only on the state of streams, but also on the definition of RER. Defining an appropriate RER may not be a direct task, but it is essential for ExA (Dincer and Zamfirescu, 2011). Exergy flow provides a thermodynamic scale to measure any resource that is considered under the form of a stream, but it is not solely an intrinsic characteristic of the stream. The exergy flow rate of a stream is a measure of its thermodynamic distance to the state of equilibrium with RER (Gaudreau, 2012). Hence, ExA is meaningless without a comprehensive RER (Valero, 2006), whose definition should meet a practical requirement: The species exergies should not be ascribed with extremely high values without reasonable discrimination of species and states. The reason is simple: If all streams of a steady-state process have very high exergy flows, process irreversibilities can be masked because the inlet and outlet flow rates of exergy would be of the same high order of magnitude, while the rate of exergy destruction is fixed and invariant with respect to the chosen RER. In other words, if the scale being used favors high scores to all items under

consideration, while letting untouched the differences among them, it is evident that this would gratuitously inflate the efficiencies of candidate processes reducing the capability to discriminate them (Ahrendt, 1980). There are studies regarding the influence of the RER choice. Some have pointed out that ExA of chemical and thermal plants are often relatively insensitive to variations in RER temperature (T_0) and pressure (P_0) (Wepfer and Gaggioli (1980); Rosen and Dincer, 2004). On the other hand, the study of Muslim et al (2005) on one-stage and two-stage crude oil distillation plants, shows that exergy efficiencies may be sensitive to the RER temperature.

In the present work the focus is on how the choice of the RER state of central species impacts ExA. In MRUs, MEG is the central species. Therefore, besides performing ExA of MRUs, another goal here is to address how the RER state of MEG affects the analysis. MEG has a very high specific exergy if measured from the conventional RER i.e. the standard atmosphere (N_2, O_2, CO_2, H_2O, Ar, etc) with MEG in chemical equilibrium with O_2, CO_2 and H_2O. Such RER gives very high specific exergy of MEG in MRU streams due to the extremely low chemical potential of ultra-rarefied MEG in chemical equilibrium with air. Consequently, since MEG is conserved in MRUs, there is a high percentage of conserved exergy in all MRUs, masking the inefficiencies of each one and hindering their discrimination; i.e. all MRUs will appear with high exergy efficiencies near 80%. This RER choice is unrealistic for the typical transitions in MRUs. Thus, a better RER is sought to eliminate this masking of efficiencies and to allow a meaningful comparison of MRUs. The only possible way is to redefine RER to reduce the high specific exergy of MEG relatively to the other species. The proposed approach is to allow MEG to *exist as an independent RER species*, not in chemical equilibrium with air. This new RER state of MEG can only be feasible if defined in an aqueous liquid in vapor-liquid equilibrium (VLE) with the atmosphere; i.e. this new RER is two-phase with MEG infinitely diluted in the aqueous liquid. To compare RER choices, ExA has been conducted according to these two RERs: (i) Approach #1: the conventional RER with gaseous MEG in chemical equilibrium with air, corresponding to the standard atmosphere water saturated via VLE with pure liquid H_2O at 25 ^oC and 1 atm; and (ii) Approach #2: RER is the standard atmosphere again in VLE with liquid water containing MEG at infinite dilution at 25 ^oC and 1 atm.

II.1.4. Sensitivity of Exergy Analysis of Offshore MRUs

MRU processes basically use distillation and flash operations to re-concentrate MEG by removing salt and water. Typical distillation and flash operations follow well-known patterns of efficiency. Thus, once exergy values are obtained using an appropriate RER definition and exergy efficiencies are in accordance to what is expected for distillation-based processes (i.e. akin to MRU operations), a sensitivity analysis can be carried out in order to evaluate the effect of key parameters related to the degree of irreversibility of operations in terms of overall exergy performance.

As any designer knows, there are a few parameters that directly control the degree of irreversibility of typical operations of distillation-based processes, namely: (i) the thermal approach (*TAPP*) in heat exchangers; and (ii) the reflux ratio (*RR*) of distillation columns. As *TAPP* increases above the minimum pinch value for a given thermal service ($TAPP^{MIN}$), the size and complexity of the exchanger decreases, but the irreversibility of the process increases, implying a rise of cooling and heating consumptions. This can be translated as a higher rate of destruction (or loss) of exergy, i.e. a fall of exergy efficiency. The reasoning is similar in the context of *RR*: as *RR* increases above the minimum pinch value for a given distillation separation (RR^{MIN}) the column height decreases, but the irreversibility increases with the rise of heating and cooling consumptions, increasing the rate of loss of exergy and lowering the exergy efficiency of the process. These patterns are demonstrated in this work after appropriately choosing the definition of RER for MRU applications.

II.1.5 Thermodynamic Efficiencies of Unit Operations of Offshore MRUs

Offshore MRUs basically utilize distillation columns and evaporation equipment, besides several heating and cooling operations. A relevant question would be: How about the range of expected values of thermodynamic efficiencies for the main MRU operations? A first point to be realized beforehand is that Thermodynamic Efficiency and Exergy Efficiency are not in

general the same thing, but both have a direct relationship and vary in the same direction. Considering only energy consuming processes as in the case of MRUs, the Thermodynamic Efficiency – not to be confused with the Thermodynamic Yield of power cycles or with the Coefficient of Performance of heat pump cycles – expresses the ratio between the minimum consumption of equivalent power to accomplish a given task and the actual consumption of equivalent power for the same task, where by equivalent power it is meant the equivalent measure in terms of mechanical power corresponding to all heating and cooling thermal duties.

On the other hand, Exergy Efficiency is based on the fact that the difference between the outlet usable exergy flow rate of streams ($\dot{B}_{out}$) and the inlet usable exergy flow rate of streams ($\dot{B}_{in}$) is related to the minimum consumption (maximum production) of power to accomplish the process task under reversible conditions, i.e. $\dot{W}^{REV} = -(\dot{B}_{out} - \dot{B}_{in})$. In the case of a power consuming process, like MRUs, the efficiency can be defined in two different ways: (i) as the ratio between the minimum power consumption $\left|\dot{W}^{REV}\right| = \left|\dot{B}_{out} - \dot{B}_{in}\right|$ and the actual equivalent power consumption; and (ii) as the ratio between the flow rate of all usable exergy leaving the process ($\dot{B}_{out} + \dot{B}_{out}^{W}$) and the corresponding flow rate of all usable inlet exergy ($\dot{B}_{in} + \dot{B}_{in}^{W}$), where the superscript *W* refers exclusively to the contribution of non-material streams like pure mechanical energy streams and the equivalent mechanical value of heat duties. As can be seen, the first definition of Exergy Efficiency is exactly the abovementioned Thermodynamic Efficiency, but the second one can give, in general, different results and is very dependent on the definition of RER, because it strongly affects the value of exergy flow rate associated to material streams. For ExA of processes, it is normally chosen the second interpretation of exergy efficiency.

Concerning the Thermodynamic Efficiency of ordinary distillation columns, it can easily be shown that ordinary distillation columns have poor thermodynamic efficiencies, invariably ranging from 0% to 20%. This is the range of Exergy Efficiency that should be expected for MRU processes. As a matter of example, it is shown in Appendix A (Supplementary

Materials) that the Thermodynamic Efficiency is only 10.31% for a nearly isobaric atmospheric binary distillation column assuming a not too sharp cut, total condenser and total reboiler operation, bubble point equimolar ideal solution feed (components “1” and ”2”), bubble point bottoms with 5% mol of “1”, bubble point distillate with 95% mol of “1”, heat of vaporization of 30 kJ/mol independent of composition, constant relative volatility $\alpha=2$, no head losses, isothermal heating medium at 200 ^{o}C, isothermal cooling medium at 50 ^{o}C, and $RR/RR^{MIN}=1.3$.

In the case of pure component products, the distillation column efficiency attains a maximum value of 15.46% at minimum reflux, decreasing – as the reflux ratio increases – initially rapidly and then slowly towards zero at total reflux. In Appendix B (Supplementary Materials) it is also shown how to combine the thermodynamic efficiencies of several power consuming operations in order to obtain the overall thermodynamic efficiency of a power consuming process with several constituent operations. It must be pointed out that the results in Appendices A and B (Supplementary Materials) are not based on exergy concepts, but only on classical Second Law Analysis, which is the unique requisite to assess Thermodynamic Efficiencies. The objective of these appendices is to shed some light on the expected range of Thermodynamic Efficiencies of distillation columns and, indirectly, of MRU processes.

II.2. Methodology

The primary objective of this work is to compare the three MRU technologies in terms of energy consumption and exergy efficiency. Secondly, it is also investigated how the choice of RER definition impacts ExA. Thirdly, a consistency cross-check is formulated and applied to validate ExA. Finally, a sensitivity analysis is performed to evaluate how the ExA results vary with parameters that control the degree of irreversibility of operations in distillation-based processes. The perturbed parameters are chosen as the thermal approach (*TAPP*) in heat exchangers; and the reflux ratio (*RR*) of the ADC of MRUs. It is expected beforehand that the increase of such parameters must lead to the decrease of both Thermodynamic Efficiencies and Exergy Efficiencies. To achieve that, process conditions and relevant parameters are

defined and steady-state process flow diagrams (PFD) of MRUs are simulated to solve mass and energy balances. Mechanical energy and heat consumptions of MRUs are accessed via simulations, as well all thermodynamic properties of the relevant material, thermal and mechanical energy streams. Heat streams are used to represent heating and cooling effects associated to a contact of material streams in a heat exchanger.

The mathematical expressions of exergy flows are derived in Sec. II.4 from the 1st and 2nd Laws of Thermodynamics applied to a multi-stream, steady-state open system representing a MRU and/or its constituent operations. An important feature of ExA is that only the material and (equivalent) mechanical energy streams crossing the boundaries that envelope the studied process have to be taken into account. From the RER definition, stationary exergy flows are calculated for the relevant streams via spreadsheets with thermodynamic properties extracted from the simulated PFD of interest. Exergy efficiencies are determined in each PFD with the exergy flows.

II.3. Implementation of MRU PFDs

II.3.1. Premises

Typical flow rates and conditions in the literature of real MRUs are used for TP, FS and SS PFDs (Nazzer and Keogh, 2006). The operating pressure of MEG boiling systems is set at 0.2 bar A, so that all boiling points lie below 140 ^{o}C to avoid thermal degradation of MEG at 162 ^{o}C or above. NaCl is the main ionic species, representing 1-3% w/w of Rich MEG, whereas the other salts – $CaCl_2$, $CaSO_4$ etc – reach only hundreds of ppm and are irrelevant in terms of thermal effects. Even so, NaCl is not included in the simulation for two reasons: Firstly, NaCl only settles in the FLS after vaporization of MEG and H_2O, which are responsible for the main energy effects associated with phase changes. To confirm this, MRU was simulated with and without NaCl and the differences in terms of heat duties were always found below 1-2% (Teixeira, 2014). Secondly, current aqueous solution models are not reliable with strong electrolytes at SVLE (i.e. VLE with NaCl saturation and precipitation) conditions, which would lead to inaccurate thermodynamic properties and consequently affect

the accuracy of ExA. Thus, after discarding NaCl, the Rich MEG stream is defined as: 100 t/d, 55% w/w H_2O + 45% w/w MEG at 25 ^oC, 1 bar. The Slip Fraction in SS is chosen as 50%. Temperature approaches (*TAPP*) in all heat exchangers are set to 5 ^oC. Inlet and outlet temperatures of gas turbine exhausts in HRWH are 600 ^oC and 300 ^oC, respectively. The temperatures of PHW and ChW are 200 ^oC and 10 ^oC, respectively. The initial and final temperatures of SW and CW are 20 ^oC – 35 ^oC and 25 ^oC – 40 ^oC, respectively. For comparisons, the temperature and pressure of Rich and Lean MEG have same values on TP, FS, SS MRUs. Thermodynamic calculations use the Glycol Property Package (Twu-Sim-Tassone TST-EOS; Twu et al., 2002) available in the simulation environment (Aspen Hysys v. 8.8).

II.3.2 Traditional Process (TP)

The PFD of the TP implementation is shown in Fig. II.1. In all figures, inlet and outlet streams are identified, respectively, in blue and red. The atmospheric distillation column (ADC) has a heat-integrated condenser, such that the Rich MEG feed is pre-heated in the condenser before entering the column. The ADC condenser is complemented with a CW finishing condenser. "Rich MEG" is fed into ADC, producing pure water as top product (≥ 99.99% mol water) and stream "2" as bottoms. Stream "2" is the Lean MEG stream, which passes through pump and heat exchanger to meet specifications.

II.3.3 Full-Stream (FS) Process

The PFD of the FS implementation is shown in Fig. II.2. As in the TP case, the ADC has a heat-integrated condenser. However, in this case, the ADC has only to remove part of water present in the Rich MEG. The ADC bottoms pass through a valve to depressurize to 0.2 bar A and feeds the FLS where it is mixed with the hot liquor from the recycle heater SHE. The hot liquor, highly concentrated in MEG, has only 20 ^oC of sensible heat above the dew point in the FLS, but it can vaporize the entire feed by direct contact because it has a much larger mass

flow rate (≈ 30:1 w/w). The FLS top vapor containing only H_2O and MEG is sent to a sub-atmospheric distillation column (SDC), producing pure water as top distillate and stream "3" as bottoms, which corresponds to Lean MEG after passing through following pump and heat exchanger. The vacuum system of SDC (vacuum compressor or ejector) must not admit high flow rates of vapor in order to keep vacuum and save power. To accomplish this, a distillate sub-cooler is employed admitting chilled water (ChW) at 10 ^{o}C to sub-cool the water distillate to 15 ^{o}C reducing its vapor pressure to protect the vacuum system. The ChW circuit is a secondary loop cooled by a water chiller using a propane refrigeration cycle, whose condenser, by its turn, is cooled by SW as sketched in Fig. II.4.

II.3.4 Slip-Stream Process (SS)

The PFD of the SS implementation is shown in Fig. II.3. As in the previous cases, ADC operates with the same configuration using a heat-integrated condenser. In this case, the ADC bottom product is divided into two streams: (i) the Slip-Stream, which follows the FS process path towards the FLS and SDC; and (ii) the Slip-Stream complement which is left unchanged to be mixed with the Lean MEG from the SDC bottoms, thereby producing the final Lean MEG product. SS uses the same FS vacuum configuration.

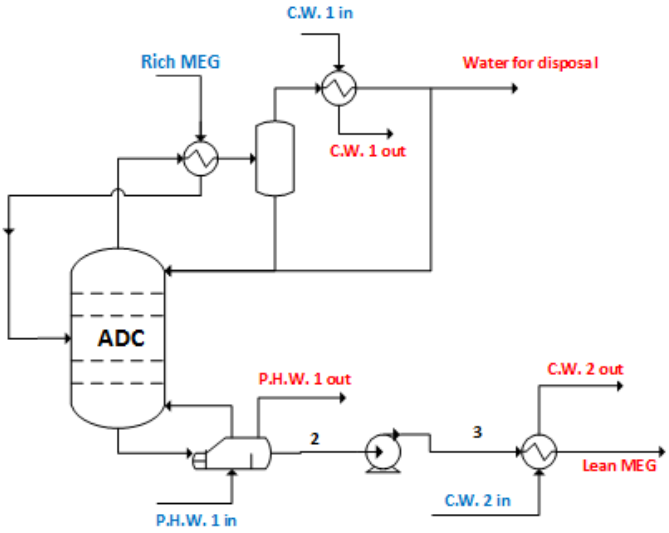

Figure II.1. Traditional Process (TP)

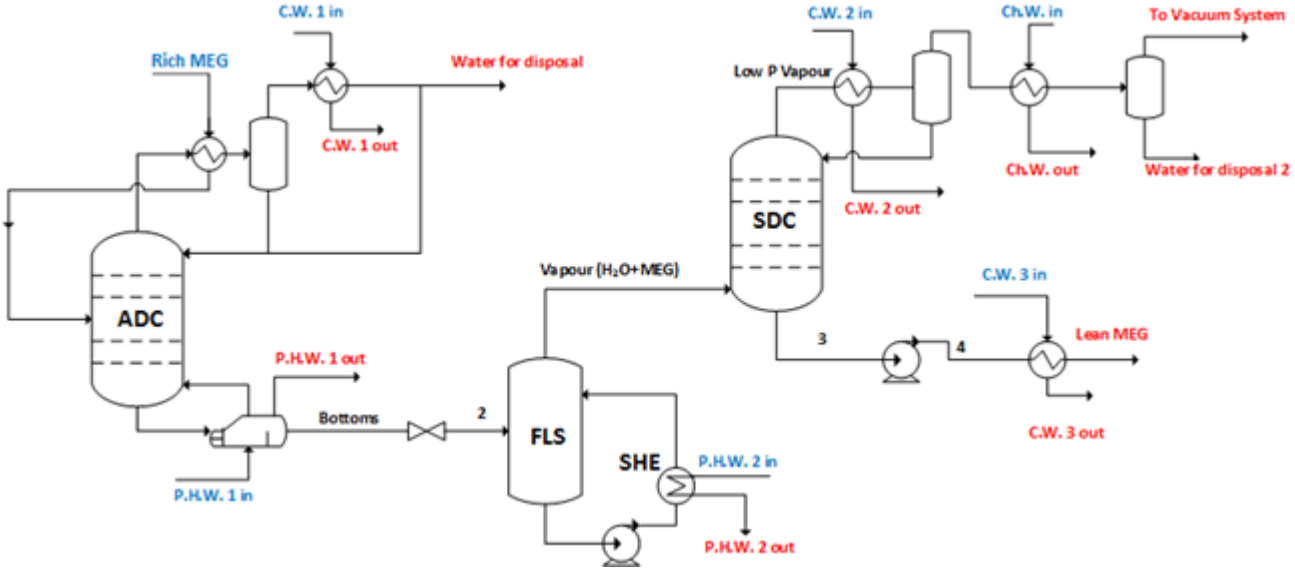

Figure II.2. Full-Stream Process (FS)

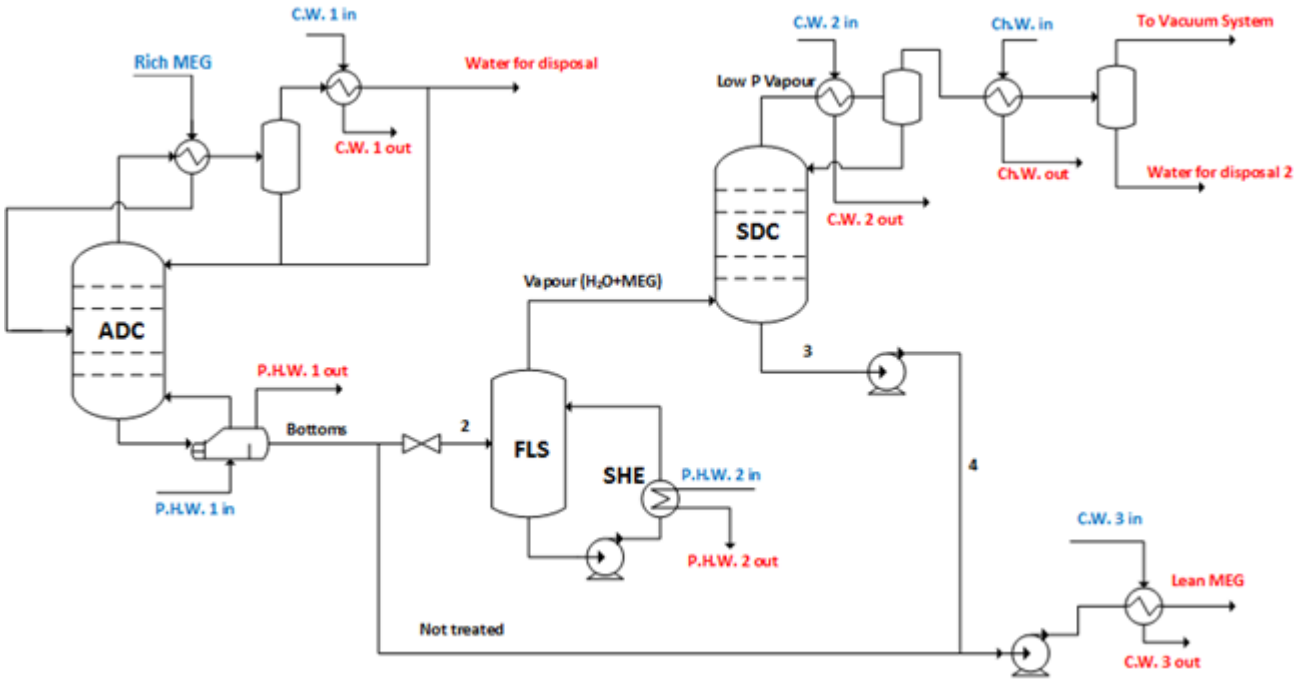

Figure II.3. Slip-Stream Process (SS)

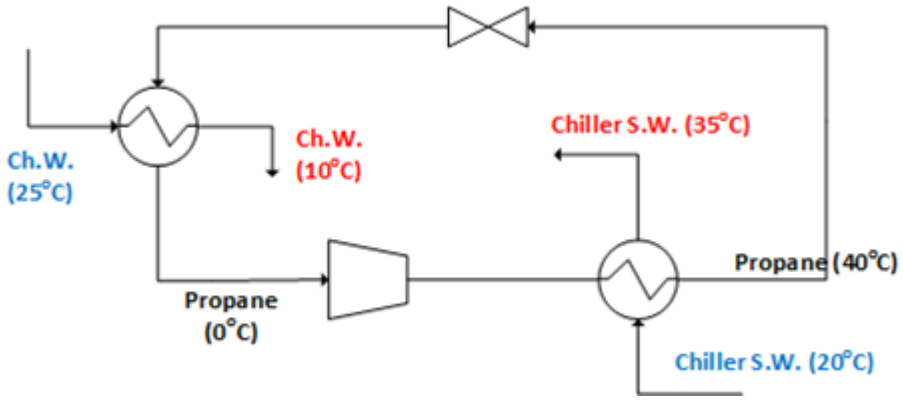

Figure II.4. Water Chiller with Propane Refrigeration Cycle Cooled by Seawater (SW)

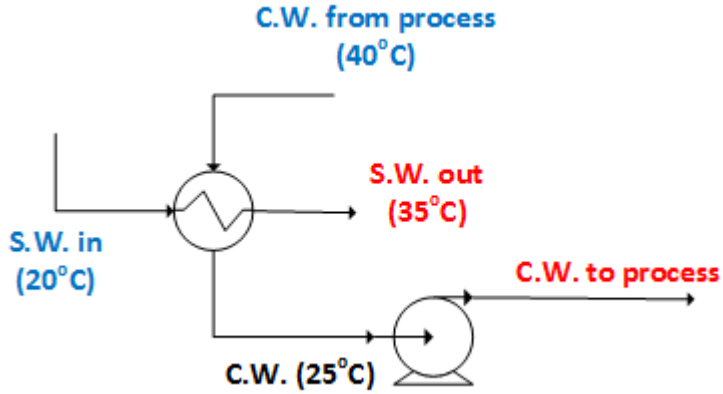

Figure II.5. Cooling Water (CW) Regeneration System Cooled by Seawater (SW)

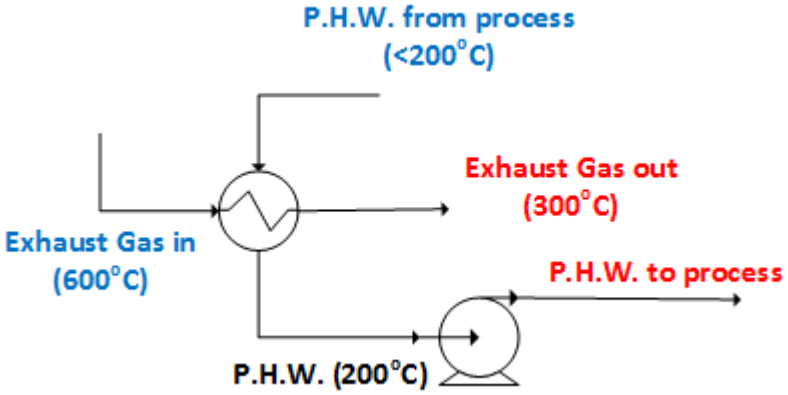

Figure II.6. Heat Recovery Water Heater (HRWH) using Gas Turbine Exhaust to Heat Pressurized Hot Water (PHW)

II.3.5 Heat Consumption of MRUs

For each PFD in Figs II.1, II.2 and II.3, mass and energy balances are solved giving thermal duties and mechanical powers for TP, FS and SS. The main heating duties (ADC reboiler and FLS recycle heater) are depicted in Table II.1, wherein the respective Lean MEG compositions and the energy required to achieve them are reported. TP has the lowest heat consumption as it is the simplest process with only one separation step which does not vaporizes MEG appreciably. On the other hand, FS has the highest heat consumption, as it vaporizes the whole Rich MEG feed. SS is the second in terms of heat consumption as the Rich MEG feed in this case is only partially distilled. It is worth of note that, in all MRUs, the heat consumption is primarily supplied by the waste heat of hot exhaust gas from EE generation gas turbines. Part of this waste heat is recovered by the HRWH (Fig. II.6) and conveyed to the unit operations by the PHW circuit (Figs. II.1, II.2 and II.3). The SW circuit (Fig. II.5) is the ultimate cold sink of the entire heat consumed by MRUs.

Table II. 1. Heat Consumptions and Lean MEG Compositions of MRU Processes

MRU	%w/w MEG of Lean MEG	Heat Consumption (kW)
TP	85.83	1734.1
FS	93.32	2289.8
SS	85.58	1889.9

II.4. Exergy Analysis (ExA)

II.4.1. Exergy Definition and Modeling

Exergy flow (in kW) is defined as the maximum power (mechanical work) obtainable when a stream reaches equilibrium with a reference RER. Therefore a generalized expression for exergy flow of streams is developed considering a general steady-state open system and its RER. According to the Second Law of Thermodynamics the Universe is an isolated system with constant mass, volume and energy, whose entropy increases as irreversible transitions occur or remains constant when only reversible transitions take place. A miniature Universe is

shown in Fig. II.7. This mini Universe has a steady-state finite open system – henceforth called the System – interacting with several different reservoirs, which are infinite systems – hence their representation with indefinite contours – that are characterized by one (or more) constant intensive parameter(s) that regulates the exchanges of certain specific extensive properties like volume, thermal energy, mass of species *1*, mass of species *2*, etc. Central points in the concept of reservoir are: (i) any finite exchange of the specific exchangeable property(ies) does not alter the reservoir characteristic intensive parameter(s); (ii) reservoirs have appropriate selective walls that allow bidirectional flow exclusively of the exchangeable property (e.g. movable, frictionless, thermally isolated piston to exchange exclusively volume; selective membrane to exchange component *1*, etc); (iii) reservoirs are uniform and always in internal equilibrium (internal reversibility), so that the Fundamental Relationship of the Internal Energy is always integrable on any transition.

The System is a rigid – rectangle in Fig. II.7 – steady-state, open system with several inlet $\{F_1, F_2, ... F_{nfs}\}$ and outlet $\{K_1, K_2, ..., K_{nps}\}$ streams where *nfs* and *nps* represent, respectively, numbers of feed and product streams. The System interacts with *nc* reservoirs of species *k* $\{R_1, R_2, ..., R_{nc}\}$, where each R_k has a constant volume and state coordinates T_0 *and* μ_k^0. In all interactions between the System and R_k, only component *k* is transferred at a certain rate with a simultaneous energy flow $\dot{\Xi}_k$. The System interacts with a volume reservoir R_V at constant pressure P_0, where interactions with R_V are adiabatic volume transfers only, with associated work (power) $\dot{W}_V$. Due to its internal reversibility and adiabatic operation, R_V entropy is constant. The System also interacts with a constant volume heat reservoir R_H at temperature T_0, through heat transfer $\dot{Q}_0$. Fig. II.7 illustrates this coupling of System and reservoirs, where the lightning shaped arrows represent transfers between System and reservoirs, such that do not necessarily entail equilibrium between them.

RER is a conceptual union of all reservoirs: species, volume and heat reservoirs $R_1, R_2, ..., R_{nc}$, R_V, R_H. Each reservoir is infinite (relatively to the System), uniform and supposed in complete (thermo-chemical-mechanical) equilibrium. All reservoirs of species (R_k) are supposed in *mutual chemical equilibrium* and at the same temperature T_0. RER is a large enough

environment where its intensive properties do not change due to interactions with the (finite) System.

Initially, the First Law is written in Eq. (II.1) for the System. Since all reservoirs are at internal equilibrium, *Internal Energy Fundamental Relationships* can be written in rate-based form as shown in Eqs. (II.2), (II.3) and (II.4). Exchange terms $\dot{Q}_0, \dot{W}, \dot{W}_V, \dot{\Xi}_k$ are defined according to the classical thermodynamic convention following the System viewpoint. The First Law is invoked to relate the exchange terms $\dot{Q}_0, \dot{W}, \dot{W}_V, \dot{\Xi}_k$ with the rate of internal energy of reservoirs as seen in the RHS of Eqs. (II.2), (II.3) and (II.4).

$$\sum_{j}^{nps} K_j \overline{H}_{K_j} = \sum_{j}^{nfs} F_j \overline{H}_{F_j} + \sum_{k=1}^{nc} \dot{\Xi}_k + \dot{Q}_0 - \dot{W} - \dot{W}_V \tag{II.1}$$

$$\dot{U}^{(R_H)} = T_0 \dot{S}^{(R_H)} = -\dot{Q}_0 \ , \dot{V}^{(R_H)} = 0 \tag{II.2}$$

$$\dot{U}^{(R_V)} = -P_0 \dot{V}^{(R_V)} = \dot{W}_V \ , \dot{S}^{(R_V)} = 0 \tag{II.3}$$

$$\dot{U}^{(R_k)} = T_0 \dot{S}^{(R_k)} + \mu_k^0 \dot{N}_k^{(R_k)} = -\dot{\Xi}_k \quad (k=1..nc) \tag{II.4}$$

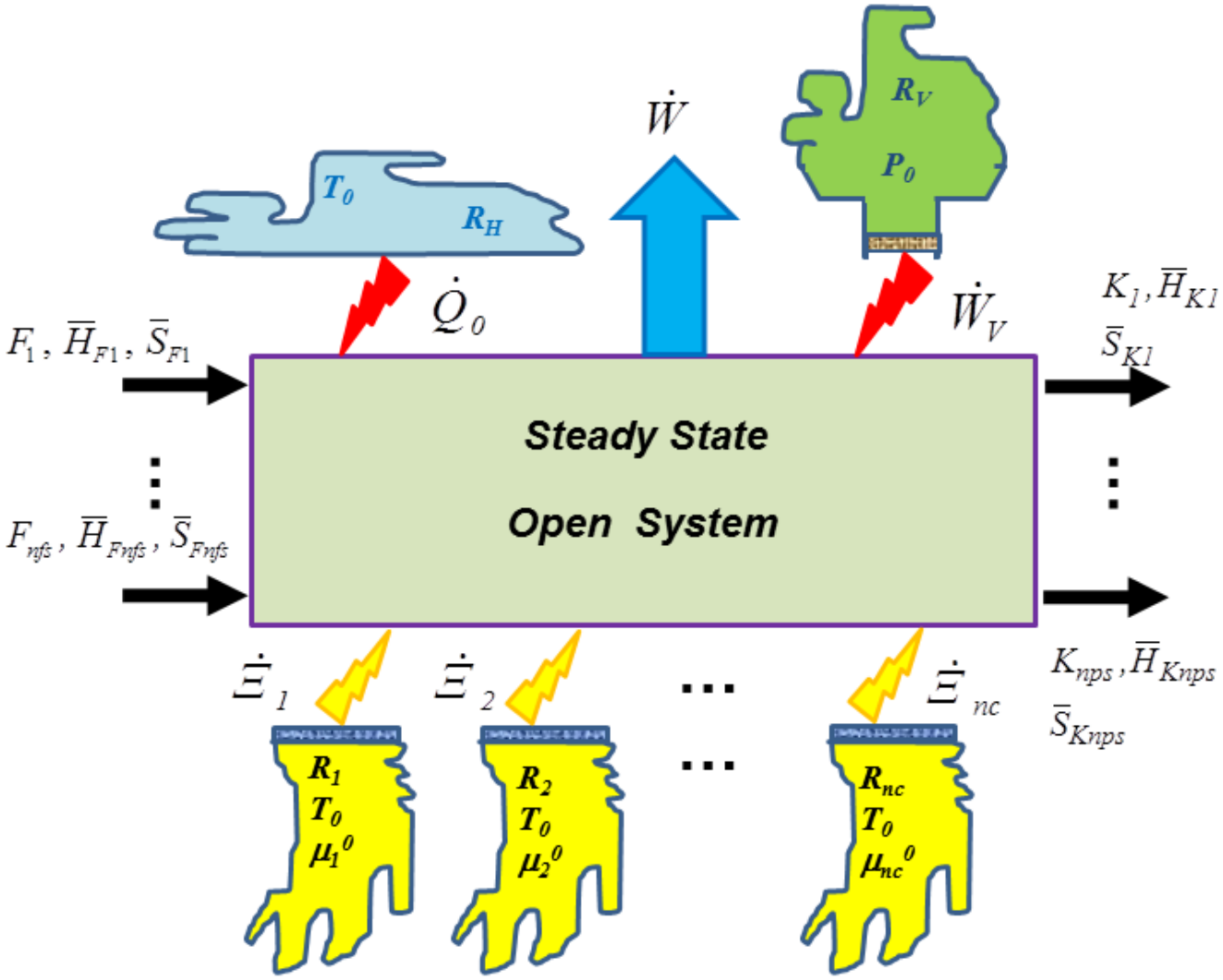

Figure II.7. Complex Steady-State Open System Interacting with Heat, Volume and Species Reservoirs

Net rates of creation of volume, entropy and species k in the Universe can be addressed respectively using Eqs. (II.5), (II.6) and (II.7), which are written for the macro-system in Fig. II.7 defined by the System coupled to reservoirs R_1,R_2,....,R_{nc}, R_V, R_H.

$$\dot{\Omega}_V = \dot{V}^{Sys} + \dot{V}^{(R_V)} + \dot{V}^{(R_H)} + \sum_{k=1}^{nc} \dot{V}^{(R_k)} - \sum_{k}^{nfs} F_k \bar{V}_{F_k} + \sum_{k}^{nps} K_k \bar{V}_{K_k} \qquad \text{(II.5)}$$

$$\dot{\Omega}_S = \dot{S}^{Sys} + \dot{S}^{(R_H)} + \dot{S}^{(R_V)} + \sum_{k=1}^{nc} \dot{S}^{(R_k)} - \sum_{j}^{nfs} F_j \bar{S}_{F_j} + \sum_{j}^{nps} K_j \bar{S}_{K_j} \qquad \text{(II.6)}$$

$$\dot{\Omega}_k = \dot{N}_k^{Sys} + \dot{N}_k^{(R_k)} - \sum_j^{nfs} F_j Y_{kF_j} + \sum_j^{nps} K_j Y_{kK_j} \qquad \text{(II.7)}$$

The steady-state condition of the System implies $\dot{V}^{Sys}$, $\dot{S}^{Sys}$ and $\dot{N}_k^{Sys}$ equal to zero. $\dot{V}^{(R_H)}$ and $\dot{V}^{(R_k)}$ are also zero because they refer to constant volume reservoirs. Similarly, $\dot{S}^{(R_V)}$ is zero because R_V operates at constant entropy. The rate of creation of volume ($\dot{\Omega}_V$) of the Universe is zero according to the definition of Universe. If the System exhibits chemical reactions, at first species are not conserved in the Universe; i.e. apparently $\dot{\Omega}_k \neq 0$. But, since species reservoirs are *in mutual chemical equilibrium*, the generation/consumption of species *k* within the System, can be compensated by a reverse consumption/generation of species *k* within reservoir R_k by simply converting/creating reversibly other species in their respective reservoirs without any change in the thermodynamic condition of the Universe. Thus, either with or without chemical reactions in the System, the creation rates of all species in the Universe can be taken as zero ($\dot{\Omega}_k = 0$). With these concepts, it can be shown that the rate of work produced by the System is given by Eq. (II.8a):

$$\begin{aligned} -\dot{W} = &\sum_j^{nps} K_j \left(\overline{H}_{K_j} + P_0 \overline{V}_{K_j} - T_0 \overline{S}_{K_j} - \sum_{k=1}^{nc} \mu_k^0 Y_{kK_j} \right) \\ &- \sum_j^{nfs} F_j \left(\overline{H}_{F_j} + P_0 \overline{V}_{F_j} - T_0 \overline{S}_{F_j} - \sum_{k=1}^{nc} \mu_k^0 Y_{kF_j} \right) + T_0 \dot{\Omega}_S \end{aligned} \qquad \text{(II.8a)}$$

The maximum rate of net work is obtained when the System operates reversibly, in other words without creation of entropy in the Universe according to the 2nd Law, i.e. $\dot{\Omega}_S = 0$. In this case, Eq. (II.8a) leads to Eq. (II.8b) which shows that the maximum rate of work production $\dot{W}^{MAX}$ (or minimum rate of work consumption $\dot{W}^{MIN}$) is defined by the negative of the difference between the total output flow rate of exergy associated with product streams leaving the System and the total input flow rate of exergy associated with the feed streams entering the System, respectively corresponding to the first and second RHS terms of Eq. (II.8b). In other words, the molar exergies of product stream K_j and of feed stream F_j must be

defined, respectively, by $\overline{B}_{K_j} \equiv \overline{H}_{K_j} + P_0\overline{V}_{K_j} - T_0\overline{S}_{K_j} - \sum_{k=1}^{nc}\mu_k^0 Y_{kK_j}$ and $\overline{B}_{F_j} \equiv \overline{H}_{F_j} + P_0\overline{V}_{F_j} - T_0\overline{S}_{F_j} - \sum_{k=1}^{nc}\mu_k^0 Y_{kF_j}$.

Exergy terms associated to material streams are calculated using only state (ratio or "density") properties belonging to the respective stream ($\overline{V},\overline{H},\overline{S},Y_k$), multiplied by ("field") parameters P_0,T_0,μ_k^0 that belong to RER. Each term summed up in the RHS of Eq. (II.8b) represents the ultimate definition of exergy flow rate associated with the respective material stream.

$$-\dot{W}^{MAX} = \sum_{j}^{nps} K_j \left(\overline{H}_{K_j} + P_0\overline{V}_{K_j} - T_0\overline{S}_{K_j} - \sum_{k=1}^{nc}\mu_k^0 Y_{kK_j} \right) - \sum_{j}^{nfs} F_j \left(\overline{H}_{F_j} + P_0\overline{V}_{F_j} - T_0\overline{S}_{F_j} - \sum_{k=1}^{nc}\mu_k^0 Y_{kF_j} \right) \qquad \text{(II.8b)}$$

The difference between Eqs. (II.8a) and (II.8b), leads to the well-known formula for the rate of lost work (lost power) in Eq. (II.8c).

$$\dot{W}^{LOST} = \dot{W}^{MAX} - \dot{W} = T_0\dot{\Omega}_S \qquad \text{(II.8c)}$$

On the other hand, besides being associated with material flows, exergy can also be associated to pure mechanical energy (power) streams which are contributing terms within $\dot{W}$ and $\dot{W}^{MAX}$. Therefore, the total inlet and outlet exergy flows can be generalized by adding material and pure mechanical exergy flows as in Eqs. (II.9) and (II.10), where $\dot{B}_{in}$, $\dot{B}_{out}$ are the exergy flow rates associated to all input and output material streams, whereas exergy flows $\dot{B}_{in}^{W}$, $\dot{B}_{out}^{W}$ are assigned to all positive pure mechanical power streams (e.g. electric energy streams and/or equivalent mechanical effects associated with heat duties) imported or exported by the System, represented by $\left|\dot{W}_j^{imported}\right|$ and $\left|\dot{W}_k^{exported}\right|$ respectively.

$$\dot{B}_{in} + \dot{B}_{in}^{W} = \sum_{j}^{nfs} F_j \left(\overline{H}_{F_j} + P_0 \overline{V}_{F_j} - T_0 \overline{S}_{F_j} - \sum_{k=1}^{nc} \mu_k^0 Y_{kF_j} \right) + \sum_{j=1}^{nwi} \left| \dot{W}_j^{imported} \right| \quad \text{(II.9)}$$

$$\dot{B}_{out} + \dot{B}_{out}^{W} = \sum_{j}^{nps} K_j \left(\overline{H}_{K_j} + P_0 \overline{V}_{K_j} - T_0 \overline{S}_{K_j} - \sum_{k=1}^{nc} \mu_k^0 Y_{kK_j} \right) + \sum_{k=1}^{nwe} \left| \dot{W}_k^{exported} \right| \quad \text{(II.10)}$$

All terms in exergy formulae Eqs. (II.9) and (II.10) can be extracted from the process simulations. The only exceptions correspond to RER parameters P_0, T_0, μ_k^0, which depend on the definition of RER. Therefore, in order to investigate which would be the best definition of RER for ExA with MRUs, two RER approaches are considered in the next subsections.

For final validation of exergy calculations, two ways of calculating lost exergy are implemented for each MRU. These two ways can corroborate each other in any application of this methodology because they use different sources of property values. The rate of lost exergy in the Universe can be calculated from: (i) the difference between total output and total input flow rates of exergy in Eq. (II.12); and (ii) from the rate of lost work in Eq. (II.8c) or Eq. (II.11), where $\dot{\Omega}_S$ is the net rate of creation of entropy in Eq. (II.6), and $\Delta\dot{B}$ arises in the LHS of the difference of Eqs. (II.10) and (II.9).

$$\dot{W}^{LOST} = T_0 \dot{\Omega}_S \quad \text{(II.11)}$$

$$\Delta\dot{B} \equiv (\dot{B}_{out} + \dot{B}_{out}^{W}) - (\dot{B}_{in} + \dot{B}_{in}^{W}) \quad \text{(II.12)}$$

II.4.2. RER Chemical Potentials of Species for RER Approach #1

RER in Approach #1 is two-phase and defined by standard atmospheric air saturated with water at $T_0=298.15\ K$ and $P_0=1\ atm$ by VLE with an infinite body of pure water, where the standard atmosphere has the following dry-basis molar fractions: $Y_{N_2} = 0.7808$, $Y_{O_2} = 0.2095$, $Y_{Ar} = 0.0094$, $Y_{CO_2} = 0.0004$. The final composition of the RER vapor phase ($Y_{N_2}^0, Y_{O_2}^0, Y_{Ar}^0, Y_{CO_2}^0, Y_{H_2O}^0$) is obtained by solving the VLE with liquid water as an idle sub-PFD, where the vapor is well approximated by an ideal gas mixture. On the other hand, it

must be recalled that commercial simulators do not export chemical potentials. Thus μ_i^0 must be obtained through enthalpy and entropy of pure species as ideal gases at T_0= *298.15 K* and P_0=*1 atm* which are corrected to mixture conditions via Eq. (II.13), where $\mu_i^{f,0}(T_0, P_0)$ is the chemical potential of pure *i* at (T_0, P_0), calculated by the simulation PFD with an idle stream of pure *i* at (T_0, P_0) via Eq. (II.14). These calculations must use the same thermodynamic model selected for the pertinent exergy flows in the MRU PFD. This ensures consistency of exergy values since all enthalpies and entropies refer to the same entropy and enthalpy datum values.

$$\mu_i^0 = \mu_i^{f,0}(T_0, P_0) + RT_0 \ln Y_i^0 \qquad \text{(II.13)}$$

$$\mu_i^{f,0}(T_0, P_0) = \bar{H}(\text{pure } i, T_0, P_0) - T_0 \bar{S}(\text{pure } i, T_0, P_0), \ (i = N_2, O_2, Ar, CO_2) \qquad \text{(II.14)}$$

In the case of water this procedure must be changed as a pure water stream at T_0 and P_0 will be recognized in liquid state. Thus, an arbitrary idle stream of pure water is created at T_0=*298.15 K* and *P=0.01 atm* which is depressurized enough to be in vapor phase as a stable pure ideal gas. The substitute versions of Eqs. (II.13) and (II.14) for water case correspond to Eqs. (II.15) and (II.16). Properties in Eq. (II.15) come from the idle water gas stream, which are complemented by Eq. (II.16) via the ideal gas chemical potential isothermal change from *0.01 atm* to P_0=*1 atm*. Another possible way to calculate μ_{H2O}^0 follows from the VLE with pure liquid water, namely, by the value of molar Gibbs energy of pure liquid water at T_0 and P_0 via Eq. (II.17) from an idle stream of liquid water with the thermodynamic package TST-EOS.

In RER Approach #1, MEG is allocated as a trace component gas in chemical equilibrium with the remaining RER species. From a practical standpoint, the trace presence of MEG is insufficient to affect the gas phase composition and the other chemical potentials. The RER chemical potential of MEG is extremely low as calculated according to a combustion chemical equilibrium among MEG, O_2, CO_2 and H_2O in Eq. (II.18) with standard states of species as *(g)* state (pure ideal gas, 25 ^oC, 1 atm). This gives μ_{MEG}^0 in Eq. (II.19).

$$\mu_i^f(T_0, 0.01\,atm) = \bar{H}(pure\ i, T_0, 0.01\,atm) - T_0\bar{S}(pure\ i, T_0, 0.01\,atm)\ (i=H_2O) \quad \text{(II.15)}$$

$$\mu_i^{f,0}(T_0, P_0) = \mu_i^f(T_0, 0.01\,atm) + RT_0 \ln\left(\frac{1\,atm}{0.01\,atm}\right) \quad (i=H_2O) \quad \text{(II.16)}$$

$$\mu_{H_2O}^0(T_0, P_0) = \bar{G}(T_0, P_0)\Big|_{Liquid\ H_2O} = \bar{H}(T_0, P_0)\Big|_{Liquid\ H_2O} - T_0\bar{S}(T_0, P_0)\Big|_{Liquid\ H_2O} \quad \text{(II.17)}$$

$$C_2H_6O_2(g) + 2.5O_2(g) \leftrightarrow 2CO_2(g) + 3H_2O(g) \quad \text{(II.18)}$$

$$\mu_{MEG}^0 = 2\mu_{CO_2}^0 + 3\mu_{H_2O}^0 - 2.5\mu_{O_2}^0 \quad \text{(II.19)}$$

II.4.3. RER Chemical Potentials of Species for RER Approach #2

In Approach #2 RER is again two-phase at $T_0=298.15\ K$ and $P_0=1\ atm$ with H_2O saturated atmospheric air in VLE with liquid H_2O. The difference from Approach #1 is that MEG is allocated *in the liquid at infinite dilution without chemical equilibrium with air*. The vapor phase uses the same dry-basis air composition of RER Approach #1, with final vapor composition obtained by solving the water VLE as before. RER chemical potentials $\mu_{N_2}^0$, $\mu_{CO_2}^0$, μ_{Ar}^0, $\mu_{O_2}^0$, $\mu_{H_2O}^0$ are calculated as in RER Approach #1 with Eqs. (II.13), (II.14), (II.15) and (II.16), with the humid air composition as Y_i^0 values. In the case of water, as the liquid phase is essentially pure water, $\mu_{H_2O}^0$ can also be obtained from the molar Gibbs energy of a pure water liquid stream with Eq. (II.20). The RER chemical potential of MEG, μ_{MEG}^0, is given by μ_{MEG}^{∞,H_2O} via Eq. (II.21) (Smith et al., 2001), where *X* represents the MEG mol fraction. The derivative term in Eq. (II.21) is obtained via numerical differentiation on the curve $\bar{G}(T_0,P_0,X) = \bar{H}(T_0,P_0,X) - T_0\bar{S}(T_0,P_0,X)$ generated with $\bar{H}(T_0,P_0,X)$, $\bar{S}(T_0,P_0,X)$ values from several composition of H_2O+MEG liquid streams at (T_0, P_0) in the simulation PFD. Graphically, Eq. (II.21) is equivalent to the intersection of the tangent line at $X_{MEG}=0$ with the line $X_{MEG}=1$, as illustrated in Fig. II.8.

$$\mu^{0}_{H_2O}(T_0,P_0)=\overline{G}(T_0,P_0,X)\big|_{X=0}=\overline{H}(T_0,P_0,X)\big|_{X=0}-T_0\overline{S}(T_0,P_0,X)\big|_{X=0} \quad \text{(II.20)}$$

$$\mu^{\infty,H_2O}_{MEG}(T_0,P_0)=\overline{G}(T_0,P_0,X)\big|_{X=0}+\frac{d\overline{G}}{dX}(T_0,P_0,X)\Big|_{X=0} \quad \text{(II.21)}$$

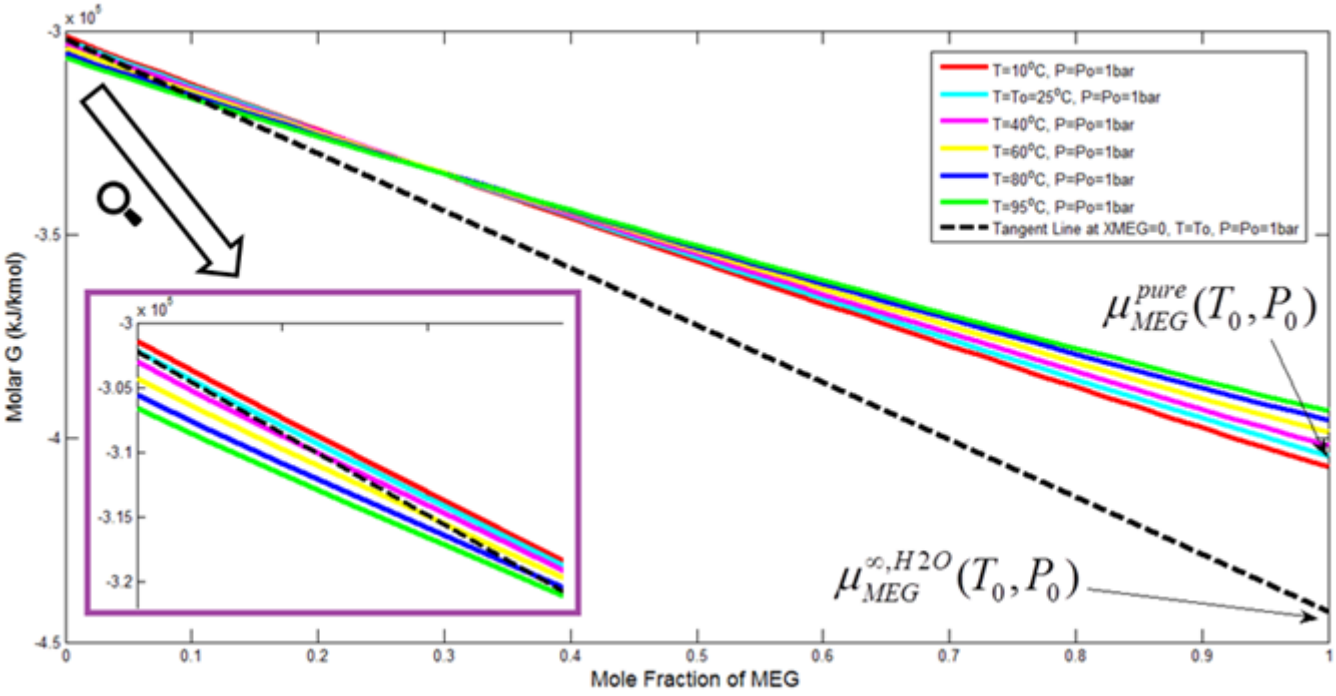

Figure II.8. Graphic Determination of the Chemical Potential of MEG Infinitely Diluted in Water

II.5. Results and Discussion

II.5.1. Exergy Analyses of MRUs by RER Approach #1 and by RER Approach #2

Table II.2 reports values of RER chemical potentials of species from both RER approaches. Exergy flows of streams via each RER approach are calculated with Table II.2. A primary indicator of consistency is that all exergy flows must always have *positive values* expressed in kW. As can be seen, μ^{0}_{MEG} is very different for RER Approaches #1 and #2, strongly affecting the numerical values of exergy flows. RER Approach #1 provides a very negative μ^{0}_{MEG} entailing Rich MEG and Lean MEG streams with very high positive values of exergy

flows of similar magnitudes as seen in Table II.3. The situation is different under RER Approach #2: exergy flows of MEG streams exhibit much lower positive values of dissimilar magnitudes, whose distinction is markedly established as seen in Table II.4.

Table II.2. Chemical Potentials of RER Species via RER Approaches #1 and #2

Species	μ_k^0 RER Approach#1 (kJ/kmol)	μ_k^0 RER Approach #2 (kJ/kmol)
N_2	-5.05×10^4	-5.05×10^4
O_2	-5.39×10^4	-5.39×10^4
Ar	-4.69×10^4	-4.69×10^4
CO_2	-4.60×10^5	-4.60×10^5
H_2O	-3.02×10^5	-3.02×10^5
MEG	-1.71×10^6	-4.43×10^5

Table II. 3. Exergy Flows of Inlet and Outlet Streams with RER Approach #1

TP		FS		SS	
Stream	**Exergy Flow Rate (kW)**	**Stream**	**Exergy Flow Rate (kW)**	**Stream**	**Exergy Flow Rate (kW)**
Rich MEG	10879.8	Rich MEG	10879.8	Rich MEG	10879.8
S.W.1 in	13.9	S.W.1 in	10.0	S.W.1 in	11.3
S.W.2 in	0.9	S.W.2 in	5.8	S.W.2 in	2.5
Exhaust Gas in	2243.4	S.W.3 in	0.4	S.W.3 in	0.8
Water for disposal	0.2	Exhaust Gas 1 in	1713.1	Exhaust Gas 1 in	1811.9
S.W.1 out	24.9	Exhaust Gas 2 in	1113.7	Exhaust Gas 2 in	524.6
S.W.2 out	1.7	Chiller S.W. in	4.9	Chiller S.W. in	2.1
Exhaust Gas out	1051.6	Water for disposal	0.1	Water for disposal	0.1
Lean MEG	10922.5	S.W.1 out	17.9	S.W.1 out	20.3
		S.W.2 out	10.5	S.W.2 out	4.6
		S.W.3 out	0.8	S.W.3 out	1.4
		Exhaust Gas 1 out	807.4	Exhaust Gas 1 out	806.2
		Exhaust Gas 2 out	440.7	Exhaust Gas 2 out	226.2
		Chiller S.W. out	8.8	Chiller S.W. out	3.8
		Water for disposal 2	0.1	Water for disposal 2	0.1
		Lean MEG	10930.3	Lean MEG	10922.3

According to RER Approach #2, MEG is allocated in a liquid phase infinitely diluted in water *without chemical equilibrium with RER species*. Although MEG is now not in the lowest exergy state in RER, this choice of reference is more practical in MRU processing because it is out of question to produce work by oxidizing MEG to CO_2 and H_2O. This entails a less negative μ^0_{MEG}, consequently giving much lower positive values of exergy flows of the Rich

and Lean MEG streams as seen in Table II.4, because μ^0_{MEG} now represents a state closer to the thermodynamic condition of MEG in the MRU streams. Comparing Tables 3 and 4 it becomes clear that values of exergy flows of MEG streams for RER Approach #1 are two orders of magnitude larger than those via RER Approach #2. The underlying reason is that Rich and Lean MEG streams have much more exergy content relatively to RER species in Approach #1 than in Approach #2, as reflected in the RER chemical potentials of MEG in Table II.2.

Table II. 4. Exergy Flows of Inlet and Outlet Streams with RER Approach #2

TP		**FS**		**SS**	
Stream	**Exergy Flow Rate (kW)**	**Stream**	**Exergy Flow Rate (kW)**	**Stream**	**Exergy Flow Rate (kW)**
Rich MEG	263.8	Rich MEG	263.8	Rich MEG	263.8
S.W.1 in	13.9	S.W.1 in	10.0	S.W.1 in	11.3
S.W.2 in	0.9	S.W.2 in	5.8	S.W.2 in	2.5
Exhaust Gas In	2243.4	S.W.3 in	0.4	S.W.3 in	0.8
Water for disposal	0.1	Exhaust Gas 1 in	1713.1	Exhaust Gas 1 in	1811.9
S.W.1 out	24.9	Exhaust Gas 2 in	1113.7	Exhaust Gas 2 in	524.6
S.W.2 out	1.7	Chiller S.W. in	4.9	Chiller S.W. in	2.1
Exhaust Gas Out	1051.6	Water for disposal	0.1	Water for disposal	0.1
Lean MEG	306.6	S.W.1 out	17.9	S.W.1 out	20.3
		S.W.2 out	10.5	S.W.2 out	4.6
		S.W.3 out	0.8	S.W.3 out	1.4
		Exhaust Gas 1 out	807.4	Exhaust Gas 1 out	806.2
		Exhaust Gas 2 out	440.7	Exhaust Gas 2 out	226.2
		Chiller S.W. out	8.8	Chiller S.W. out	3.8
		Water for disposal 2	0.1	Water for disposal 2	0.1
		Lean MEG	314.9	Lean MEG	306.4

The differences between RER Approaches #1 and #2 also impact directly exergy efficiencies as seen in Table II.5. Exergy efficiencies are calculated as ratios between output and input flow rates of exergy (in kW) taken, respectively, from Eqs. (II.10) and (II.9). As calculated with Tables 3 and 4, both approaches give rise to the same rate of lost exergy (kW). However, RER Approach #1 leads to Rich and Lean MEG streams with very high positive exergy flows (≈ 11000 kW) both of a much greater magnitude than exergy losses (exergy destruction) associated to irreversibilities, which amounts 1142.2 kW for TP, 1626.6 kW for FS and 1300.8 kW for SS. As MEG is not consumed in the MRUs, total inlet and outlet exergy flow rates associated with Rich and Lean MEG streams have huge magnitudes with only ≈ 1000 kW to ≈ 1600 kW of lost exergy. Hence, with RER Approach #1, the output exergy flow rate has a small relative fall to the input exergy flow rate – i.e. they are close in magnitude – entailing high exergy efficiencies near 80%. The exaggerate magnification of exergy content of Lean MEG and Rich MEG, as viewed by RER Approach #1, precludes a satisfactory perception of the difference between these exergy flows, resulting in very high exergy efficiencies for all MRU processes if RER Approach #1 is used.

On the other hand, RER Approach #2 provides much lower positive values of exergy flows associated with Rich and Lean MEG streams (≈ 260 kW to ≈ 315 kW). Therefore much lower (but more meaningful) exergy efficiencies are obtained, since the same rate of exergy is lost in both cases of RER definition. This leads to more realistic efficiencies by RER Approach #2, which are closer to what is expected for distillation-based processes (Appendix A, Supplementary Materials).

Table II. 5. Overall Exergy Efficiencies (%) of MRU Processes via RER Approaches #1 and #2

MRU	RER Approach #1	RER Approach #2
TP	83.10%	12.13%
FS	78.96%	9.76%
SS	82.21%	11.48%

Another instance to compare the performances of ExA according to RER Approaches #1 and #2 is related to the determination of exergy efficiencies of unit operations of MRUs. Fig. II.9 depicts exergy efficiencies of the processing units of TP, FS and SS for ExA via RER Approach #1, while Fig. II.10 presents analogous results for ExA via RER Approach#2. As expected, the main sinks of exergy (i.e. units with major rates of exergy destruction) correspond to the distillations columns: ADC is the largest sink, whereas FLS is the smallest sink among the main units. However, only RER Approach #2 is capable of revealing this kind of detail, while RER Approach #1 gives a worse discrimination of exergy efficiencies of process units and of the entire PFDs. In other words, RER Approach #2 allows ExA to indicate on which blocks of MRU processes, design efforts should be concentrated so as to minimize energy degradation and improve overall energy consumption. In this case, the distillation columns, and particularly ADC in TP, FS and SS, should be considered with more care. This is in accordance with what is expected for ordinary distillation columns (Appendix A, Supplementary Materials), since the reboiler of ADC represents a great source of irreversibility thanks to a large average *TAPP* and heat consumption. The efficiency of ADC should be compared with the better exergy efficiency of SDC which does not have reboiler and uses the supply of enthalpy conveyed by the vapor stream from FLS.

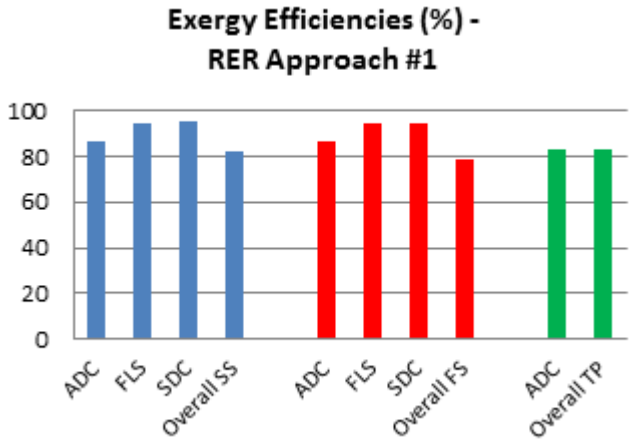

Figure II.9. Exergy Efficiency of Process Units of SS, FS and TP via RER Approach #1

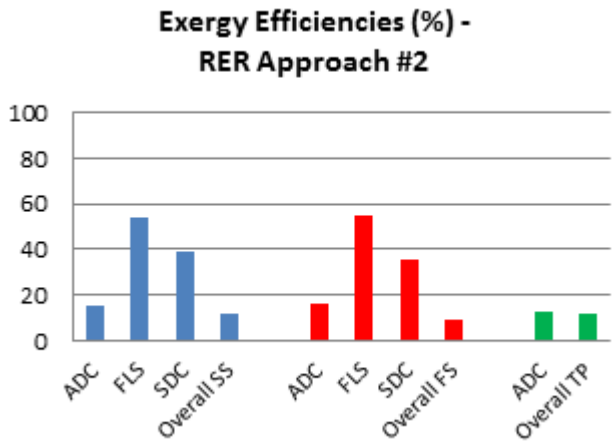

Figure II.10. Exergy Efficiency of Process Units of SS, FS and TP via RER Approach #2

Figs. II.11 and II.12 illustrate Sankey Diagrams for TP, FS and SS MRUs under RER Approaches #1 and #2, respectively. In Figs. II.11 and II.12 the widths of arrows are proportional to the respective exergy flow rates, thereby depicting the distribution of exergy flows of TP, FS and SS. It is remarkable the very different relative impacts of the rate of lost exergy according to RER Approach #1 and #2. RER Approach #2 allows a more impacting and meaningful role of the rate of lost exergy when compared with the respective main input flow of exergy, namely, the stream of hot exhaust gas. In other words, ExA with RER Approach #2 (Fig. II.12) makes clear that the main input of exergy to drive the transformation of Rich MEG into Lean MEG is just the stream of hot exhaust gas from the gas turbines. RER Approach #2 also reveals that the rate of destroyed exergy totals about 50-60% of the input exergy conveyed by hot exhaust gas. Exergy is also wasted (but not destroyed) by the output of useless exergy associated to waste streams: waste exhaust gas, warm SW and disposal water, which respond for approximately 40% of the input exergy with hot exhaust gas. In summary, about 90-100% of the main input of exergy (hot exhaust gas) is wasted by irreversible destruction or dispersed into the environment by waste streams.

In frank opposition with the above correct revelation, RER Approach #1 creates an illusory landscape where the main input of exergy to all MRU processes would correspond to the Rich MEG stream, which is portrayed as carrying an exergy flow 4.5 times bigger than the exergy

flow of hot exhaust gas. This is a wrong and undesirable message. Rich MEG does not have such a role of resource stream; instead, it is just the raw feed to be upgraded to Lean MEG. The role of “resource stream” pertains to the hot exhaust gas, which is the real carrier of exergy to drive all MRUs. This feature configures a sensible weak facet of RER Approach #1. In other words, RER Approach #2 is the really useful RER definition for ExA with MRUs.

Despite the different efficiency magnitudes via RER Approaches #1 and #2, in both cases TP is the most exergy efficient, while FS is the lesser efficient, with SS at intermediate post. Such results are consistent but unfair to FS, because the three MRUs do not have isonomic targets. TP is the simplest MRU, having basically an ADC tower for removing part of the water from Rich MEG. The other MRUs have higher consumptions of heat and EE since they distillate a greater part of water and evaporate partially or totally the fed MEG. Therefore, no wonder TP has the best efficiency: it has only one primary sink of exergy (ADC) responding by its comparatively lesser exergy loss. FS and SS also have, from the outset, an ADC with similar targets, but extend the separation beyond the ADC limits. Between FS and SS, FS performs a harder effort by vacuum-distilling a greater material flow and also producing a more concentrated Lean MEG, demanding more heat and more EE to drive vacuum and chiller systems. The higher heat duties imply higher circulation of PHW, which in turn demands higher heat recovery from hot exhaust gas, as shown in Sec. II.3.5. Therefore, FS has to have the highest rate of exergy input with similar rate of output exergy, consequently exhibiting the lowest exergy efficiency.

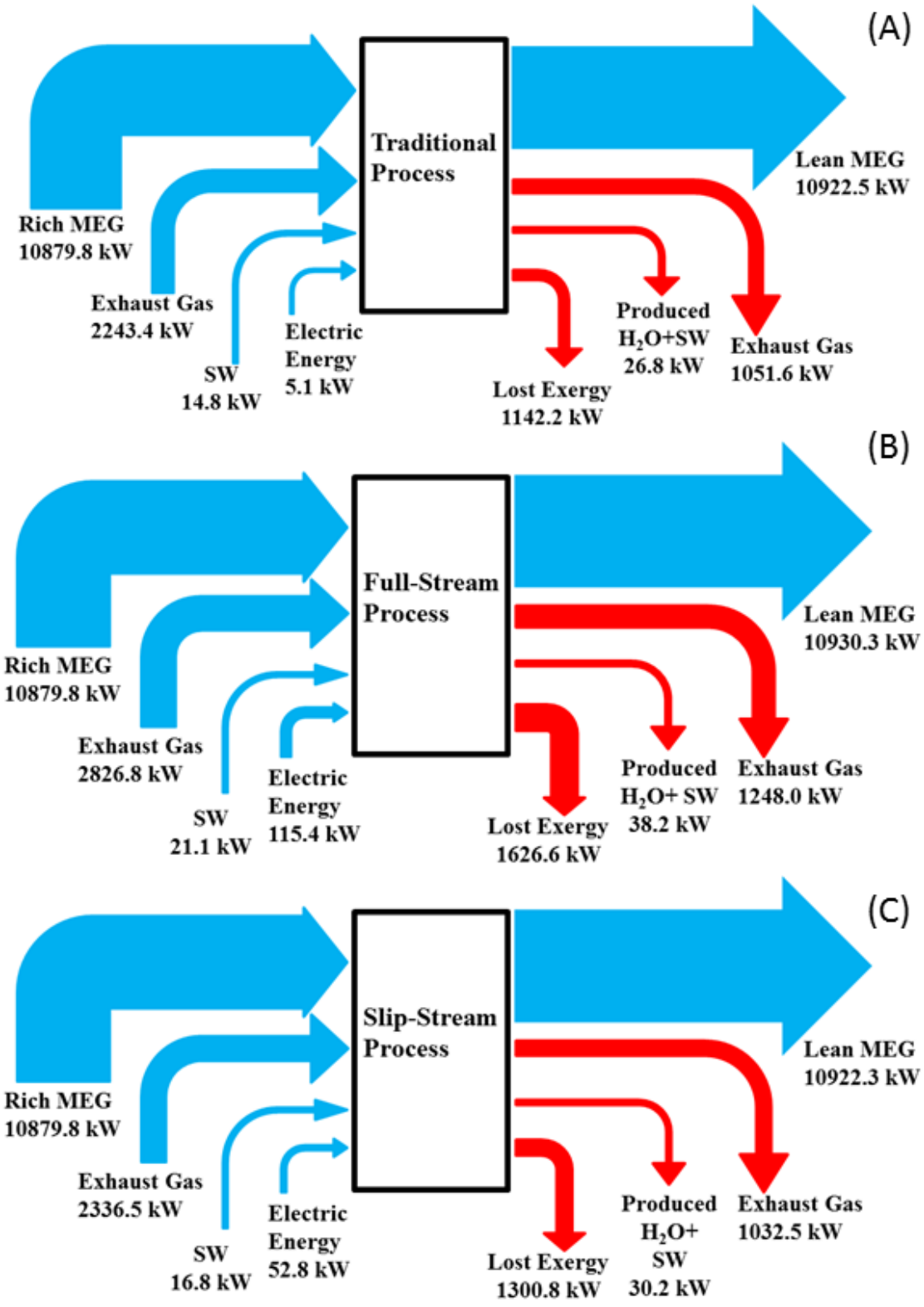

Figure II.11. Sankey Diagrams for ExA with RER Approach #1: (A) TP; (B) FS; (C) SS

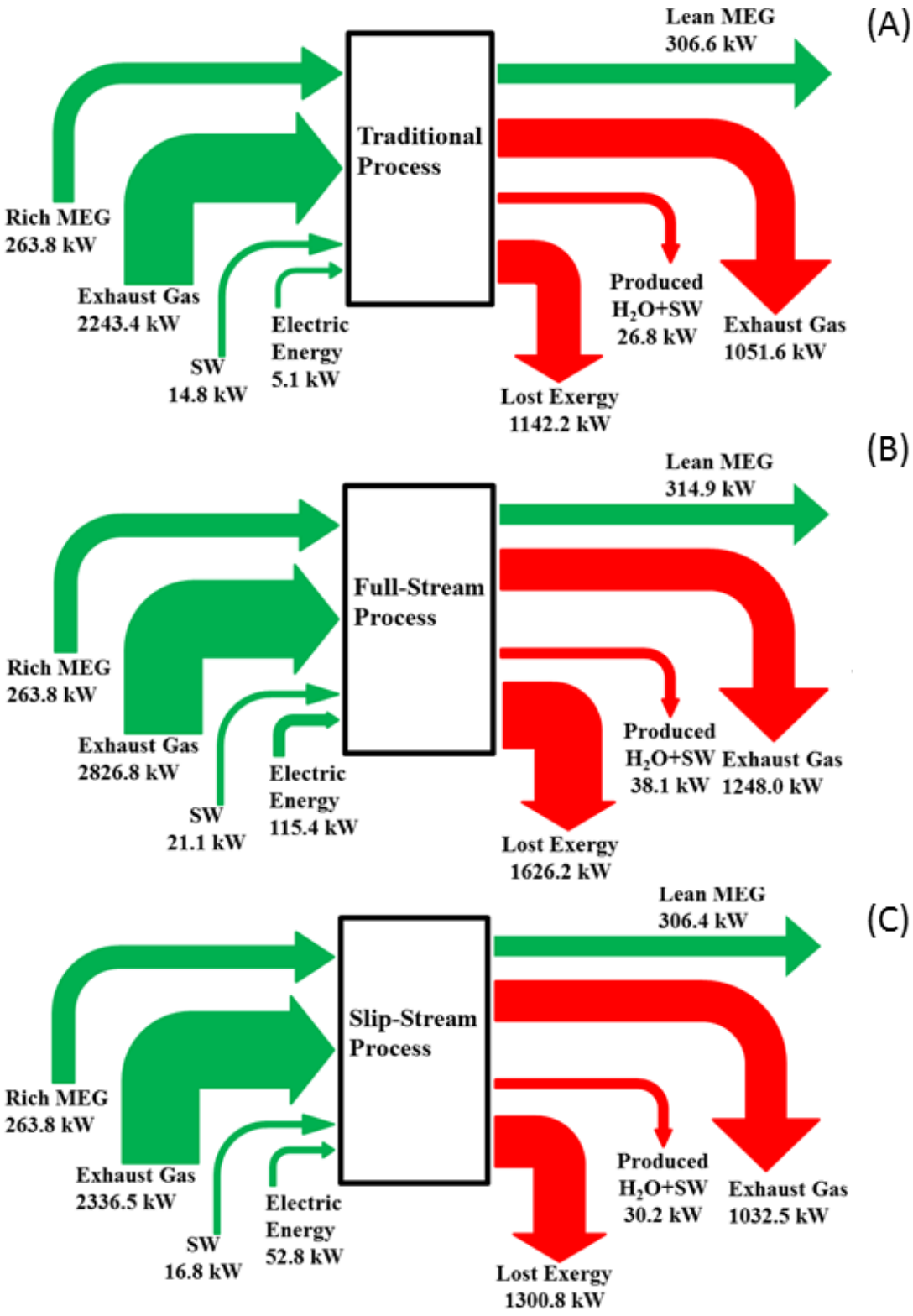

Figure II.12. Sankey Diagrams for ExA with RER Approach #2: (A) TP; (B) FS; (C) SS

II.5.2. Consistency Cross-Check of Exergy Analysis

Exergy calculation in this work can have its consistency tested by carrying out independent calculations of the rate of lost exergy. As discussed in Sec. II.4.1, there are two ways to do that, respectively via Eqs. (II.11) and (II.12). The rate of lost exergy estimated with Eq. (II.12) demands only the exergy flows of MRU streams already displayed in Tables 3 and 4. On the other hand, the rate of lost exergy can also be given by the lost work formula in Eq. (II.11), which now demands estimating the rate of creation of entropy in the Universe $\dot{\Omega}_S$ associated with MRU operation. To estimate $\dot{\Omega}_S$ Eq. (II.6) is used by dropping the first four terms due to steady-state regime and reservoir definition and operation. The volume reservoir R_V is naturally isentropic, whereas the heat reservoir R_H has zero entropy creation because there is no transfer to it since all cooling duties targeted on SW streams. Similarly, all species reservoirs R_1,R_2,....,R_{nc}, do not create entropy because there is no transfer to/from them in all MRUs, since all involved compounds are continuously fed via inlet streams and disposed of by outlet streams without any chemical reaction; i.e. there is no contact with species reservoirs which are left unchanged. Thus, $\dot{\Omega}_S$ is determined by only using the flow rates of entropy associated with feed, product and waste streams of the MRUs.

This comparison is shown in Tables 6 and 7 for RER Approaches #1 and #2, respectively. The displayed figures in columns $\dot{W}^{LOST}$ and $\Delta\dot{B}$ of both Tables 6 and 7 are concordant and corroborate each other, with discrepancies of low magnitude always below 1%, thereby ensuring consistency of results.

Table II.6. Cross-Check of Exergy Calculations: Comparison of Rates of Lost Exergy via Eqs. (II.11) & (II.12) with RER Approach #1

MRU	$\dot{W}^{LOST}$ (kW)	$\Delta\dot{B}$ (kW)	Discrepancy (%)
TP	1150.5	1142.2	0.72%
FS	1617.3	1626.6	-0.58%
SS	1292.5	1300.8	-0.64%

Table II.7. Cross-Check of Exergy Calculations: Comparison of Rates of Lost Exergy via Eqs. (II.11) & (II.12) with RER Approach #2

MRU	$\dot{W}^{LOST}$ (kW)	$\Delta\dot{B}$ (kW)	Discrepancy (%)
TP	1150.5	1142.2	0.72%
FS	1617.3	1626.2	-0.55%
SS	1292.5	1300.8	-0.64%

II.5.3. Sensitivity Analysis of Exergy Efficiencies of MRU Processes

Certain equipment design parameters have direct influence on the degree of irreversibility associated with the operation of the equipment in question, concomitantly with inverse influence on the respective size and capital cost. Typical examples are the temperature approach (*TAPP*) of heat exchangers and the reflux ratio (*RR*) of distillation columns. Concerning the impacts of *TAPP* on the overall exergy efficiency of the process, the chain of influences of *TAPP* is the following: the greater the *TAPP*, the smaller the exchangers, the greater the degree of irreversibility of exchangers, the greater the consumption of thermal utilities, the greater the rate of exergy destruction, the lower the exergy efficiency of exchangers and the lower the exergy efficiency of the plant. The chain of influences is similar for the *RR* of a given column: the greater the *RR*, the smaller the distillation column, the greater its consumption of thermal utilities, the greater the column degree of irreversibility, the greater its rate of exergy destruction, the lower the exergy efficiency of the column and the lower the exergy efficiency of the plant.

From the standpoint of the perspective of the exergy methodology presented in this work, it is worthwhile to assess (and verify) the chains of influences of such design parameters – like *TAPP* and *RR* – closely related to the degree of irreversibility of processes. To accomplish this, the common *TAPP* of three specific heat exchangers – ADC reboiler, SHE of FLS and the sub-cooler at the top of SDC using ChW – and, separately, the *RR* of ADC are monotonically increased in order to observe the respective impacts on the exergy efficiencies of MRUs using both RER approaches. This sensitivity analysis is implemented for all MRUs

under the following assumptions relative to the specific base case of each MRU in Sec. II.5.1: (i) transfer areas and overall heat transfer coefficients of exchangers are kept with values from the respective base cases; (ii) temperature change of the hot exhaust gas stream kept from 600 ^{o}C to 300 ^{o}C as in all base cases; (iii) number of stages and distillate flow rate of ADC kept with values from the respective base cases.

The results of the influence of temperature approach (*TAPP*) on the exergy efficiencies of all MRUs are shown on Table II.8, where the first row of Table II.8 corresponds to the base cases in Sec. II.5.1, Table II.5, which used thermal approach of 5 ^{o}C for the exchangers of TP, FS and SS. As expected, the rising of *TAPP* from 5 ^{o}C to 25 ^{o}C increases the irreversibility related to heat exchanges, monotonically reducing the exergy efficiency of MRUs. With RER Approach #1 the unrealistic large efficiencies are reduced by approximately almost 1% with *TAPP=25 ^{o}C*, whereas with RER Approach #2, this fall is approximately of 4%.

The results of the influence of reflux ratio (*RR*) of ADC on the exergy efficiency of the ADCs of TP, FS and SS are seen on Table II.9, whereas the influences of *RR* on the overall efficiency of MRUs follow on Table II.10. The results corresponding to the base cases of TP, FS and SS (Table II.5) are recognized for *RR=0.28* on Table II.10. As easily seen, the overall exergy efficiencies of all MRUs are much more sensitive to changes on the *RR* of ADC. With RER Approach #1 the unrealistic large efficiencies are reduced by approximately almost 5% as *RR* doubles from 0.2 to 0.4, whereas with RER Approach #2, this fall is approximately of 20%. To explain this, firstly, it must be recalled that ADC is spotted in Fig. II.9 and, especially Fig. II.10 (which adopts the appropriate RER definition), as the main exergy sink in all MRUs. Secondly, from Fig. II.10 it can be seen that the exergy efficiencies of all MRUs are "dragged" to the efficiency of ADC in consequence of its prominent role as main exergy degrader. Thirdly, Appendices A and B (Supplementary Materials) aggregate useful information on thermodynamic efficiency of distillation columns, like its strong dependence on *RR* and how it impacts the overall efficiency of a power consuming process. Appendix A showed that common distillation columns have low thermodynamic efficiencies that fall initially very rapidly and then asymptotically to zero (Fig. A-4) as the reflux ratio increases from minimum to total reflux. Appendix B showed how the fall of the thermodynamic

efficiency of a column can impact the overall process efficiency in the case of power consuming flowsheets like MRUs.

Table II. 8. Influence of Temperature Approach on MRU Exergy Efficiency (%)

	RER Approach #1			RER Approach #2		
TAPP **(°C)**	**TP**	**FS**	**SS**	**TP**	**FS**	**SS**
5*	83.10*	78.96*	82.21*	12.13*	9.76*	11.48*
10	82.94	78.79	82.05	12.01	9.67	11.37
15	82.76	78.61	81.89	11.88	9.57	11.26
20	82.58	78.43	81.73	11.75	9.48	11.15
25	82.40	78.24	81.56	11.61	9.39	11.04

* base case values

Table II.9. Influence of Reflux Ratio (*RR*) on the Exergy Efficiency (%) of ADC

	RER Approach #1			RER Approach #2		
RR	**TP**	**FS**	**SS**	**TP**	**FS**	**SS**
0.20	*85.07*	*88.28*	*87.61*	*14.60*	*17.76*	*17.02*
0.22	*84.66*	*87.93*	*87.26*	*14.21*	*17.28*	*16.58*
0.24	*84.24*	*87.57*	*86.91*	*13.82*	*16.80*	*16.15*
0.26	*83.81*	*87.20*	*86.54*	*13.44*	*16.33*	*15.72*
0.28	*83.36*	*86.81*	*86.16*	*13.07*	*15.87*	*15.30*
0.30	*82.90*	*86.40*	*85.77*	*12.70*	*15.41*	*14.88*
0.32	*82.43*	*85.98*	*85.37*	*12.33*	*14.95*	*14.47*
0.34	*81.93*	*85.54*	*84.95*	*11.97*	*14.50*	*14.07*
0.36	*81.42*	*85.09*	*84.52*	*11.62*	*14.06*	*13.67*
0.38	*80.89*	*84.62*	*84.07*	*11.27*	*13.62*	*13.28*
0.40	*80.35*	*84.12*	*83.60*	*10.92*	*13.19*	*12.89*

Table II. 10. Influence of ADC Reflux Ratio (*RR*) on Overall Exergy Efficiency (%)

	RER Approach #1			RER Approach #2		
RR	**TP**	**FS**	**SS**	**TP**	**FS**	**SS**
0.20	84.81	80.18	83.53	13.55	10.44	12.46
0.22	84.40	79.89	83.22	13.19	10.27	12.21
0.24	83.98	79.59	82.89	12.83	10.10	11.97
0.26	83.55	79.27	82.56	12.48	9.93	11.72
0.28	83.10	78.95	82.21	12.13	9.76	11.48
0.30	82.64	78.61	81.85	11.79	9.58	11.23
0.32	82.17	78.26	81.48	11.45	9.40	10.99
0.34	81.68	77.90	81.10	11.12	9.22	10.74
0.36	81.17	77.52	80.70	10.79	9.04	10.50
0.38	80.64	77.12	80.29	10.47	8.86	10.25
0.40	80.09	76.71	79.86	10.15	8.67	10.01

II.6. Conclusions

ExA is conducted for MRU processes designed to operate on offshore NG production rigs to treat the Rich MEG stream producing Lean MEG stream via distillation-based technologies. To do this, firstly the PFDs of the MRUs under consideration – TP: Traditional Process; FS: Full-Stream; and SS: Slip-Stream – are solved within a professional simulation environment. Then two RER Approaches are chosen: (i) usual RER Approach #1, a two-phase environment where the gas phase corresponds to the dry-basis standard atmosphere in VLE with pure liquid water at 25 ^{o}C and 1 atm containing traces of MEG in the gas phase under oxidative chemical equilibrium with CO_2, H_2O and O_2; and (ii) novel RER Approach #2, again a two-phase environment consisting of dry-basis atmospheric air in VLE with liquid water containing MEG at infinite dilution, but *not in chemical equilibrium*. Both approaches calculated the same rate of lost exergy for the same MRU. But Approach#1 seems inappropriate because its calculated exergy flows of Rich MEG and Lean MEG streams are two orders of magnitude greater, leading to exergy efficiencies near 80% for all MRUs, masking results of equipment efficiencies and hindering the discrimination of performances of units and processes in terms of exergy degradation. On the other hand, RER Approach #2 defines the RER condition of MEG as a liquid infinitely diluted in water, entailing that the exergy flows of Rich MEG and Lean MEG streams are much lower in magnitude, giving exergy efficiencies of MRUs with values around 10%-11% which are reasonable values for distillation-based processes (Appendices A and B, Supplementary Materials). Besides, RER Approach #2 allows much better discrimination of exergy efficiencies and better identification of exergy sinks in all studied MRUs. RER Approach #1, although consistent and correct, failed to provide discrimination of exergy performances and realistic results, whereas the proposed novel RER Approach #2 is able to provide much more realistic and meaningful exergy efficiency values. Under RER Approach #2 the existing irreversibilities are more easily revealed and, thus, affect with more impact the calculation of exergy efficiencies, better discriminating them. Hence, it is highlighted the importance of setting an appropriate RER definition, which is relevant to a successful ExA. By means of ExA, with appropriate RER

choice, commercial MRUs are weighted with the respective main exergy sinks accurately identified and the respective exergy efficiencies correctly determined.

In this work all exergy calculations for any unit or process passed a consistency cross-check by means of calculating the rate of lost exergy according to two different ways, which gave less than 1% of discrepancy, namely: (i) via the differences of input and output flow rates of exergy; and (ii) via the lost power formula with the rate of entropy creation in the Universe. A comprehensive sensitivity analysis of the ExA is also conducted asserting coherently how unit and MRU efficiencies respond with the increase of design parameters – temperature approach and reflux ratio of ADC – whose values are directly translated as degree of irreversibility in the respective operations.

II.7 Appendices A and B. Supplementary Materials

Appendix A: Thermodynamic Efficiency of a Steady-State Binary Distillation Column.

Appendix B: Thermodynamic Efficiency of a Steady-State Process with Several Power Consuming Operations.

II.8 Acknowledgments

A.M. Teixeira and L.O. Arinelli acknowledge financial support from PETROBRAS S.A. and ANP-Brazil (PRH-ANP / MCT via PRH-13 of Escola de Química, UFRJ). J.L. de Medeiros and O.Q.F. Araújo acknowledge financial support from PETROBRAS S.A. and CNPq-Brazil.

II.9 References

Ahrendts J. Reference states, Energy, 5(8), 666-677, 1980. http://dx.doi.org/10.1016/0360-5442(80)90087-0.

Alharooni K, Barifcani A, Pack D, Gubner R, Ghodkay V. Inhibition effects of thermally degraded MEG on hydrate formation for gas systems. Journal of Petroleum Science and Engineering. 2015; 135(1):608-617. http://dx.doi.org/10.1016/j.petrol.2015.10.001

Al-Muslim H, Dincer I, Zubair SM. Effect of reference state on exergy efficiencies of one- and two-stage crude oil distillation plants. International Journal of Thermal Science. 44(1), 65-73. 2005. http://dx.doi.org/10.1016/j.ijthermalsci.2004.04.015

Araújo, O.Q.F., Reis, A.C., de Medeiros, J.L., do Nascimento, J.F., Grava, W.M., Musse, A.P., Comparative analysis of separation technologies for processing carbon dioxide rich natural gas in ultra-deepwater oil fields, Journal of Cleaner Production 2016. http://dx.doi.org/10.1016/j.jclepro.2016.06.073

Bianchi M, Branchini L, De Pascale A, Melino F, Peretto A, Valentini E. Thermo-economic evaluation of orc system in off-shore applications. Proceedings of the ASME Turbo Expo 2014: Turbine Technical Conference and Exposition. Paper No. GT2014-25170. http://dx.doi.org/10.1115/GT2014-25170

Bikkina C, Radhakrishnan N, Jaiswal S, Harrington R, Charlesworth M. Development of MEG regeneration unit compatible corrosion inhibitor for wet gas systems. 2012. In: SPE Asia Pacific Oil & Gas Conference and Exhibition, Oct22–24, Perth.

Boroumandjazi G, Rismanchi B, Saidur R. A review on exergy analysis of industrial sector. Renewable and Sustainable Energy Reviews. Elsevier; Nov 2013; 27:198–203. http://dx.doi.org/10.1016/j.rser.2013.06.054

Dincer, I and Zamfirescu, C. Sustainable Energy Systems and Applications. Springer Science and Business Media, LLC 2011. http://dx.doi.org/10.1007/978-0-387-95861-3_1

Gaudreal K, Fraser R, Murphy S. The characteristics of the exergy reference environment and its implications for sustainability-based decision-making. Energies 2012, 5(7), 2197-2213; http://dx.doi.org/10.3390/en5072197

GE Aviation. 2013. http://www.geaviation.com/press/marine/marine_2003415.html [Accessed 25 Jun 2016]

Gupta G, Singh S K. Hydrate Inhibition - Optimization In Deep Water Gas Field. 2012. SPE 153504. http://dx.doi.org/10.2118/153504-MS

Haghighi H, Chapoy A, Burgess R, Tohidi B. Experimental and thermodynamic modelling of systems containing water and ethylene glycol: Application to flow assurance and gas processing. Fluid Phase Equilibria 2009; 276(1):24–30. http://dx.doi.org/10.1016/j.fluid.2008.10.006

Latta T M, Palejwala A A, Tipson S K, Haigh N P. Design Considerations for Mitigating the Impact of Contaminants in Rich MEG on Monoethylene Glycol Recovery Unit MRU Performance. Offshore Technology Conference Asia. 2016. OTC-26456-MS. http://dx.doi.org/10.4043/26456-MS

Montazaud, T. Precipitation of carbonates in the pretreatment process for regeneration of ethyleneglycol. Master Thesis, Norwegian University of Science and Technology, 2011.

Myhre J. Electrical Power Supply to Offshore Oil Installations by High Voltage Direct Current Transmission. Doctoral Thesis. Norwegian University of Science and Technology, 2001.

Nazeri M, Tohidi B, Chapoy A. An Evaluation of Risk of Hydrate Formation at the Top of a Pipeline. 2012; SPE 160404. http://dx.doi.org/10.2118/160404-MS

Nazzer C A, Keogh J. Advances in Glycol Reclamation Technology. Offshore Technology Conference 2006;18010. http://dx.doi.org/10.4043/18010-MS

Nguyen T-V, Pierobon L, Elmegaard B, Haglind F, Breuhaus P, Voldsund M. Exergetic assessment of energy systems on North Sea oil and gas platforms. Energy. Volume 62, 2013. Pages 23-36. http://dx.doi.org/10.1016/j.energy.2013.03.011

PARAT Halvorsen AS. Offshore Heating Solutions. 2008. http://www.parat.no/media/2993/offshore.pdf. [Accessed 25 Jun 2016]

Rosen M A, Dincer I. Effect of varying dead-state properties on energy and exergy analyses of thermal systems. International Journal of Thermal Sciences. 43(2), 121-13. February 2004. http://dx.doi.org/10.1016/j.ijthermalsci.2003.05.004

Seiersten M, Brendsdal E, Deshmukh S, Dugstad A, Endrestøl G, Ek A et al. Development of a Simulator for Ethylene Glycol Loops Based on Solution Thermodynamics and Particle Formation Kinetics. NACE-10131; CORROSION 2010.

Sloan ED, Koh CA. Clathrate hydrates of natural gases. 3rd ed. CRC Press, Taylor & Francis Group; 2008.

Smith J M, Van Ness H C and Abbott M M, Introduction to Chemical Engineering Thermodynamics, 6th edition. McGraw-Hill, p. 359-361; 2001.

Teixeira A M. Exergetic Analysis of Processes for Monoethylene Glycol (MEG) Recovery in Offshore Platforms. MSc Dissertation, TPQBq, Escola de Quimica, Federal University of Rio de Janeiro, 2014.

Twu C H, Sim W D, Tassone V. A versatile liquid activity model for SRK, PR and a new cubic equation-of-state TST. Fluid Phase Equilibria, Volumes 194–197, 30 March 2002, Pages 385-399. http://dx.doi.org/10.1016/S0378-3812(01)00663-X

Valero A. Exergy accounting: Capabilities and drawbacks. Energy. 31(1), 164-180, January 2006. http://dx.doi.org/10.1016/j.energy.2004.04.054.

Wepfer W J, Gaggioli R A. Reference datums for available energy. Thermodynamics: Second Law Analysis, in: ACS Symposium Series, vol. 122, American Chemical Society, Washington, DC, 1980, pp. 77–92.

CHAPTER III – RECOVERY OF THERMODYNAMIC HYDRATE INHIBITORS METHANOL, ETHANOL AND MEG WITH SUPERSONIC SEPARATORS IN OFFSHORE NATURAL GAS PROCESSING

This article was published in Journal of Natural Gas Science and Engineering Vol. 52 (2018) pp. 166-186 (doi: 10.1016/j.jngse.2018.01.038

Recovery of Thermodynamic Hydrate Inhibitors Methanol, Ethanol and MEG with Supersonic Separators in Offshore Natural Gas Processing

Alexandre Mendonça Teixeira[1a], Lara de Oliveira Arinelli[2a], José Luiz de Medeiros[*a] and Ofélia de Queiroz F. Araújo[3a]

[a]Escola de Química, Federal University of Rio de Janeiro. Av. Horacio Macedo, 2030, Bl. E, 21949–900, Rio de Janeiro, RJ, Brazil

*Corresponding author: jlm@eq.ufrj.br

[1]alexandremtxr@gmail.com, [2]lara.arinelli@gmail.com, [3]ofelia@eq.ufrj.br

Abstract

In offshore natural gas (NG) production, hydrate formation is a big concern that can impact the production and even stop NG flow. In this context, the injection of Thermodynamic Hydrate Inhibitors (THIs) in wellheads is widely employed in order to avoid these undesirable problems on subsea flowlines to gas processing rigs. However, in the main three-phase high-pressure separator in the gas rig, THI losses for gas phase are significant, particularly when the adopted THI is volatile like methanol and ethanol. This work discloses a new supersonic separator (SS) THI recovery process – SS-THI-Recovery – that treats the gas effluent from three-phase high-pressure separator achieving four simultaneous results: (i) gas water dew-point adjustment (WDPA); (ii) gas hydrocarbon dew-point adjustment (HCDPA); (iii) production of C3+ (propane and heavier) liquids as LPG; and (iv) recovery of almost all THI which would be lost in the gas otherwise. The proposition employs a supersonic separator (SS) battery followed by an anti-hydrates separator (LTX), a liquid-liquid THI extraction step and auxiliary THI distillation. SS-THI-Recovery was evaluated with HYSYS 8.8 simulator using methanol, ethanol and monoethylene glycol (MEG) as THIs. Supposing that the THI in the gas phase would be totally lost along with the exported gas otherwise, with SS-THI-Recovery the losses of methanol, ethanol and MEG were reduced by 91.9%, 79.3% and 99.2%, respectively, and such recovery factors could be further improved by increasing water flow rate in liquid-liquid THI extraction. Such high THI recovery entails reduction of THI costs with make-up, storage and transportation. Additionally, SS-THI-Recovery process is

simple, with low footprint, and of easy implementation even for non-volatile THIs like MEG. Furthermore, the produced NG is ready for commercialization, dismissing additional treatment steps, not counting the commercial value of LPG. Therefore, new SS-THI-Recovery process configures an innovative and profitable alternative for gas treatment and THI recovery on gas processing offshore platforms.

Keywords: Thermodynamic Hydrate Inhibitor, THI Recovery, Supersonic Separator, Three-Phase Supersonic Flow, Multiphase Sound Speed, HYSYS Unit Operation Extension

Abbreviations

1D One-Dimensional; ADC Atmospheric Distillation Column; BIP Binary Interaction Parameter; BP Bubble Point; ChW Chilled Water (10^oC-25^oC); CFD Computational Fluid Dynamics; CPA Cubic Plus Association; CSM Colorado School of Mines; CW Cooling Water (30^oC–45^oC); ECS Equilibrium Closed System; EOS Equation of State; FLS Flash-Evaporator; GHET Gas-Hydrate Equilibrium Temperature; HC Hydrocarbons; HCDP Hydrocarbons Dew Point; HCDPA Hydrocarbon Dew Point Adjustment; HPS High-Pressure Three-Phase Separator; LLE Liquid-Liquid equilibrium; LLS Liquid-Liquid Separator; LPG Liquefied Petroleum Gas; LTX Low Temperature Separator; L+W Liquid HCs and Water; MEG Monoethylene Glycol; $MMsm^3/d$ Millions of standard m^3 per day; NG Natural Gas; PEC Phase-Equilibrium *c*; PFD Process Flow Diagram; PHW Pressurized Hot Water (200^oC); PVT Pressure, Volume & Temperature; SAFT Statistical Associating Fluid Theory; SDC Sub-atmospheric Distillation Column; SRK Soave-Redlich-Kwong; SS Supersonic Separator; THI Thermodynamic Hydrate Inhibitor; THI-RU THI Recovery Unit; UOE Unit Operation Extension; VLE Vapor-Liquid Equilibrium; VLWE Vapor-Liquid-Water Equilibrium; WDP Water Dew Point; WDPA Water Dew Point Adjustment.

Nomenclature

A : *Flow area section (m^2)*

$c(T,P,\underline{Z})$: *Sound speed property of multiphase equilibrium fluid at (T, P, $\underline{Z}$) (m/s)*

$\overline{C}_P \equiv \left(\frac{\partial \overline{H}}{\partial T}\right)_{P,\underline{Z}}$: *Molar isobaric heat capacity of multiphase fluid (J/kg.K)*

$\hat{C}_P \equiv \left(\frac{\partial \hat{H}}{\partial T}\right)_{P,\underline{Z}}$: *ECS isobaric heat capacity per unit of mass (J/kg.K)*

D_I, D_T, D_O : *SS inlet/throat/outlet internal diameters (m)*

F : *Molar flow rate of multiphase fluid (mol/s)*

$\overline{G}^E / RT$: *Dimensionless Gibbs free energy of excess*

$\overline{H}, \hat{H}$: *Multiphase fluid molar enthalpy (J/mol) and ECS enthalpy per unit of mass (J/kg)*

L, L_C, L_D : *SS lengths: total/converging/diverging sections (m)*

L^{LAVAL} : *Laval nozzle length (m)*

L^{Shock} : *SS axial position just before normal shock (=L^{LAVAL}) (m)*

$Ma=v/c$: *Mach Number*

Ma^{Shock} : *Ma just before normal shock and before condensate withdrawal*

M_M : *Molar mass (kg/mol)*

nc : *Number of components*

P : *Pressure (bar, Pa)*

$\overline{S}$: *Molar entropy of multiphase fluid (J/K.mol)*

T : *Temperature (K)*

v : *Axial velocity of non-segregated multiphase fluid (m/s)*

x : *SS axial position (m)*

$\underline{Z}$: *Multiphase fluid vector (nc x 1) of total mol fractions for non-reactive systems*

$\underline{Z}$: *ECS preparation vector (nc x 1) of total mol fractions for reactive systems*

Greek Symbols

α, β : *SS converging/diverging wall angles (deg)*

$\eta^{EXP}\%, \eta^{CMP}\%$: *SS expansion/compression adiabatic efficiencies (%)*

ρ : *Multiphase fluid density (kg/m³)*

$\gamma' \equiv \overline{C}'_P / \overline{C}'_V$: *Ratio of molar heat capacities of an ideal gas*

$\Xi_P \equiv \left(\frac{\partial \rho}{\partial P}\right)_{T,\underline{Z}}$: *Derivative of ρ with P at const. T, $\underline{Z}$ for multiphase fluid or for ECS (kg/Pa.m^3)*

$\Xi_T \equiv \left(\frac{\partial \rho}{\partial T}\right)_{P,\underline{Z}}$: *Derivative of ρ with T at const. P, $\underline{Z}$ for multiphase fluid or for ECS (kg/K.m^3)*

Subscripts

AS, BS : *Just after normal shock and just before normal shock and after condensate withdrawal*

C, D : *Converging, Diverging sections*

E : *SS entrance*

I, O, T : *SS inlet, outlet, throat*

k : *Species index*

L : *SS HC liquid at L^{Shock}*

$L+W$: *Two-phase HC+Water condensate at* L^{Shock}

Superscripts

$'$: *Refers to ideal gas properties*

$in\ \ out$: *Inlet, outlet*

$,$

$LAVAL$: *Laval nozzle*

$Shock$: *At maximum Mach Number, just before normal shock and condensate withdrawal*

$Throat$: *SS Throat*

III.1. Introduction

A relevant category of problems in the exploration and production of natural gas (NG) in offshore environments, particularly at ultra-deep waters, comprehends flow assurance issues as consequence of gas hydrate equilibrium in subsea systems. Such equilibrium is basically favored by three factors: (i) presence of production water along with the gas; (ii) high pressure conditions in flowlines; (iii) low pipe external temperatures of 0^oC to 4^oC associated to high depths. Management of gas hydrate equilibrium is considered as the most critical aspect in flow assurance strategies, since hydrate obstructions respond for most of the economic and safety impacts on flowline operation, and can completely stop production for several days or months and, in the worst case, can lead to pipeline abandonment (Nazeri et al., 2012).

Gas hydrates are crystalline structures of water and light hydrocarbons which coexist in equilibrium with gas and free water at low temperatures and high pressures in NG production, transportation and processing systems. Formation of gas hydrates may cause clogging, overburdening of compression systems and even stoppage of NG flow, representing serious operational concerns. Further, the removal of plugs of gas hydrates and its remediation, once they are formed, can be a costly, dangerous and time-consuming procedure. As a result, flow assurance is strongly dependent on successful strategies for inhibition of gas hydrate equilibrium and formation.

As NG flows in pipeline, its temperature and pressure vary. In most subsea pipelines, after the wellhead, the production stream cools down and may reach the temperature of seabed before arriving at processing facilities. Thus, humid NG temperature in pipelines should be always higher than local equilibrium hydrate temperature so as to prevent hydrate formation. In this

context, thermodynamic hydrate inhibitors (THIs) are highlighted by their mechanism of hydrate inhibition: THIs reduce the fugacity of water in the liquid phase, stabilizing it in the liquid and shifting the hydrate equilibrium border to lower temperatures and/or higher pressures, therefore removing from the system the thermodynamic conditions for hydrate equilibria at the (*T*,*P*) of operation.

The most adopted strategy for gas hydrate inhibition is the continuous injection of fresh THIs in wellheads, such that THI flows along with gas and production fluids, stabilizing the free water phase, avoiding gas hydrate equilibrium and consequently ensuring unimpeded flow. Generally, THI is injected in gas wellheads mixing with gas, condensate and production water (possibly saline). This mixture returns to the gas processing platform as a multiphase flow in the flowlines, comprising a THI-water-salts denser phase, a condensate phase rich in heavy (C3+) hydrocarbons (HCs) and the gas phase. The incoming stream has its phases separated in the high pressure three-phase separator (HPS): (i) a bottom aqueous phase containing THI, water and salts; (ii) an intermediate HC condensate phase, if present; and (iii) an upper gas phase. The THI-water-salts phase is sent to a distillation-based plant for THI recovery and regeneration – the THI Recovery Unit or THI-RU – so as to enable the reinjection of re-concentrated and desalinized THI in production wellheads.

The gas phase from the HPS consists of raw NG with vaporized water and THI in equilibrium with the THI-water-salts phase. The raw NG phase is evidently the greatest of the three, with the highest flow rate. Therefore, without the appropriate treatment, some vaporized THI will remain in the raw NG and will be lost, entailing replacement costs.

Not considering some ionic salts, hydroxylated compounds – e.g. short chain alcohols and glycols – are the most common THIs injected in wellheads, especially methanol, ethanol and monoethylene glycol (MEG). For several decades, MEG and methanol have been the most common chemicals injected in offshore environment as THIs in gas production pipelines and related facilities. Ethanol is also used, particularly in regions where it has a sufficiently large and established market (e.g. Brazil). Among these THIs, MEG is the less volatile with lower losses to the HPS gas phase (Haghighi et al., 2009).

THIs are recovered and re-purified in THI Recovery Units (THI-RU) from the THI-water-salts bottom phase of HPS to be recycled to wellheads. However, in the case of methanol and ethanol there are significant losses to vapor phase due to their higher volatilities. In addition, they may become undesirable contaminants of sales gas, and may lead to gas depreciation.

As the anti-hydrate action of THIs is a colligative property, the molar ratio THI:water in the aqueous phase is a design specification in anti-hydrate services in gas offshore fields. Therefore, the mass flow rate of injected methanol is always lesser than the MEG counterpart thanks to the much smaller molar mass of methanol which is about half of MEG's. This represents, at first, a comparative advantage of methanol against MEG since chemicals are bought by weight. Nevertheless, the net molar flow rate of liquid methanol entering into the water phase could be much less than the MEG counterpart thanks to a higher THI effectiveness and also thanks to its higher vaporization to the gas phase, which lowers its effectiveness as only the moles of liquid in the aqueous phase can actually act as THI. Thus, the make-up requirements of methanol lost into the sales gas configures a major operating expense of methanol THI systems, which represents a comparative disadvantage relatively to MEG (Son and Wallace, 2000). Moreover, all losses of THIs to the gas phase from the HPS are unrecoverable by THI-RU plants, as such plants only recover THI from the bottom THI-water-salts phase from the HPS (Teixeira et al., 2016).

Whichever the case, in the context of NG offshore rigs, the gas phase leaving the HPS separator contains non-negligible amounts of THI, especially when the THI is a volatile alcohol. Currently, the THI present in the HPS gas is totally lost with the exported gas, leading to THI costs of make-up, storage and transport. In other words, there is a need for operations that could efficiently recover THI from the effluent HPS gas phase and reduce its losses.

This work discloses and analyzes a new and original process employing supersonic separator (SS), liquid water injections, water extraction of THI, and some heat consumption to drive a small atmospheric distillation for water recovery. This combination of resources can, cost-effectively, dramatically reduce THI losses to the final gas phase, simultaneously executing water dew point adjustment (WDPA) and hydrocarbon dew point adjustment (HCDPA) of the

final treated gas, thus making it suitable for direct commercialization. Besides, this new process does not aggregate high costs and also can recover condensed C3+ hydrocarbons (LPG) from HCDPA, which represents a potential tertiary factor of revenues.

This new process is referred here as SS-THI-Recovery and should not be confused with the conventional THI-RU processes that recover THIs from the bottom THI-water phase from the HPS. In other words, SS-THI-Recovery explores a THI recovery niche that was neglected by THI-RU technologies; i.e. it is complementary to THI-RUs and does not compete with them. Several embodiments of SS-THI-Recovery process consolidated a pending patent in Brazilian Patent and Trademark Office (Teixeira et al., 2017).

Therefore, the subject of the present work, namely, SS-THI-Recovery, is totally original, new, based on breakthrough separation technologies – such as SS – and is thoroughly technically assessed here to confirm its capabilities. SS-THI-Recovery is technically evaluated via process simulations with HYSYS 8.8 by using process flow diagrams (PFDs) where SS-THI-Recovery operates integrated to THI-RU processes, complementing them. Such simulations used thermodynamic modeling appropriate to handle complex polar systems containing NG, water, MEG, methanol, ethanol and HCs by means of the CPA Equation of State (CPA-EOS). In addition, the supersonic separator (SS) is rigorously thermodynamically modeled via a HYSYS Unit Operation Extension (UOE), namely, SS-UOE developed in a previous work (Arinelli et al., 2017). SS-UOE rigorously handles multiphase – single-phase, two-phase and three-phase – equilibrium supersonic flow and phase-split in SS and calculates the correct multiphase – single-phase, two-phase or three-phase – equilibrium sound speed (c) with another HYSYS UOE, namely, PEC-UOE also from another previous work (de Medeiros et al., 2017).

The remaining of this work is organized as follows. Sec. III.2 discusses the pertinent review on the technical background of this work comprising THI-RUs, CPA-EOS, and modeling of SS and multiphase equilibrium sound speed with SS-UOE and PEC-UOE. Sec. III.3 discloses two processing schemes of SS-THI-Recovery, respectively appropriate for recovery of methanol and ethanol as THIs and of MEG as THI. Sec. III.4 presents the simulation results,

technical analysis and discussion, while the concluding remarks are objects of Sec. III.5 which ends the paper.

III.2. Technical Background

To present and to analyze the proposed processes for recovery of THIs from gas phase via supersonic separators and water injections – SS-THI-Recovery – some technical subsidiary items have to be preliminarily accessed and reviewed, namely: (i) THI Recovery Units (THI-RU); (ii) thermodynamic modeling of polar systems via CPA-EOS; and (iii) rigorous simulation of supersonic separators (SS) with multiphase supersonic flow including calculation of the thermodynamic multiphase equilibrium sound speed within HYSYS 8.8 environment.

III.2.1. THI Recovery Units (THI-RU)

In any offshore NG producing system using THIs, there is a closed loop connecting the subsea service points for THI injection and a gas processing rig. The gas processing starts with the high-pressure three-phase separator (HPS), which receives the multiphase (gas dominated) feed and separates it into: (i) bottom THI-water-salts phase; (ii) intermediate HCs condensate phase; and (iii) raw NG phase. The HCs condensate is collected, the gas is dispatched to some conditioning step before exportation and the THI-water-salts liquid phase goes to the THI Recovery Unit, or THI-RU, for re-purification of THI by removing water and salts. The recovered lean THI receives some complementary make-up and is recycled back to service points. The key point to be perceived here is that THI-RU plants only recover THI from liquid streams. They all assume the THI in the HPS gas as process loss, to be compensated by THI make-up, which represents an evident direct cost according to the THI-RU logic.

THI-RU processes for THIs methanol and ethanol are very simple and basically the same, as shown in PFD A in Fig III.1, the implemented process flow diagram (PFD) of THI-RU for

methanol and ethanol as THIs. It consists of an atmospheric distillation column (ADC), where THI – methanol or ethanol – is recovered at the top at *≈85%w/w* (*≈15%w/w* H_2O), and water is produced as bottoms with *THI ≤ 100 ppm* and possibly with salts. After expansion from the HPS (not shown in Fig III.1) to atmospheric pressure, the Rich THI liquid feed is pre-heated in a heat exchanger with ADC bottoms, which is essentially hot water at *≈100°C*. ADC has a partial condenser releasing vent gases to flare, safely removing light HCs and other volatile contaminants from the THI-water feed. The condenser is cooled by process cooling water (CW) at 30°C, whose flow rate adjusts distillate temperature and vent flow rate. The recovered THI – methanol or ethanol – receives some THI make-up to recompose the THI service stream. The cooled water product is discarded (possibly with salts) into the sea.

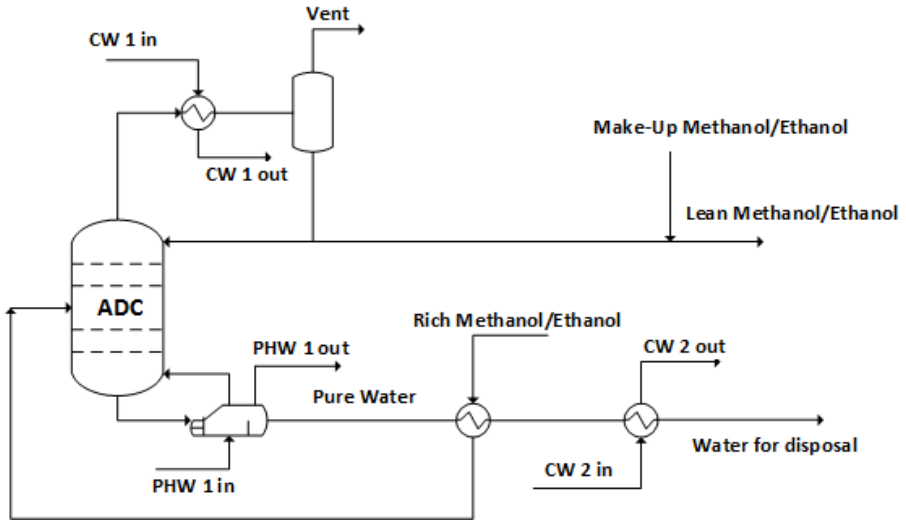

Figure III.1. PFD A: THI-RU for THI=Methanol or THI=Ethanol

Consider now the MEG THI-RU. Differently from the previous THI-RU for methanol or ethanol, salts may accumulate in the THI loop, because MEG is recovered as columns bottoms together with salts due to its higher boiling point relatively to water. Hence, besides MEG re-concentration, the removal of salts is required as well, to avoid accumulation of salts, scaling and equipment fouling. The salt-handling factor orients the classification of current MEG THI-RU technologies into three major process categories: (i) Traditional; (ii) Full-Stream; and (iii) Slip-Stream. The first is too simple and is in disuse because it cannot handle

salts, while the Slip-Stream has intermediate cost-effective capabilities and the Full-Stream is the most complete in terms of resources. This work considers only the Full-Stream MEG THI-RU.

Full-Stream MEG THI-RU is shown in PFD B, Fig III.2. It treats Rich MEG (MEG-water-salts) with three serial steps after expanding the THI-water phase from HPS to atmospheric pressure. The first step is an atmospheric distillation column (ADC) that removes *≈50%* of water and gases (HCs, CO_2) with bottoms at *≈119°C*. In the second step, ADC bottoms (MEG *≈70%w/w*) go to a vacuum Flash-Evaporator (FLS) at *≈0.25 bar*, wherein the feed instantaneously vaporizes at $\approx 125^{o}C$ by direct contact with a high flow rate of recycled hot liquor at $\approx 135^{o}C$ from the spiral heat exchanger (SHE) heated by pressurized hot water (PHW) at $\approx 200^{o}C$ (Teixeira et al., 2016). In the FLS all MEG and water are vaporized from the feed, excluding dissolved solids, which precipitate in FLS bottom. In the third step, MEG and water vapor from FLS feed a sub-atmospheric distillation column without reboiler (SDC) at *P=0.2 bar*, to be split into pure distillated water ($THI \leq 100\ ppm$) and Lean MEG ($\approx 15\%w/w\ H_2O$) as bottoms (Nazzer and Keogh, 2006). SDC operates under vacuum to ensure low bottom temperatures ($T \approx 103^{o}C$), thereby preventing thermal degradation of MEG (above $\approx 162^{o}C$), which reduces THI performance (Alharooni et al., 2015). FLS temperature is controlled to retard degradation of MEG, whose products glycolic, acetic and formic acids (Psarrou et al., 2011) lead to higher operating costs associated to MEG make-up and corrosion by acids (Ikeh et al., 2016; Dong et al., 2008). The SDC vacuum system must not admit vapors in order to keep vacuum and save power. This is accomplished by a sub-cooler with chilled water (ChW) at $10^{o}C$ that cools the water distillate to $15^{o}C$ reducing its vapor pressure (Teixeira et al., 2016). The recovered THI (MEG) is made up recomposing the THI service stream. Distillated water and FLS salts are discarded into the sea.

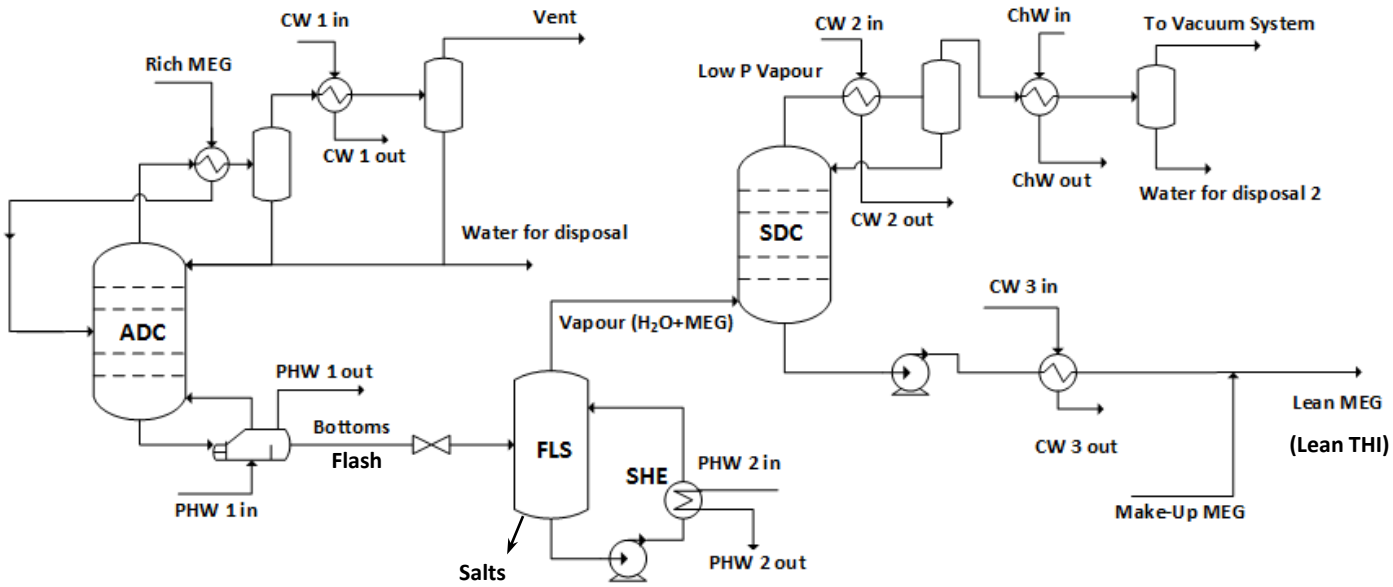

Figure III. 2. PFD B: THI-RU for THI=MEG

III.2.2. CPA Equation of State

Classical cubic equations of state (EOS) are widely used for calculating thermodynamic properties and phase equilibria of pure components and mixtures. However, it is well known that cubic EOS combined with the classical van der Waals mixing rules are insufficient when strongly polar or associated compounds – such as water, alcohols or glycols – are present along with HCs. Hence, the precise description of phase equilibria of such mixtures requires more sophisticated EOS's, such as the CPA-EOS (*cubic-plus-association*), which has an additional non-cubic term for polar effects/association via Wertheim's Theory, essentially the association term from SAFT (*Statistical Associating Fluid Theory*). When no association contributions are present, the CPA-EOS reduces to SRK-EOS, also widely employed in gas and petroleum industries. The purpose of CPA-EOS is to add the free energy of association based on SAFT to the free energy of SRK-EOS, in order to describe mixtures of associating species such as water and hydroxylated compounds (Karakatsani and Kontogeorgis, 2013).

Several studies in the literature have investigated the suitability of CPA-EOS for mixtures with polar compounds of interest to the oil and gas industry, achieving a good agreement

between predictions and experimental data. CPA-EOS proved to be successful for multicomponent mixtures containing, for example: alcohols, water and polar compounds (Folas et al., 2005); HCs, methanol and water (Haghighi et al., 2009); NG and water (Karakatsani and Kontogeorgis, 2013); and MEG and HCs (Tzirakis et al., 2016).

Following these works, CPA-EOS was selected in the present study to model the thermodynamics of high-pressure NG systems containing water and THIs methanol, ethanol and MEG, including the respective two-phase VLE (vapor-liquid equilibrium) and three-phase VLWE (vapor-liquid-water equilibrium) loci. HYSYS 8.8 is appropriate for simulating processes with associating compounds by means of its CPA-EOS Thermodynamic Package, which comprises improved methanol binary interaction parameters (BIPs) as well as BIPs databank for water, MEG and HCs for phase-equilibrium systems (Aspentech, 2015). The absence of ethanol-water BIPs in HYSYS 8.8 databank was overcome by using $k_{Ethanol\text{-}H2O} = -0.11$ from Folas et al. (2005).

Despite the well-known suitability of CPA-EOS for handling multiphase NG systems with water, methanol, ethanol and MEG, it may be argued that such polar systems should be more appropriately attacked via classical *gamma-phi* approaches with CPA-EOS restrained to the gas phase, while the two liquid (hydrocarbon and aqueous) phases are modeled via activity coefficient ($\overline{G}^E / RT$) excess formulae. Despite *gamma-phi* approaches are known to represent VLWE polar systems when appropriately calibrated, there are several reasons that do not recommend them for SS applications with complex high-pressure NG systems containing water and hydroxylated THIs.

In the first place, $\overline{G}^E / RT$ models also depend on BIPs that normally were calibrated with VLE and LLE (but not with VLWE) data at low pressures (i.e. far from VLE critical points), while SS applications with NG are normally at high or very high pressures, invariably passing near to VLE critical points.

In the second place, SS applications with NG systems demand full description of the complete phase-behavior of the SS feed, including its VLE critical neighborhood, while *gamma-phi* approaches are impotent to handle VLE critical neighborhoods, for the simple reason that they

cannot recognize VLE critical points, neither were developed with such finality. It is well-known that only self-contained single free-energy thermodynamic models – like PVT EOS's – that encompass vapor and liquid phases can represent VLE critical phenomena.

In the third place, SS applications demand precise continuous calculation of Mach Number (*Ma*) along the SS flow path, which, by its turn, demands accurate prediction of the multiphase sound speed (*c*), a mixed thermodynamic property related to PVT properties and thermal properties as shown in Eqs. (1a) and (1b), where M_M is the molar mass (kg/mol) and $\underline{Z}$ is the vector of species total mol fractions. As shown by de Medeiros et al. (2017), the multiphase sound speed (*c*) of non-reactive systems is an equilibrium multiphase property that can be calculated by Eq. (1a), where all PVT and thermal properties ($\rho, \Xi_P, \Xi_T, \overline{C}_P$) are equilibrium multiphase properties defined in Eq. (1b). On the other hand, for reactive systems the multiphase multi-reactive sound speed (*c*) should be calculated by Eq. (1c), where $\rho, \Xi_P, \Xi_T, \hat{C}_P$ now represent equilibrium closed system (ECS) properties defined in Eq. (1d) with $\hat{C}_P$,$\hat{H}$, $\underline{Z}$ standing for ECS isobaric heat capacity per unit of mass, ECS enthalpy per unit of mass and ECS preparation vector of species total mol fractions. In the present work, the single-phase, two-phase or three-phase sound speeds were calculated along the SS flow path by unit operation extension PEC-UOE for HYSYS 8.8 using Eqs. (1a) and (1b) as no chemical reactions occurs in the SS flow path (this is not the case if supersonic reactors, SR's, are being considered instead of SS's). In PEC-UOE all multiphase properties in Eq. (1a) are determined via Eq. (1b) with HYSYS *Flash(P,T)* multiphase equilibrium tool. This long preamble is only to put into discussion the fact that conventional $\overline{G}^E / RT$ models do not incorporate PVT frameworks, so that they are also impotent to handle the PVT behavior of liquid phases to which they are attached. Thus, $\overline{G}^E / RT$ models cannot be used to address the entities in Eq. (1a) for liquid phases (the hypothesis of incompressible liquids has to be ruled out as it leads to infinite sound speed). In other words, an appropriate EOS has to be used with the liquid phases to address their PVT behavior necessary to calculate the multiphase equilibrium sound speed in Eq. (1a).

In summary, the final verdict is that SS processing of complex high-pressure raw NG systems containing water and hydroxylated compounds – methanol, ethanol and MEG – can only be

addressed with adequate EOS formalisms capable to handle multiphase VLWE including PVT and thermal behaviors of all phases. For all that exist in the literature, CPA-EOS is easily recognized as the appropriate thermodynamic modeling resource to adequately handle the SS applications of interest in the present study.

$$c = \frac{1}{\sqrt{\Xi_P - (M_M T / \rho^2)\Xi_T^2 / \overline{C}_P}} \tag{III.1a}$$

$$\Xi_P \equiv \left(\frac{\partial \rho}{\partial P}\right)_{T,\underline{Z}}, \quad \Xi_T \equiv \left(\frac{\partial \rho}{\partial T}\right)_{P,\underline{Z}}, \quad \overline{C}_P \equiv \left(\frac{\partial \overline{H}}{\partial T}\right)_{P,\underline{Z}} \tag{III.1b}$$

$$c = \frac{1}{\sqrt{\Xi_P - (T / \rho^2)\Xi_T^2 / \hat{C}_P}} \tag{III.1c}$$

$$\Xi_P \equiv \left(\frac{\partial \rho}{\partial P}\right)_{T,\underline{Z}}, \quad \Xi_T \equiv \left(\frac{\partial \rho}{\partial T}\right)_{P,\underline{Z}}, \quad \hat{C}_P \equiv \left(\frac{\partial \hat{H}}{\partial T}\right)_{P,\underline{Z}} \tag{III.1d}$$

III.2.3. Simulation and Design of Supersonic Separators and the Multiphase Equilibrium Sound Speed

Supersonic separators (SS) can simultaneously provide water dew point adjustment (WDPA) and hydrocarbon dew point adjustment (HCDPA) of NG feeds by accelerating the gas at supersonic velocities, causing expansion and deep temperature fall, resulting that water and HCs with three or more carbon atoms (C3+) condense by the extreme cooling and are collected. Hence, SS executes selective WDPA and HCDPA in a single operation, reducing requirements of equipment and footprint (Machado et al., 2012). Besides the advantages of its compact size, low weight and absence of rotating parts, Feygin et al. (2006) alleged that SS is also low intensive in capital and operational costs for NG conditioning.

The present work extends – as far as authors can see, for the first time in the literature – the applicability of SS systems beyond NG WDPA+HCDPA by also using it to simultaneously recover THIs present in the raw NG to be treated. To reinforce this characteristic, the SS feed receives a small injection of complementary liquid water – no matter how paradoxical this seems to be – in order to improve the extraction of THI to the water phase along the SS flow path. In other words, the high-pressure SS feed is two-phase (gas+water) from the outset, which means that the SS simulation should be capable to handle two-phase feeds that will turn into a three-phase supersonic flow along the SS flow path as more water, THI and C3+ HCs condense along the SS nozzle due to the extreme fall of temperature.

SS comprises a static swirling device, followed by a Laval nozzle, a cyclonic separation section and a final diffuser, where the Laval nozzle comprehends a converging section, a throat and a diverging section. The final SS diffuser is understood as continuation of the diverging section of the Laval nozzle after the separation section for collecting liquid material formed in the Laval. The flow accelerates from subsonic to $Ma=1$ at the throat ($Ma^{Throat}=1$) and then becomes supersonic ($Ma>1$) through the diverging section, where intense fall of temperature and pressure occurs. Due to the elevated rate of disappearance of enthalpy to create kinetic energy, water and C3+ change to low enthalpy phases, forming super-cooled liquid droplets centrifugally collected by lateral vanes in the separation section. Fig III.3 illustrates a sketch of the essential components of SS assuming linear diameter profiles, with

the Laval nozzle ending at the normal shock front, followed by the final diffuser, a continuation of the Laval diverging section. The normal shock is an idiosyncrasy of supersonic flow in the diverging section against a downstream positive pressure gradient. In such situation, the supersonic flow is metastable and, as Mach Number (*Ma*) rises above 1, it suddenly performs the normal shock transition becoming subsonic, recompressed and hotter.

Fig III.3 only shows the SS elements strictly necessary for design and simulation. However, real SS devices have certain important accessories not depicted in Fig III.3, such as: (i) swirling vanes, a set of fixed blades positioned before the converging section that impel the fluid in rotatory motion; and (ii) collecting vanes – or separation section – a set of wall narrow ports positioned at the pre-shock where the condensed material is centrifugally collected from the rotating fluid.

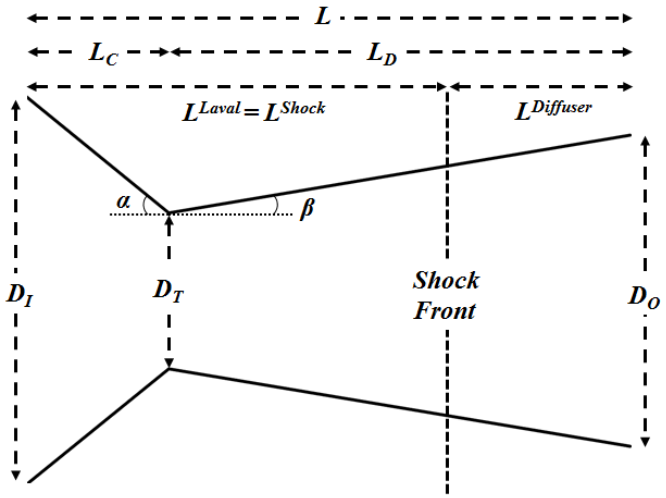

Figure III. 3. SS Basic Scheme with Linear Diameter Profiles

Presently, there is no process simulator offering SS units ready for inclusion in PFDs. In a previous work (Arinelli et al., 2017) a thermodynamically rigorous SS Unit Operation Extension, SS-UOE, was developed to be inserted into HYSYS 8.8 PFDs in order to simulate SS operations. SS-UOE simulates and finishes the SS design at steady-state within HYSYS environment. SS-UOE embodies a pure phenomenological 1D (one-dimensional) SS model that comprises rigorous thermodynamic and phase equilibrium calculations along the 1D axial SS compressible flow path, so that it can operate with water saturated NG including the

possibility of multiphase SS feeds. SS-UOE correctly handles three-phase 1D axial compressible flow with the gradual appearance and segregation of two-phase HCs and water (L+W) condensate. Two-phase (L+W) condensate is a result from WDPA+HCDPA and is collected in the SS separation section giving rise to the L+W condensate stream exported by SS-UOE, which emulates the action of SS collecting vanes. After L+W removal, the remaining dry saturated vapor 1D compressible flow is normally still supersonic, so that it passes through the normal shock transition becoming superheated, subsonic and recompressed, a transition also rigorously modeled by SS-UOE. After the normal shock, the gas performs 1D compressible subsonic flow through the ending diffuser (Fig III.3) where its temperature and pressure continuously rises reversibly until the SS outlet. The SS discharge pressure (backpressure) is lower than the feed pressure, so that there is a net head loss associated with SS operation, whose main source of irreversibility is the normal shock transition, where entropy is created adiabatically. SS head loss raises with the intensity of normal shock, which, by its turn, rises with the pre-shock supersonic Mach Number, Ma^{Shock} ($Ma^{Shock}>1$). As Ma^{Shock} rises above 1, the fall of temperature increases in the supersonic section of SS prior to condensate removal and also the irreversibility through normal shock, which moves downstream towards the outlet, lowering the fraction of pressure recovery at SS outlet. SS-UOE can also model other sources of irreversibility (e.g. friction) by allowing the user to specify adiabatic efficiencies through the expansion step ($\eta^{EXP}\%$) and/or through the compression step ($\eta^{CMP}\%$).

SS operation is specified at the user interface of SS-UOE by inputting the following parameters: (i) feed entering conditions F_E, T_E, P_E, $\underline{Z}_E$, respectively, flow rate (mol/s), temperature (K), pressure (bar) and component mol fractions; (ii) adiabatic efficiencies of SS expansion and compression steps ($\eta^{EXP}\%$, $\eta^{CMP}\%$); (iii) Mach Number just before normal shock and before condensate withdrawal (Ma^{Shock}); and (iv) Laval nozzle geometric parameters (Fig III.3) D_I, D_O, α, β, respectively inlet and outlet diameters, and converging and diverging wall angles. The feed stream set of parameters is automatically rescued by SS-UOE from HYSYS PFD and, reciprocally, the calculated SS product streams are exported by SS-UOE to the HYSYS PFD. SS-UOE finishes the SS design for each simulation, determining

the gas and L+W condensate outlet conditions, the SS head loss and the complete SS design including lengths L_C , L_D , L^{Shock}, $L^{Diffuser}$ and throat diameter D_T (Fig III.3) so that $Ma^{Throat}=1$.

Along SS flow path, *Ma* must be correctly evaluated at all SS flow points for any fluid condition – single-phase, two-phase or three-phase equilibrium – which demands correct determination of the sound speed (*c*) also for any fluid condition – single-phase, two-phase or three-phase equilibrium. Within SS-UOE, the determination of the thermodynamic phase-equilibrium *c* is accomplished by another HYSYS extension, PEC-UOE, which rigorously calculates *c* of multiphase compressible flow via Eqs. (1a) and (1b) using the thermodynamic package that was selected in the simulation (de Medeiros, 2017). In this work, all SS simulations involve water, HCs and one hydroxylated compound among MEG, methanol and ethanol. Therefore, SS simulations were conducted using CPA-EOS as thermodynamic model, rendered by HYSYS CPA Thermodynamic Package and Data Bank as discussed in Sec. III.2.2.

Due to the low temperature ($\approx -15^oC$ to $\approx -40^oC$) achieved in the two-phase L+W condensate ejected by SS carrying water as a super-cooled liquid, there is always potential for gas hydrates and ice formation, even in the present case where some THI exists in the L+W condensate. Such hydrates and ice would form in the downstream processing outside the SS, as the cold L+W condensate is at the same high pressure of SS gas outlet (Arinelli et al., 2017). Hence, to avoid hydrates, the ejection of cold L+W condensate is directed to a bottom-heated vessel known in the SS literature as LTX separator. LTX is fed on the top with cold L+W condensate under direct contact with ascending gas from the LTX bottom kept above $\approx 20^oC$ to prevent hydrates in the exiting L+W bottoms. This direct contact produces at the LTX top a small slip-gas stream at same pressure of the SS gas outlet, which carries some water vapor. The slip-gas is added to the main dry gas from SS outlet because the resulting water content will be still within WDPA range. The coupling of the LTX slip-gas with the SS gas outlet means that the LTX is at the SS outlet pressure, as well as the L+W condensate, whose discharge is correctly computed by SS-UOE at this pressure. As shown in Arinelli et al. (2017), LTX can be implemented in the PFD as two cascaded flashes: a bottom *Flash(P,T)* double-connected to a top *Flash(P,H)*, which emulates the direct adiabatic contact of SS L+W

condensate and warm vapor from the bottom of LTX. This kind of interconnected flashes cluster is easily solved by HYSYS 8.8 without convergence issues.

As occurs with centrifugal compressors, industrially there are some particularities in SS operation that have to be observed to achieve adequate performance. Given a SS nozzle design in Fig III.3, for successful SS operation it is necessary and sufficient that sonic flow (*Ma=1*) be attained at the throat. Thus, the sonic throat condition will be lost if the inlet flow rate decreases (other things constant) or if the inlet pressure increases (other things constant), because such events reduce the inlet velocity displacing the new sonic condition downstream the actual throat. In this case sonic flow is unattainable because beyond the actual throat there is a diverging section that will recompress the subsonic flow slowing it down. A first diagnosis of this situation would blame such effects as SS shortcomings that could hold back SS utilization. But this is an unfair interpretation of a kind of phenomenon that, mutatis mutandis, also occur with other important equipment such as centrifugal compressors with a given design, whose operational regime can be disrupted by surge effects caused by sudden falls of suction pressure or flow rate. In other words, in both cases – centrifugal compressors and SS nozzles – control algorithms must protect the operational point and avoid disruptions.

The truth is that a given SS geometry is designed for a given inlet Mach Number (Ma^{in}), not for a given inlet pressure or for a given inlet flow rate. Therefore, if the feed flow rate falls for some reason, a control algorithm should decrease the feed pressure by throttling the flow to increase the inlet velocity restoring the design inlet Ma^{in}. In the same way, if the inlet pressure falls, the control algorithm should throttle the inlet flow rate to decrease the inlet velocity restoring Ma^{in}. A reverse reasoning, mutatis mutandis, also works if “falls” is replaced by “rises”, “decrease” by “increase” (and vice-versa), and “throttling” by “compressing” or “impelling”.

This behavior can be easily demonstrated for a given SS nozzle expanding an ideal gas with approximately constant ratio of heat capacities ($\gamma' \equiv \overline{C}'_P / \overline{C}'_V \cong const.$). For such ideal gas it can be easily shown that Eqs. (III.2a), (III.2b) and (III.2c) correctly describe 1D isentropic compressible flow through a converging-diverging SS nozzle, where ^{in} refers to inlet conditions, *A* represents the flow area section and Eq. (III.2d) is obtained from Eq. (III.2a) by

substituting *Ma=1*. Thus, given a SS geometry in Fig III.3 (with defined parameters A^{in}, A^{out}, A^{Throat}, *L*, etc) and inlet temperature T^{in}, Eq. (III.2d) shows that there is a unique Ma^{in} for the chosen A^{Throat}/A^{in} ratio in order to attain sonic throat flow. Therefore Eqs (III.2a) and (III.2b) show that *Ma* and *T* profiles will accomplish the design objectives (i.e. a supersonic *Ma>1* condition in the diverging section with very low temperature $T << T^{in}$) if the inlet Mach Number is kept at this correct Ma^{in} calculated by Eq. (III.2d), no matter whether P^{in} had to be manipulated away from its design value to ensure constancy of Ma^{in} under changes of inlet flow rate. In other words, P^{in} is manipulated to accommodate different inlet flow rates (and vice-versa) for a given SS nozzle design properly working with sonic throat. Another defensive strategy to protect the operational point of SS nozzles for NG processing – which can be complemented by the previously discussed protective throttling schemes – is to install a battery of several smaller SS nozzles that are individually activated (or deactivated) by the control algorithm according to the total feed flow rate to be processed, such that each SS nozzle is always fed with its design Ma^{in}.

$$\frac{A}{A^{in}} = \frac{Ma^{in}}{Ma}\left\{\frac{1+\left(\frac{\gamma'-1}{2}\right).(Ma)^2}{1+\left(\frac{\gamma'-1}{2}\right).(Ma^{in})^2}\right\}^{\frac{\gamma'+1}{2(\gamma'-1)}} \qquad \text{(III.2a)}$$

$$\frac{T}{T^{in}} = \frac{1+\left(\frac{\gamma'-1}{2}\right).(Ma^{in})^2}{1+\left(\frac{\gamma'-1}{2}\right).(Ma)^2} \qquad \text{(III.2b)}$$

$$\frac{P}{P^{in}} = \left\{\frac{1+\left(\frac{\gamma'-1}{2}\right).(Ma^{in})^2}{1+\left(\frac{\gamma'-1}{2}\right).(Ma)^2}\right\}^{\frac{\gamma'}{\gamma'-1}} \qquad \text{(III.2c)}$$

$$\frac{A^{Throat}}{A^{in}} = Ma^{in}\left\{\frac{1+\left(\frac{\gamma'-1}{2}\right)}{1+\left(\frac{\gamma'-1}{2}\right).(Ma^{in})^2}\right\}^{\frac{\gamma'+1}{2(\gamma'-1)}} \qquad \text{(III.2d)}$$

III.3. SS-THI-Recovery Processes

Two PFDs – PFD C in Fig III.4 and PFD D in Fig III.5 – were developed to implement SS-THI-Recovery for methanol, ethanol and MEG as THIs. These SS-THI-Recovery PFDs are shown already integrated to the respective conventional THI-RUs PFDs discussed in Sec. III.2.1, so that THIs are now recovered from the two main effluents leaving the high-pressure three-phase HPS separator, namely: (i) from the gas effluent by SS-THI-Recovery; and (ii) from the THI-water bottoms effluent by the conventional THI-RU process. THI could also be recovered from the small HCs condensate effluent (if any) from HPS by merely sending this stream to be water-washed in the liquid-liquid separator (LLS) in the terminal section of SS-THI-Recovery.

III.3.1. PFDs of SS-THI-Recovery Already Integrated to THI-RUs

Figs. III.4 and III.5 illustrate PFDs of SS-THI-Recovery integrated to THI-RU, where PFD C of Fig III.4 is dedicated to methanol and ethanol as THIs, while PFD D of Fig III.5 is appropriate to MEG as THI. SS-THI-Recovery operates with the gas effluent from HPS, while THI-RU is fed with the THI-water bottoms from HPS and with a THI-water stream coming from SS-THI-Recovery. This latter THI-water stream conveys all THI effectively recovered by SS-THI-Recovery.

In their first sections, PFDs C (Fig III.4) and D (Fig III.5) have no differences. The gas from HPS goes to one or more parallel SS nozzles according to the gas flow rate (about ≈*3 MMsm*^{3}*/d* can be handled by a single *6"* inlet SS nozzle at 50 bar). As SS-THI-Recovery is

based on THI capture using water as agent, sufficient (possibly liquid) water is necessary in the SS gas feed – however paradoxical it may appear. Therefore, in order to overcome fluctuations in the water content of the HPS gas due to changes in the field composition, a small stream of pure liquid water is added to the SS feed to guarantee the formation of two liquid phases in the SS flow path, thus effectively extracting THI and water from the gas and HCs phases, as THI and water are mutually attracted to each other due to their physical-chemical affinity. Water is added in the SS feed at a typical 3:1 ratio of water moles per mol THI. It should be noted that higher water:THI ratios are also possible, which improves THI capture; but at the expenses of increasing SS size as well as investment costs. In order to allow high pressure recovery in SS (about *≈84%* in the present case) to reduce compression costs, SS is specified with a not too high Ma^{Shock} ($Ma^{Shock} \approx 1.5$), so that temperature falls to about $\approx -38^{o}C$ in the SS supersonic section, condensing at least *≈99.5%* of water and at least *≈95%* of THI in the SS feed, jointly with heavy HCs (C3+). The two-phase L+W condensate is ejected from SS into the high-pressure LTX vessel whose bottom temperature is $\approx +20^{o}C$. The top slip-gas from LTX is added to the exiting dry gas from SS, while the warm L+W condensate leaves the LTX as bottoms, where a good portion of all condensed THI resides in the aqueous phase. The LTX bottoms goes to a high-pressure liquid-liquid separator (LLS) where more warm water is added to improve extraction of THI from HCs phase. Water is added into LLS typically at 4:1 ratio of water moles per mol THI in HPS gas. Again, higher water ratios can be used so as to increase THI recovery from HCs phase; but at the expenses of increasing LLS size, entailing higher fixed costs, besides operating costs to recover such added water by distillation. The LLS bottom THI-water phase is heated and expanded to atmospheric pressure, while the HCs phase is heated and expanded to an intermediate pressure (*≈20 bar*) producing a raw LPG product (C3+) and residual gas (mainly CH_4 and C_2H_6), which is recompressed and returns to the main gas header, conveying the final NG product with specified WDP and HCDP, practically without THI.

At this point, PFDs C and D become different. In PFD C (Fig III.4) for SS-THI-Recovery with methanol and ethanol as THIs, the atmospheric THI-water stream from LLS goes to a small atmospheric distillation column producing THI-water at the top and fresh water (*99.99%)* as bottoms. The objective of this column is to recover pure water bottoms, which

has no salt and provides all the fresh water consumed in the SS-THI-Recovery to be injected in SS and LLS. The THI-water distillate from the small atmospheric distillation is recycled to the atmospheric flash that receives the depressurized THI-water bottoms from HPS. The atmospheric THI-water liquid from this flash feeds the THI-RU process (PFD A, Fig III.1), whose main products is lean THI (*≈85%w/w*) and an aqueous (possibly salted, *THI ≤ 100 ppm*) bottoms to be discarded into the sea.

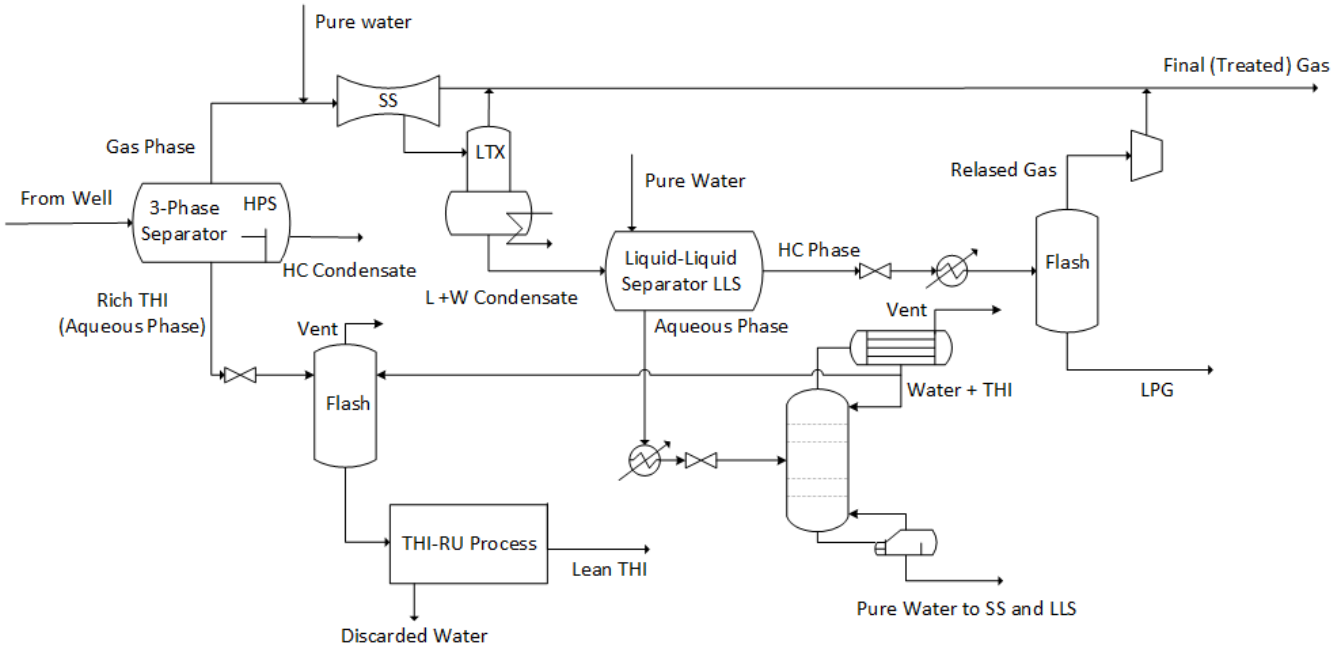

Figure III.4. PFD C: SS-THI-Recovery Process for Methanol or Ethanol as THI

On the other hand, in PFD D (Fig III.5) for SS-THI-Recovery with MEG as THI, there is no need for atmospheric distillation in the SS-THI-Recovery PFD because fresh water is naturally recovered as top distillate in the THI-RU columns (PFD B, Fig III.2). Therefore, the atmospheric THI-water stream from LLS goes directly to the atmospheric flash that receives the depressurized THI-water bottoms from HPS. The atmospheric THI-water liquid from this

flash feeds the THI-RU (PFD B, Fig III.2), whose main products is lean THI (*≈85%w/w*), a slurry of salts and fresh distillated water (*≈99.99%w/w, THI ≤ 100 ppm*), which provides all the consumption of fresh water in the SS-THI-Recovery process, besides a large excess of water that has to be discarded into the sea alongside with the salts from FLS bottom (PFD B, Fig III.2).

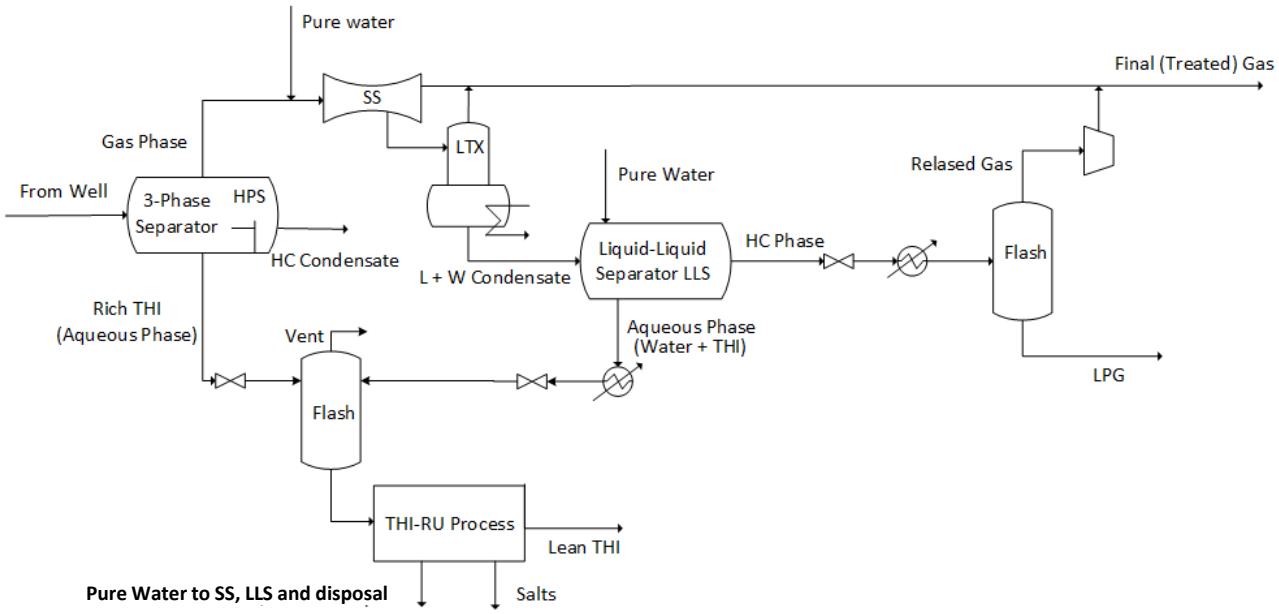

Figure III.5. PFD D: SS-THI-Recovery Process for MEG as THI

The utilization of SS nozzles in PFDs C and D could at first be misunderstood as similar to ejector applications. But they do not have too much in common, besides the fact that both use converging-diverging nozzles. Ejectors are fed with hot low pressure steam as driving fluid that expands through a converging-diverging nozzle #1 to supersonic velocities (*Ma>1*) at sub-atmospheric pressures and not too low temperatures. Nozzle #1 discharges its supersonic sub-atmospheric flow into the inlet of a larger converging-diverging nozzle #2, whose inlet is also connected to a vapor stream which is aspired by the sub-atmospheric discharge of nozzle #1. Successful ejector operation demands that the mixing of the supersonic driving fluid from nozzle #1 and the aspired vapors still results in supersonic flow, so that the converging-

diverging nozzle #2 could reversibly compress and slow down the flow to atmospheric subsonic discharge. No expressive cooling effect is observed in ejector operation and also there is no normal shock as the nozzle #1 supersonic flow is slowed down to subsonic almost reversibly in nozzle #2. On the other hand, SS has no driving fluid and its feed is at high pressures. SS expands the high-pressure NG feed to supersonic flow (*Ma>1*) and very low temperatures. Particularly in SS-THI-Recovery, a small flow rate of liquid water is injected in the SS inlet to drag THI from the gas and liquid HC phases towards the aqueous phase at very low temperatures generated through the SS flow path. Evidently the gas phase is much larger in comparison with the liquid HC and water phases as only *≈3%mol* of two-phase L+W condensate is typically produced in SS-THI-Recovery. After removal of L+W condensate in the SS separation section, the remaining dry vapor is still supersonic (*Ma>1*) so that it performs a normal shock transition to a hotter and recompressed subsonic flow that is further recompressed through the ending diffuser until the SS discharge. Therefore three simultaneous main tasks are executed in the SS-THI-Recovery application: (i) NG WDPA via deep gas dehydration; (ii) NG HCDPA via removal of condensable HCs; and (iii) high THI recovery from the gas phase. These results differ enormously from what occurs in an ejector application.

III.3.2. SS-THI-Recovery Simulation Premises [P1] to [P14]

The following premises were adopted for steady-state simulation of the SS-THI-Recovery processes using methanol, ethanol (PFD C, Fig III.4) and MEG (PFD D, Fig III.5) as THIs. Certain specific information (such as H_2O:THI injection ratios) can be found in the description of SS-THI-Recovery in Sec. III.3.1.

[P1] Process simulation: HYSYS 8.8 with Thermodynamic Package CPA-EOS using HYSYS Library of Component Data and CPA-EOS BIPs. **[P2]** Salts and electrolytes: Not considered in simulations. **[P3]** Raw NG producing scenario: (i) wellhead conditions *P=300 bar* and *T=40°C*; (ii) raw NG dry basis flow rate of *6 MMsm^3/d* with following dry-basis %mol composition: *85.48% CH_4, 8.26% C_2H_6, 3.06% C_3H_8, 0.47% iC_4H_{10}, 0.85% nC_4H_{10}, 0.20%*

iC_5H_{12}, 0.24% nC_5H_{12}, 0.21% C_6H_{14}, 0.06% C_7H_{16}, 0.53% N_2, 0.64% CO_2; (iii) production water flow rate of *75 m^3/d*. **[P4]** Determination of Gas Hydrate Equilibrium Temperature (*GHET*) in HYSYS 8.8: Two methods are available CSM (Colorado School of Mines) and Ng & Robinson; CSM was selected as it gives better *GHET* prediction for CH_4 under high pressures (Hould et al., 2015). **[P5]** Subsea flowline conditions: seabed temperature of *$T=5^oC$*; maximum pipeline pressure of *P=80 bar*, giving by CSM *$GHET=18.9^oC$* without THI, which justifies THI injection. **[P6]** Lean THI composition: All lean THI streams with *85%w/w* THI and *15%w/w* water. **[P7]** Dosages of lean THI injection in raw NG stream: Lean THI flow rates were designed to achieve same inhibiting effect, i.e. same *GHET* suppression calculated by CSM for worst pipeline conditions of *P=80 bar* and *$T=5^oC$*, by selecting *$GHET=1^oC$* under THI presence or *GHET* suppression of *17.9^oC*. **[P8]** Simulation of SS nozzles: Via HYSYS extension SS-UOE (Arinelli et al., 2017) with phase-equilibrium sound speed via HYSYS extension PEC-UOE (de Medeiros et al., 2017), both running with CPA-EOS. **[P9]** Specification of SS nozzles in SS-UOE: *$Ma^{Shock}=1.5$*, *$\eta^{EXP}\%=\eta^{CMP}\%=100\%$*, *$D_I=0.15$ m*, *$D_O=0.12$ m*, *$\alpha=12.67^o$*, *$\beta=2.66^o$*. **[P10]** SS PFD configuration: Two 6" SS nozzles with a single LTX for collecting cold L+W condensate. **[P11]** Compressors and pumps: *75%* adiabatically efficient. **[P12]** Intercoolers (Condensers): Gas (Liquid) at *45^oC*, thermal approach of *15^oC*, head loss of *0.5 bar*. **[P13]** Heating utility: PHW (*200^oC, 20 bar*). **[P14]** Cooling utilities: CW (*30^oC-45^oC, 4 bar*), ChW (*10^oC-25^oC, 4 bar*).

III.4. Results and Discussion

Table III.1 summarizes for methanol, ethanol and MEG as THIs, the respective lean THI injection flow rates and resulting THI compositions in the THI-water phase after injection in raw NG at service points. Gas flowline service points are supposed at *P=80 bar* and *T=5°C* according to premises [P3], [P4], [P5], [P6] and [P7]. SS-THI-Recovery processes for methanol and ethanol as THIs (PFD C, Fig III.4) and for MEG as THI (PFD D, Fig III.5) were simulated according to process premises [P1] to [P14] assuming THI injection data from Table III.1.

Table III.1. Lean THI Composition, THI Flow Rates and THI Composition in Water Phase

THI	*Lean THI Composition*	*Flow Rate of Lean THI Injection*	*THI Composition in Aqueous Phase (80 bar, 5^oC)*
Methanol	*85% w/w*	*79.7 kmol/h*	*31.2% w/w*
Ethanol	*85% w/w*	*99.0 kmol/h*	*43.1% w/w*
MEG	*85% w/w*	*108.7 kmol/h*	*51.1% w/w*

Table III.2 summarizes the specifications, design and performance of SS batteries as calculated by SS-UOE for SS-THI-Processes with THIs methanol, ethanol (PFD C, Fig III.4) and MEG (PFD D, Fig III.5). Specific results for each THI recovery are presented in the following sub-sections. As seen in Table III.2, SS batteries demand only two SS nozzles for each THI, with same inlet and outlet diameters (D_I, D_O), same converging and diverging angles (α, β) and same Ma^{Shock}, but obtaining little differences in terms of: (i) throat positions $L_C \approx 0.20\ m$; (ii) total nozzle lengths $L \approx 0.84\ m$; (iii) throat diameters $D_T \approx 0.06\ m$; (iv) normal shock locations $L^{Shock} \approx 0.26\ m$; (v) minimum before-shock temperatures $T_{BS} \approx -38.5^oC$ and pressures $P_{BS} \approx 15\ bar$; (vi) L+W condensate mol fraction $\approx 3\%$; and (vii) Mach Number after condensate removal $Ma_{BS} \approx 1.3$. In all SS cases the gas feed pressure is $P_E = 50\ bar$, while the final backpressures are all around $P^{Discharge} \approx 42\ bar$ corresponding to pressure recoveries of $\approx 84\%$, denoting excellent performances. Table III.2 also shows that, in all cases, the lean NG at SS outlet is perfectly specified in terms of WDP (around $\approx 15\ ppm\ mol\ H_2O$) and HCDP (after losing $\approx 40\%$ of its C3+), with a final NG (after adding slip-gas from LTX and LPG flash) also WDP and HCDP specified (around $\approx 21\ ppm\ mol\ H_2O$), while the SS THI recoveries were all above $\approx 95\%$.

Table III.2. SS Specifications, SS Nozzle Designs and SS Performances for SS-THI-Recovery with MeOH, EtOH and MEG as THIs

Specified Items	***MeOH***	***EtOH***	***MEG***	***Calculated by SS-UOE***	***MeOH***	***EtOH***	***MEG***
No.of SS	*2*	*2*	*2*	$D_T(m)$	*0.0603*	*0.0603*	*0.0601*
$D_I(m)$	*0.1500*	*0.1500*	*0.1500*	$L_C(m)$	*0.1995*	*0.1996*	*0.2000*
$D_O(m)$	*0.1200*	*0.1200*	*0.1200*	$L_D(m)$	*0.6430*	*0.6432*	*0.6453*
$\alpha(^o)$	*12.67*	*12.67*	*12.67*	$L(m)$	*0.8425*	*0.8428*	*0.8453*
$\beta(^o)$	*2.66*	*2.66*	*2.66*	$L^{Shock}(m)$	*0.2628*	*0.2627*	*0.2626*
Ma^{Shock}	*1.5*	*1.5*	*1.5*	$L^{Diff}(m)$	*0.5797*	*0.5801*	*0.5827*
$\eta^{EXP}\%$	*100*	*100*	*100*	$P_{BS}(bar)$	*14.95*	*14.95*	*14.98*
$\eta^{CMP}\%$	*100*	*100*	*100*	$T_{BS}(^oC)$	*-38.37*	*-38.52*	*-39.31*
$P^{Feed}(bar)$	*50*	*50*	*50*	Ma_{BS}	*1.293**	*1.294**	*1.388**
$T^{Feed}(^oC)$	*25.28*	*25.24*	*25.00*	$P^{Discharge}(bar)$	*42.05*	*42.08*	*42.24*
$MMsm^3/d$	*3.019*$^\$$	*3.013*$^\$$	*3.001*$^\$$	$T^{Discharge}(^oC)$	*30.68*	*30.58*	*29.89*
$\%C3^{+Feed}$	*5.06%*$^\&$	*5.07%*$^\&$	*5.09%*$^\&$	*%Condensate*	*3.21%*$^\&$	*3.05%*$^\&$	*2.77%*$^\&$
$ppmH_2O^{Feed}$	*4960*$^\&$	*3500*$^\&$	*593*$^\&$	$REC\%H_2O^\#$	*99.71%*	*99.60%*	*97.31%*
$ppmTHI^{Feed}$	*1508*$^\&$	*1097*$^\&$	*1*$^\&$	$REC\%THI^\#$	*95.23%*	*98.42%*	*100.0%*
				%P Recovery	*84.10%*	*84.17%*	*84.48%*
				$ppmH_2O^{GasSS}$	*15*$^\&$	*14*$^\&$	*16*$^\&$
				$ppmH_2O^{FinalNG}$	*20*$^\&$	*21*$^\&$	*21*$^\&$

III.4.1. Results of SS-THI-Recovery for Methanol as THI

The gas from HPS in PFD C, Fig III.4, receives *45 kmol/h* of water (about 3:1 water moles per THI mol) at the admission of two parallel SS nozzles. Each SS nozzle processes $\approx 3\ MMsm^3d$ of raw gas with $Ma^{Shock}=1.5$ producing two-phase L+W condensate at *-39.6°C* with final gas discharge pressure (backpressure) of $P^{Discharge}=42.1\ bar$. The L+W cold condensate is ejected into LTX whose bottom is at *20ºC*. In this case, the slip-gas from LTX has zero flow rate.

Fig III.6 reports SS profiles of several dependent variables versus *x* as obtained by SS-UOE, where *x* is the SS axial spatial coordinate. SS linear diameter profiles are shown in Fig III.6a with throat position at *x=0.1995 m*. With linear diameter profiles it is easily seen in Fig III.6a that the flow area section gradient is nonzero ($dA/dx \neq 0$) at both sides of the throat. This

entails some consequences on the shape of profiles of dependent variables as the throat is crossed at sonic speed, as will be shown shortly. Figs. III.6b, III.6c, III.6d, III.6e, III.6f and III.6g depict respective profiles of *P(bar), T(K), c(m/s), Ma*, molar vapor fraction and % condensed of HCs, CO_2, H_2O and MeOH versus *x*. Fig III.6f shows, from the outset, that the gas starts the SS flow path with less than *100%* vapor due to the excess of liquid water injected in SS inlet, which is confirmed in Fig III.6g showing *≈90%* of condensed water at *x=0*; i.e. SS flow is two-phase from the beginning. This is a keystone of the proposed SS-THI-Recovery: a small excess of liquid water is admitted in SS feed to guarantee a permanent water phase along SS flow path to continuously extract THI from the gas and from the forming liquid HC phase.

As gas accelerates, *T, P, c* decrease and *Ma* increases until $x=L^{Shock}=0.2628\ m$, where *Ma* attains the specified maximum value of $Ma^{Shock}=1.5$ with minimum before-shock temperature and pressure of $T_{BS}=-38.37^{o}C$, $P_{BS}=14.95\ bar$, minimum molar vapor fraction of *96.79%* and minimum sound speed $c\approx 328\ m/s$. The multiphase sound speed (Fig III.6d) continuously decreases from *x=0* to $x=L^{Shock}=0.2628\ m$ due to increasing condensation and cooling, both continuously causing increase of multiphase properties such as density (ρ) and isothermal compressibility ($\Xi_P=(\partial\rho/\partial P)_{T,\underline{Z}}$), which, by their turn, decrease the multiphase sound speed (de Medeiros et al., 2017). At the throat ($x=L_C=0.1995\ m$), SS axial flow becomes sonic with *Ma=1*, which is accompanied by SS signatures represented by $\pm\infty$ gradient singularities clearly identified in Figs. III.6b, III.6c, III.6d and III.6e as shown in Eq. (3), where *v* is the axial flow velocity and *Ma=v/c*.

$$\frac{dT}{dx}\to-\infty,\ \ \frac{dP}{dx}\to-\infty,\ \ \frac{dv}{dx}\to+\infty,\ \ \frac{dc}{dx}\to-\infty,\ \ \frac{dMa}{dx}\to+\infty\ \ \left(Ma\to 1^{-},\ \frac{dA}{dx}\neq 0\right) \tag{3}$$

SS signatures in Eq. (3) are rigorous thermodynamic conditions that can be proved (de Medeiros et al., 2017, Supplementary Materials) for any compressible isentropic supersonic flow through converging-diverging nozzles provided $dA/dx\neq 0$ at the throat, where the flow is sonic. These signatures are valid (if $dA/dx\neq 0$) for either ideal gas or single-phase real gas or two-phase VLE mists or three-phase VLWE mists or any multiphase-equilibrium

compressible fluid. On the other hand, the $dc/dx \rightarrow -\infty$ singularity is proven only for a multiphase sonic compressible flow *with a dominant gas phase* as occurs in the present case, where the vapor fraction is always above *96%* mol. The vapor fraction (Fig III.6f) starts to fall more intensely at $x=0.18\ m$, where a sudden concomitant increase of condensation of HCs, THI and H_2O occur as confirmed in Fig III.6g. This point corresponds to the first inflexion of *c* profile in Fig III.6d ($x=0.18\ m$). The second inflexion point of *c* profile in Fig III.6d occurs at $x \approx 0.20\ m$, just after the throat, where the condensation profiles sudden lose intensity as temperature falls less rapidly and water condensation is practically complete (Fig III.6g). The two inflexion points of *c* profile in Fig III.6d show that PEC-UOE correctly handles the calculation of sound speed across phase transition boundaries in multiphase flow.

After condensate removal at $x=L^{Shock}=0.2628\ m$, *Ma* falls to $Ma_{BS}=1.293$, but is still supersonic, so that the normal shock occurs at this point with sudden recompressing discontinuities that recover part of the initial (*T,P*) and turn the flow into subsonic. After normal shock, gas velocity and *Ma* decrease through the diffuser with *T* and *P* smoothly increasing until the SS gas outlet with final $T^{Discharge}=30.68^oC$, $P^{Discharge}=42.05\ bar$.

By last, Fig III.6h represents the plane *P x T* with HCDP curve of the feed (hotter), HCDP curve of treated lean gas (colder), WDP curve of the two-phase feed and with SS flow path superimposed, all calculated with CPA-EOS. The SS path consists of expansion from two-phase humid vapor ($T_E=25.28^oC$, $P_E=50\ bar$) below the feed WDP curve from the beginning, penetrating deeply into the VLE feed envelope until $T_{BS}=-38.37^oC$, $P_{BS}=14.95\ bar$, and then suddenly recompressing via the linear shock-jump back to superheated vapor, followed by smooth recompression and heating through the diffuser.

The L+W condensate from LTX, with *95.23%* of THI recovery and *99.71%* of water recovery, goes to the LLS separator (Fig III.4) at $P=42.1\ bar$ and $T=20^oC$, where more water is injected at $60\ kmol/h$ and 20^oC (4:1 water moles per THI mol in the HPS gas). The capture of THI by the aqueous phase increases by raising the water injected into LLS, as shown in Fig III.7. On the other hand, the higher the LLS water flow rate, the higher the size and costs of LLS and the higher the heat consumption to recover water in the small distillation column (Fig III.4) to be injected in SS feed and LLS. Table III.3a shows how LLS water flow rate

affects the heat consumption of THI-RU in PFD A (Fig III.1) – under constant specification of lean THI at *85% w/w* THI – and the heat consumption in the distillation column for recovery of fresh water (*99.99%w/w* H_2O). The plain fact is that the heat consumption of Methanol THI-RU is practically invariant, while the heat to recover fresh water by distillation rises with the increase of LLS water flow rate. The top HC phase from LLS (Fig III.4) is depressurized to *P=20 bar* and heated to $T=50^oC$ before the LPG flash, releasing gas (mainly CH_4 and C_2H_6), while the bottoms correspond to raw LPG, whose composition is shown in Table III.6 for comparison with other THIs. Table III.3b presents all pertinent stream results of SS-THI-Recovery for methanol as THI according to PFD C (Fig III.4), while Table III.7 summarizes its main yield results for comparison with other THIs.

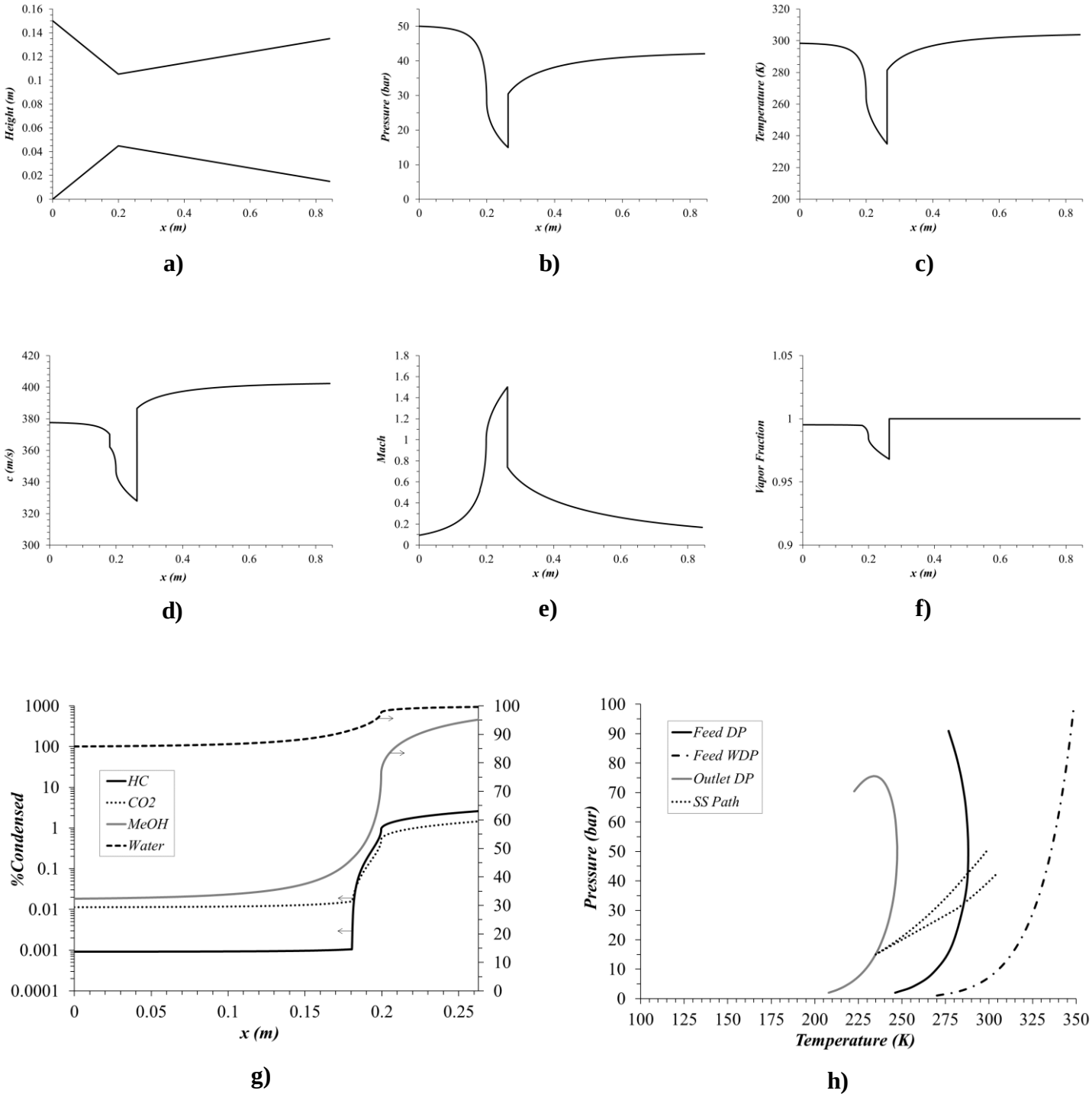

Figure III.6. SS Profiles for SS-THI-Recovery with Methanol: (a) Flow Section; (b) *P* (bar); (c) *T* (K); (d) Sound Speed *c* (m/s); (e) *Ma*; (f) Mol Vapor Fraction; (g) %Condensed HCs, CO_2, H_2O, THI; (h) Plane *T x P* with SS Path, HCDP and WDP Curves of SS Feed and HCDP Curve of Lean Gas

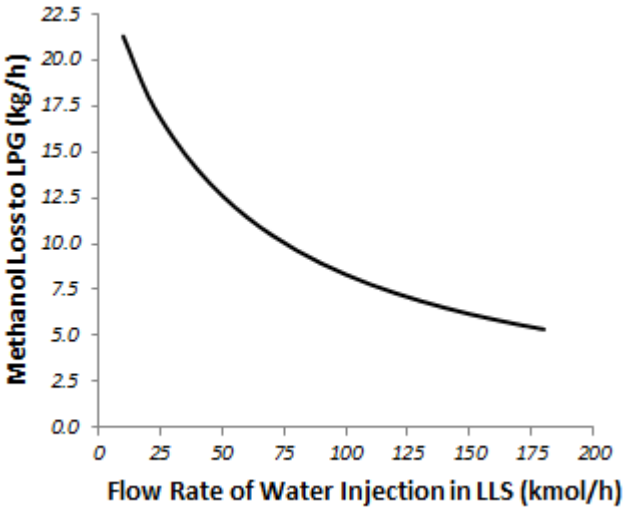

Figure III.7. Methanol Loss to LPG versus Water Flow Rate in LLS

Table III.3a. SS-THI-Recovery for Methanol as THI: Water Injected in LLS versus Heat Consumptions of THI-RU and Water Recovery Distillation

Water Injected in LLS (kmol/h)	*Heat Consumption (kW) of THI-RU*	*Heat Consumption (kW) of Water Recovery Distillation*
60	*2188*	*866.8*
70	*2189*	*885.3*
80	*2190*	*903.7*
90	*2191*	*921.9*
100	*2191*	*939.9*
110	*2192*	*957.9*
120	*2193*	*975.8*

Table III.3b. Streams of SS-THI-Recovery for Methanol as THI

System	*SS & LTX*					*LLS Vessel*		*LPG Flash*		*NG Header*	*Water Recovery Distillation*		*HPS**	*THI-RU*		
Stream [#]	*HPS Gas* [$]	*SS Feed*	*L+W Condensate*	*L+W LTX*	*SS Gas*	*Aqueous Bottoms*	*HCs Top*	*Gas*	*Raw LPG*	*Final NG*	*Distillate*	*Bottom*	*Aqueous THI*	*Flash Vent*	*ADC Vent*	*Lean THI* [&]
T(°C)	25	25.3	-39.6	20	30.7	20.2	20.2	50	50	31.3	45	113.6	25	27.3	45	45.1
P(bar)	50	50	42.1	42.1	42.1	40.3	40.3	20	20	42.1	1.7	1.8	50	1.6	1	1
MMsm^3/d	6.012	3.019	0.097	0.193	5.845	0.073	0.155	0.035	0.120	5.88	0.012	0.061	0.147	4.10^{-4}	1.10^{-5}	0.46
%Vapor	100	99.5	0	0	100	0	0	100	0	100	0	0	0	100	100	0
%CH_4	85.29	84.93	9.83	9.83	87.41	0.10	12.20	39.32	4.23	87.13	0.04	0.00	0.26	78.04	50.77	0.03
%C_2H_6	8.24	8.21	10.75	10.75	8.12	0.02	13.39	24.07	10.25	8.22	0.02	0.00	0.02	7.09	2.11	0.00
%C_3H_8	3.05	3.04	18.02	18.02	2.54	0.01	22.45	20.48	23.04	2.65	0.01	0.00	0.01	2.41	0.48	0.00
%i-C_4H_{10}	0.47	0.47	6.68	6.68	0.26	0.00	8.33	4.11	9.57	0.28	0.00	0.00	0.00	0.21	0.02	0.00
%C_4H_{10}	0.85	0.84	14.92	14.92	0.38	0.00	18.60	7.37	21.90	0.42	0.01	0.00	0.00	0.74	0.10	0.00
%i-C_5H_{12}	0.20	0.20	5.04	5.04	0.04	0.00	6.29	1.32	7.75	0.05	0.00	0.00	0.00	0.03	0.00	0.00
%C_5H_{12}	0.24	0.24	6.37	6.37	0.04	0.00	7.94	1.40	9.86	0.04	0.00	0.00	0.00	0.11	0.01	0.00
%C_6H_{14}	0.21	0.21	6.34	6.34	0.01	0.00	7.90	0.51	10.07	0.01	0.00	0.00	0.00	0.10	0.00	0.00
%C_7H_{16}	0.06	0.06	1.85	1.85	0.00	0.00	2.30	0.07	2.96	0.00	0.00	0.00	0.00	0.03	0.00	0.00
%CO_2	0.64	0.64	0.29	0.29	0.65	0.02	0.35	0.91	0.19	0.65	0.03	0.00	0.02	4.97	7.11	0.02
ppm H_2O	663	4960	---	---	15	---	324	859	167	20	---	---	---	---	---	---
% H_2O	---	---	15.43	15.43	---	88.39	---	---	---	---	31.54	100	82.11	1.96	3.77	23.70
ppm THI	1514	1508	---	---	74	---	2015	3021	1719	92	---	0.3	---	---	---	---
%THI	---	---	4.48	4.48	---	11.47	---	---	---	---	68.34	---	17.58	4.15	35.55	76.24

*[#] %mol; [$] Before water injection; [&] After THI make-up; * No liquid HC phase*

III.4.2. Results of SS-THI-Recovery for Ethanol as THI

HPS gas with traces of ethanol and water receives *30 kmol/h* of injected water (≈3:1 water moles per THI mol) at the entrance of two parallel SS nozzles, each one processing *≈3 MMsm^{3}d* of raw gas with $Ma^{Shock}=1.5$ producing two-phase L+W condensate at *-39.7°C* with final gas pressure of $P^{Discharge}=42.1$ *bar*. L+W condensate is ejected into LTX whose bottom is at *20ºC*, again without slip-gas.

Fig III.8 reports SS profiles of several variables versus *x* obtained by SS-UOE. The SS linear diameter profiles are shown in Fig III.8a with throat position at *x=0.1996 m*, again with $dA/dx \neq 0$ at both sides of the throat. Figs. III.8b, III.8c, III.8d, III.8e, III.8f and III.8g depict respective profiles of *P(bar), T(K), c(m/s), Ma*, molar vapor fraction and % condensed of HCs, CO_2, H_2O and EtOH versus *x*. Fig III.8f shows, from the outset, that the gas starts the SS flow path with less than *100%* vapor due to the excess of liquid water injected in SS feed, which is confirmed in Fig III.8g with *≈85%* of condensed water at *x=0* already dragging *≈35%* of condensed EtOH; i.e. SS flow is two-phase from the beginning, as mentioned early, a basic point in SS-THI-Recovery. As gas accelerates, *T, P, c* decrease and *Ma* increases until $x=L^{Shock}=0.2627$ *m*, where *Ma* attains the specified maximum value $Ma^{Shock}=1.5$ with minimum temperature and pressure $T_{BS}=-38.52^oC$, $P_{BS}=14.95$ *bar*, minimum molar vapor fraction of *96.95%* and minimum sound speed *c≈329 m/s*.

As before, the multiphase sound speed (Fig III.8d) continuously decreases from *x=0* to $x=L^{Shock}=0.2627$ *m* due to increasing condensation and cooling, both continuously causing increase of multiphase properties such as density (ρ) and isothermal compressibility ($\Xi_P=(\partial\rho/\partial P)_{T,\underline{Z}}$), which damp the multiphase *c*. At the throat ($x=L_C=0.1996$ *m*), SS axial flow becomes sonic with *Ma=1*, again accompanied by SS signatures as $\pm\infty$ gradient singularities clearly identified in Figs. III.8b, III.8c, III.8d and III.8e according to Eq. (3), since $dA/dx \neq 0$ at both sides of the throat. Again, the observed $dc/dx \rightarrow -\infty$ singularity in Fig III.8d is proven only (de Medeiros et al., 2017) for a multiphase sonic compressible flow *with a dominant gas phase*, a characteristic of the present case whose SS vapor fraction is always above *96.9%* mol. The vapor fraction (Fig III.8f) starts to fall more intensely at *x=0.185 m*,

where a sudden concomitant increase of condensation of HCs, THI and H_2O occur (Fig III.8g). Again, this point corresponds to the first inflexion of *c* profile (Fig III.8d). The second inflexion point in Fig III.8d occurs at $x \approx 0.21\ m$, just after the throat, where the condensation profiles become less intense as temperature falls less rapidly and water condensation is complete (Fig III.8g). Again, the two inflexion points (Fig III.8d) show that PEC-UOE correctly handles the calculation of *c* across phase transition boundaries in multiphase flow with complex polar systems.

After condensate removal at $x=L^{Shock}=0.2627\ m$, *Ma* falls to $Ma_{BS}=1.294$, but as it is still supersonic, normal shock occurs at this point discontinuously recompressing the gas, recovering part of the initial (*T,P*) and turning the flow into subsonic. After normal shock, gas velocity and *Ma* decrease through the diffuser with *T* and *P* smoothly increasing until the SS gas outlet with final $T^{Discharge}=30.58^oC$, $P^{Discharge}=42.08\ bar$.

Fig III.8h represents the plane *P x T* with HCDP curve of the feed, VLE envelope of the treated lean gas, WDP curve of the two-phase feed and with SS path superimposed, all calculated with CPA-EOS. The SS path consists of expansion from two-phase humid vapor ($T_E=25.24^oC$, $P_E=50\ bar$) below the feed WDP curve from the beginning, penetrating the VLE feed envelope until $T_{BS}=-38.52^oC$, $P_{BS}=14.95\ bar$, and then suddenly recompressing via the linear shock-jump back to superheated vapor, followed by smooth recompression through the diffuser.

The L+W condensate from LTX, with *98.42%* of THI recovery and *99.60%* of water recovery, goes to LLS separator (Fig III.4) at $P=42.1\ bar$ and $T=20^oC$, where more water is injected at *40 kmol/h* and 20^oC (4:1 water moles per THI mol in the HPS gas). As before, the capture of THI by the aqueous phase increases by raising the water injected into LLS (Fig III.9), evidently with increasing costs. Table III.4a shows how LLS water flow rate affects the heat consumption of THI-RU in PFD A (Fig III.1) – under constant specification of lean THI at *85% w/w* THI – and the heat consumption in the distillation column (Fig III.4) for recovery of fresh water (*99.99%w/w* H_2O). Analogously to the MeOH case, the heat consumption of Ethanol THI-RU is practically invariant, while the heat to recover fresh water by distillation rises with the increase of LLS water flow rate. The top HC phase from LLS (Fig III.4) is

depressurized to *P=20 bar* and heated to $T=50^{o}C$ before the LPG flash, releasing gas (mainly CH_4 and C_2H_6), while the bottoms correspond to raw LPG, whose composition is also in Table III.6 for comparison with other THIs. Table III.4b presents all pertinent stream results of SS-THI-Recovery for ethanol as THI (PFD C, Fig III.4), while Table III.7 summarizes its main yield results.

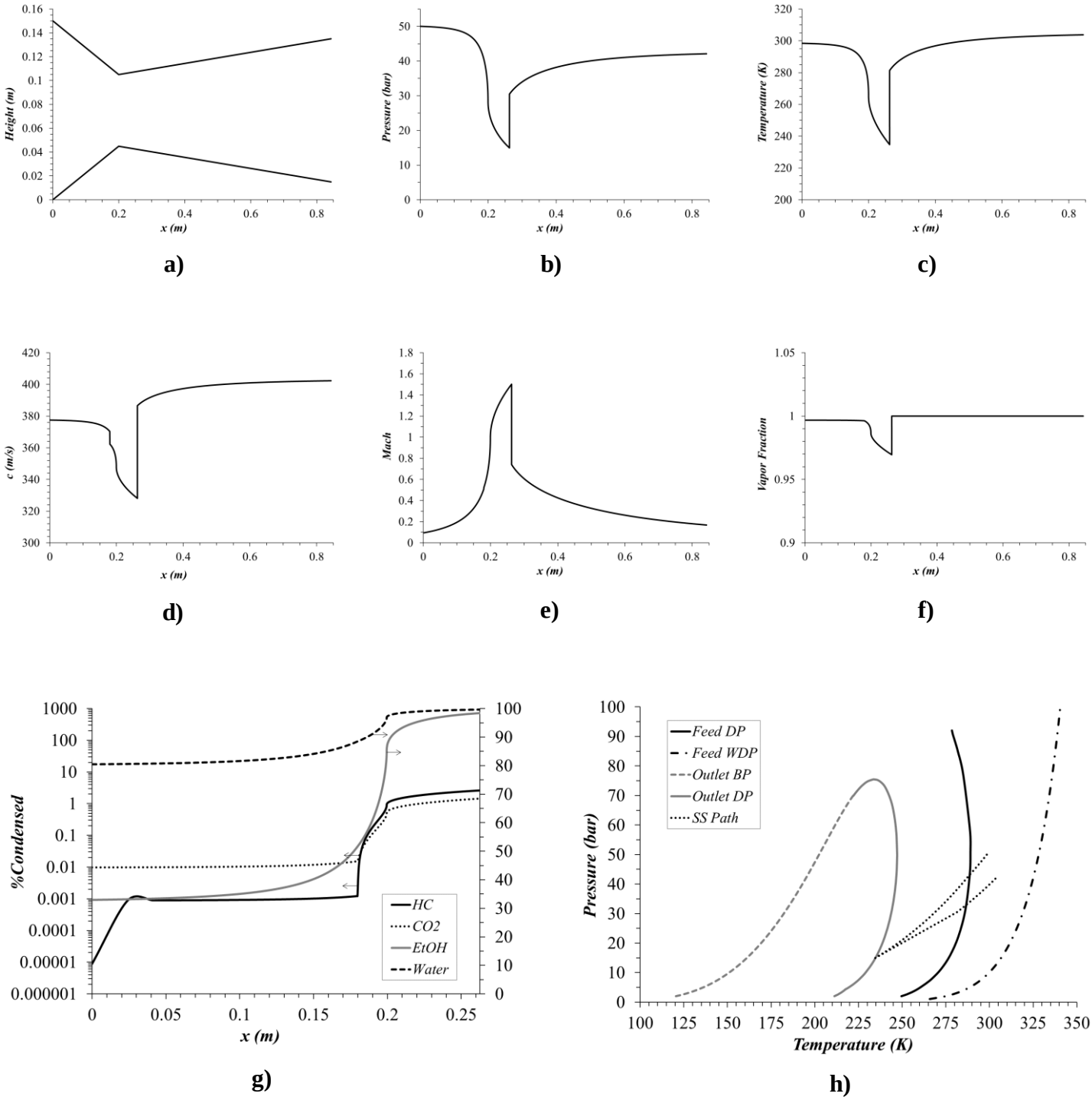

Figure III.8. SS Profiles for SS-THI-Recovery with Ethanol: (a) Flow Section; (b) *P* (bar); (c) *T* (K); (d) Sound Speed *c* (m/s); (e) *Ma*; (f) Mol Vapor Fraction; (g) %Condensed HCs, CO_2, H_2O, THI; (h) Plane *T x P* with SS Path, HCDP and WDP Curves of SS Feed and VLE Envelope of Lean Gas

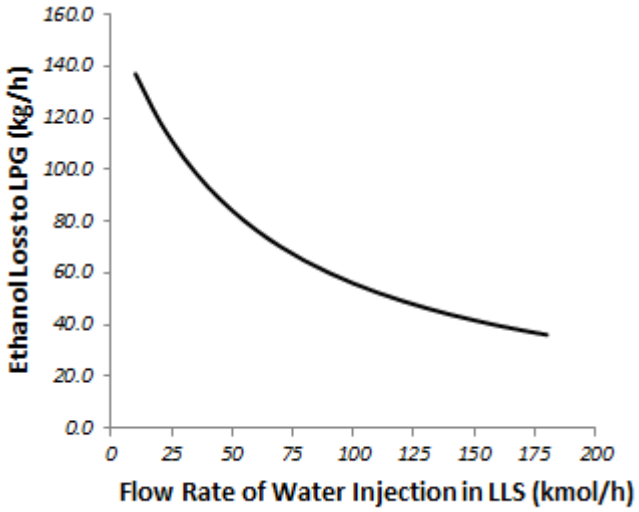

Figure III.9. Ethanol Loss to LPG versus Water Flow Rate in LLS

Table III. 4a. SS-THI-Recovery for Ethanol as THI: Water Injected in LLS versus Heat Consumption of THI-RU and Water Recovery Distillation

Water Injected in LLS (kmol/h)	*Heat Consumption (kW) of THI-RU*	*Heat Consumption (kW) of Water Recovery Distillation*
40	*2529*	*746.1*
50	*2534*	*772.8*
60	*2539*	*797.9*
70	*2542*	*821.9*
80	*2545*	*844.9*
90	*2548*	*867.1*
100	*2550*	*888.7*

Table III.4b. Streams of SS-THI-Recovery for Ethanol as THI

System	*SS & LTX*					*LLS Vessel*		*LPG Flash*		*NG Header*	*Water Recovery Distillation*		*HPS**	*THI-RU*		
Stream [#]	*HPS Gas* [$]	*SS Feed*	*L+W Condensate*	*L+W LTX*	*SS Gas*	*Aqueous Bottoms*	*HCs Top*	*Gas*	*Raw LPG*	*Final NG*	*Distillate*	*Bottom*	*Aqueous THI*	*Flash Vent*	*ADC Vent*	*Lean THI* [&]
T(°C)	25	25.2	-39.7	20	30.6	20.6	20.6	50	50	31.3	45	115.5	25	27.4	45	44.5
P(bar)	50	50	42.1	42.1	42.1	40.3	40.3	20	20	42.1	1.6	1.7	50	1.6	1	1
MMsm^3/d	6.009	3.013	0.092	0.184	5.843	0.049	0.158	0.036	0.122	5.88	0.009	0.040	0.152	9.10^{-4}	3.10^{-6}	0.057
%Vapor	100	99.7	0	0	100	0	0	100	0	100	0	0	0	100	100	0
%CH_4	85.33	85.09	10.46	10.46	87.44	0.12	12.17	39.44	4.23	87.15	0.06	0.00	0.48	75.95	66.99	0.04
%C_2H_6	8.25	8.22	11.47	11.47	8.12	0.02	13.37	24.11	10.24	8.22	0.03	0.00	0.06	9.29	3.93	0.01
%C_3H_8	3.05	3.05	19.21	19.21	2.54	0.01	22.40	20.45	22.97	2.65	0.03	0.00	0.02	3.86	0.99	0.01
%i-C_4H_{10}	0.47	0.47	7.10	7.10	0.26	0.00	8.28	4.08	9.50	0.28	0.00	0.00	0.00	0.34	0.05	0.00
%C_4H_{10}	0.85	0.85	15.82	15.82	0.37	0.00	18.45	7.31	21.70	0.42	0.01	0.00	0.01	1.33	0.23	0.00
%i-C_5H_{12}	0.20	0.20	5.33	5.33	0.04	0.00	6.21	1.30	7.64	0.05	0.00	0.00	0.00	0.08	0.00	0.00
%C_5H_{12}	0.24	0.24	6.72	6.72	0.03	0.00	7.84	1.38	9.73	0.04	0.00	0.00	0.00	0.28	0.03	0.00
%C_6H_{14}	0.21	0.21	6.67	6.67	0.01	0.00	7.78	0.50	9.90	0.01	0.00	0.00	0.00	0.24	0.02	0.00
%C_7H_{16}	0.06	0.06	1.95	1.95	0.00	0.00	2.27	0.06	2.91	0.00	0.00	0.00	0.00	0.07	0.00	0.00
%CO_2	0.64	0.64	0.31	0.31	0.65	0.02	0.35	0.91	0.19	0.65	0.04	0.00	0.03	4.35	6.51	0.03
ppm H_2O	630	3500	---	---	14	---	480	1129	291	21	---	---	---	---	---	---
% H_2O	---	---	11.42	11.42	---	89.20	---	---	---	---	40.84	100	77.89	1.91	4.47	30.83
ppm THI	1100	1097	---	---	18	---	8036	2773	9569	35	---	0.1	---	---	---	---
%THI	---	---	3.54	3.54	---	10.62	---	---	---	---	58.99	---	21.49	2.09	16.59	69.08

*[#] %mol; [$] Before water injection; [&] After THI make-up; * No liquid HC phase*

III.4.3. Results of SS-THI-Recovery for MEG as THI

Even in the case of low volatile THIs, such as MEG, SS-THI-Recovery can be successfully applied, but now with less impressive gains. The flow rate of water injected into HPS gas at SS inlet is now much lesser than in MeOH and EtOH cases, as MEG has a minuscule flow rate in HPS gas thanks to its very low volatility. Hence, HPS gas receives only 0.036 kmol/h of water (≈3:1 water moles per THI mol) at the entrance of two parallel SS nozzles, each nozzle processing $\approx 3\ MMsm^3d$ of raw gas with $Ma^{Shock}=1.5$ producing two-phase L+W condensate at $-40.6°C$ with final gas pressure of $P^{Discharge}=42.2\ bar$. L+W condensate is ejected into LTX whose bottom is at $20ºC$, again without slip-gas.

Fig III.10 reports SS profiles of several variables versus x obtained by SS-UOE. The SS linear diameter profiles are shown in Fig III.10a with throat position at $x=0.2\ m$, again with $dA/dx \neq 0$ at both throat sides. Figs. III.10b, III.10c, III.10d, III.10e, III.10f and III.10g depict respective profiles of *P(bar), T(K), c(m/s), Ma*, molar vapor fraction and % condensed of HCs, CO_2, H_2O and MEG versus x. Fig III.10f shows that the gas starts the SS flow path 100% vapor as the injected water was insufficient to saturate SS feed, a fact confirmed in Fig III.10g, which shows $\approx 0\%$ of condensed water at $x=0$. In spite of this, the added water has an important role during SS condensation as it drags MEG to the aqueous phase, a key point in SS-THI-Recovery. As gas accelerates, T, P, c decrease and Ma increases until $x=L^{Shock}=0.2626\ m$ where Ma attains the specified maximum value $Ma^{Shock}=1.5$ with minimum temperature and pressure $T_{BS}=-39.31^oC$, $P_{BS}=14.98\ bar$, minimum molar vapor fraction of 97.33% and minimum sound speed $c\approx 328\ m/s$. The colder before-shock state is a reflex of the lower degree of condensation in SS-MEG-Recovery case relatively to MeOH and EtOH cases.

As before, the multiphase sound speed (Fig III.10d) continuously decreases from $x=0$ to $x=L^{Shock}=0.2626\ m$ due to increasing condensation and cooling, both continuously causing increase of multiphase properties such as density (ρ) and isothermal compressibility ($\Xi_P = (\partial\rho / \partial P)_{T,\underline{Z}}$), which severely damp the multiphase c.

At the throat ($x=L_C=0.2\ m$), SS axial flow becomes sonic with $Ma=1$, again accompanied by SS signatures as $\pm\infty$ gradient singularities identified in Figs. III.10b, III.10c, III.10d and III.10e according to Eq. (3), since $dA/dx \neq 0$ at both sides of the throat. Again, the $dc/dx \rightarrow -\infty$ singularity is observed in Fig III.10d, but it is proven only (de Medeiros et al., 2017) for a multiphase sonic compressible flow *with a dominant gas phase* as occurs in the present case, whose SS vapor fraction is always above *97%*mol. The vapor fraction (Fig III.10f) starts to fall more intensely at $x=0.18\ m$, where a sudden concomitant increase of condensation of HCs, THI and H_2O occur (Fig III.10g). Again, this point corresponds to the first inflexion of c profile (Fig III.10d). The second and more subtle inflexion point in Fig III.10d occurs at $x \approx 0.21\ m$, after the throat, where the condensation profiles become less intense as temperature falls less rapidly and MEG condensation is complete (Fig III.10g). Again, the two inflexion points (Fig III.10d) show that PEC-UOE correctly handles the calculation of c across phase transition boundaries in multiphase flow with complex polar systems.

After condensate removal at $x=L^{Shock}=0.2626\ m$, Ma falls to $Ma_{BS}=1.388$, a fall less pronounced than MeOH and EtOH analogues due to lower condensation and lower removal of liquids in the MEG case. This dry supersonic state triggers the normal shock, which occurs at this point discontinuously recompressing the gas, recovering part of the initial (T,P) and turning the flow into subsonic. After normal shock, gas velocity and Ma decrease through the diffuser with T and P smoothly increasing until the SS gas outlet with final $T^{Discharge}=29.89^oC$, $P^{Discharge}=42.24\ bar$.

Fig III.10h represents the plane $P\ x\ T$ with VLE envelope of the feed, VLE envelope of the treated lean gas (slenderer), WDP curve of the feed and with SS path superimposed, all calculated with CPA-EOS. Now, the SS path consists of expansion from superheated vapor ($T_E=25^oC$, $P_E=50\ bar$) little above the feed WDP curve, which confirms that the water added to SS feed was not sufficient for saturation in the SS-MEG-Recovery case. As there is less condensing water and THI, there is lower release of condensation enthalpy, so that the SS path attains a colder final condition, penetrating a little more deeply into the VLE feed envelope until $T_{BS}=-39.31^oC$, $P_{BS}=14.98\ bar$. At this point, the SS path suddenly

recompresses via the linear shock-jump back to superheated vapor, followed by smooth recompression through the diffuser.

The L+W condensate from LTX, with *100%* of THI recovery and *97.31%* of water recovery, goes to LLS separator (PFD D, Fig III.5) at *P=42.24 bar* and *T=20^{o}C*, where more water is injected at *0.048 kmol/h* and *20^{o}C* (4:1 water moles per THI mol in the HPS gas). The capture of THI by the aqueous phase increases by raising the water injected into LLS (Fig III.11), evidently with increasing costs. In the MEG case, PFD D (Fig III.5) does not need a distillation for fresh water recovery, as water can be recovered as top distillates (*99.99% water*) of THI-RU columns. Therefore, Table III.5a only shows how LLS water flow rate affects the heat consumption of THI-RU in PFD B (Fig III.2) under constant specification of lean THI at *85% w/w* THI. Differently from MeOH and EtOH cases, the heat consumption of MEG THI-RU increases with the increase of water flow rate in LLS. This is a direct consequence of a higher water load to THI-RU, which needs to be evaporated and distilled to keep constant lean MEG composition. The top HC phase from LLS (Fig III.5) is depressurized to *P=20 bar* and heated to *T=50^{o}C* before the LPG flash, releasing gas (mainly CH_4 and C_2H_6) that is returned to the header of treated NG, while the LLS bottoms correspond to raw LPG, whose composition is also shown in Table III.6 for comparison with other THIs. Table III.5b presents all pertinent stream results of SS-THI-Recovery for MEG as THI according to PFD D (Fig III.5), while Table III.7 summarizes its main yield results.

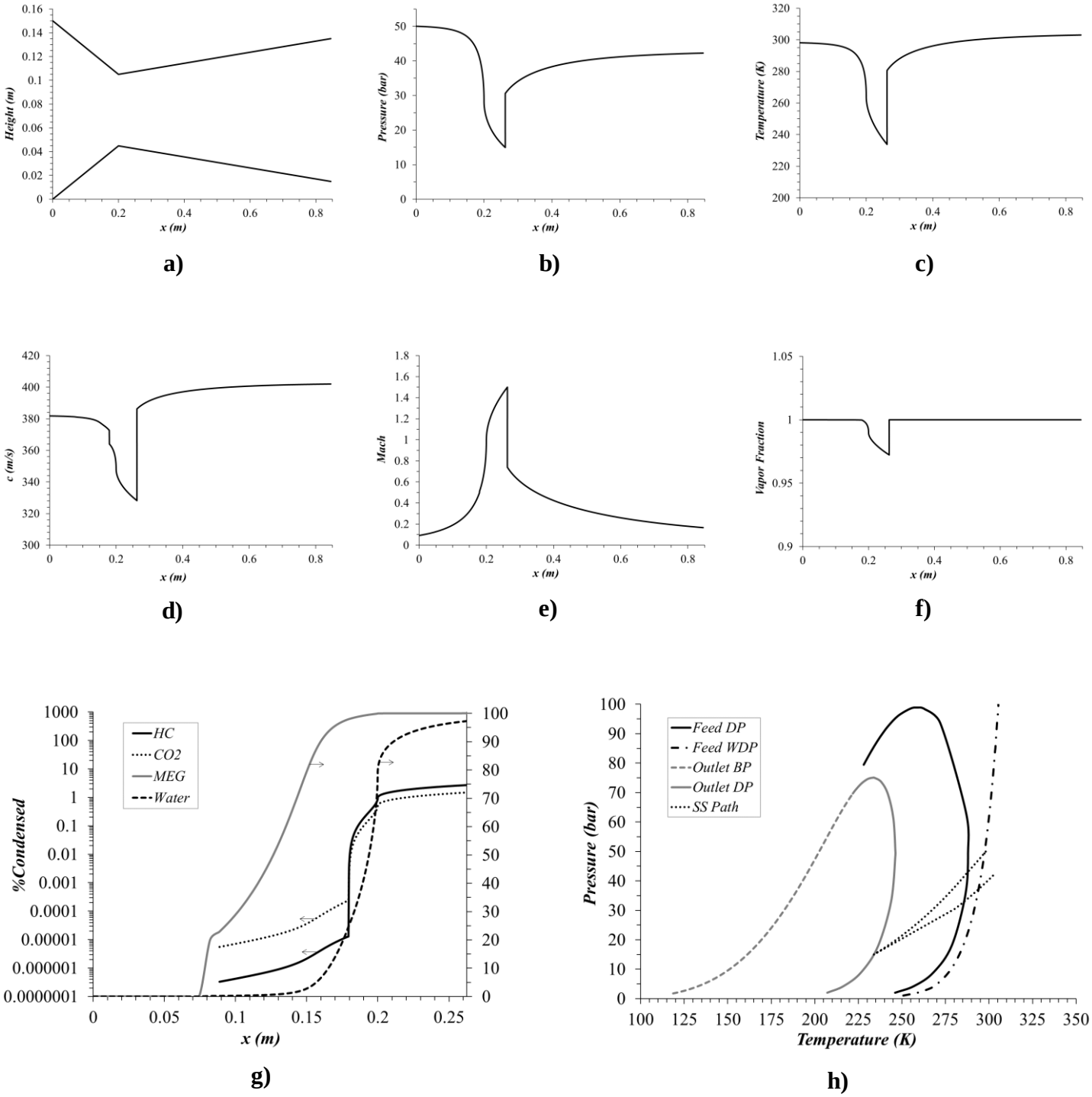

Figure III.10. SS Profiles for SS-THI-Recovery with MEG: (a) Flow Section; (b) *P* (bar); (c) *T* (K); (d) Sound Speed *c* (m/s); (e) *Ma*; (f) Mol Vapor Fraction; (g) %Condensed HCs, CO_2, H_2O, THI; (h) Plane *T x P* with SS Path, VLE Envelopes of SS Feed and Lean Gas and WDP Curve of SS Feed

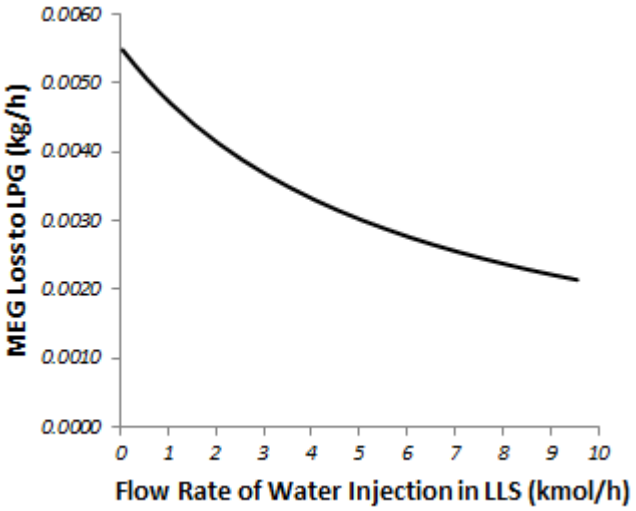

Figure III.11. MEG Loss to LPG versus water Flow Rate in LLS

Table III. 5a. SS-THI-Recovery for MEG as THI: Water Injected in LLS versus Heat Consumption of MEG THI-RU

Water Injected in LLS (kmol/h)	*Heat Consumption (kW) of THI-RU*
0.048	*4099.6*
1	*4113.0*
2	*4127.2*
3	*4141.7*
4	*4156.2*
5	*4170.7*
6	*4185.1*

Table III.5b. Streams of SS-THI-Recovery for MEG as THI

System			*SS & LTX*			*LLS Vessel*		*LPG Flash*		*NG Header*	*HPS**	*THI-RU*		
Stream [#]	*HPS Gas* [$]	*SS Feed*	*L+W Condensate*	*L+W LTX*	*SS Gas*	*Aqueous Bottoms*	*HCs Top*	*Gas*	*Raw LPG*	*Final NG*	*Aqueous THI*	*Flash Vent*	*ADC Vent*	*Lean THI* [&]
T(°C)	*25*	*25*	*-40.6*	*20*	*29.9*	*20*	*20*	*50*	*50*	*30.6*	*25*	*25*	*45*	*45*
P(bar)	*50*	*50*	*42.2*	*42.2*	*42.2*	*42.2*	*42.2*	*20*	*20*	*42.2*	*50*	*1.6*	*1*	*1*
MMsm^3/d	*6.003*	*3.001*	*0.083*	*0.166*	*5.837*	*0.003*	*0.163*	*0.039*	*0.124*	*5.876*	*0.164*	*5.10^{-4}*	*4.10^{-5}*	*0.063*
%Vapor	*100*	*100*	*0*	*0*	*100*	*0*	*0*	*100*	*0*	*100*	*0*	*100*	*100*	*0*
%CH_4	*85.43*	*85.43*	*12.19*	*12.19*	*87.51*	*0.05*	*12.44*	*38.76*	*4.19*	*87.19*	*0.21*	*70.09*	*26.17*	*0.00*
%C_2H_6	*8.25*	*8.25*	*13.48*	*13.48*	*8.11*	*0.01*	*13.76*	*24.44*	*10.41*	*8.21*	*0.04*	*13.77*	*14.23*	*0.00*
%C_3H_8	*3.06*	*3.06*	*22.51*	*22.51*	*2.50*	*0.00*	*22.98*	*20.98*	*23.61*	*2.63*	*0.02*	*5.18*	*6.82*	*0.00*
%i-C_4H_{10}	*0.47*	*0.47*	*8.19*	*8.19*	*0.25*	*0.00*	*8.36*	*4.16*	*9.68*	*0.28*	*0.00*	*0.41*	*0.33*	*0.00*
%C_4H_{10}	*0.85*	*0.85*	*18.10*	*18.10*	*0.36*	*0.00*	*18.48*	*7.40*	*21.96*	*0.41*	*0.01*	*1.67*	*3.27*	*0.00*
%i-C_5H_{12}	*0.20*	*0.20*	*5.99*	*5.99*	*0.04*	*0.00*	*6.11*	*1.30*	*7.62*	*0.04*	*0.00*	*0.08*	*0.04*	*0.00*
%C_5H_{12}	*0.24*	*0.24*	*7.53*	*7.53*	*0.03*	*0.00*	*7.69*	*1.38*	*9.67*	*0.04*	*0.00*	*0.33*	*0.54*	*0.00*
%C_6H_{14}	*0.21*	*0.21*	*7.41*	*7.41*	*0.01*	*0.00*	*7.56*	*0.50*	*9.78*	*0.01*	*0.00*	*0.26*	*0.48*	*0.00*
%C_7H_{16}	*0.06*	*0.06*	*2.16*	*2.16*	*0.00*	*0.00*	*2.20*	*0.06*	*2.87*	*0.00*	*0.00*	*0.07*	*0.14*	*0.00*
%CO_2	*0.64*	*0.64*	*0.35*	*0.35*	*0.65*	*0.01*	*0.35*	*0.89*	*0.18*	*0.65*	*0.03*	*6.25*	*38.32*	*0.00*
ppm H_2O	*590*	*593*	*---*	*---*	*16*	*---*	*253*	*683*	*118*	*21*	*---*	*---*	*---*	*---*
% H_2O	*---*	*---*	*2.09*	*2.09*	*---*	*99.74*	*---*	*---*	*---*	*---*	*75.96*	*1.60*	*9.61*	*37.68*
ppm THI	*1*	*1*	*42*	*42*	*0*	*---*	*0.3*	*0.1*	*0.4*	*0*	*---*	*17*	*0*	*---*
%THI	*---*	*---*	*---*	*---*	*---*	*0.20*	*---*	*---*	*---*	*---*	*23.72*	*---*	*---*	*62.32*

[#] *%mol;* [$] *Before water injection;* [&] *After THI make-up; * No liquid HC phase*

III.4.4. Discussion

The new SS-THI-Recovery process was successfully demonstrated to recover THIs methanol, ethanol and MEG from the gas phase leaving the HPS in any gas processing rig connected to offshore THI loops for NG production. SS-THI-Recovery can be installed as a simple appendix of THI-RU plants that traditionally recover THI from the THI-water phase from HPS bottoms. SS-THI-Recovery generates two revenue factors and one cost-reducing factor to the gas processing rig: (i) NG is produced with WDPA and HCDPA, ready for commercialization and/or exportation; (ii) Raw LPG which can be refined producing commercial LPG and solvents; and (iii) THI is recovered from the HPS gas, reducing its losses from *79%* to *99%* depending on the THI.

Table III.6 depicts the compositions of the Raw HPS gas, the final treated NG and of the Raw LPG obtained with SS-THI-Recovery process for methanol, ethanol and MEG as THIs, while Table III.7 presents the main yield results of SS-THI-Recovery for methanol, ethanol and MEG as THIs. All SS-THI-Recovery cases present similar compositions and yields for the produced Raw LPG and final treated NG, the two main sources of revenues with SS-THI-Recovery, jointly with the reduction of THI make-up costs. These products were left in perfectly marketable conditions with good yield by SS-THI-Recovery: the Raw LPG product with *≈15%mol* C1-C2, *≈55%mol* C3-C4, *≈30%mol* C5+, while the NG is within the appropriate WDP and HCDP ranges. Raw LPG has commercial value because it can be further reprocessed in refineries to produce *55%mol* of directly marketable commercial LPG (C3-C4), *30%mol* of solvents (C5+) and *15%mol* of fuel gas. As ethanol has higher affinity for HCs, relatively to methanol and MEG, it is present in Raw LPG with a higher final content (*≈1% mol*). On the other hand, as MEG has extremely high affinity for H_2O and has low volatility, it was well extracted in the LLS and did not accumulate significantly in LPG nor in final NG.

Table III.7 clearly shows that SS-THI-Recovery from HPS gas is effective and has good performance for the three mostly used THIs: methanol, ethanol and MEG. THI losses are reduced by at least *79%* (for Ethanol as THI), admitting that THI present in HPS gas would be totally lost without this new process. For methanol, losses are reduced by *91.9%* with SS-

THI-Recovery, while MEG losses are reduced by *99.2%*. Hence, SS-THI-Recovery effectively reduces THI losses to HPS gas. Consequently, it is economically advantageous, as it means, besides the two aforementioned associated revenues factors, lower THI make-up costs, as well as lower indirect costs of THI transportation and storage in gas processing rigs.

Therefore, volatile THIs like methanol and ethanol can be made more competitive against MEG, since the main reason for not employing volatile THIs are their huge losses to HPS gas. Fig III.12 illustrates how total THI losses can be reduced by using the new SS-THI-Recovery process, when compared with not using such process, supposing that THI in HPS gas would be totally lost in gas processing and exportation. Further, the SS-THI-Recovery process would also bring reduction in footprint and weight due to the lower volume of THI storage, which is a relevant factor in offshore rigs. Finally, the produced NG is ready for export and commercialization and does not require additional treatment steps.

At first, one could conjecture that SS-THI-Recovery is an unnecessary alternative because a simple wash with chilled or ambient temperature water could recover the *≈1000 ppm* of THI from the HPS gas as suggested by the SS profiles for MeOH and EtOH cases respectively in Figs. III.6g and III.8g. These figures show that about *35%* of THI is already recovered just by contacting raw NG with liquid water at the SS inlet temperature under 3:1 water/THI mol ratio. Unfortunately there are several facts that evidence this conjecture as comparatively inferior to SS-THI-Recovery.

In the first place, due to the high triple point temperature of water, chilled water cannot be used below 0^oC, while it is clearly seen in Figs. III.6c, III.6e, III.8c and III.8e, that only below -13^oC the recovery of THIs surpasses *60%* with low water/THI ratio of only 3:1 in mol. On the other hand, it must be added that water freezing is not an issue in SS-THI-Recovery, because water behaves as a metastable super-cooled liquid during the few milliseconds of contact at $\approx -38^oC$ in the supersonic section of SS nozzles. Besides, water freeze-out is also impeded to occur in SS-THI-Recovery since – thanks to the water/THI capture ratio of 3:1 – in the SS supersonic section the water phase has about *25%mol* of THI methanol or ethanol or MEG, all known to be excellent depressors of the freezing point of water.

In the second place, it must be realized that the raw gas is originally warm at 25^oC and its flow rate is enormous – about $6MMsm^3/d \approx 5500\ t/d$ in our examples, but it could be higher in real cases. Therefore, the cold water flow rate to contact such gigantic warm raw gas flow rate with ordinary contacting devices would be also huge; otherwise the supposed cold contact temperature is not attained. How much would be the cost of such huge cold water flow rate to contact the raw gas to capture just about $\approx 1000\ ppm$ of THI? Moreover, how much would cost such gigantic battery of scrubber or knock-out vessels (in case of inline mixers) operating at high gas pressure (*50 bar*)? Similar issues will also exist if only ambient temperature water is used for water-wash the raw NG. That is, the water flow rate will also have to be ponderable in order to provide a sufficient contact in ordinary contacting devices, otherwise one has to be satisfied with a mediocre recovery of only $\approx 35\%$ as seen in the ambient temperature SS inlet in Figs. III.6g and III.8g. Besides, ambient temperature water-wash will also require some investment with high-pressure scrubbers or knock-out vessels (in case of inline mixers).

In the third place, even assuming that a huge flow rate of cold water could be feasible to wash the raw gas, how much would cost the associated gigantic water refrigeration service? And how about the distillation costs to process huge flow rate of "rich" water leaving such gas scrubbers with something like $\approx 2000\ ppm$ of THI ($2\%mol$)?

In the fourth place, contacting raw gas with cold or even ambient temperature water does not produce HCDPA and would saturate the raw NG with water, implying that WDPA and HCDPA still have to be applied to the raw NG by means of conventional dehydration and HC removal processes, both costly and very footprint intensive operations in offshore gas processing platforms.

Counterpointing this water-wash conjecture, it is easily seen that the proposed SS-THI-Recovery process is fairly superior and much more practical. SS-THI-Recovery uses much less fresh water much more efficiently and without any need of refrigeration. Only about 3:1water/THI mol ratio at ambient temperature is necessary in the SS inlet, because water-THI contact will occur much more intensively at $\approx -38^oC$ during only a few milliseconds of residence time through the SS flow path. Additionally, to process such huge raw NG flow rate of $6MMsm^3/d$ only two 6" SS nozzles and a LTX vessel are necessary, with about $\approx 84\%$ of

pressure recovery (i.e. the head loss in the SS nozzles is only of *≈16%*), which means a low power demand to recompress the gas to its original pressure. It is also worth of mention that the required LTX is not a particularly large vessel as it is fed with only the cold L+W condensate (about *≈3%* of the raw NG inlet flow rate) ejected through the separation vanes of the SS nozzles. Besides its efficient, low footprint demanding and not too costly recovery of THI from the raw NG, SS-THI-Recovery also simultaneously treats the raw NG executing WDPA+HCDPA and producing raw LPG with commercial value. In this regard it must be mentioned that WDPA and HCDPA are produced by SS-THI-Recovery with sufficient grade for NG commercialization and transport through subsea pipelines. As shown in Table III.6 and considering all THI cases, the final treated NG has less than *≈21 ppm* of water, less than *≈92 ppm* THI and less than *≈3.5%mol* C3+, while the untreated raw NG from HPS has more than *≈600 ppm* H_2O, more than *≈1000 ppm* THI (except in MEG case) and more than *≈5%mol* C3+.

Table III.6. SS-THI-Recovery: %Mol Compositions of Raw HPS Gas, Produced Raw LPG and Treated Final NG for Methanol, Ethanol and MEG as THIs

	Raw HPS Gas			***Produced Raw LPG***			***Treated Final NG***		
THI	***MeOH***	***EtOH***	***MEG***	***MeOH***	***EtOH***	***MEG***	***MeOH***	***EtOH***	***MEG***
$MMsm^3/d$	*6.012*	*6.009*	*6.003*	*0.120*	*0.122*	*0.124*	*5.88*	*5.88*	*5.88*
P (bar)	*50*	*50*	*50*	*19.5*	*19.5*	*19.5*	*42.1*	*42.1*	*42.2*
T (^oC)	*25*	*25*	*25*	*45*	*45*	*45*	*31.3*	*31.2*	*30.6*
%CH_4	*85.29*	*85.33*	*85.43*	*4.23*	*4.23*	*4.19*	*87.13*	*87.15*	*87.19*
%C_2H_6	*8.24*	*8.25*	*8.25*	*10.25*	*10.24*	*10.41*	*8.22*	*8.22*	*8.21*
%C_3H_8	*3.05*	*3.05*	*3.06*	*23.04*	*22.97*	*23.61*	*2.65*	*2.65*	*2.63*
%i-C_4H_{10}	*0.47*	*0.47*	*0.47*	*9.57*	*9.50*	*9.68*	*0.28*	*0.28*	*0.28*
%C_4H_{10}	*0.85*	*0.85*	*0.85*	*21.90*	*21.70*	*21.96*	*0.42*	*0.42*	*0.41*
%i-C_5H_{12}	*0.20*	*0.20*	*0.20*	*7.75*	*7.64*	*7.62*	*0.05*	*0.05*	*0.04*
%C_5H_{12}	*0.24*	*0.24*	*0.24*	*9.86*	*9.73*	*9.67*	*0.04*	*0.04*	*0.04*
%C_6H_{14}	*0.21*	*0.21*	*0.21*	*10.07*	*9.90*	*9.78*	*0.01*	*0.01*	*0.01*
%C_7H_{16}	*0.06*	*0.06*	*0.06*	*2.96*	*2.91*	*2.87*	*0.00*	*0.00*	*0.00*
%CO_2	*0.64*	*0.64*	*0.64*	*0.19*	*0.19*	*0.18*	*0.65*	*0.65*	*0.65*
ppm H_2O	*663*	*630*	*590*	*167*	*291*	*118*	*20*	*21*	*21*
ppm THI	*1514*	*1100*	*1*	*1719*	*9569*	*0.4*	*92*	*35*	*0*

Table III. 7. Yield Results of SS-THI-Recovery for Methanol, Ethanol and MEG as THIs

	THI		
	MeOH	*EtOH*	*MEG*
THI flow rate in HPS[&] gas	*505.7 kg/h*	*527.8 kg/h*	*0.74 kg/h*
Loss of THI to final NG[*]	*30.0 kg/h*	*16.2 kg/h*	*0.00023 kg/h*
Loss of THI to Raw LPG[*]	*11.5 kg/h*	*93.3 kg/h*	*0.0055 kg/h*
Total flow rate of injected THI	*1943.7 kg/h*	*3142.7 kg/h*	*4195.8 kg/h*
Fraction of injected THI in HPS[&] gas	*26.0 %*	*16.8%*	*0.0176%*
THI loss to final NG[*] and Raw LPG[*]	*2.1 %*	*3.48%*	*0.000137%*
Reduction of THI losses to HPS gas[*]	*91.9 %*	*79.3%*	*99.22%*
THI loss in THI-RU Process	*1.35 kg/h*	*1.59 kg/h*	*0.0009 kg/h*
Total THI loss[#] without SS-THI-Recovery	*26.1%*	*16.8%*	*0.024%*
Total THI loss[*] with SS-THI-Recovery	*2.3%*	*3.6%*	*0.00016%*

[*]with the proposed SS-THI-Recovery process; [#]without the proposed SS-THI-Recovery process; [&]high-pressure three-phase separator

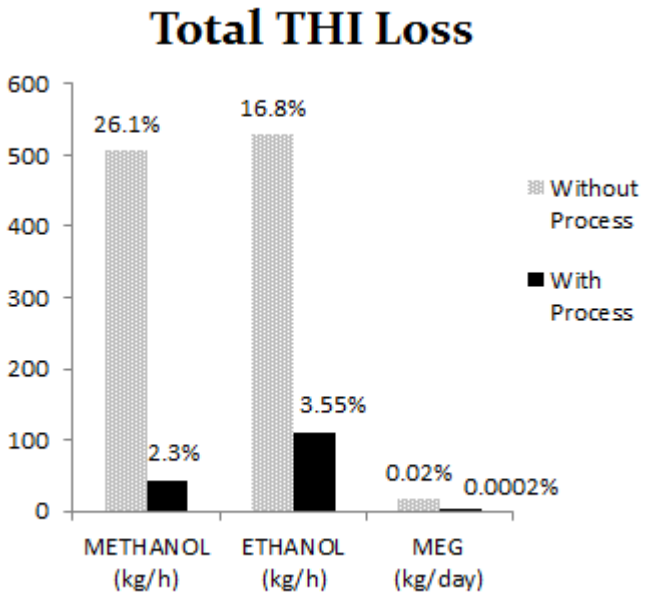

Figure III.12. Total THI Losses with/without SS-THI-Recovery Process

III.5. Conclusions

A new process using supersonic separator (SS) to recover THI commonly lost to gas phase from the high-pressure three-phase separator (HPS) of gas processing rigs is disclosed and analyzed. The new process – SS-THI-Recovery – uses supersonic separators (SS), water injections, LTX separator and a high-pressure liquid-liquid separator (LLS) to recover THIs originally being lost in gas phase.

SS is a recent separating technology that promotes a partial depressurization of a gas feed achieving low temperatures in its supersonic section, which allows to condense and to collect water, THI and heavy HCs (C3+), hence simultaneously executing WDPA and HCDPA of the gas, besides recovering THIs from gas phase. As super-cooled water is produced in SS nozzles of SS-THI-Recovery, the two-phase L+W condensate is ejected from SS directly to a so-called LTX separator to impede hydrate and ice formation.

A keystone of the new SS-THI-Recovery is that liquid water should be injected into the SS inlet with the raw NG feed. The injected water flow rate is proportional (≈3:1 mol/mol) to the THI flow rate in order to provide a permanent water liquid phase along SS flow path to drag THI from the vapor phase and from the forming C3+ liquid phase, so as to recover it to the aqueous phase ejected into the LTX. This stratagem – however paradoxical it may appear, as it proposes to soak raw NG with liquid water – worked perfectly, as shown in Secs. III.4.1, III.4.2 and III.4.3, respectively for THIs MeOH, EtOH and MEG.

Evidently, new SS-THI-Recovery could only be quantitatively demonstrated – without prototypes and experiments – if a competent and precise simulation resource is available for solving SS nozzles with three-phase VLWE supersonic flow and also able to calculate, with accuracy, the three-phase VLWE thermodynamic sound speed property. Moreover, to be reliable, calculations must use appropriate EOS's to handle multiphase equilibrium and multiphase properties for complex polar systems containing HCs, water and hydroxylated THIs. All these requisites were met in this work making its results of confidence. New SS-THI-Recovery was simulated in HYSYS 8.8 using SS-UOE (Arinelli et al., 2017), a thermodynamically rigorous HYSYS UOE for simulating SS with multiphase equilibrium

flow path in connection with PEC-UOE (de Medeiros et al., 2017), another UOE for calculating the phase-equilibrium sound speed property in multiphase flow. All SS calculations by SS-UOE and PEC-UOE adopted CPA-EOS (Folas et al., 2005), a widely recognized EOS to handle multiphase systems with water, hydroxylated THIs and HCs.

It is also important to realize that our SS and sound speed approaches are not based on Computational Fluid Dynamics (CFD). Instead, our methods are totally based on equilibrium thermodynamics with rigorous phase-split algorithms – e.g. *Flash(P,S), Flash(P,H) and Flash(P,T)* rendered by HYSYS 8.8 – continuously running along the SS flow path (Arinelli et al., 2017). On the other hand, it is fairly known that ordinary CFD SS simulations with raw NG feeds cannot generate correct phase behavior and phase-change effects along the SS flow path. Thus, a typical symptom of ordinary CFD SS simulations with raw NG are the incredibly low temperatures attained in the SS supersonic section; evidently a consequence of ignoring enthalpy releases from condensations under adiabatic SS regime. Thus, checks based on the 2nd Law of Thermodynamics applied to such CFD SS solutions with raw NG feeds promptly reveal adiabatic destruction of entropy at the pre-shock thanks to the improperly attained colder temperature. This is a forbidden outcome according to the 2nd Law, which states that entropy, once created, is indestructible and can only be moved away via non-adiabatic transfers, otherwise it must stay in the stream. Unfortunately, the literature is plenty of "entropy-killer" CFD solutions of SS with raw NG. Some of them were detected in Arinelli et al. (2017) via 2nd Law checks using reliable EOS and allowing phase-changes.

The thermodynamic rigor of our SS simulations involving three-phase VLWE supersonic flow was amply showed in the results of SS-THI-Recovery for MeOH (Sec. III.4.1), EtOH (Sec. III.4.2) and MEG (Sec. III.4.3). Nevertheless, taking into account that the subject is eminently thermodynamic, a thorough use of classical thermodynamic diagrams could be argued. Therefore, the capabilities of our methods are shown here for MeOH, EtOH and MEG cases of SS-THI-Recovery by drawing the respective SS Paths on $T \times \bar{S}$ diagrams. As SS nozzles operate adiabatically, $T \times \bar{S}$ diagrams also have the property of evidencing 2nd Law violations in SS simulations. Using only $T \times \bar{S}$ planes, Fig. III.13 depicts the same SS paths shown in Figs. III.6, III.8 and III.10, respectively for SS-THI-Recovery with MeOH (Figs.

III.13a and III.13b), EtOH (Figs. III.13c and III.13d) and MEG (Figs. III.13e and III.13f). The $T\,x\,\bar{S}$ on the right (Figs. III.13b, III.13d and III.13f) are magnifications of the respective $T\,x\,\bar{S}$ on the left (Figs. III.13a, III.13c and III.13e). WDP, HCDP, BP loci of feed and lean gas are also drawn in $T\,x\,\bar{S}$ coordinates. In MeOH and EtOH cases the SS paths start already below the WDP loci – i.e. their SS feeds have liquid water – while in MEG case the SS path starts a little above WDP locus. All SS paths then proceed isentropically downwards (A→B paths in Figs. III.13b, III.13d and III.13f) until below the HCDP+BP dome of the lean gas, implying three-phase VLWE equilibrium. This is the coldest SS point with maximum *Ma* at the pre-shock. As L+W condensates are withdrawn, all SS paths now move isothermally to the right (B→C paths in Figs. III.13b, III.13d and III.13f) towards the lean gas HCDP. At theirs HCDP's the lean gases are dry but still supersonic. This is the theoretical best point for the normal shock, which is the only irreversible entropy creating step in all SS simulations as SS pre-shock expansions and after-shock compressions are isentropic by Premise [P9], Sec. III.3.2 (SS-UOE could also handle non-isentropic expansion and compression steps, if adiabatic efficiencies $\eta^{EXP}\%$ and $\eta^{CMP}\%$ are chosen lesser than 100%). All SS paths now cross their normal shock fronts, where sudden heating, recompression and entropy creation occur, only seen in the magnified diagrams (C→D inclined rectilinear paths in Figs. III.13b, III.13d and III.13f). After the shock, all SS paths perform isentropically upwards (D→E paths in Figs. III.13b, III.13d and III.13f) continuously recompressing and heating the superheated lean gas flow until the SS outlet.

The assessment of SS-THI-Recovery performances shows that at least 91% of MeOH, 79% of EtOH and 99% of MEG that would be lost to HPS gas can be successfully recovered by this new process. Additionally, such recoveries could be further raised by increasing the flow rate of water injected in the high-pressure liquid-liquid separator (LLS) after LTX. Such high THI recoveries entail a very significant reduction of cost associated with THI make-up, storage and transportation. Moreover, SS-THI-Recovery process is simple, with low footprint and easy implementation, even for less volatile THIs like MEG. SS-THI-Recovery also aggregates two revenue factors: (i) Treated NG is ready for exportation and commercialization, without noticeable flared inventories and additional treatment; and (ii) Raw LPG is a liquid

commodity with commercial value ready to be sold to refineries to produce commercial LPG, solvents and fuel gas. Hence, SS-THI-Recovery is an innovative, useful and potentially economically feasible alternative for NG treatment and THI recovery in offshore gas platforms.

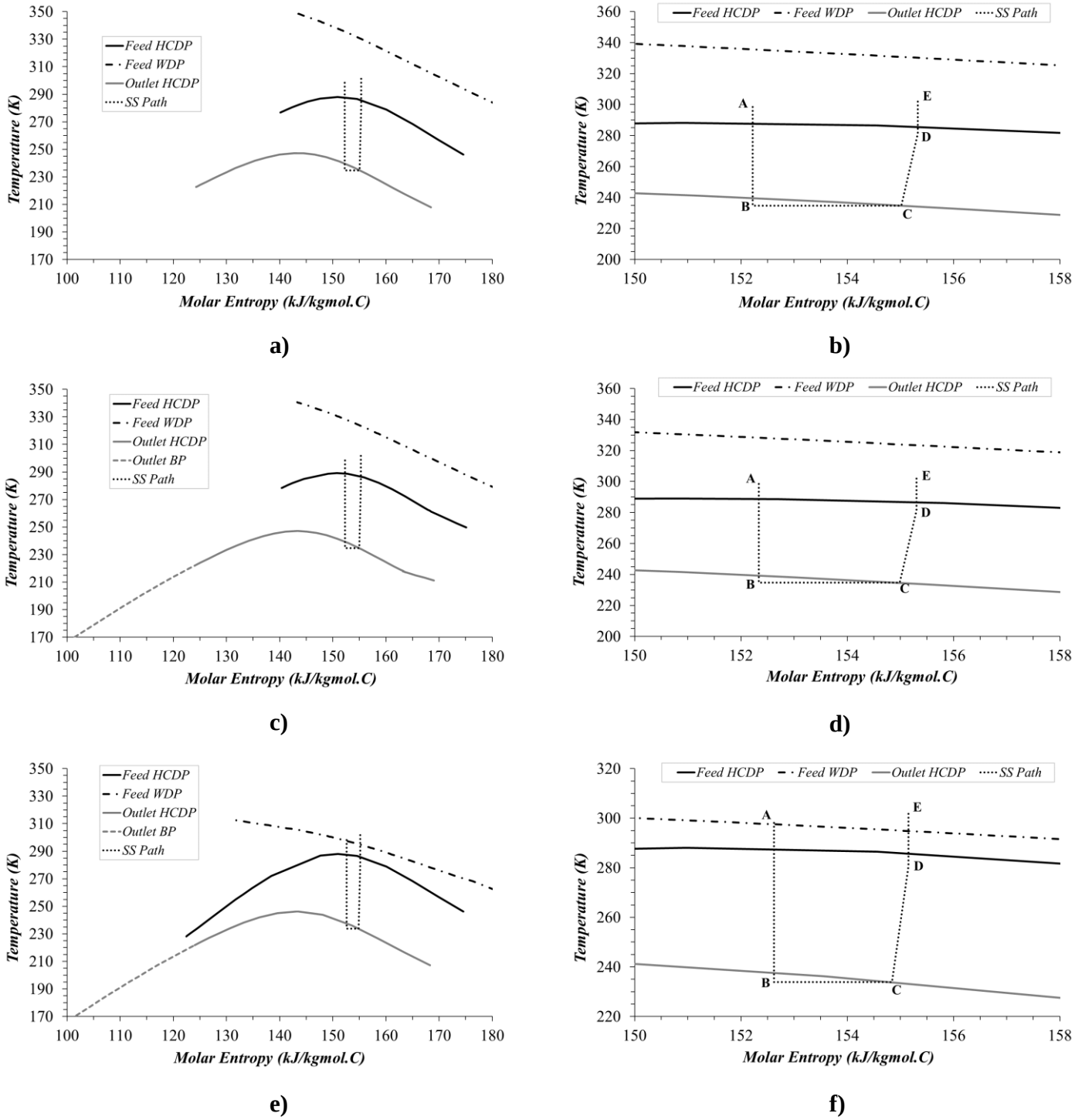

Figure III.13. SS Paths on Plane $T\ x\ \bar{S}$ for SS-THI-Recovery: (a) MeOH Case with Feed WDP and HCDP Loci and Lean Gas HCDP Locus; (b) Magnification of MeOH Case SS Path; (c) EtOH Case with Feed WDP and HCDP Loci and Lean Gas HCDP and BP Loci; (d) Magnification of EtOH Case SS Path; (e) MEG Case with Feed WDP and HCDP Loci and Lean Gas HCDP and BP Loci; (f) Magnification of MEG Case SS Path

III.6 Acknowledgments

Authors acknowledge financial support from Petrobras S.A. J.L. de Medeiros and O.Q.F. Araújo also acknowledge financial support from CNPq-Brazil.

III.7. References

Aspentech (Ye, V. and Rumyanteseva, I). Jump Start: CPA and Methanol Partitioning. A Brief Tutorial, 2015, Aspen Technology Inc.

Alharooni K., Barifcani A., Pack D., Gubner R., Ghodkay V., 2015. Inhibition effects of thermally degraded MEG on hydrate formation for gas systems. Journal of Petroleum Science and Engineering. 135(1):608-617. http://dx.doi.org/10.1016/j.petrol.2015.10.001

Arinelli L.O., Trotta T.A.F., Teixeira, A.M., de Medeiros, J.L., Araújo O.Q.F., 2017. Offshore Processing of CO2 Rich Natural Gas with Supersonic Separator versus Conventional Routes. Journal of Natural Gas Science and Engineering. Vol. 46, pp. 199-221. http://dx.doi.org/10.1016/j.jngse.2017.07.010

de Medeiros, J.L., Arinelli, L.O., Araújo, O.Q.F., 2017. Speed of sound of multiphase and multi-reactive equilibrium streams: a numerical approach for natural gas applications. Journal of Natural Gas Science and Engineering. Vol. 46, pp. 222-241. https://doi.org/10.1016/j.jngse.2017.08.006

Dong, L., ZhenYu, C., XingPeng, G., 2008. The effect of acetic acid and acetate on CO2 corrosion of carbon steel. Anti-Corros. Methods Mater. 55 (3), 130-134. http://dx.doi.org/10.1108/00035590810870437

Feygin, V., Imayev, S., Alfyorov, V., Bagirov, L., Dmitriev, L., Lacey, J., 2006. Supersonic gas technologies, in: 23rd World Gas Conference. International Gas Union, Amsterdam, The Netherlands.

Folas, G.K., Gabrielsen, J., Michelsen, M.L., Stenby, E.H., Kontogeorgis, G.M., Application of the Cubic-Plus-Association (CPA) Equation of State to Cross-Associating Systems. Ind. Eng. Chem. Res. 2005, 44, 3823−3833

Haghighi H., Chapoy A., Burgess R., Tohidi B., 2009. Experimental and thermodynamic modelling of systems containing water and ethylene glycol: Application to flow assurance and gas processing. Fluid Phase Equilibria; 276(1):24–30. http://dx.doi.org/10.1016/j.fluid.2008.10.006

Hould N., Elanany M.S., Aleisa R.M., Al-Majnouni K.A., Al-Malki A., Abba I., 2015. Evaluating polymeric inhibitors of ethane clathrate hydrates. Journal of Natural Gas Science and Engineering, Volume 24, Pg 543–549. http://doi.org/10.1016/j.jngse.2015.03.041

Ikeh, L., Enyi, G.C., Nasr, G.G., 2016. Inhibition Performance of Mild Steel Corrosion in the Presence of CO2, HAc and MEG. 2016. http://doi.org/10.2118/179942-MS

Karakatsani E.K., Kontogeorgis G.M., 2013. Thermodynamic Modeling of Natural Gas Systems Containing Water. Ind. Eng. Chem. Res. 2013, 52, 3499−3513. http://dx.doi.org/10.1021/ie302916h

Machado, P.B., Monteiro, J.G.M., de Medeiros, J.L., Epsom, H.D., Araújo, O.Q.F., 2012. Supersonic separation in onshore natural gas dew point plant. J. Nat. Gas Sci. Eng. 6, 43–49. http://dx.doi.org/10.1016/j.jngse.2012.03.001

Nazzer C.A., Keogh J., 2006. Advances in Glycol Reclamation Technology. Offshore Technology Conference; 18010. http://dx.doi.org/10.4043/18010-MS

Nazeri, M., Tohidi, B., Chapoy, A., 2012. An Evaluation of Risk of Hydrate Formation at the Top of a Pipeline. Society Of Petroleum Engineers. SPE-160404-MS. http://doi.org/10.2118/160404-MS

Psarrou, M.N., Jøsang L.O., Sandengen K., Østvold T., 2011. Carbon Dioxide Solubility and Monoethylene Glycol (MEG) Degradation at MEG Reclaiming/Regeneration Conditions. Journal of Chemical & Engineering Data. 56 (12), 4720-4724. http://dx.doi.org/ 10.1021/je200709h

Son K.V., Wallace C., 2000. Reclamation/regeneration of glycols used for hydrate inhibition. Deep Offshore Technology. http://reclaim.com/wp-content/uploads/2013/10/reclamation-regeneration-of-glycols-used-for-hydrate-inhibition.pdf [Accessed 14 June 2017]

Teixeira, A.M., Arinelli, L.O., de Medeiros, J.L., Araújo, O.Q.F., 2016. Exergy Analysis of Monoethylene Glycol Recovery Processes for Hydrate Inhibition in Offshore Natural Gas Fields. Journal of Natural Gas Science & Engineering, Volume 35, pp. 798-813. http://dx.doi.org/10.1016/j.jngse.2016.09.017

Teixeira, A.M., Arinelli, L.O., de Medeiros, J.L., Araújo, O.Q.F., 2017. Processo para recuperar inibidores termodinâmicos de hidratos de gás de cargas de gás natural utilizando separador supersônico simultaneamente ajustando ponto de orvalho de hidrocarbonetos e ponto de orvalho de água do gás final Brazilian Patent Application No. BR 10 2017 015092 5. Filed in July 13, 2017.

Tzirakis F., Karakatsani E., Kontogeorgis G.M, 2016. Evaluation of the Cubic-Plus-Association Equation of State for Ternary, Quaternary, and Multicomponent Systems in the Presence of Monoethylene Glycol. Ind. Eng. Chem. Res. 55(43), pp 11371–11382.

CHAPTER IV - ECONOMIC LEVERAGE AFFORDS POST-COMBUSTION CAPTURE OF 43% OF CARBON EMISSIONS: SUPERSONIC SEPARATORS FOR METHANOL HYDRATE INHIBITOR RECOVERY FROM RAW NATURAL GAS AND CO_2 DRYING

Article published in Journal of Environmental Management, Vol. 236 (2019), pp 534-550 (doi: 10.1016/j.jenvman.2019.02.008).

Economic Leverage Affords Post-Combustion Capture of 43% of Carbon Emissions: Supersonic Separators for Methanol Hydrate Inhibitor Recovery from Raw Natural Gas and CO_2 Drying

Alexandre Mendonça Teixeira[1a], Lara de Oliveira Arinelli[2a], José Luiz de Medeiros[*a] and Ofélia de Queiroz F. Araújo[3a]

[a]Escola de Química, Federal University of Rio de Janeiro. Av. Horacio Macedo, 2030, Bl. E, 21949–900, Rio de Janeiro, RJ, Brazil

*Corresponding author: jlm@eq.ufrj.br

[1]alexandremtxr@gmail.com, [2]lara.arinelli@gmail.com, [3]ofelia@eq.ufrj.br

Abstract

Offshore oil/gas productions are power intensive and CO_2 emitters from gas-fired power generation. This work investigates supersonic separator as a strategy for affording post-combustion capture backed up by cost reductions. Conventional offshore gas processing usually loses thermodynamic hydrate inhibitor methanol in processing and exported gas. This work analyses a supersonic separator variant gas processing simultaneously reducing methanol losses. Such process dramatically improves gas-plant profitability via cost-reduction of methanol make-up and power-consumption, simultaneously increasing revenues from liquefied-petroleum-gas by-product. This economic leverage affords post-combustion carbon capture, including subsequent CO_2 dehydration and compression for exportation of high-pressure liquid CO_2. This corresponds to abate 43% of CO_2 emissions boosting revenues via enhanced oil recovery. Moreover, CO_2 is dehydrated via another supersonic separator operating with minimum head-loss, minimizing compression costs. Despite its much higher investment, the new process with carbon capture presents higher net value (865.63 MMUSD) than the conventional processing without carbon capture (829.31 MMUSD), being economically feasible and more environmentally adequate with cleaner natural gas production and successful CO_2 management. The new process is superior in several scenarios and particularly favored by oil prices above 55 USD/bbl. Rising oil price from 40 to 100 USD/bbl, the new process net value rises 29%, whereas the conventional counterpart rises only 7.5%. In addition, as a plausible future scenario, CO_2 taxation favors the new process, which always

has superior economic performance, even without CO_2 taxation. In summary, implementing supersonic separators in offshore natural gas processing aiming at anti-hydrate recovery and CO_2 dehydration for enhanced oil recovery creates economic leverage sustaining Carbon Capture & Storage without loss of competitiveness. This result, backed up by rigorous thermodynamic simulations and economic-environmental assessments, configure an original achievement to the literature.

Keywords: Supersonic Separator; Methanol Hydrate Inhibitor; CO_2 Capture and Storage; Post-Combustion Capture; Supersonic Separator CO_2 Drying

Abbreviations

BP Bubble-Point; C3+ Propane and Heavier; CCS Carbon Capture and Storage; CDU CO_2 Compression and Dehydration Unit; CFD Computational Fluid Dynamics; CPA-EOS Cubic-Plus-Association Equation-of-State; CW Cooling-Water *[30°C,45°C]*; FG Fuel-Gas; HCDP Hydrocarbon Dew-Point; HCDPA Hydrocarbon Dew-Point Adjustment; HPS High-Pressure Three-Phase Separator; JT Joule-Thomson; LLS Liquid-Liquid Separator; NGL Natural Gas Liquids; LPG Liquefied-Petroleum-Gas; LTX Anti-Hydrate Separator; MEA Monoethanolamine; $MMSm^3/d$ Millions of standard m^3 per day; MRU Methanol Recovery Unit; NG Natural Gas; PCC-MEA Post-Combustion Capture with Aqueous MEA; PHW Pressurized Hot Water (*210°C*); PR-EOS Peng-Robinson Equation-of-State; SS Supersonic Separator; SW Seawater *[25°C,35°C]*; TEG Triethylene Glycol; UOE Unit Operation Extension; USD U.S. Dollars; WDP Water Dew-Point; WDPA Water Dew-Point Adjustment; WHRU Waste Heat Recovery Unit.

Nomenclature

AP : *Annual profit (USD/y)*

c(P,T,$\underline{Z}$) : *Multiphase-equilibrium sound speed property for multicomponent systems (m/s)*

COM : *Annual cost of manufacturing (USD/y)*

CRM, CUT : *Annual costs of raw materials and utilities (USD/y)*

D_I, D_O : : *SS inlet/outlet internal diameters (m)*

FCI, GAP : *Fixed capital investment (USD) and gross annual profit (USD/y)*

GHET : *Gas-hydrate equilibrium temperature (K)*

Ma, Ma^{Shock} : *Mach Number and Ma before normal shock and condensate withdrawal*

Ma_{BS}, Ma_{AS} : *Ma just before shock and after condensate withdrawal, and Ma just after shock*

N : *Horizon (years)*

nc ; *Number of components*

NPV, REV : *Net present value (USD) and revenues (USD/y)*

P, P_{BS}, P_{AS} : *Pressure and pressures just before shock and just after shock (bar)*

T, T_{BS}, T_{AS} : *Temperature and temperatures just before shock and just after shock (K)*

v : *Multiphase flow velocity (m/s)*

x : *SS axial position (m)*

$\underline{Z}$: *Vector (nc x 1) of species mol fractions*

Greek Symbols

α, β : *SS converging/diverging wall angles (deg)*

$\eta^{EXP}\%, \eta^{CMP}\%$: SS expansion/compression adiabatic efficiencies (%)

ρ : *Density of multiphase fluid (kg/m^3)*

$\Xi_P = \left(\frac{\partial \rho}{\partial P}\right)_{T,\underline{Z}}$: *Multiphase isothermal compressibility (derivative of ρ with P at const. T, $\underline{Z}$) ($kg/Pa.m^3$)*

IV.1. Introduction

There is a growing concern over the increasing atmospheric concentration of greenhouse gases related to human activity, particularly CO_2, since global concentration of this gas in the atmosphere is the main cause of planet climate change and contributes to increase Earth's mean temperature. Therefore, management of CO_2 emissions is a critical issue. Offshore oil and gas industries are large contributors to CO_2 global emissions, as oil-gas platforms are power-intensive for processing and transporting hydrocarbons. In this context, the main CO_2 emissions in oil-gas platforms correspond to exhausts from gas-fired power generation (Cruz et al., 2018).

Many efforts have been recently made with an increasing research on CO_2 mitigation processes associated to energy generation, including pre-combustion, post-combustion and oxy-combustion for Carbon Capture and Storage (CCS) (Olajire, 2010). CCS consists of separation of CO_2 from industrial sources, compression, drying and transportation to storage geologic sites or to enhanced oil recovery (EOR) (Araújo and de Medeiros, 2017). Post-combustion is the most mature alternative for carbon capture, wherein chemical absorption is the only mature technology for large-scale post-combustion capture (PCC) of CO_2 but at expense of high heat-consumption for solvent regeneration (Araújo et al., 2015). On the terrain of new CO_2 mitigation options, Anwar et al., 2018 cites alternative ways for capturing CO_2 in the context of CCS, such as CO_2 capture by algae, CO_2 capture through nanotechnology and CO_2 capture via biochar. In connection with this, Sepehri and Sarrafzadeh (2018) also report a new biological process driven by CO_2 chemical reduction with potential to be used in CO_2 mitigation as well. These few mentions do not have the intent to be exhaustive and only represent a very small sample of all alternative CO_2 mitigation technologies currently being studied. Evidently, they all have some potential, but unfortunately lack successful industrial-scale experience, a decisive factor. Therefore, only a very mature PCC like chemical absorption can be relevant in the present study.

In the scenario of offshore natural gas (NG) processing, gas-fired turboshafts (i.e. gas-turbine shafts with driven machines) constitute the main power-producing system. Turboshaft exhausts have a CO_2 content around $\approx$*5-6%*, as well as low-pressure near atmospheric, so that

PCC with aqueous MEA (PCC-MEA) is preferred (Nguyen et al., 2016). Limitations of driving-force – i.e. CO_2 fugacity – indicate that state-of-the-art membrane permeation is unlikely to compete with PCC-MEA for capturing CO_2 from turboshaft exhausts, so that PCC-MEA remains as the most efficient and cost-effective capture alternative for exhausts of offshore NG processing (Maitland, 2016).

IV.1.1. CCS Plants in Offshore Natural Gas Processing

In addition to the high heat-ratio for PCC-MEA solvent regeneration, compression and dehydration costs associated to the CO_2 stream from PCC-MEA are significant as well, since it must be compressed from $P \approx 1\ atm$ to the EOR export pressure ($P \approx 350\ bar$). The union of PCC-MEA, CO_2 compressors, CO_2 drying and pumping, configures what is called here a complete CCS plant. In other words, CCS plant is much more than merely CO_2 capture via PCC-MEA. It must be able as well to compress, dry and pump liquid or supercritical CO_2 at high-pressure.

Due to high costs and investment for solvent regeneration and CO_2 compression, the decision to install a complete CCS unit is mainly driven by economics. Urech et al. (2013) consider that CCS will only become competitive if new policies limiting emissions or taxing CO_2 are established. In this sense, some countries have already adopted carbon taxation to reduce emissions (Nguyen et al., 2016) and it is believed that the pressure on technological development will only reach sufficient strength under carbon taxes (Lundgren et al., 2018). From an engineering standpoint, carbon taxes can catalyze CCS progress towards technological maturity, when considered as production costs to be avoided by CO_2 abatement and adequate destination (Wiesberg et al., 2017).

Therefore, a decisive factor for CCS implementation in offshore NG processing is carbon taxation. If sufficiently high, the investment of a CCS unit is likely to be more economical than paying taxes during project lifetime. In another perspective, CCS implementation is favored via the development of more efficient processes of superior economic performance, either from higher revenues and/or lower costs, thus making budget room for affording CCS.

Particularly, this work investigates several aspects of novel offshore NG processing as a strategy for implementing emissions abatement via a complete CCS plant backed up by cost reduction and revenues increase.

In the offshore NG industry, NG transportation from production sites to the final destination is a great challenge, particularly in ultra-deepwater oil-gas fields located *≈200 km* from coast, wherein the most appropriate transportation is through submarine pipelines. Raw NG has contaminants that can cause obstructions and damages to the pipeline in such conditions of high-pressure and low-temperatures. Therefore, it is essential to treat the gas on offshore rigs for safe transportation and sales specification. Firstly, NG must be dehydrated via water dew-point adjustment (WDPA) to avoid gas-hydrates and corrosion in NG transporting. Secondly, propane and heavier hydrocarbons (C3+) should be removed from the raw gas via hydrocarbon dew-point adjustment (HCDPA) by means of Joule-Thomson (JT) expansion and/or refrigeration, avoiding condensation in pipelines exposed to low external seabed temperatures. In addition, JT expansion produces natural gas liquids (NGL), a source of revenues. Furthermore, offshore NG fields require continuous injection of thermodynamic hydrate inhibitor methanol in wellheads to avoid gas-hydrates in subsea flowlines. However, when methanol is employed as anti-hydrate, there are high losses to gas phase, entailing direct make-up costs and indirect transport/storage costs. Therefore, one way for achieving economic leverage to implement CCS units is by means of a nonconventional offshore gas processing performing simultaneously WDPA+HCDPA and reducing losses of anti-hydrate methanol.

IV.1.2. Supersonic Separator for NG Processing

The supersonic separator (SS) is a new technology for raw NG processing (Wang and Hu, 2018). SS simultaneously executes WDPA and HCDPA of raw NG by accelerating the gas at supersonic velocities, causing expansion and temperature drop, inducing water and C3+ condensation and posterior centrifugal withdrawal via collecting vanes at the end of the

supersonic section. Hence, SS executes selective WDPA+HCDPA in a single operation, reducing equipment sizes and footprint (Machado et al., 2012).

SS with linear diameter profiles is sketched in Fig. 1, where α and β are wall angles; L_C, L_D and L are converging, diverging and total lengths and D_I, D_T and D_O represent respectively inlet, throat and outlet diameters. SS comprises a static swirling device, followed by a Laval nozzle, a condensate separation section and the ending diffuser ($L^{Diffuser}$). The Laval comprises converging section, throat and diverging section, which ends at the liquid-collecting section, normally followed by a normal shock zone and the ending diffuser, the continuation of the previous diverging section.

SS phenomenology is regulated by the flow Mach Number ($Ma=v/c$) where v is axial flow velocity and c represents the sound speed property (c). The flow accelerates from subsonic to $Ma=1$ at the throat and then becomes supersonic ($Ma>1$) through the diverging section, accompanied by temperature and pressure falls as enthalpy is converted into kinetic energy, forcing water and C3+ to change to (sub-cooled) liquid droplets, centrifugally impelled towards lateral vanes in the liquid-collecting section. After liquid withdrawal, if the flow is still supersonic, the spontaneous normal shock occurs suddenly turning the flow into sub-sonic and adiabatically rising temperature, pressure and entropy. For adequate SS operation, condensate recovery must occur upstream the shock; otherwise re-vaporization across the shock would destroy separation. A critical SS specification is the maximum attained Ma, or Ma^{Shock}, which is the Ma value at the Laval end, before shock and condensate withdrawal. After condensate removal, normally Ma becomes lesser than Ma^{Shock}, though still supersonic and sufficient for shock. This value is represented as Ma_{BS} (Ma just before shock) so that the shock effectively occurs at Ma_{BS} and not at Ma^{Shock}. The sub-sonic Ma after shock is represented as Ma_{AS}, so that, in general, $Ma_{AS}<1<Ma_{BS}<Ma^{Shock}$ (Arinelli et al., 2017). SS with linear diameter profiles (Fig. 1) is specified with the feed stream and D_I, D_O, α, β, $\eta^{CMP}\%$, $\eta^{EXP}\%$, Ma^{Shock}, where $\eta^{CMP}\%$, $\eta^{EXP}\%$ represent adiabatic compression/expansion efficiencies in SS. SS design should determine (Fig. 1) lengths L, L_C, L_D, L^{LAVAL}, $L^{Diffuser}$, throat diameter D_T, gas and condensate product streams and SS head-loss.

Rigorous thermodynamic modeling of SS for condensing feeds (e.g., raw NG) was provided in Arinelli et al. (2017) by means of a SS Unit Operation Extension (UOE) developed for HYSYS 8.8, namely SS-UOE. SS-UOE rigorously handles multiphase supersonic compressible flows – e.g., gas, C3+ liquid and water – with any equation-of-state (EOS) available in the HYSYS palette of thermodynamic models such as Peng-Robinson EOS (PR-EOS) and Cubic-Plus-Association EOS (CPA-EOS). For correct *Ma* determination in SS flow path, the phase-equilibrium sound speed (*c*) property is rigorously calculated in SS-UOE via another UOE, PEC-UOE, developed in de Medeiros et al. (2017). SS-UOE and PEC-UOE can handle SS simulation with any chemical system, provided an appropriate EOS is available in HYSYS. Examples of utilization of SS-UOE and PEC-UOE are found in previous works Arinelli et al. (2017) and de Medeiros et al. (2017) for water-saturated raw NG and Teixeira et al. (2018) for raw NG saturated with thermodynamic hydrate inhibitors (e.g., methanol). All these systems develop three-phase (gas-water-C3+) supersonic compressible flow in SS flow path.

Recent studies have focused on alternative SS applications beyond WDPA and HCDPA of NG. The work of Teixeira et al. (2018) presented a new "out-of-the-box" process for recovering thermodynamic hydrate inhibitors – e.g., methanol – from raw gas employing SS with water injection. Such process was shown to dramatically reduce methanol losses, as well as performing HCDPA+WDPA for NG exportation and producing liquefied-petroleum-gas (LPG) attaining higher profitability relatively to conventional offshore gas processing. In other words, this SS-based process was able to increase revenues and lower costs relatively to conventional gas processing, being a candidate for NG conditioning capable to sustain CCS plants rendering a cleaner production. In addition, SS-based processes require lower footprint, as SS's are highly compact units with high capacities, liberating space for a CCS unit on the offshore rig.

In order to provide a convincing validation of the present SS-UOE modeling, Appendix D brings a comparison of SS-UOE results against the data of a previous SS work from Arina using computational fluid dynamics (CFD) as described in Yang et al. (2014). The concordance of the SS-UOE results with Arina's data is almost perfect. There is only a subtle discrepancy: the axial pressure profile of Arina (Fig. D.1) crosses the shock front at $x \approx 70$ *mm*

following a highly inclined linear path – a typical crippled CFD outcome – which rigorously should be a true vertical discontinuity as shown in the correct axial pressure profile of SS-UOE.

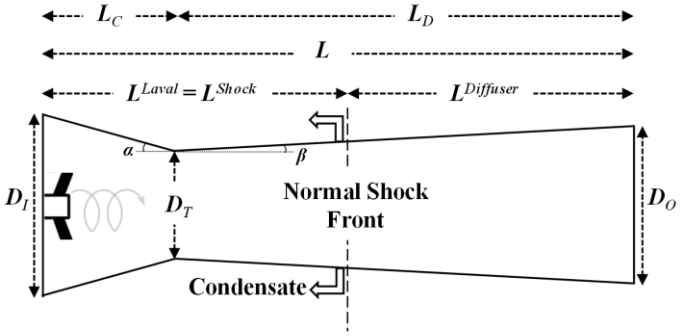

Figure IV.1. SS sketch with linear diameter profiles.

IV.1.3. The Present Work

The literature scarcely addressed economic and environmental analyses of SS-based NG processing in comparison with conventional alternatives, or even economic feasibility of CO_2 capture backed up by cost reduction provided by new SS-based NG processing. Machado et al. (2012) performed a technical-economic comparison of SS and conventional technologies for onshore conditioning of raw NG. However, environmental issues such as CCS or CO_2 emissions were not addressed. Sánchez and de Oliveira Jr. (2015) compared exergy performances of offshore rigs with/without CCS concluding that CCS turns the plant more environmentally adequate in renewability-exergy indexes, but economics and SS were not addressed.

The present work discloses a new SS-based NG offshore processing simultaneously recovering anti-hydrate methanol denominated SS-MeOH-Recovery. The economic leverage of SS-MeOH-Recovery makes possible to afford a complete CCS plant to abate CO_2 emissions of gas rigs. The CCS plant comprises PCC-MEA and also an original compression and dehydration unit (CDU) for exporting EOR-grade liquid CO_2. The dehydration of compressed CO_2 from PCC-MEA is executed with another SS at $P \approx 50$ *bar* designed for minimum head-loss – minimally impacting compression costs – and simultaneously recovering water fulfilling make-up requirements of PCC-MEA. The feasibility and

competitiveness of the new CCS-integrated gas processing with SS-MeOH-Recovery are proved by simulating and economically comparing two process alternatives using anti-hydrate methanol: (i) conventional gas processing without CCS; and (ii) SS-MeOH-Recovery integrated to a complete CCS plant, both alternatives coupled to an obligatory Methanol Recovery Unit (MRU) for methanol-water separation.

In summary, the present work approaches technological aspects not yet being considered in the current literature; namely: (i) SS-MeOH-Recovery is a new gas processing alternative prescribing a SS to treat raw NG carrying water and anti-hydrate methanol, representing a hard simulation problem which was tackled with rigorous three-phase (gas, liquid C3+ and water-methanol) compressible flow, rigorous three-phase sound speed property and rigorous thermodynamic modeling with CPA-EOS, all these features clearly inexistent in other SS literature studies (excepting our previous work Teixeira et al., 2018); (ii) the present work proves, for the first time, that the economic benefits of SS-MeOH-Recovery can sustain PCC-MEA abating a significant part of CO_2 emissions and the associated dehydration/compression costs for the separated CO_2, while keeping competitiveness relatively to conventional gas processing without PCC-MEA in several scenarios. Therefore, lowering CO_2 emissions via PCC-MEA and achieving a cleaner production was possible by the economic leverage of the more efficient SS-MeOH-Recovery relatively to the conventional counterpart. This analysis is centered in economically sustainable CCS implementation in offshore NG processing using original SS units designed with rigorous thermodynamic simulations. Such thermodynamic-economic-environmental assessment is an original contribution to the current literature.

IV.2. Technical Background and Methods

To implement and assess new SS-based offshore gas processing and provide integration with CCS plants, several related technical aspects and methods have to come into discussion at this point.

IV.2.1. Overview of Offshore Gas Processing

Fig. IV.2 depicts an overview of typical gas processing on an offshore NG field. It must be noticed beforehand that the CCS module is only a possibility, as Fig. IV.2 contemplates a conventional gas-rig normally deprived of CCS from exhausts. Another aspect is gas-hydrate formation in subsea pipelines, a major concern in offshore NG systems, since gas-hydrate obstructions can lead to economic and safety issues on flowline operation (Nazeri et al., 2012). Since deep-water offshore scenarios present thermodynamic conditions favouring gas-hydrate formation, such as high-pressure, low external temperature *[≈0°C,10°C]* and gas contact with free water, hydrate inhibition is mandatory to ensure continuous production and flow assurance (Teixeira et al., 2016). Therefore, lean methanol is a common thermodynamic hydrate inhibitor injected in well-heads such that it flows with production fluids, displacing the gas-hydrate equilibrium temperature (*GHET*) to values lesser than system temperature, thus removing the thermodynamic conditions for hydrate formation. Consequently, production fluids reach the platform as a multiphase gas-dominated stream feeding the high-pressure three-phase separator (HPS). HPS splits the feed into: (i) bottom water-methanol-salts liquid (Rich-Methanol); (ii) hydrocarbon condensate, if present; and (iii) an upper gas (HPS-Gas).

Rich-Methanol from HPS goes to the Methanol Recovery Unit (MRU) for re-purification of methanol by removing water and salts via distillation. The recovered lean methanol is recycled back to service points after receiving make-up. The hydrocarbon condensate (if present) is collected for stabilization and the HPS-Gas goes to WDPA and HCDPA conditioning and follows to compression for exportation.

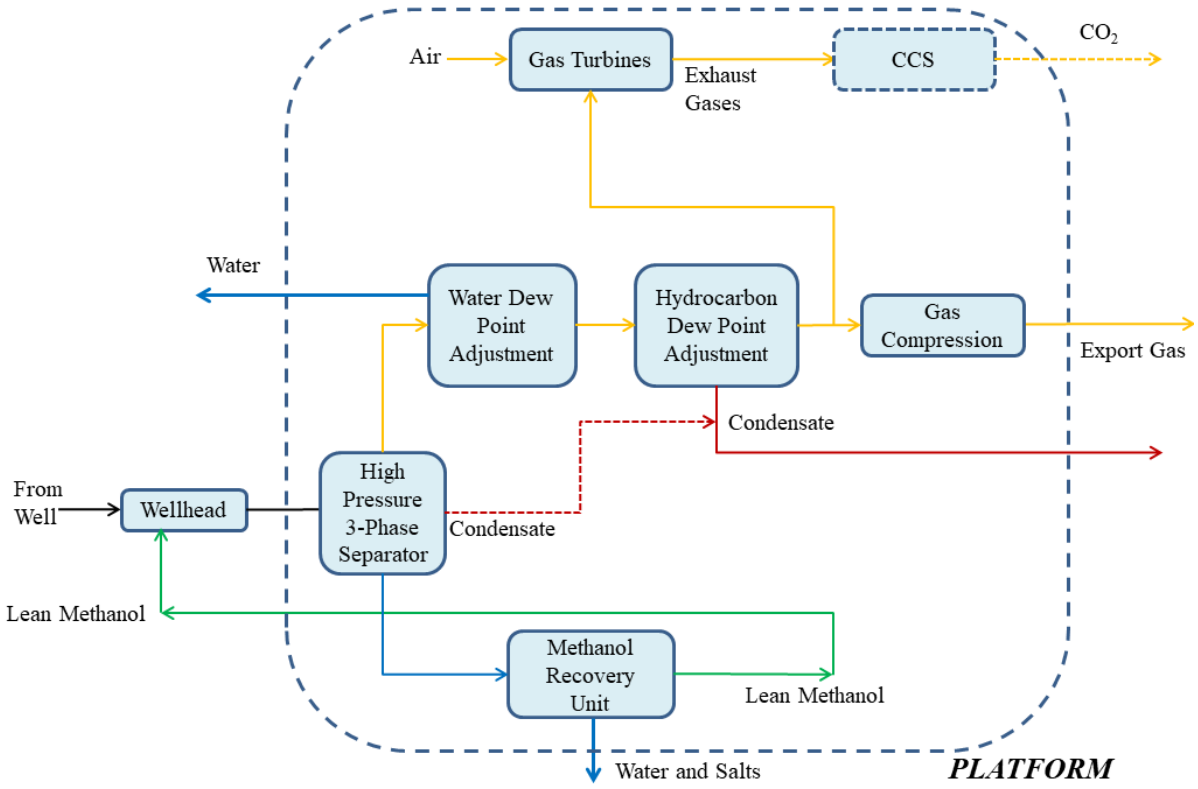

Figure IV.2. Overview of offshore gas-processing platform.

As explained before, turboshafts and gas-turbines are widely used for on-site power generation and as mechanical drives in offshore oil-gas producing and processing facilities (Araújo et al., 2016). The temperature of exhaust from gas-turbines with power output rating up to *50 MW* (both industrial heavy-duty and aero-derivatives) ranges between *400°C–600°C* (Bianchi et al., 2014). The waste heat from exhaust gas is partly recovered in waste heat recovery units (WHRU) to heat liquid hot utilities (Araújo et al., 2016), such as thermal fluid (TF, $T=280^oC$) or pressurized hot water (PHW, $T=210^oC$), while the remaining heat is released with flue-gases to the atmosphere. TF or PHW circulate in loop supplying heat to platform facilities. PHW is preferred, as it involves relatively low risks. Up-to-date systems frequently adopt the PHW as a costless heating solution for reboilers and heaters. The main cooling utility in offshore rigs is cooling-water (CW, $T \in [35^oC,45^oC]$), which is kept in closed-loop cooled with seawater (SW, $T \in [25^oC,35^oC]$). In this work, all heating duties are

considered supplied by PHW at $T=210^oC$ and SW is considered aspired from surface waters of tropical seas at $T=25^oC$, being returned to the sea at $T=35^oC$ (Teixeira et al., 2016).

Gallo et al. (2017) quantifies electricity and heat demands of a general platform processing oil and NG, with *6 MMSm^{3}d* of NG capacity. Electricity is generated by four *30MW* turboshafts (one spare included). They report *80MW* of peak electricity consumption during platform lifetime for such NG capacity. Turboshafts burn fuel-gas (FG) produced in the platform and always generate power for the maximum electricity demand on the platform. Each turboshaft operates in cogeneration mode, so that its exhausts feed a WHRU producing PHW at $T=210^oC$. The WHRU ratio of heat-recovery adopted in this work is *75MW-PHW* per *100MW-power* (Araújo et al., 2016). Considering a total power generation of *80MW* (Gallo et al., 2017) and the WHRU heat-recovery ratio, there is *60MW* of PHW heating capacity.

Exhausts from WHRUs represent the main CO_2 emissions from NG processing. It could be abated if a CCS plant is employed. In addition, the captured CO_2 can generate revenues if it is injected in oil fields for EOR (Araujo and de Medeiros, 2017).

IV.2.2. Methanol Recovery Unit (MRU)

In gas rigs, Rich-Methanol from the HPS (Fig. IV.2) is treated in the Methanol Recovery Unit (MRU) for water and salts removal, enabling recycle of Lean-Methanol to well-heads. Fig. IV.3 depicts the MRU consisting of an atmospheric distillation column with *≈85%w/w* methanol top distillate, and water (with salts) as bottoms with less than *100ppm* methanol appropriate for sea disposal. After expansion from HPS to atmospheric pressure, Rich-Methanol is pre-heated with column bottoms. The condenser is cooled with CW, whose flow rate adjusts distillate temperature and vent-gas flow rate. The distillate receives methanol make-up forming the Lean-Methanol stream for reinjection (Teixeira et al., 2018).

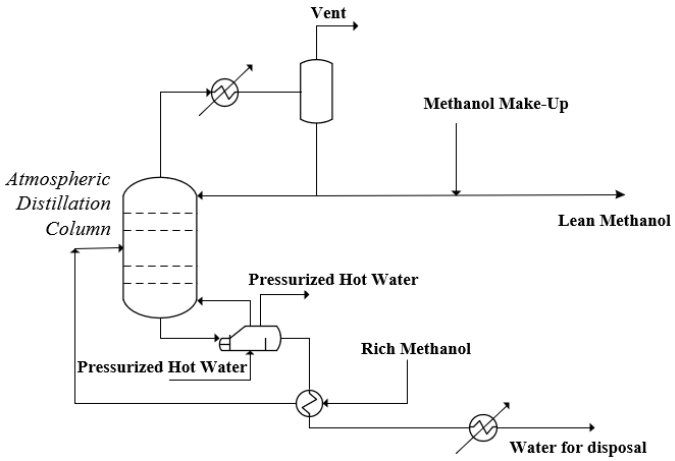

Figure IV.3. MRU: methanol recovery unit.

IV.2.3. Conventional Offshore NG Processing

Fig.4 depicts the conventional NG processing where the HPS-Gas passes through WDPA and HCDPA and is compressed for exportation. Regarding WDPA, there are several methods for high-capacity dehydration of high-pressure NG. NG dehydration using triethylene glycol (TEG) absorption is the conventional way (Mokhatab et al., 2006). In the TEG absorber, raw NG counter-currently contacts Lean-TEG, so that Dry-Gas leaves as top product and Rich-TEG as bottoms. Rich-TEG is sent to a regeneration atmospheric distillation, where Lean-TEG is recovered as bottoms, returning to the absorber after heat exchange with cold Rich-TEG. The top-distillate from the TEG regenerator is liquid water with some methanol recovered, which returns to the MRU.

Regarding HCPDA, the conventional option is Joule-Thomson (JT) expansion, wherein the Dry-Gas from WDPA experiences temperature drop through isenthalpic expansion condensing C3+ (NGL). NGL by-product (with commercial value) is recovered, while the treated gas goes to exportation compressors.

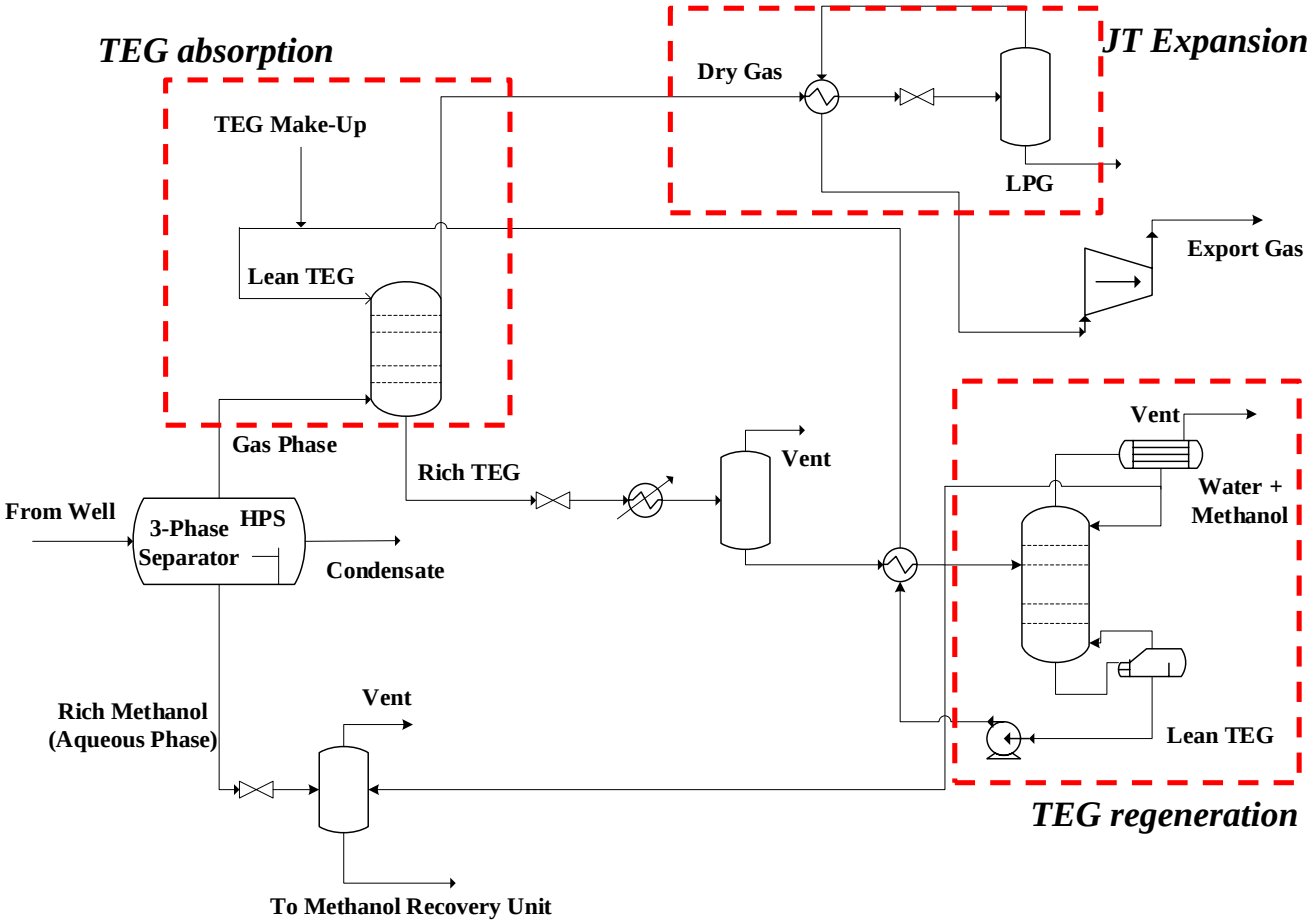

Figure IV.4. Conventional processing of HPS-Gas (dashed-red).

IV.2.4. SS-MeOH-Recovery

Teixeira et al. (2018) disclosed a new process for methanol recovery from the raw gas leaving the HPS (Figs. IV.2 and IV.4). This process – so-called SS-MeOH-Recovery in Fig. IV.5 – expands HPS-Gas through SS with small water injection. Besides recovering methanol, SS-MeOH-Recovery produces LPG with commercial value and exportable NG with appropriate HCDPA and WDPA.

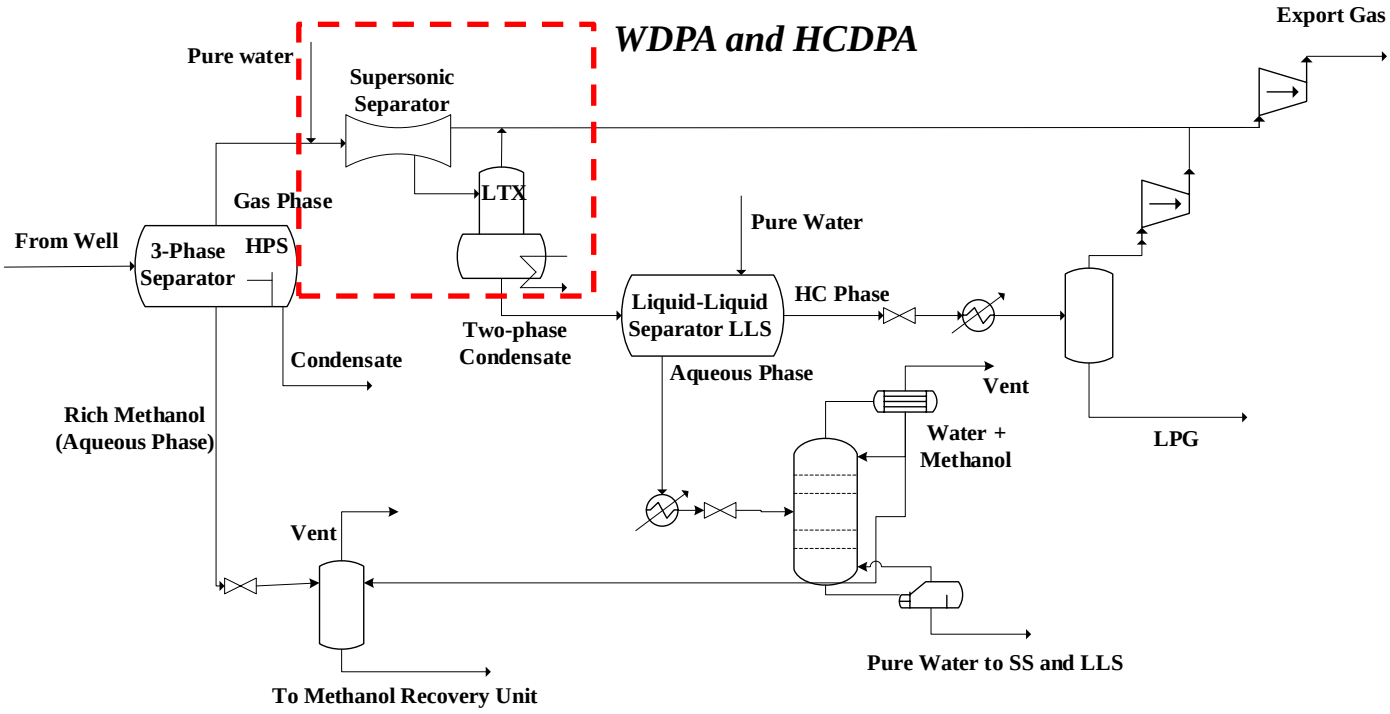

Figure IV.5. NG processing via SS-MeOH-Recovery.

HPS-Gas goes to one or more parallel SS according to its flow rate. As SS-MeOH-Recovery is based on methanol capture using water as agent, sufficient water is necessary in SS feed. Therefore, in order to overcome fluctuations of water content of HPS-Gas, a small flow rate of liquid water ($H_2O/MeOH=3mol/mol$) is injected in the SS inlet to guarantee methanol extraction in SS flow path thanks to water-methanol physical-chemical affinity. The SS of SS-MeOH-Recovery performs three simultaneous tasks: it recovers methanol and executes WDPA and HCDPA of HPS-Gas. Therefore the SS condensate is two-phase: there is the water-methanol bottom condensate and a C3+ top condensate. Despite the presence of methanol (an anti-freezing agent) in SS condensate, this condensate is sent to a heated LTX vessel with bottom temperature of $\approx 30^oC$ to avoid ice and gas-hydrates. The LTX top slip-gas, if present, joins the SS lean gas, while the warm two-phase condensate leaves the LTX bottom, where a good portion of condensed methanol resides in the aqueous phase. The two-phase LTX bottoms go to a high-pressure liquid-liquid separator (LLS). The LLS receives a small injection of water ($H_2O/MeOH=4mol/mol$) to enhance methanol extraction. LLS bottom aqueous condensate is heated and expanded to atmospheric pressure, while the top C3+ condensate is heated and expanded to an intermediate pressure ($\approx 20\ bar$) producing LPG

(C3+) and residual gas (CH_4+C_2H_6), which is recompressed to the main gas header, containing the final NG product with WDPA/HCDPA grades and practically exempt of methanol. The aqueous LLS bottoms are expanded to a small atmospheric distillation column producing methanol-water as top distillate and bottom fresh water (*99.99%mol*). The objective of this column is to recover pure water, which has no salt and provides all the fresh water injected in SS and LLS, while its methanol-water distillate joins the Rich-Methanol from HPS to MRU. To allow high pressure recovery of *≈85%* reducing compression costs, SS is specified with a low Ma^{Shock} (Ma^{Shock}*≈1.5*), so that in the SS supersonic section temperature falls to *-39°C* condensing at least *≈99.7%* of water, C3+ and *≈95%* of methanol in the SS feed.

IV.2.5. CCS Plant: PCC-MEA and CO_2 Compression and Drying

PCC-MEA is chosen for capturing CO_2 from turboshaft exhausts with only *≈5%mol* CO_2, but presenting issues such as high capture-ratio (*10-18* $kg^{Solvent}/kg^{CO2}$) entailing high solvent circulation, high heat-ratio for regeneration (*2-4* MJ/kg^{CO2}) and a low-pressure CO_2 product requiring compression and dehydration for EOR (Botero et al., 2009). In offshore rigs the PHW generated in WHRUs can be used to meet the high thermal demand of PCC-MEA. Therefore, PCC-MEA heat demand is considered cost-free up to the maximum WHRU heat-recovery of *75 MW-PHW* per *100 MW-power* (Araújo et al., 2016).

Fig. IV.6 depicts the PCC-MEA plant for CO_2 capture from exhausts leaving the WHRUs at *≈300°C*. Exhausts are pre-cooled with CW in a direct-contact column before CO_2 absorption. This direct-contact also saturates flue-gas with water preventing solvent dehydration in the counter-current absorber. Decarbonated flue-gas leaves the absorber as top product, while the bottom product Rich-MEA with captured CO_2 is sent to the atmospheric regeneration stripper after pre-heating with hot Lean-MEA from the regenerator reboiler. The regenerator has a top condenser cooled with CW to avoid losses of water and MEA with CO_2 gas product. In spite of this, saturation water at *45°C* and few ppms of MEA join the CO_2 top product containing *≈90%mol* CO_2 and *≈10%mol* H_2O at *1 atm*. Such saturation water with traces of MEA is

recovered a posteriori as high-pressure condensates from the CO_2 compression and dehydration unit (CDU) in Fig. IV.7. As high-pressure water condensates have some content of dissolved CO_2, they are directed to the regenerator bottom (Make-up Water stream) avoiding atmospheric release of such CO_2 (Fig. IV.6).

The CO_2 top product from the atmospheric regenerator follows to the compression and dehydration unit (CDU) shown in Fig. IV.7. In the CDU CO_2 is dried at high-pressure with an *ad hoc* SS. Firstly, a four-stage compression train brings this stream to $P=50\ bar$, being subsequently heated to 50^oC before entering the dehydration SS. This temperature is necessary for good SS performance so as to avoid extreme compressibility of CO_2 due to critical proximity below 45^oC at $P=50\ bar$. The condensate ejected from SS at $T\approx-18^oC$ and $P\approx50\ bar$ containing water and some liquid CO_2 is sent to a LTX with bottom temperature at $\approx30^oC$ to avoid ice and CO_2-hydrates. The warm LTX condensate joins other high-pressure water-CO_2 condensates from the knock-out vessels, returning to the bottom of the atmospheric PCC-MEA regenerator. Dry CO_2 at $T\approx52^oC$ and $P\approx50\ bar$ leaving the dehydration SS with $99.76\%mol$ CO_2 and $127ppm\text{-}mol$ H_2O is compressed in the last compressor to $P\approx120\ bar$ and emerges liquefied in the subsequent intercooler at $T=40^oC$. Liquid dry CO_2 is then pumped to final export pressure $P=350\ bar$.

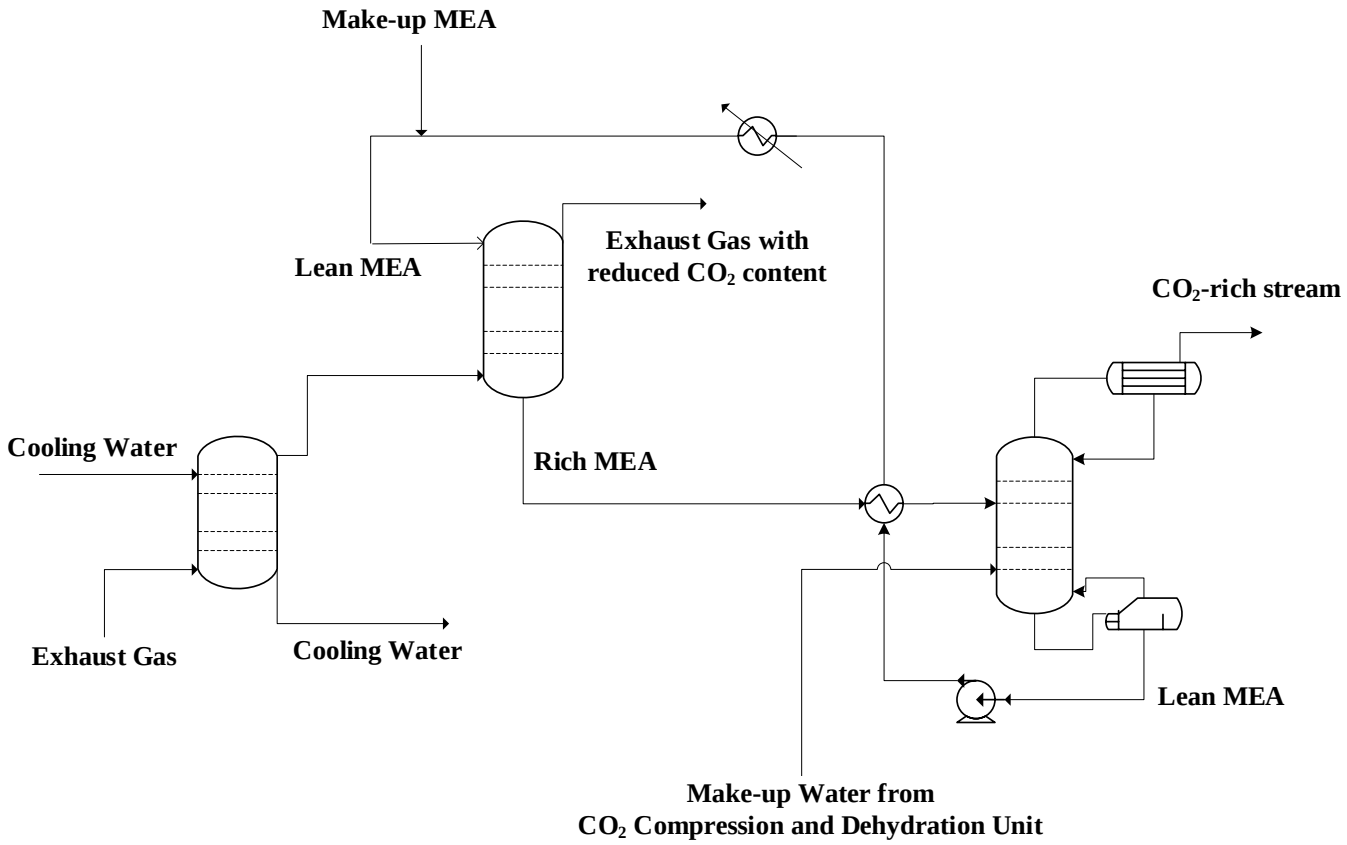

Figure IV.6. PCC-MEA for CO_2 capture from turboshaft exhausts.

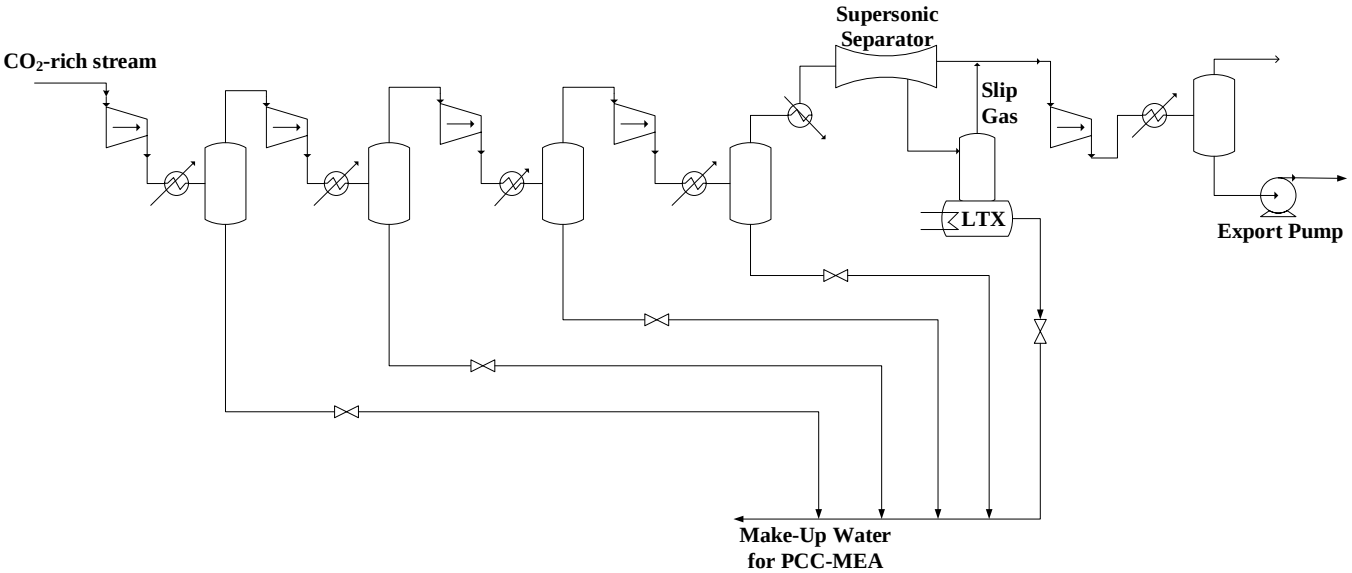

Figure IV.7. Compression and dehydration unit (CDU) for CO_2 product to EOR

IV.3. Process Assumptions and Economic Premises

The main objective of this work is to evaluate if the economic gain provided by SS-MeOH-Recovery compared to the conventional gas processing using methanol anti-hydrate is enough to afford the proposed CCS unit for abatement of CO_2 emissions. To achieve that, process conditions and relevant parameters were defined and steady-state flowsheets of conventional NG processing without CCS and SS-MeOH-Recovery with CCS, both coupled to MRU, were implemented in HYSYS environment. Then power, heat consumptions, flow rates and pertinent parameters were assessed via simulations. Following this, equipment items were sized, module costing technique (Turton et al., 2009) was applied for estimating Fixed Capital Investment (*FCI, MMUSD*) associated to equipment items and the Net Present Value (*NPV, MMUSD*) for project lifetime (20 years of operation) was obtained for both alternatives. Process economic analysis was handled with the method of Turton et al. (2009) and formulas reported in Granjo and Oliveira (2015) for estimating Cost of Manufacturing (*COM, MMUSD/y*), Revenues (*REV, MMUSD/y*), Cost of Raw Materials (*CRM, MMUSD/y*), Gross Annualized Profit (*GAP, MMUSD/y*), Depreciation (*DEPR, MMUSD/y*), Annualized Profit (*AP, MMUSD/y*) and Net Present Value (*NPV, MMUSD*). The relationships between such economic variables are detailed in Appendix C.

Process simulation was conducted in HYSYS 8.8 with appropriate thermodynamic modeling via CPA-EOS for both SS-MeOH-Recovery and conventional gas processing, with the following exceptions: (i) TEG plant employed HYSYS Glycol Package; (ii) PCC-MEA was simulated with HYSYS Acid-Gas Package; (iii) CO_2 compression and dehydration unit (CDU) was simulated with PR-EOS. The CPA-EOS was chosen for flowsheet sections containing light hydrocarbons, water and methanol, as it is the only fully-tested thermodynamic model appropriate to handle complex polar and associating multiphase systems (Folas et al., 2005). On the other hand, the influence of NaCl and calcium salts (e.g., $CaCl_2$, $CaSO_4$, etc.) in production waters was neglected in simulations, since their presence would require a different thermodynamic model (CPA-EOS cannot handle electrolytes), whereas current aqueous solution models have limited reliability with strong electrolytes. In this regard, NaCl is the main ionic species, representing about 0.1%w/w-1%w/w in water-methanol production streams, while other salts reach much lower levels. The truth is that salts

at such concentrations cannot influence too much the heat effects – basically dominated by water and methanol latent heats – but bring certain obstacles to VLE modeling. So, the thermal effects associated to electrolytes presence were considered negligible and such species were removed from the process model as justified in previous studies (Teixeira et al., 2016).

Simulation and design of SS nozzles was made via HYSYS extension SS-UOE (Arinelli et al., 2017), a thermodynamically rigorous HYSYS UOE for simulating SS with multiphase equilibrium flow path in connection with PEC-UOE (de Medeiros et al., 2017) for correct determination of the phase-equilibrium sound speed property (c) in multiphase flow. Such tools are capable to rigorously handle calculation of thermodynamic properties for multiphase systems with CPA-EOS/PR-EOS and complex phase-behavior and phase-change perfectly obeying the 2nd Law of Thermodynamics. The LTX vessels in SS-MeOH-Recovery and in CDU were modeled via two cascaded flashes (P-H and P-T flashes) as shown in Arinelli et al., 2017. Table IV.1 lists economic premises for economic analysis, Table IV.2 lists assumptions adopted for process simulation and equipment sizing and Table IV.3 lists complementary assumptions for simulation of SS-MeOH-Recovery with CCS. The specifications of SS nozzles in SS-UOE are given in Table IV.4 for both cases in which SS is employed (SS-MeOH-Recovery and CDU). Table IV.4 also depicts the converged design of SS nozzles and important calculated variables such as outlet flow rates and variables (T,P,$ppmH_2O$), pressure-recovery and just before-shock variables (T_{BS},P_{BS},Ma_{BS}).

Table IV.1. Economic Premises

Item	Premises
FCI	*FCI extrapolation to operational capacities via 0.6 rule (Turton et al., 2009).* *$FCI^{OFFSHORE}$ = 2.2* $FCI^{ONSHORE*}$* *FCI^{SS} and FCI^{LTX} extrapolated from onshore FCI^{SS} and FCI^{LTX} for 6MMSm³/d of capacity[a].* *Liquid-Inventories = 1.2*(Volume-Vessels + 0.16*Volume-Columns)*
COM	*CO_2 tax: 65 USD/ton* *Power-Ratio of Fuel-Gas (FG) for power generation: 191.5MW-power/MMSm³d* *Costless thermal utilities: SW, CW, PHW*
Prices	*Raw NG=0; Methanol=425USD/ton; TEG=3000USD/ton; MEA=1000USD/ton.* *LPG/NGL: via percentages of oil price (C2=30%; C3=55%; C4=75%; C5+= 95%[a])* *Crude oil=70USD/bbl* *Export NG=3.2USD/MMBTU; Export CO_2=1 bbl-oil/ton[b]* *Fuel-Gas (FG)=3.2USD/MMBTU*
Economic Parameters	*Horizon=20 years (invariant feed and process conditions)* *Construction: triennial investment allocation of 20%/30%/50%* *Annual interest rate: i=10%* *Depreciation(USD/y)=10%FCI(USD)* *Operation=8000 h/y* *Working-Capital(USD)=5%FCI(USD)* *Income Tax Rate: ITR=34%* *CEPCI=550.3 (Sept, 2015)*

*[a]Machado et al., 2012; [b]McCoy, 2008; *Rech, 2012.*

Table IV.2. Assumptions for Process Simulations and Equipment Sizing

Item	Premises
Raw-NG producing scenario	*Well-head: P=300 bar, T=40°C* *Pipeline at well-head: P=80 bar, T=5°C (seabed)* *Raw-NG (dry-basis): 6 MMSm³/d, %mol composition CH_4=85.48%, C_2H_6=8.26%, C_3H_8=3.06%, iC_4H_{10}=0.47%, nC_4H_{10}=0.85%, iC_5H_{12}=0.20%, nC_5H_{12}=0.24%, C_6H_{14}=0.21%, C_7H_{16}=0.06%, N_2=0.53%, CO_2=0.64%* *Production water: 75m³/d* *High-Pressure Separator (HPS): T=25°C, P=50 bar*
GHET	*Via HYSYS 8.8 Colorado School of Mines method* *At P=80 bar, T=5°C, no methanol ⇒ GHET=18°C* *Target for lean methanol injection: GHET=1°C at P=80 bar, T=5°C*
Conventional NG Processing	*Thermodynamic Package: HYSYS CPA-EOS (TEG Unit with Glycol Package)* *Lean TEG: TEG=98.5%w/w* *TEG flow rate determined such that ppmH_2O in final NG < 50 ppm* *Pressure drop in JT expansion such that HCDP ≤ 0°C@45 bar*
Exported NG	*P=100 bar, HCDP≤ 0°C@45 bar, H_2O<50ppm mol*
MRU Atmospheric Distillation Column	*Top distillate: Methanol=85%w/w, H_2O=15%w/w;* *Bottoms: Methanol ≤ 100ppm mol*
Heat Exchangers	*ΔP^{SHELL}=0.5 bar, ΔP^{TUBES}=0.5 bar, $\Delta T^{APPROACH}$=10°C* *Intercoolers: T^{GAS}=40°C, Condensers: $T^{DISTILLATE}$=45°C*
Stage-Compressor	*Compression-ratio ≤3.0, Intercooler T^{GAS}=40°C* *Adiabatic-efficiency: η=75%, Electric-drive*
Pumps	*Adiabatic-efficiency: η=75%*
Vessels	*P^{DESIGN}=1.15*$P^{OPERATION}$ (rounded up to 10 multiple)*
Heating utility	*Pressurized Hot Water (PHW): T=210°C, P=20 bar*
Cooling utility	*Cooling-Water (CW): T∈[30°C,45°C], P=4 bar.*
Rig Total Power Demand	*80MW[a]*
Gas-Turbines	*Fuel-Gas (FG) %mol: CH_4=97%, CO_2=3%* *FG Power-Ratio[b]=191.5MW/MMSm³d (total combustion, 100% excess air)* *Air %mol: CO_2=0.04%, H_2O=2.02%, O_2=20.69%, N_2=77.25%*
WHRUs	*PHW-Load=60MW (from 75MW-PHW/100MW-Power[b])*

[a] *Gallo et al. (2017).* [b] *Araujo et al. (2016).*

Table IV.3. Complementary Assumptions for Simulation of SS-MeOH-Recovery with CCS

Item	Premises
SS-MeOH-Recovery	*Thermodynamic Package: CPA-EOS* *SS: Two nozzles, single LTX, Water Injection Molar Ratio: H_2O/MeOH=3* *SS Specifications: Table IV.3* *LLS: Water Injection Molar Ratio H_2O/MeOH=4*
PCC-MEA	*Thermodynamic Package: HYSYS Acid-Gas Package* *Lean Solvent: MEA=20%w/w, Heat-Ratio: 3.8 MJ/tCO_2* *Available heat for regenerator: 60 MW minus gas processing heat demand*
CO_2 Dehydration/Compression	*Thermodynamic Package: PR-EOS* *SS: Single nozzle with LTX* *SS Specification: see Table IV.3* *CO2-EOR product: P= 350 bar, H_2O < 200ppm mol*

** Premises of Table IV.2 are also valid for common general aspects of this case (e.g. MRU, equipment sizing criteria, etc.)"*

IV.4. Results

Table IV.4 presents the specifications, design results and some outlet variables of SS nozzles prescribed for SS-MeOH-Recovery process and for CO_2 dehydration (CDU) in the CCS plant integrated to SS-MeOH-Recovery. It is interesting to see that the SS feed in SS-MeOH-Recovery has only *1508ppm mol* of methanol, but this small content was almost entirely captured by SS reducing dramatically the costs of SS-MeOH-Recovery with raw materials. Secs. IV.4.1 and IV.4.2 discuss specific results for these two SS units: the SS in SS-MeOH-Recovery and the SS for CO_2 drying in the CCS plant. Sec. IV.4.3 presents technical and economic results and comparisons for the two offshore NG processing plants subjected to analysis: (i) the SS-MeOH-Recovery integrated to CCS plant; and (ii) the conventional gas plant without CCS plant.

Table IV.4. SS specifications and calculated designs for SS-MeOH-Recovery and CDU

Specified Items	***SS-MeOH-Recovery***	***CDU***	***Calculated by SS-UOE***	***SS-MeOH-Recovery***	***CDU***
No.of SS	*2*	*1*	$D_T(m)$	*0.0644*	*0.0178*
$D_I(m)$	*0.1500*	*0.0800*	$L_C(m)$	*0.1992*	*0.1383*
$D_O(m)$	*0.1200*	*0.0580*	$L_D(m)$	*0.6407*	*0.4321*
$\alpha(^o)$	*12.67*	*12.67*	$L(m)$	*0.8399*	*0.5704*
$\beta(^o)$	*2.66*	*2.66*	$L^{Shock}(m)$	*0.2626*	*0.1446*
Ma^{Shock}	*1.5*	*1.3*	$L^{Diff}(m)$	*0.5773*	*0.4258*
$\eta^{EXP}\%$	*100*	*100*	$P_{BS}(bar)$	*14.79*	*19.69*
$\eta^{CMP}\%$	*100*	*100*	$T_{BS}(^oC)$	*-38.88*	*-17.63*
$P^{Feed}(bar)$	*50*	*50.27*	Ma_{BS}	*1.399*[*]	*1.284*
$T^{Feed}(^oC)$	*25.28*	*50.00*	$P^{Discharge}(bar)$	*42.67*	*49.78*
$MMSm^3/d$	*3.019*[$]	*0.180*	$T^{Discharge}(^oC)$	*31.91*	*51.82*
$\%C3^{+Feed}$	*5.06%*[&]	-	*%Condensate*	*3.22%*[&]	*0.34%*[&]
$ppmH_2O^{Feed}$	*4960*[&]	*3340*[&]	$REC\%H_2O^{\#}$	*99.71%*	*96.21%*
$ppmMeOH^{Feed}$	*1508*[&]	-	$REC\%MeOH^{\#}$	*95.30%*	-
			%P Recovery	*85.32%*	*99.22%*
			$ppmH_2O^{SS\text{-}Gas}$	*15*[&]	*127*[&]
			$ppmH_2O^{FinalNG}$	*20*[&]	-

[*] *After 2-phase condensate withdrawal.* [$] *Total feed flow rate of each nozzle.* [&] *Molar basis.* [#] *% Recovered.*

IV.4.1. SS Results for SS-MeOH-Recovery

Figs. IV.8 and IV.9 report SS profiles of several dependent variables versus SS axial position *x(m)* or pertinent to the plane *P x T* as obtained by SS-UOE. SS linear diameter profiles are shown in Fig. IV.8a with throat position at *x=0.1992m* and molar vapor-fraction profile along SS nozzle. Figs. IV.8b and IV.8c depict respective axial profiles of *P(bar)* and *Ma*, and *T(K)* and the sound speed property *c(m/s)*. Fig. IV.9a reports the condensation profile (%condensed) of hydrocarbons (HCs), CO_2, H_2O and MeOH versus *x*, while Fig. IV.9b depicts the SS path on plane *P x T* jointly with the hydrocarbon dew-point (HCDP) loci of SS feed and lean gas product, and the water dew-point (WDP) locus of the SS feed. Fig. IV.8a shows that the gas begins the SS flow path already with some liquid fraction (i.e., the SS feed is two-phase with less than *100%* vapor fraction) due to the injection of liquid water in SS inlet for better methanol capture. This feature is also noted in Fig. IV.9a that shows *≈90%* of condensed water at *x=0*.

As gas accelerates, *T,P,c* decrease and *Ma* increases until $x=L^{Shock}=0.2626m$, where *Ma* attains the specified maximum value of $Ma^{Shock}=1.5$ with minimum temperature and pressure respectively of $T=T_{BS}=-38.88^{o}C$ and $P=P_{BS}=14.79\ bar$ (Table IV.4). The multiphase sound speed (Fig. IV.8c) continuously decreases from *x=0* to $x=L^{Shock}=0.2626m$ due to increasing condensation and cooling, both continuously causing increase of multiphase properties such as density (ρ) and isothermal compressibility ($\Xi_P=(\partial\rho/\partial P)_{T,\underline{Z}}$), which, by their turn, decrease the multiphase sound speed (de Medeiros et al., 2017). At the throat ($x=L_C=0.1992m$), SS axial flow becomes sonic with $Ma\rightarrow 1^{-}$, which is accompanied by SS signatures (de Medeiros et al., 2017) represented by $\pm\infty$ spatial gradient singularities at the throat clearly identified in Figs. IV.8a, IV.8b, IV.8c as shown in Eq. (IV.1), where *v* is the axial flow velocity, *Ma=v/c* and *A(x)* is the flow section area function of *x*.

$$\frac{dT}{dx}\rightarrow-\infty,\ \frac{dP}{dx}\rightarrow-\infty,\ \frac{dv}{dx}\rightarrow+\infty,\ \frac{dc}{dx}\rightarrow-\infty,\ \frac{dMa}{dx}\rightarrow+\infty \qquad \left\{ Ma\rightarrow 1^{-},\ \frac{dA}{dx}\neq 0 \right. \tag{IV.1}$$

SS throat $\pm\infty$ spatial gradient singularities only exist if the nozzle design is such that $dA/dx \neq 0$ at the throat as occurs in linear diameter profile nozzles in Fig. IV.1. Further, the two inflexion points of *c* profile in Fig. IV.8c confirm that PEC-UOE correctly handles the calculation of sound speed (*c*) across phase transition boundaries in multiphase compressible flow.

After condensate removal at $x=L^{Shock}=0.2628m$, *Ma* falls to $Ma_{BS}=1.399$ (still supersonic), so that the normal shock occurs with sudden recompression recovering part of the initial (*T,P*) and turns the flow into subsonic. After normal shock, gas velocity and *Ma* decrease through the diffuser, while (*T,P*) smoothly increases until the SS gas outlet with final $T^{Discharge}=31.91^{o}C$, $P^{Discharge}=42.67\ bar$.

Fig. IV.9b represents the plane *P x T* with the SS path and feed and lean gas HCDP loci and feed WDP locus, all rendered with CPA-EOS. The HCDP locus of the feed is the hotter one, and the lean gas HCDP locus is the coldest one, while the two-phase feed WDP locus is the hottest locus. The SS flow path starts somewhere between the feed HCDP and feed WDP loci, consequence of its *ab initio* two-phase condition with injected free liquid water. The SS path expands the two-phase feed ($T_{Feed}=25.28^{o}C$, $P_{Feed}=50\ bar$) deeply crossing the feed HCDP locus initiating C3+ condensation and increasing water and methanol condensation until the minimum temperature point ($x=L^{Shock}=0.2628m$) where $Ma=Ma^{Shock}$, $T=T_{BS}=-38.37^{o}C$ and $P=P_{BS}=14.95\ bar$. At this point, about $\approx 2\%$ of hydrocarbons (HCs) condensed (Fig. IV.9a), while water and methanol were practically $\approx 100\%$ and $\approx 96\%$ condensed respectively (though a small part of methanol is dissolved in the C3+ phase). The two-phase condensate water-methanol and C3+ phases are collected at this point $x=L^{Shock}=0.2628m$ at constant temperature ($T=T_{BS}=-38.37^{o}C$) and pressure ($P=P_{BS}=14.95\ bar$). After condensate removal *Ma* falls to $Ma_{BS}=1.399$ sufficient for normal shock occurrence. The manifestation of normal shock is seen as a sudden fall of *Ma* to subsonic value (Fig. IV.8b), as a sudden compression (Fig. IV.8b) and as sudden heating (Fig. IV.8c), all at $x=L^{Shock}=0.2628m$. Fig. IV.9b also depicts the shock on the plane *P x T* as a rectilinear jump back to higher (*T,P*). Just after shock, the gas is superheated compressed vapor. From this point on, the gas flows sub-

sonically through the ending diffuser (Fig. IV.1) slowly regaining temperature and pressure (Figs. IV.8b, IV.8c and IV.9b).

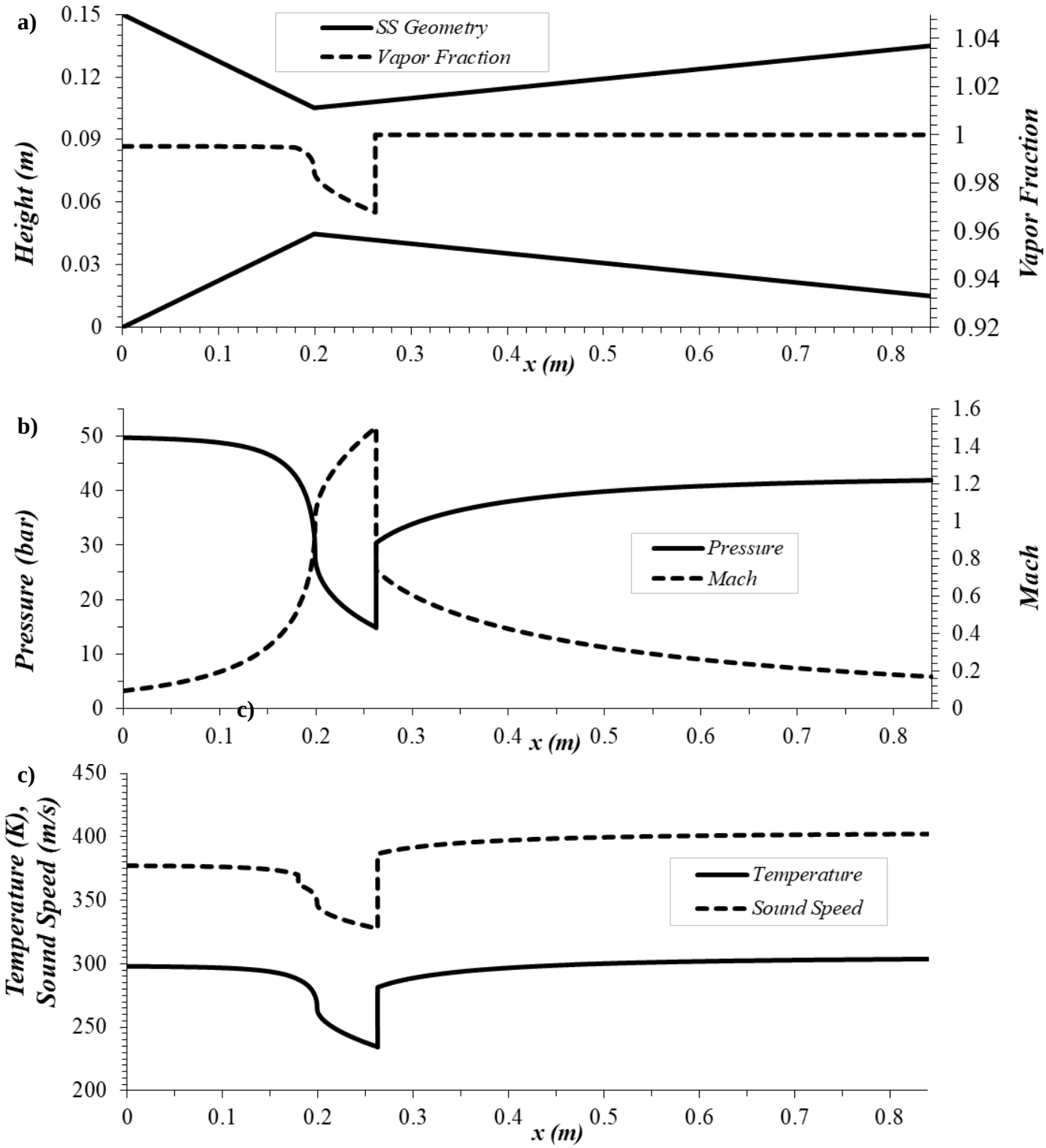

Figure IV.8. SS axial profiles for SS-MeOH-Recovery: (a) SS walls and molar vapor-fraction vs *x*(m); (b) *P(bar)* and *Ma* vs *x*(m); (c) *T(K)* and *c* (m/s) vs *x*(m);

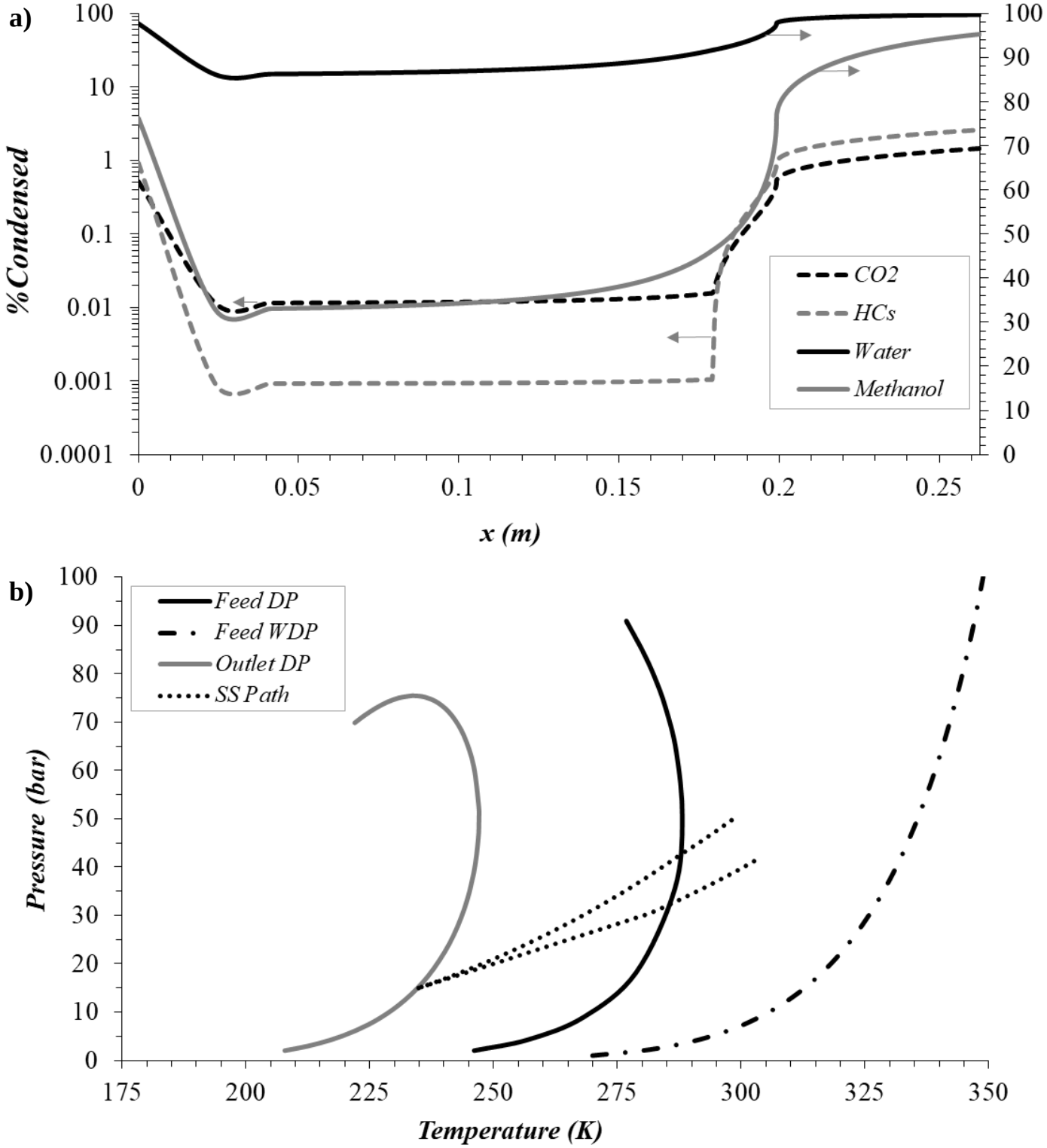

Figure IV.9. SS profiles for SS-Methanol-Recovery: (a) %condensed hydrocarbons (HCs), CO_2, H_2O, and methanol vs *x*(m); (b) plane *P x T* with SS path, HCDP and WDP loci of SS feed and HCDP locus of lean gas.

IV.4.2. SS Results for CO_2 Dehydration (CDU)

Fig. IV.10 reports SS profiles as obtained by SS-UOE. SS linear diameter profiles are again observed in Fig. IV.10a with throat position at *x=0.1383 m* and molar vapor-fraction profile along SS nozzle. Figs. IV.10b, IV.10c, IV.10d depict respective profiles of *P(bar)* and *Ma*, *T(K)* and *c(m/s)*, and profiles of % condensed H_2O and CO_2 versus *x(m)*. Fig. IV.10e depicts SS path on *P x T* plane with the WDP locus of feed CO_2 and the bubble-point and dew-point loci of feed CO_2 and of dry CO_2. The gas begins the SS flow path *100%* vapor, as noted in Fig. IV.6a and Fig. IV.6d which shows *0%* of condensed water at *x=0*. Variables *P,T,c,Ma* follow similar patterns as observed in Fig. IV.8, again with SS signatures ($\pm\infty$ spatial gradient singularities) at the throat. In Fig. IV.10e, the dew-point loci practically coincide with the respective bubble-point loci for both feed CO_2 and dry CO_2, so that both feed and product VLE envelopes, besides having minuscule thicknesses, are practically coincident. The SS path now starts above the WDP curve, then crossing it when water starts condensing jointly with a small quantity of CO_2 possibly dissolved in water. The SS path attains the point of maximum specified Mach $Ma=Ma^{Shock}=1.3$ and minimum temperature at $x=L^{Shock}=0.1446m$ touching the dew-point locus of dry CO_2 at $T=T_{BS}=-17.63^oC$, $P=P_{BS}=19.69\ bar$. At this point, the condensed carbonated water is collected, causing a fall of *Ma* to $Ma_{BS}=1.284$. After condensate removal, the flow is still supersonic and normal shock occurs, causing sudden recompression and heating to a subsonic state of superheated vapor flow. The shock is seen on plane *P x T* as a reasonable rectilinear jump back to higher (*T*,*P*). From this point on, dry CO_2 experiences smooth recompression and heating through the ending diffuser.

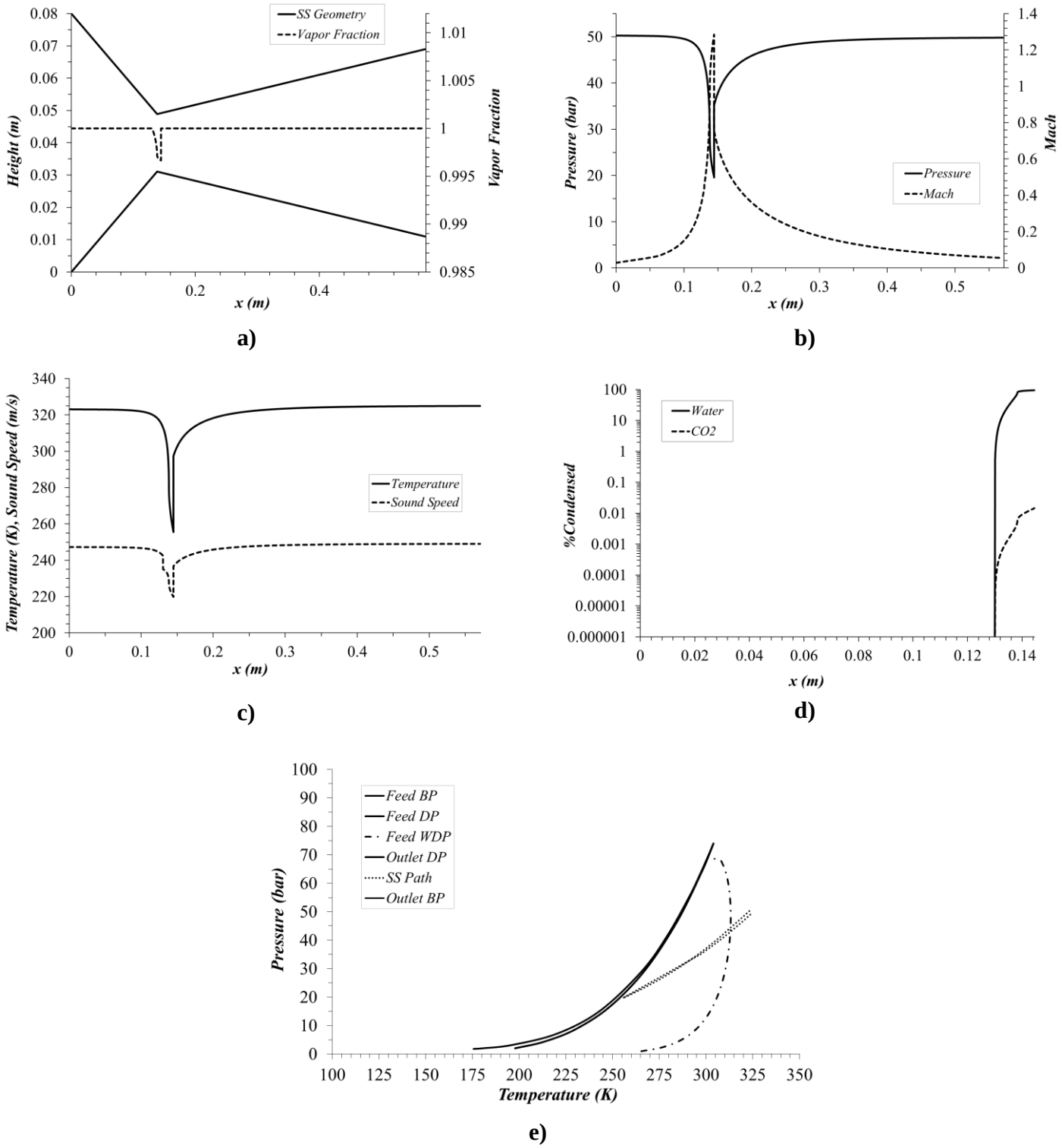

Figure IV.10. SS axial profiles for CO_2 dehydration: (a) SS walls and mol vapor-fraction vs *x*(m); (b) *P(bar)* and *Ma* vs *x*(m); (c) *T(K)* and *c (m/s)* vs *x*(m); (d) %condensed CO_2 and H_2O vs *x*(m); (e) plane *P x T* with SS path, dew-point, bubble-point and WDP loci of CO_2 feed and dry CO_2.

IV.4.3. Technical and Economical Results of SS-MeOH-Recovery and Conventional Gas Plant

Table IV.5 reports technical results obtained by simulation. Power consumption is higher for the conventional gas plant relatively to SS-Methanol-Recovery, since JT expansion requires a higher pressure drop to adjust HCDP. On the other hand, the 1st SS unit for methanol recovery presents high pressure recovery (*≈85%*), entailing less compression power to reach export gas specifications. The 2nd SS for CO_2 drying (CDU) presents an even higher pressure recovery (*≈99%*) thanks to a lower supersonic Ma^{Shock}, entailing less intense shock irreversibility in this SS. Despite the huge CO_2 compression ratio (*1 bar* to *350 bar*), total power required in CDU is only a fraction of the power demand for gas exportation, due to a comparatively much smaller CDU flow rate (*≈0.3 MMSm³d vs ≈6 MMSm³d*). Further, MRU heat demand is higher for SS-MeOH-Recovery, since this process recovers a greater amount of methanol and water from the gas phase and sends it to the MRU, entailing a higher flow rate of water-methanol stream to be treated. In addition, SS-MeOH-Recovery has higher heating duties (e.g., distillation for water recovery) than conventional gas processing (e.g., TEG regenerator). In both cases, MRU heat demand represents the largest share of total heat demand. In SS-MeOH-recovery, CO_2 capture is limited, by premise, to the availability of costless heat for the MEA regenerator. Thus, the available heat of *56.5MW* allows to capture *43.3%* of all CO_2 emissions by the CCS unit, representing a very significant emissions reduction. As expected, the exhaust gas is the major emitter of CO_2 (*≈99.7%* of total emissions).

Fig. IV.11 shows the *FCI* discrimination, while Table IV.6 summarizes economic results. Fig. IV.11 shows that compressor *FCI* of SS-MeOH-Recovery with CCS is lower than the conventional gas processing counterpart. On the other hand, heat exchanger *FCI* is higher for SS-MeOH-Recovery with CCS due to higher heat demand in PHW reboilers. Moreover, the *FCI* of PCC-MEA and CDU represent a big share (*≈35.6%)* of total *FCI* for SS-MeOH-Recovery with CCS. From Table IV.6, despite its lower costs of utilities (*CUT*), raw materials (*CRM*) and CO_2 taxation, SS-MeOH-Recovery with CCS still presents higher *COM* than the conventional gas processing. The underlying reason is that *COM* has a fixed-cost component

proportional to *FCI*, which is *≈100%* higher for SS-MeOH-Recovery with CCS. NG revenues are higher for conventional gas processing due to the higher NG flow rate, since less hydrocarbon content was extracted to LPG. On the other hand, the LPG revenues are *≈200%* higher for SS-MeOH-Recovery due to higher LPG extraction by SS relatively to JT expansion. In addition, the CO_2 revenues of SS-MeOH-Recovery with CCS are also significant. It is impressive that the CO_2 and LPG revenues of SS-MeOH-Recovery compensate its higher *FCI*, *COM* and lower NG revenues. Consequently, SS-MeOH-Recovery with CCS attained a higher annual profit (*AP*) which makes its *NPV* after 20 years of operation higher than the conventional gas processing counterpart (without CCS). Fig. IV.12 depicts the *NPV* profile during project lifetime for both alternatives, showing that SS-MeOH-Recovery with CCS is economically feasible, with superior *NPV*, while abating significant percentage of CO_2 emissions.

Finally, a sensitivity analysis is conducted in order to evaluate the resilience of the SS-MeOH-Recovery with CCS feasibility when relevant economic parameters (NG price, oil price and CO_2 tax) fluctuate. Results are reported in Table IV.7 and are illustrated in Figs. IV.13, IV.14 and IV.15. As a function of oil price, LPG price strongly affect process revenues, then oil price was varied from *40USD/bbl* to *100USD/bbl*. It is evident that SS-MeOH-Recovery with CCS is benefited from high oil prices, being strictly economically feasible for oil prices above *≈55USD/bbl*. As NG price rises, the difference of *NPV* of alternatives becomes smaller because conventional gas processing produces a higher export gas flow rate. Nevertheless, SS-MeOH-Recovery with CCS remains economically superior in all studied cases excepting the two cases with oil prices lower than *55USD/bbl*. Further, SS-MeOH-Recovery with CCS is also benefited from increasing CO_2 taxes and is economically feasible even without CO_2 taxation (provided oil is rated above *≈55USD/bbl*).

Table IV.5. Technical results: CO_2 emissions (ton/d) and power/heat demands (MW).

	Conv. Gas Plant No CCS	***SS-MeOH-Recovery With CCS***
Design Power Generation[a]		
Turboshafts & Gas-Turbines	*80 MW*	*80 MW*
Design Heat Availability[b]		
WHRU	*60 MW*	*60 MW*
Power consumption		
Gas Processing	*14.22 MW*	*8.27 MW*
CO_2 Compression & Dehydration (CDU)	-	*1.69 MW*
Heat Demand		
MRU	*1.9 MW*	*2.2 MW*
Gas Processing	*2.2 MW*	*3.5 MW*
Available Heat for PCC-MEA	-	*56.5 MW*
CO_2 Capture (%)	-	***43.3%***
CO_2 Emisions*		
Turboshaft Flue-Gas	*770.6 ton/d*	*436.6 ton/d*
TEG Unit Vent	*0.4 ton/d*	-
TEG Regenerator Vent	*0.0 ton/d*	-
SS-MeOH-Recovery Vent	-	*0.3 ton/d*
*Water-Recovery Distillation **Vent***	-	*0.0 ton/d*
Pre-MRU Vent	*1.0 ton/d*	*1.0 ton/d*
MRU Distillation Vent	*0 ton/d*	*0.0 ton/d*
Total	***772.1 ton/d***	***437.8 ton/d***

** Vents converted to CO_2 equivalent via total combustion flare. [a]Gallo et al., (2017). [b]Araújo et al. (2016)*

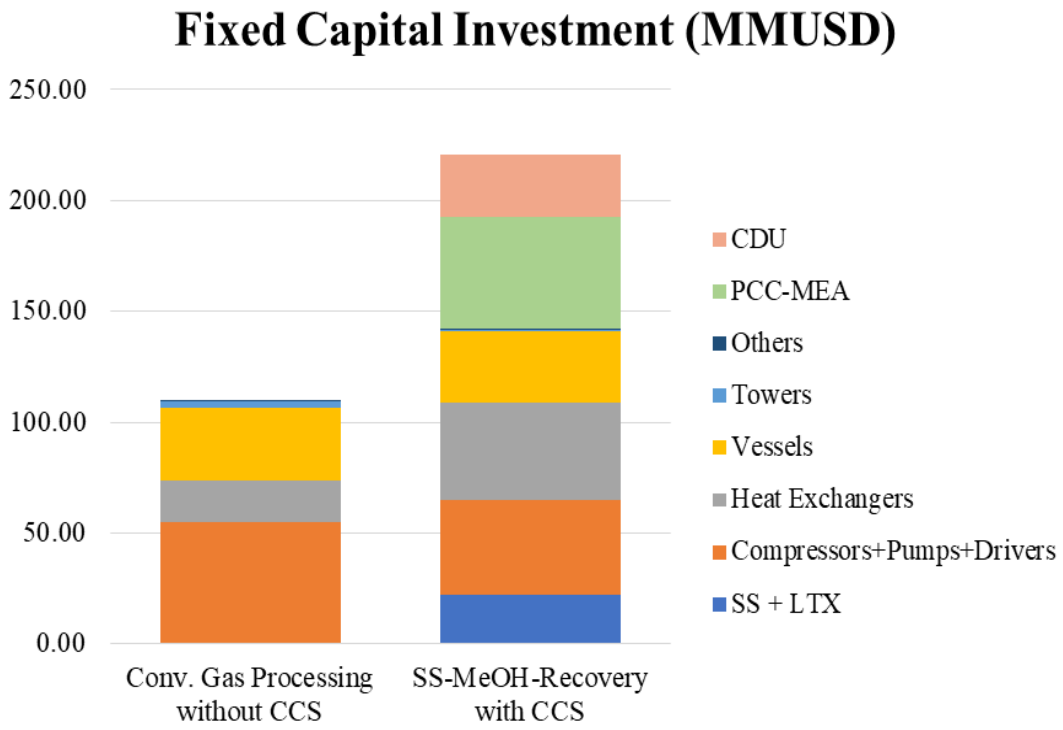

Figure IV. 11. Composition of *FCI* of gas processing alternatives

Table IV. 6. Summary of economic results.

	Conv. Gas Plant No CCS	***SS-MeOH-Recovery With CCS***
FCI (MMUSD)	*109.48*	*220.78*
SS + LTX	*-*	*22.08*
Compressors, Pumps & Drivers	*54.65*	*42.72*
Heat Exchangers	*19.28*	*43.76*
Vessels	*32.52*	*32.53*
Towers	*2.70*	*0.74*
TEG Inventory	*0.07*	*-*
THI Inventory	*0.26*	*0.25*
PCC-MEA	*-*	*50.47*
CDU	*-*	*28.23*
CRM (MMUSD/y)[a]	*1.47*	*0.15*
CUT (MMUSD/y)[b]	*3.00*	*2.07*
CO_2 Emissions (t/d)	*772.1*	*437.8*
CO_2 Tax (MMUSD/y)[c]	*17.40*	*9.87*
COM (MMUSD/y)	*43.05*	*52.92*
REV (MMUSD/y)[d]	*255.58*	*290.38*
NG Revenues	*238.89*	*229.67*
LPG Revenues	*16.68*	*52.74*
CO_2 Revenues	*-*	*7.98*
GAP (MMUSD/y)[e]	*212.52*	*237.46*
AP (MMUSD/y)[f]	*143.99*	*164.23*
NPV (MMUSD)	***829.31***	***865.63***

[a]Cost of raw materials. [b]Cost of utilities. [c]Cost of CO_2 taxation at 65 USD/t. [d]Revenues. [e]Gross annual profit .[f]Annual Profit.

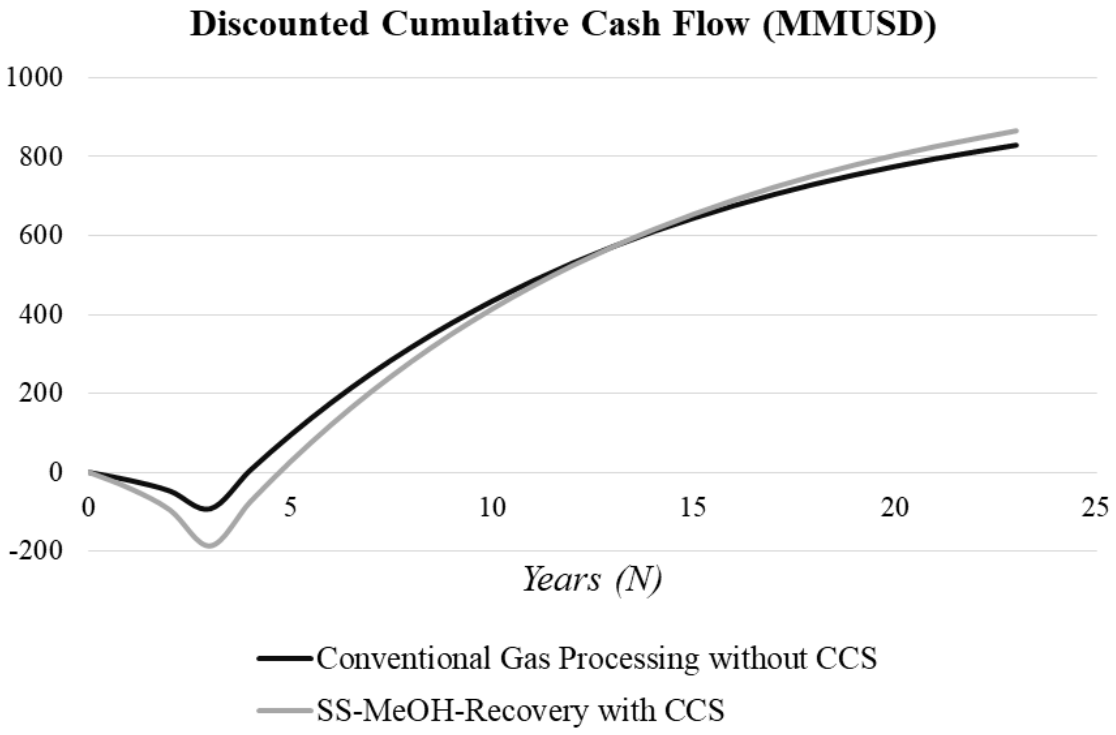

Figure IV.12. Profiles of net present value (*NPV*) of process alternatives.

Table IV.7. *NPV* sensitivity to oil price, NG price and CO_2 tax.

	NPV (MMUSD)		
	Conventional Gas Plant No CCS	***SS-MeOH-Recovery With CCS***	***ΔNPV***
Oil Price (USD/bbl)			
40	*799.12*	*755.77*	*-43.35*
50	*809.19*	*792.40*	*-16.78*
60	*819.24*	*829.00*	*9.76*
*70**	*829.31**	*865.63**	*36.33**
80	*839.36*	*902.22*	*62.86*
90	*849.43*	*938.86*	*89.43*
100	*859.48*	*975.45*	*115.97*
NG Price (USD/MMBTU)			
2.7	*674.16*	*715.82*	*41.65*
*3.2**	*829.31**	*865.63**	*36.33**
3.7	*984.45*	*1015.45*	*31.00*
4.2	*1139.59*	*1165.26*	*25.67*
CO_2 tax (USD/tonCO_2)			
0	*902.77*	*907.29*	*4.52*
30	*868.86*	*888.06*	*19.20*
*65**	*829.31**	*865.63**	*36.33**
90	*801.05*	*849.61*	*48.56*
120	*767.15*	*830.38*	*63.24*

**Base case values (Table IV.1)*

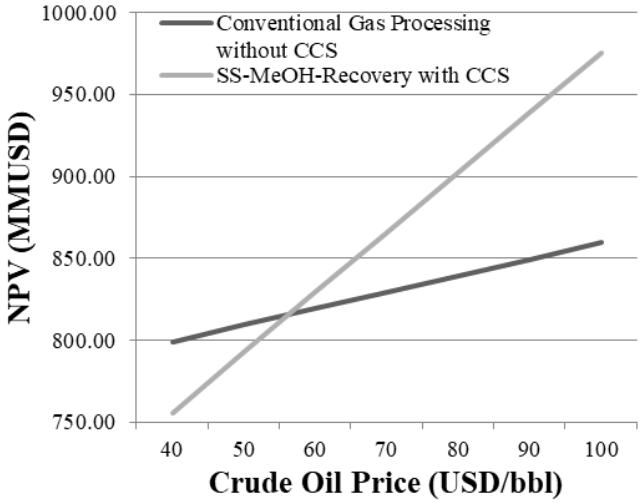

Figure IV.13. Influence of oil price on *NPV*.

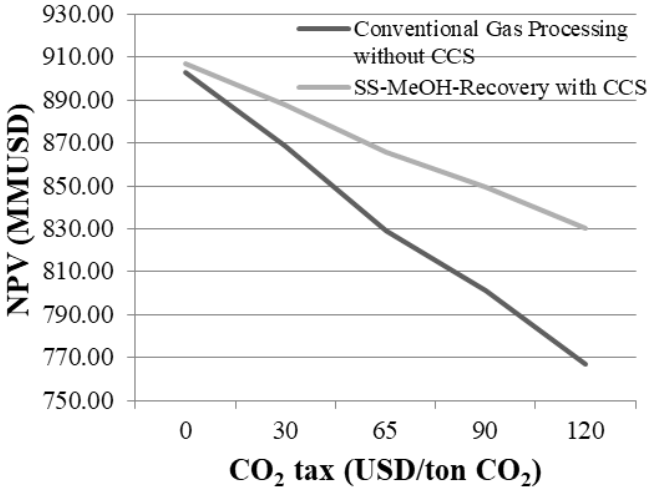

Figure IV.14. Influence of CO_2 taxation on *NPV*.

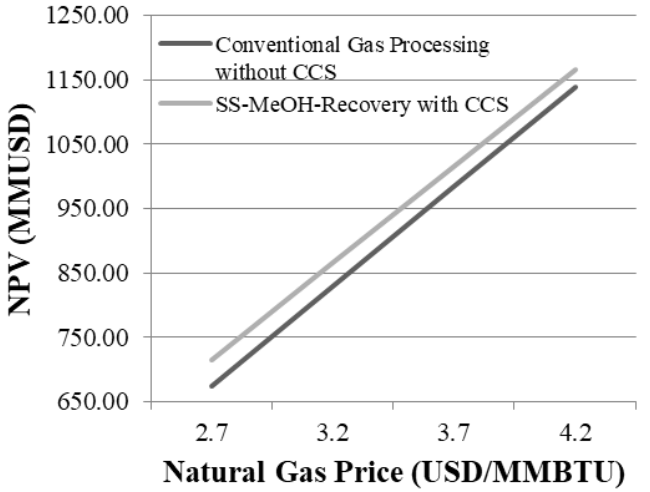

Figure IV.15. Influence of NG price on *NPV*.

IV.5. Conclusions

The economic and technical advantages of SS-based gas processing are investigated as a strategy for implementing CCS backed up by cost reduction and revenues increase via new more efficient gas processing. The advantages of such SS-based process, so-called SS-MeOH-Recovery, capable to recover methanol as anti-hydrate simultaneously conditioning natural gas and exporting valuable LPG product, coupled to a Methanol Recovery Unit, attained sufficient economic leverage to allow the new SS-MeOH-Recovery gas processing to afford a

PCC-MEA unit and associated compression and dehydration costs for CO_2 exportation as EOR agent. This CO_2 product represents new revenue – inexistent in the conventional gas processing – as CO_2 can be traded for oil in EOR applications.

Consequently, SS-MeOH-recovery with CCS plant outperforms the conventional gas processing (without CCS) in scenarios of high oil prices and high carbon taxes or even without carbon taxes and with oil prices above *≈55USD/bbl*. In addition, a novel CCS unit employing SS for CO_2 drying was disclosed, allowing the dehydration of CO_2 product with negligible head-loss, requiring minimum compression power for exportation and also contributing to improve process economics and reducing carbon emissions.

Therefore, SS-MeOH-Recovery in conjunction with MRU and novel SS-based CCS plant in offshore environment is shown to produce sufficient economic benefits that can afford a CCS plant with capacity to abate *≈43%* of CO_2 emissions, while maintaining economic superiority relative to the conventional gas processing. SS-MeOH-Recovery is superior on both economic and environmental grounds, providing a cleaner production of NG and LPG and configuring successful CO_2 management.

IV.6. Acknowledgments

Authors acknowledge financial support from Petrobras S.A. (0050.0096933.15.9). JL de Medeiros and OQF Araújo acknowledge financial support from CNPq-Brazil (311076/2017-3).

IV.7 References

Anwar M.N., Fayyaz, A., Sohail, N.F., Khokhar, M. F., Baqar, M., Khan, W.D., Rasool, K., Rehan, M., Nizami, A.S., CO2 capture and storage: A way forward for sustainable environment. Journal of Environmental Management, 226, 131–144, 2018. doi: 10.1016/j.jenvman.2018.08.009

Araújo, O.F.Q., Medeiros, J.L., Yokoyama, L., Morgado, C.R.V., Metrics for sustainability analysis of post-combustion abatement of CO2 emissions: Microalgae mediated routes and

CCS (carbon capture and storage), Energy, 92, 556-568, 2015. doi: 10.1016/j.energy.2015.03.116

Araújo O.Q.F., Reis A.C., de Medeiros J.L., Nascimento J.F., Grava W.M., Musse A.P.S., Comparative analysis of separation technologies for processing carbon dioxide rich natural gas in ultra-deepwater oil fields. J. of Clean. Production, 155, 12-22, 2016. doi: 10.1016/j.jclepro.2016.06.073.

Araújo O.Q.F. and de Medeiros J.L., Carbon capture and storage technologies: present scenario and drivers of innovation. Current Opinion in Chemical Engineering, 17, 22–34, 2017. doi: 10.1016/j.coche.2017.05.004

Arinelli, L.O., Trotta, T.A. F., Teixeira, A.M., de Medeiros, J.L., Araújo, O.Q.F., Offshore Processing of CO2 Rich Natural Gas with Supersonic Separator versus Conventional Routes. J. of Nat. Gas Sci. and Eng., 46, 199-221, 2017. doi: 10.1016/j.jngse.2017.07.010

Bianchi, M,, Branchini, L., de Pascale, A., Melino., F., Peretto, A., Valentini, E. Thermoeconomic evaluation of orc system in off-shore applications. Proceedings of the ASME Turbo Expo 2014: Turbine Technical Conference and Exposition. 2014. Paper GT2014-25170. doi: 10.1115/GT2014-25170

Botero, C., Finkenrath M., Bartlett, M., Chu, R., Choi G., Chinn, D., Redesign, Optimization, and Economic Evaluation of a Natural Gas Combined Cycle with the Best Integrated Technology CO2 Capture. Energy Procedia, 1, 3835–3842, 2009. Doi: 10.1016/j.egypro.2009.02.185

Cruz, M.A., de Medeiros, J.L. Araújo, O.Q.F., Deep seawater intake for primary cooling in tropical offshore processing of natural gas with high carbon dioxide content: Energy, emissions and economic assessments. J. of Nat. Gas Sci. and Eng., 56, 193-211, 2018. doi: 10.1016/j.jngse.2018.06.011

de Medeiros, J. L., Arinelli, L. O., Araújo, O. Q. F. Speed of Sound of Multiphase and Multi-Reactive Equilibrium Streams: A Numerical Approach for Natural Gas Applications. J. of Nat. Gas Sci. and Eng., 46, 222-241, 2017. doi: 10.1016/j.jngse.2017.08.006

Folas, G.K., Gabrielsen, J., Michelsen, M.L., Stenby, E.H., Kontogeorgis, G.M., Application of the Cubic-Plus-Association (CPA) Equation of State to Cross-Associating Systems. Ind. Eng. Chem. Res., 44, 3823−3833, 2005. doi: 10.1021/ie048832j

Gallo, W.L.R., Gallego, A.G., Acevedo, V.L., Dias, R., Ortiz, H.Y., Valente, B.A. Exergy analysis of the compression systems and its prime movers for a FPSO unit. Journal of Natural Gas Science and Engineering, 44, 287-298. 2017. doi: 10.1016/j.jngse.2017.04.023

Granjo J.F.O., Oliveira N.M.C. Process Simulation and Techno-Economic Analysis of the Production of Sodium Methoxide. Ind. & Eng. Chem. Res., 55, 1, 156-167, 2016. doi: 10.1021/acs.iecr.5b02022

Lundgren, T., Marklund, O., Samakovlis, E., Zhouc, W., Carbon prices and incentives for technological development. Journal of Environmental Management, 150, 393-403, 2015. doi: 10.1016/j.jenvman.2014.12.015

Machado, P.B., Monteiro, J.G.M., de Medeiros, J.L., Araújo, O.Q.F., Supersonic separation in onshore natural gas dew point plant, J. of Nat. Gas Sci. and Eng., 6, 43-49, 2012. doi:10.1016/j.jngse.2012.03.001

Maitland, G.C., Carbon capture and storage: concluding remarks. Faraday Discuss. Vol. 192, pp 581-599, 2016. doi:10.1039/C6FD00182C

McCoy, S.T., The Economics of CO2 Transport by Pipeline and Storage in Saline Aquifers and Oil Reservoirs. PhD Thesis, Carnegie Mellon University, USA, 2008

Mokhatab, S., William, A.P, Speight, J.G., Handbook of natural gas transmission and processing. Burlington: Elsevier; 2006, ISBN 978-0-7506-7776-9.

Nazeri, M., Tohidi, B., Chapoy, A. An Evaluation of Risk of Hydrate Formation at the Top of a Pipeline. Society of Petroleum Engineers. SPE-160404-MS. 2012. doi: 10.2118/160404-MS

Nguyen, T-V., Tock, L., Breuhaus, P., Maréchal, F., Elmegaard, B., CO2-mitigation options for the offshore oil and gas sector, Applied Energy, 161, 673-694, 2016. doi: 10.1016/j.apenergy.2015.09.088

Olajire, A. A., CO2 capture and separation technologies for end-of-pipe applications - A review, Energy, 35, 2610-2628, 2010. doi:10.1016/j.energy.2010.02.030

Rech, O., 2012. Oil & gas costs perspectives: focus on conventional oil & gas projects. In: 10th ASPO Conference

Sánchez, Y.A.C. and de Oliveira Jr., S., Exergy analysis of offshore primary petroleum processing plant with CO2 capture, Energy, 88, 46-56, 2015. doi: 10.1016/j.energy.2015.05.130

Sepehri, A. and Sarrafzadeh, M. H., Effect of nitrifiers community on fouling mitigation and nitrification efficiency in a membrane bioreactor. Chemical Engineering and Processing - Process Intensification, Vol. 128, June 2018, pp. 10-18. doi: 10.1016/j.cep.2018.04.006

Teixeira, A.M., Arinelli, L.O., de Medeiros, J.L., Araújo, O.Q.F., Exergy Analysis of Monoethylene Glycol Recovery Processes for Hydrate Inhibition in Offshore Natural Gas Fields. Journal of Natural Gas Science & Engineering, 35, 798-813, 2016. doi: 10.1016/j.jngse.2016.09.017

Teixeira, A.M., Arinelli, L.O., Medeiros, J.L., Araújo, O.Q.F., Recovery of thermodynamic hydrate inhibitors methanol, ethanol and MEG with supersonic separators in offshore natural gas processing. J. of Nat. Gas Sci. and Eng., 52, 166-186, 2018. doi: 10.1016/j.jngse.2018.01.038

Turton R, Bailie RC, Whiting WB, Shaeiwitz JA. Analysis, Synthesis, and Design of Chemical Processes. 3rd ed. New Jersey: Prentice Hall Int. 2009

Urech, J., Tock, L., Harkin, T., Hoadley, A., Maréchal, F., An assessment of different solvent-based capture technologies within an IGCC-CCS power plant. Energy, 64, 268-276, 2013. doi: 10.1016/j.energy.2013.10.081

Wang Y., Hu, D. Experimental and numerical investigation on the blade angle of axial-flow swirling generator and drainage structure for supersonic separators with diversion cone. Chemical Engineering Research and Design. 133, 155–167, 2018. doi: 10.1016/j.cherd.2018.03.008

Wiesberg, I.L., Brigagão, G.V., de Medeiros, J.L., Araújo, O.Q.F., Carbon dioxide utilization in a microalga-based biorefinery: Efficiency of carbon removal and economic performance under carbon taxation. Journal of Environmental Management, 203, 3, 988-998, 2017. Doi: 10.1016/j.jenvman.2017.03.005[

Yang, Y., Wen, C., Wang, S., Feng, Y., Theoretical and numerical analysis on pressure recovery of supersonic separators for natural gas dehydration. Applied Energy 2014, 132, 248-253, doi 10.1016/j.apenergy.2014.07.018

CHAPTER V – FURTHER RESEARCH

This Chapter gathers some additional results complementing the previous Chapters, as well as results obtained from parallel research regarding the natural gas processing of fields with high and ultra-high CO_2 content.

V.1 - Sustainable Carbon Capture via Recovery of Thermodynamic Hydrate Inhibitors with Supersonic Separators in Offshore Natural Gas Processing

This work complements the results obtained in CHAPTER IV which proved that, when THI=methanol, SS-THI-Recovery dramatically improves offshore gas plant profitability via cost-reduction of THI make-up and power consumption, simultaneously increasing revenues from LPG. In CHAPTER IV, such economic leverage was shown to afford a post-combustion carbon capture plant with MEA and the heat required by MEA plant in regeneration section was considered cost-free and provided by the waste heat recovery from exhausts, which limits the amount of captured CO_2. In this case, 43% of CO_2 emissions abatement was achieved.

However, CHAPTER IV only addressed methanol as THI, and depending on the choice of THI, power consumption and heat requirements for the gas plant are different, as well as the available heat for CO_2 capture. In addition, MEG is the most employed THI in the world, and ethanol is widely employed in countries of high industrial production. Therefore, a complete comparison with other THIs taking into account the different process requirements and CO_2 capture ratio should be performed as well so as to provide a comprehensive understanding of all alternatives by means of simulation and economic evaluation, therefore indicating the best THI alternative from both environmental and economic perspective.

Similarly to CHAPTER IV, economic and environmental assessments were conducted for two offshore gas processing plants coupled to THI-RU plant for THI recovery with/without PCC-MEA for CO_2 abatement. Now, three THIs – methanol, ethanol and MEG – were individually

considered, and only the post-combustion carbon capture plant with MEA was considered in the CCS, i.e the compression and dehydration unit for CO_2-rich stream was not considered.

Flowsheets were simulated in HYSYS 8.8 employing SS-UOE (a rigorous SS thermodynamic model handling multiphase – aqueous THI, hydrocarbon condensate and gas – supersonic compressible flow) in connection with PEC-UOE (rigorously calculating phase-equilibrium sound speed (c)), as explained in previous Chapters. Both SS-UOE and PEC-UOE used the Cubic-Plus-Association Equation-of-State (CPA-EOS) for full phase-split and calculation of multiphase properties, respectively for multiphase compressible flow in SS units and for calculating the multiphase sound speed (c).

SS-THI-Recovery coupled to THI-RU and PCC-MEA was economically compared against conventional gas processing also with THI-RU but without PCC-MEA. The superior performance of SS-THI-Recovery was sufficient to afford the PCC-MEA capturing at least ≈43% of all CO_2 emissions from the offshore rig power plant (Table V.1), yet maintaining economic superiority to conventional gas processing without PCC-MEA in all scenarios (Table V.2). All THIs presented similar results, with ethanol showing superior economic performance, despite occupying an intermediate position in CO_2 abatement.

Table V.1. Performances of processes: CO_2 capture, power and heat demands.

THI	***Methanol***		***Ethanol***		***MEG***	
	Conventional Gas Plant THI-RU	***SS-THI-Recovery THI-RU PCC-MEA***	***Conventional Gas Plant THI-RU***	***SS-THI-Recovery THI-RU PCC-MEA***	***Conventional Gas Plant THI-RU***	***SS-THI-Recovery THI-RU PCC-MEA***
Power Demand(MW)	*14.2*	*8.4*	*14.2*	*8.4*	*13.9*	*8.6*
Heat Demand (MW)	*2.3*	*4.1*	*2.7*	*4.3*	*4.2*	*5.1*
Available heat for CO_2 capture (MW)	-	*55.9*	-	*55.7*	-	*54.9*
CO_2 capture (%)	**-**	***43.4***	**-**	***43.3***	**-**	***43.1***

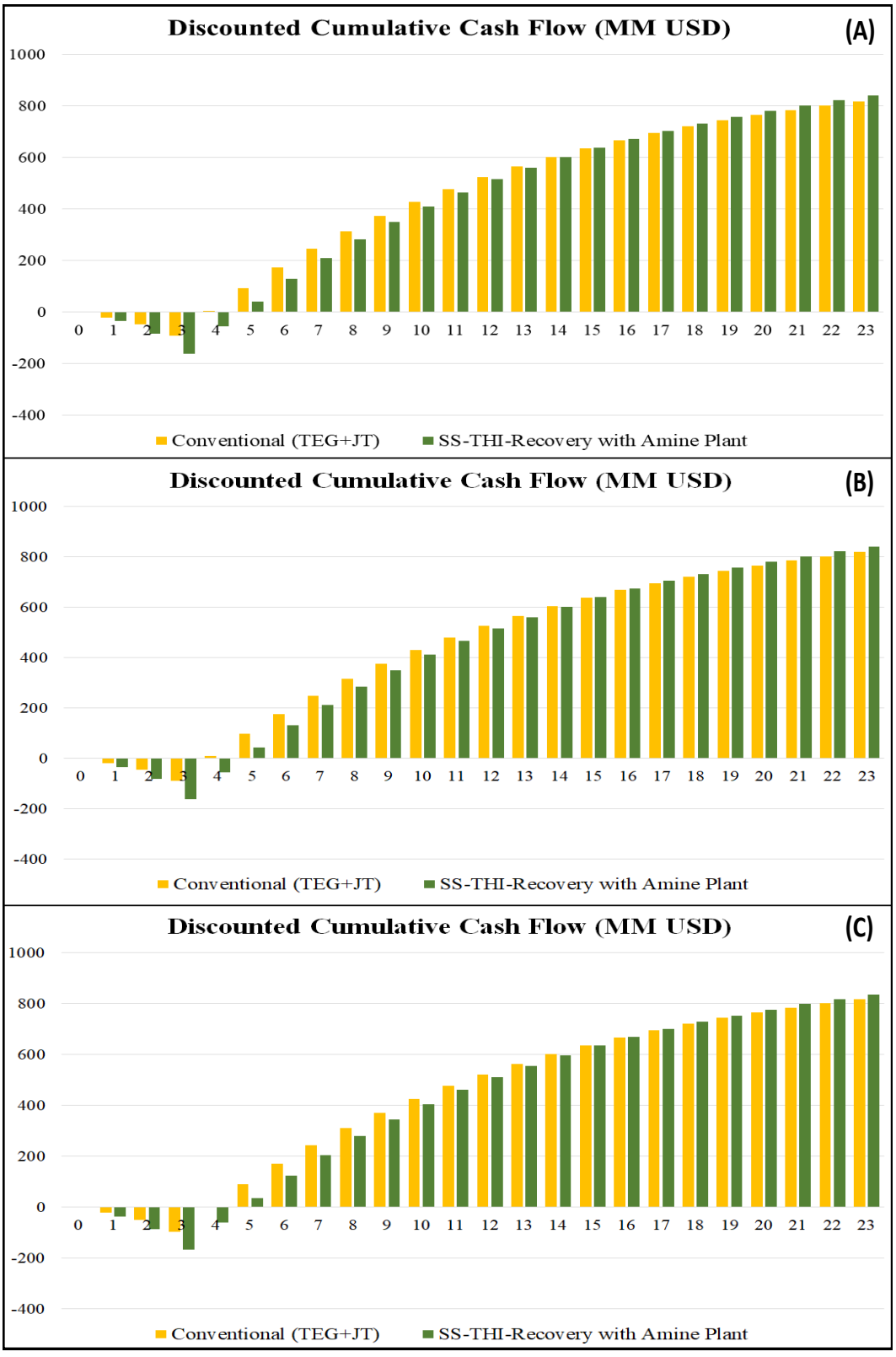

Figure V.1. *NPV* versus year: (A) THI=methanol, (B) THI=ethanol, (C) THI=MEG.

Table V.2. Economic results including carbon taxation costs.

THI	*Methanol*		*Ethanol*		*MEG*	
	Conv. Gas Plant THI-RU	*SS-THI-Recovery THI-RU PCC-MEA*	*Conv. Gas Plant THI-RU*	*SS-THI-Recovery THI-RU PCC-MEA*	*Conv. Gas Plant THI-RU*	*SS-THI-Recovery THI-RU PCC-MEA*
FCI (MMUSD)	*109.48*	*190.68*	*103.57*	*187.01*	*113.29*	*193.62*
CRM (MMUSD/y)[a]	*1.47*	*0.15*	*2.37*	*0.6*	*0.01*	*0.00*
CUT (MMUSD/y)[b]	*3.00*	*1.71*	*2.97*	*1.71*	*2.90*	*1.75*
CO_2 Emissions (t/d)	*770.6*	*436.9*	*770.6*	*437.4*	*770.6*	*439.6*
CCTX (MMUSD/y)[c]	*17.37*	*9.85*	*17.37*	*9.86*	*17.37*	*9.91*
COM (MMUSD/y)	*43.02*	*46.90*	*43.02*	*46.80*	*41.78*	*47.35*
REV (MMUSD/y)[d]	*253.19*	*274.70*	*252.42*	*274.72*	*252.44*	*275.53*
GAP (MMUSD/y)[e]	*210.17*	*227.80*	*209.39*	*227.92*	*210.66*	*228.18*
AP (MMUSD/y)[f]	*142.43*	*156.83*	*141.72*	*156.79*	*142.89*	*157.18*
NPV (MMUSD)[g]	***819.37***	***843.50***	***819.76***	***846.23***	***819.09***	***843.23***

[a]Cost of raw materials. [b]Cost of utilities. [c]Cost of CO_2 taxation at 65 USD/t. [d]Revenues. [e]Gross annual profit; [f]Annual profit. [g] For N=23 years.

Fig. V.1 illustrates NPV over time for all processes. Comparatively, all THIs presented similar performances, with ethanol being slightly superior in economic grounds and methanol being the most effective in CO_2 capture (Table V.2). Nevertheless, all THIs are shown to be appropriate for complying with the goal of reducing CO_2 emissions with superior economic performance.

Similarly to CHAPTER IV, sensitivities studies on main economic parameters were also conducted and are presented in Tables V.3, V.4 and V.5

.

Table V.3. Impact of CO_2 tax on *NPV* (MMUSD) of processes.

THI	*Methanol*			*Ethanol*			*MEG*		
CO_2 tax (USD/tCO_2)	*Conv. Gas Plant THI-RU*	*SS-THI-Recovery THI-RU PCC-MEA*		*Conv. Gas Plant THI-RU*	*SS-THI-Recovery THI-RU PCC-MEA*		*Conv. Gas Plant THI-RU*	*SS-THI-Recovery THI-RU PCC-MEA*	
			ΔNPV			*ΔNPV*			*ΔNPV*
0	*892.70*	*885.07*	*-7.62*	*893.08*	*887.85*	*-5.24*	*892.41*	*885.06*	*-7.35*
30	*858.86*	*865.89*	*7.03*	*859.24*	*868.64*	*9.40*	*858.57*	*865.76*	*7.19*
65[*]	*819.37*[*]	*843.50*[*]	*24.13*[*]	*819.76*[*]	*846.23*[*]	*26.47*[*]	*819.09*[*]	*843.23*[*]	*24.15*[*]
90	*791.17*	*827.51*	*36.34*	*791.55*	*830.22*	*38.66*	*790.88*	*827.15*	*36.26*
120	*757.33*	*808.32*	*50.99*	*757.71*	*811.01*	*53.30*	*757.04*	*807.84*	*50.80*

[*] *Adopted for economic analysis*

Table V.4. Impact of oil price on *NPV* (MMUSD) of processes.

THI	*Methanol*			*Ethanol*			*MEG*		
Oil Price (USB/bbl)	*Conv. Gas Plant THI-RU*	*SS-THI-Recovery THI-RU PCC-MEA*		*Conv. Gas Plant THI-RU*	*SS-THI-Recovery THI-RU PCC-MEA*		*Conv. Gas Plant THI-RU*	*SS-THI-Recovery THI-RU PCC-MEA*	
			ΔNPV			*ΔNPV*			*ΔNPV*
45	*804.29*	*796.03*	*-8.26*	*805.72*	*798.61*	*-7.12*	*804.93*	*794.46*	*-10.47*
50	*809.32*	*811.88*	*2.56*	*810.40*	*814.48*	*4.08*	*809.65*	*810.73*	*1.08*
55	*814.34*	*827.69*	*13.35*	*815.08*	*830.35*	*15.27*	*814.37*	*826.96*	*12.59*
60[*]	*819.37*[*]	*843.50*[*]	*24.13*[*]	*819.76*[*]	*846.23*[*]	*26.47*[*]	*819.09*[*]	*843.23*[*]	*24.15*[*]
65	*824.41*	*859.36*	*34.95*	*824.43*	*862.10*	*37.67*	*823.79*	*859.46*	*35.67*
70	*829.44*	*875.16*	*45.72*	*829.10*	*877.97*	*48.87*	*828.51*	*875.74*	*47.22*
75	*834.47*	*890.97*	*56.50*	*833.79*	*893.85*	*60.06*	*833.23*	*891.97*	*58.73*
80	*839.49*	*906.78*	*67.29*	*838.46*	*909.72*	*71.26*	*837.95*	*908.24*	*70.29*
85	*844.53*	*922.64*	*78.11*	*843.14*	*925.59*	*82.46*	*842.67*	*924.47*	*81.80*
90	*849.56*	*938.44*	*88.88*	*847.81*	*941.42*	*93.61*	*847.38*	*940.70*	*93.32*

[*] *Adopted for economic analysis*

Table V.5. Impact of NG price on *NPV* (MMUSD).

THI	*Methanol*			*Ethanol*			*MEG*		
NG Price (USD/MMBTU)	*Conv. Gas Plant THI-RU*	*SS-THI-Recovery THI-RU PCC-MEA*		*Conv. Gas Plant THI-RU*	*SS-THI-Recovery THI-RU PCC-MEA*		*Conv. Gas Plant THI-RU*	*SS-THI-Recovery THI-RU PCC-MEA*	
			ΔNPV			*ΔNPV*			*ΔNPV*
2.7	*664.23*	*693.35*	*29.12*	*664.44*	*696.16*	*31.72*	*663.77*	*693.38*	*29.61*
3.2[*]	*819.37*[*]	*843.50*[*]	*24.13*[*]	*819.76*[*]	*846.23*[*]	*26.47*[*]	*819.09*[*]	*843.23*[*]	*24.15*[*]
3.7	*974.52*	*993.65*	*19.13*	*975.08*	*996.30*	*21.22*	*974.41*	*993.09*	*18.68*
4.2	*1129.66*	*1143.80*	*14.14*	*1130.39*	*1146.37*	*15.97*	*1129.73*	*1142.94*	*13.21*

[*] *Adopted for economic analysis*

Similarly to the conclusions of CHAPTER IV, high oil prices strongly beneficiates SS-THI-Recovery with PCC-MEA because LPG is one of its important revenues and LPG price is proportional to oil price. The conventional gas plant is less beneficiated by rising oil prices because its LPG is residual and its major revenue is NG exportation, whose price does not correlate with oil price. Similarly, the higher the carbon taxes, the higher the *ΔNPV* of SS-THI-Recovery with PCC-MEA relative to the conventional plant because the former significantly reduced its CO_2 emissions. Finally, as NG prices rise, the difference of economic performances of both alternatives vanishes – with SS-THI-Recovery always superior. Both processes have similar NG revenues, but with great difference in LPG revenues, which is more than *≈200%* higher for SS-THI-Recovery.

Comparatively, all THIs presented similar performances, with ethanol being slightly superior in economic grounds and methanol being the most effective in CO_2 capture. Nevertheless, all

THIs are shown to be appropriate for complying with the goal of reducing CO_2 emissions with superior economic performance.

Therefore, lowering CO_2 emissions by implementing PCC-MEA and achieving a cleaner production was made viable by an economic leverage provided by the more efficient SS-THI-Recovery relatively to the conventional counterpart for any THI. Such analysis in the context of offshore gas processing is backed up by rigorous thermodynamic simulations and economic-environmental assessments, bringing important conclusions and insights regarding the choice of THI and its impacts.

V.2 - Offshore processing of CO_2 rich natural gas with supersonic separator versus conventional routes

This work was published in Journal of Natural Gas Science and Engineering, Vol. 46, p. 199-221, 2017 (doi: 10.1016/j.jngse.2017.07.010) (Appendix E.12).

This work was the first in the literature to study the use of supersonic separators for conditioning humid CO_2-rich natural gas and comparing its performance with conventional routes (TEG absorption, JT expansion and Membrane Permeation (MP)) by means of process simulation. Such approach was fully based on thermodynamics, in frontal contrast with CFD approaches present in the literature. MP and SS models are disclosed, giving rise to Unit Operation Extensions (UOE) to be inserted in HYSYS 8.8 PFDs for simulation of MP and SS units, namely, MP-UOE and SS-UOE. Such developed tools were able to provide graphical SS profiles and SS paths. Fig. V.2. illustrates an example of SS flow path in *P x T* plane obtained by SS-UOE.

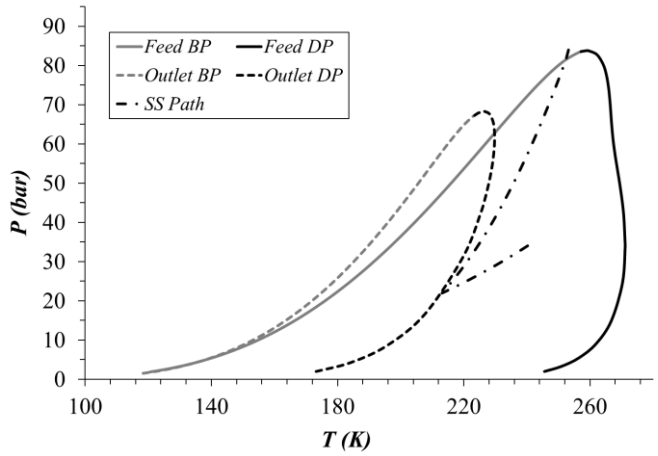

Figure V.2. Plane *P x T* for SS Path in Cases 3-3x: (i) Feed VLE Envelope; (ii) SS Path; (iii) Final NG VLE Envelope.

SS-UOE and MP-UOE were applied in the simulation of four process configurations investigated for offshore conditioning of a water saturated NG with *44%* of CO_2 content. Conventional Case 1 comprised TEG WDPA, JTE HCDPA and MP CO_2 removal. Alternatives Cases 2, 3, 3x were proposed applying SS for WDPA+HCDPA or SS for CO_2 removal.

PFDs A, B, C, D and E are shown in Figs. V.3-V.7. Case 1 (referring to the conventional process) consists of PFDs A and B, while Case 2 executes SS WDPA+HCDPA and MP CO_2 removal employing PFDs C and B, Case 3 executes SS CO_2 removal with PFDs A and D and Case 3x is a variant with PFDs A and E.

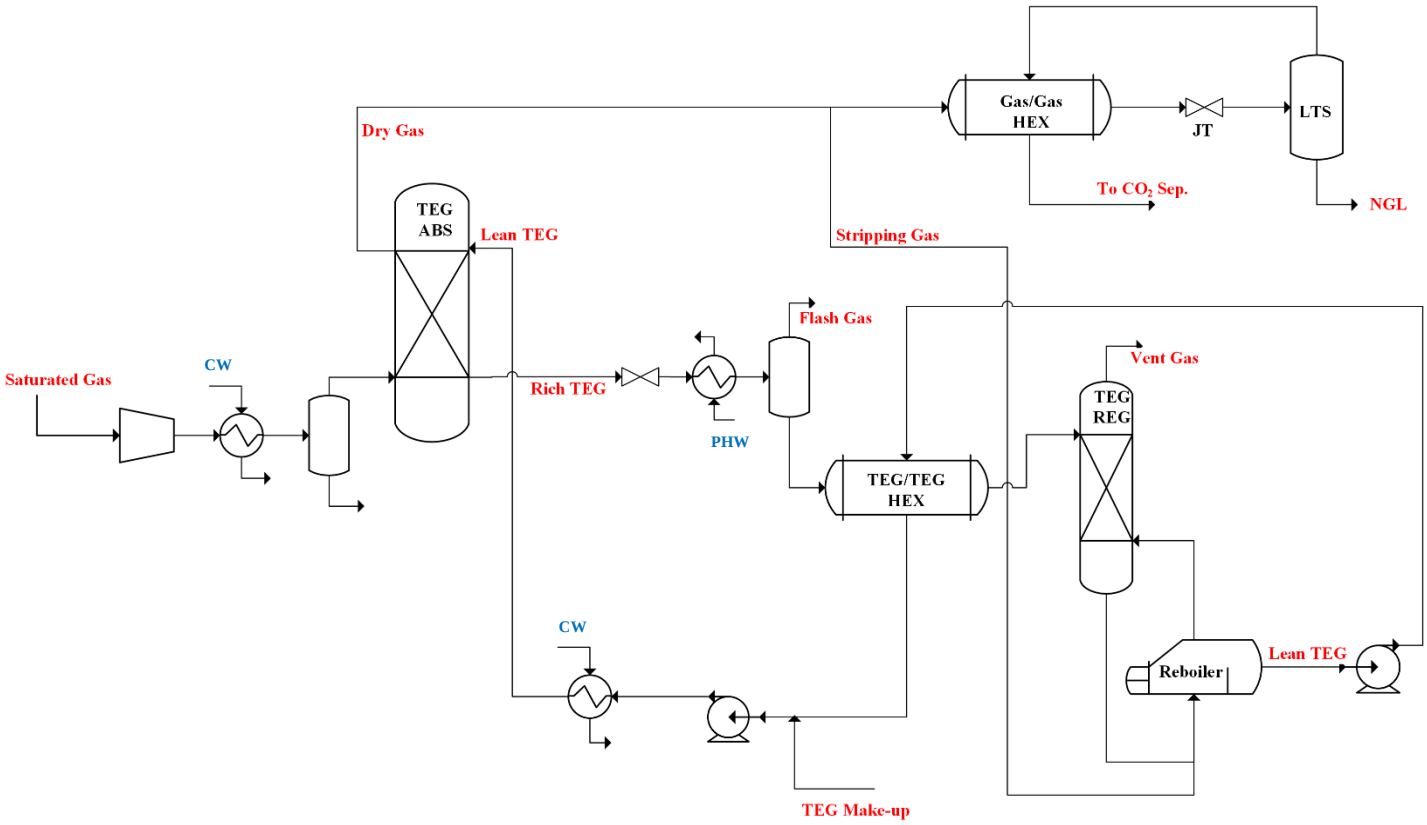

Figure V. 3. PFD A: TEG WDPA & JTE HCDPA.

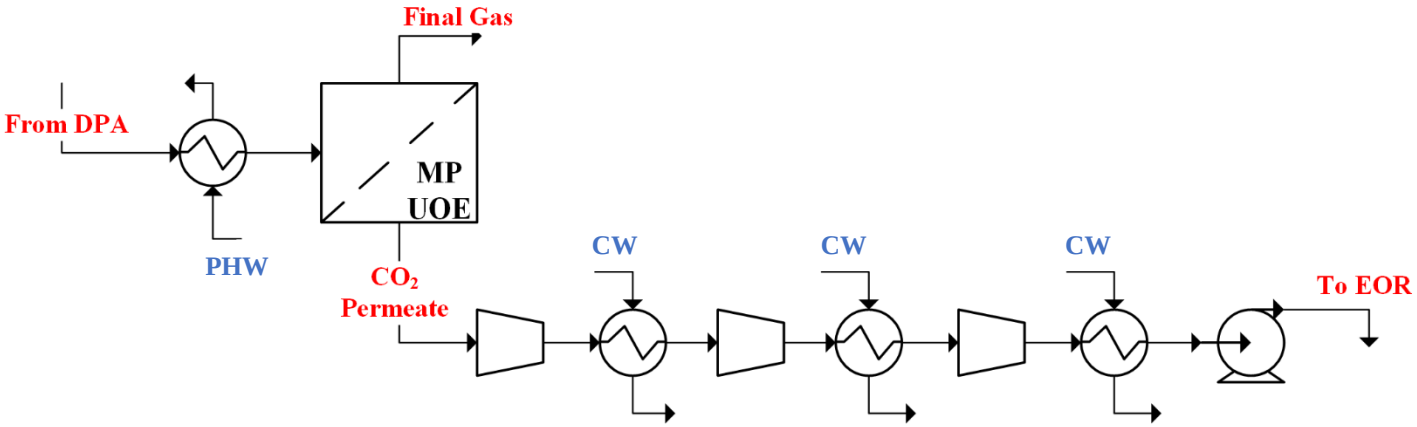

Figure V.4. PFD B: MP CO_2 Removal & Compression to EOR.

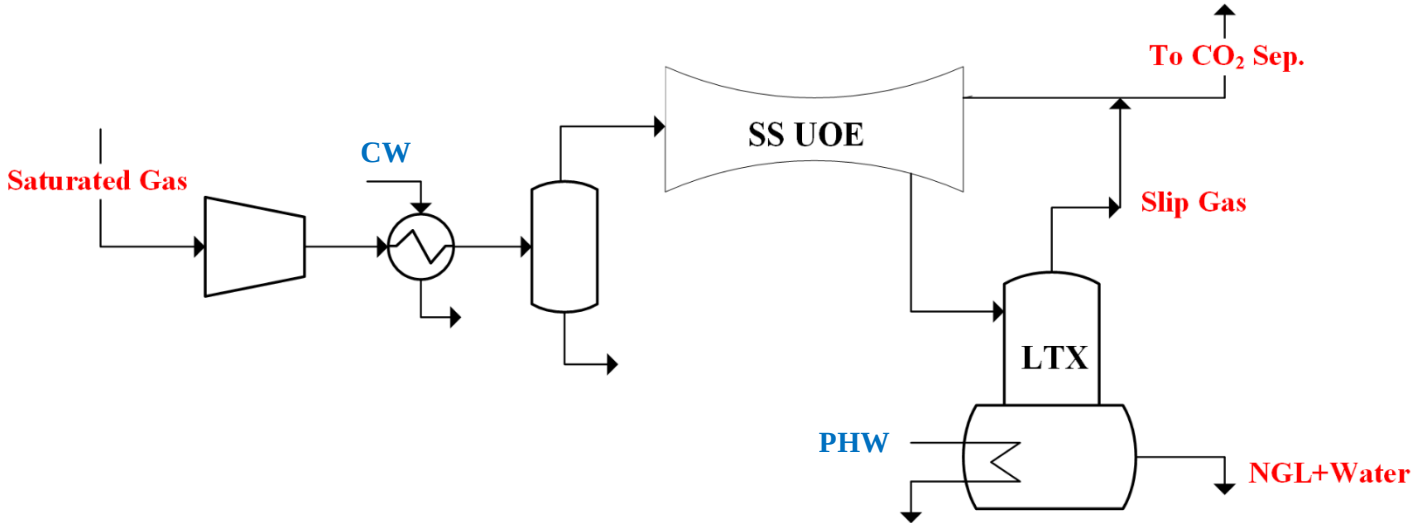

Figure V.5. PFD C: SS WDPA+HCDPA with LTX.

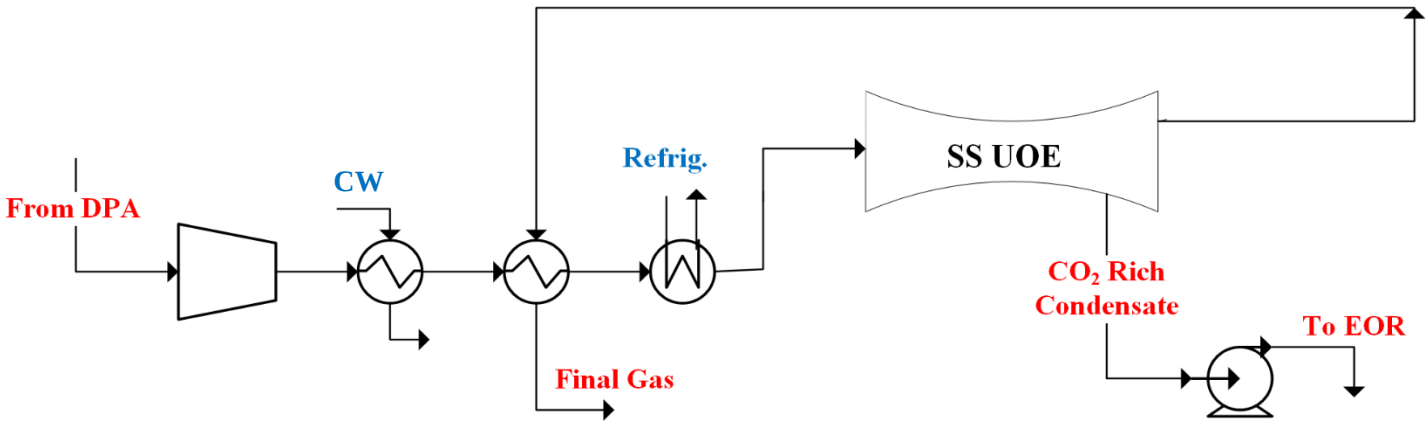

Figure V.6. PFD D: SS CO_2 Removal. Condensate Pumped to EOR.

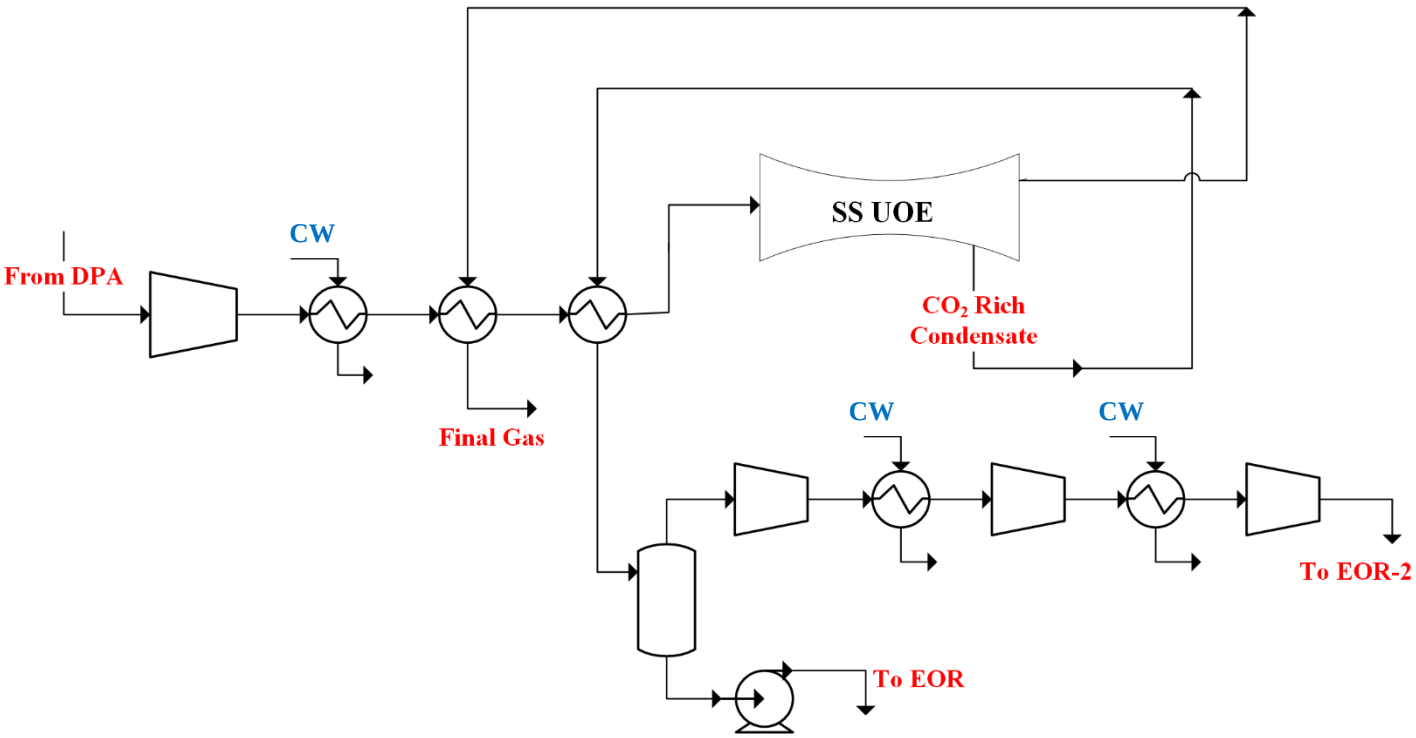

Figure V.7. PFD E: SS CO_2 Removal. Feed Cooled by Final NG and Condensate. Compression/Pumping to EOR

Power consumption was assessed for all process configurations, including the power required by a CO_2 refrigeration cycle to cool the SS feed in Case 3, which is not present in Case 3x. Fig. V.8 depicts an illustrative graphic for power consumption of such alternatives.

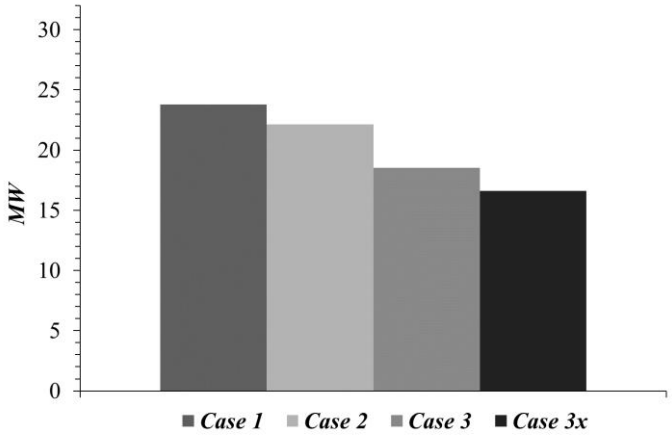

Figure V.8. Power Consumptions of Cases 1, 2, 3 and 3x

Compared to Case 1, Case 2 demands *6.9%* less power due to lower SS feed pressure in PFD C, while Case 3 demands *22.1%* less power, a consequence of extracting high pressure SS condensate with direct pumping to EOR, whereas Case 1 prescribes an expensive 3-stage compression from *4 bar* to *250 bar* for the same purpose. Case 3x avoids investment with refrigeration, demanding *10.3%* less power than Case 3 and *30.2%* less than Case 1.

This work also highlights that raw NG should be previously treated for WDPA+HCDPA to allow exclusive CO_2 condensation under deep temperature fall, and in the case of CO_2 rich NG, CO_2 freeze-out must also be avoided to prevent plugging, i.e. SS flow path should be controlled so that CO_2 freeze-out border is not crossed (there is a maximum admissible *Ma* in SS flow path to prevent CO_2 freeze-out) (Fig. V.9).

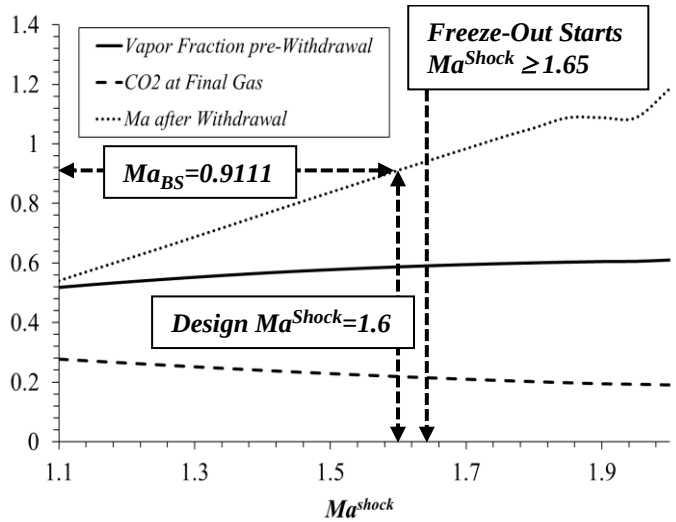

Figure V. 9. Influence of Ma^{Shock} in SS Operation for Cases 3-3x: (i) Vapor Fraction pre-Withdrawal; (ii) Final $\%CO_2$; (iii) Ma after Withdrawal (Ma_{BS}); (iv) Operation Point $Ma^{Shock}=1.6$ & $Ma_{BS}=0.9111$.

A sensitivity analysis of SS performance was also conducted by means of parametric inclusion of adiabatic efficiencies for expansion-compression paths in SS-UOE. Fig. V.10 illustrates pressure profiles for different values of adiabatic efficiencies.

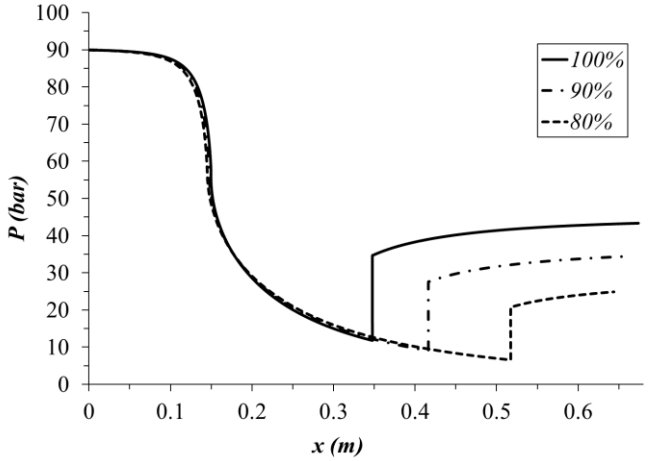

Figure V.10. SS Pressure Profiles for $\eta^{EXP}\%=\eta^{CMP}\%=\{80\%, 90\%, 100\%\}$

V.3 - Supersonic separator for cleaner offshore processing of natural gas with high carbon dioxide content: Environmental and economic assessments.

This work was published in Journal of Cleaner Production, Vol. 233, p. 510-521, 2019 (doi: 10.1016/j.jclepro.2019.06.115) (Appendix E.13)

This work approaches a cleaner CO_2-rich natural gas processing scheme for offshore platforms based on full utilization of supersonic separators (SS). Considering the processing of raw natural gas with 44%mol CO_2 similarly to Section V.2, this work shows that SS can replace conventional alternatives for water dew-point adjustment (WDPA), hydrocarbon dew-point adjustment (HCDPA) as well as CO_2 removal. All results were obtained via rigorous simulations, including simulation of supersonic separators via multiphase supersonic compressible flow and its inseparable rigorous determination of the multiphase sound speed.

This work thermodynamically, environmentally and economically investigates this new concept of offshore CO_2-rich NG processing using two consecutive SS units for WDPA+HCDPA and CO_2 removal, the so-called SS-SS alternative. SS-SS results are compared with conventional CO_2-rich gas processing – which applies TEG absorption for WDPA, Joule-Thomson expansion for HCDPA and membrane permeation (MP) for CO_2 removal – and with an intermediate gas processing scheme where SS is used only for WDPA+HCDPA and membrane-permeation (MP) is kept for CO_2 removal, the so-called SS-MP alternative.

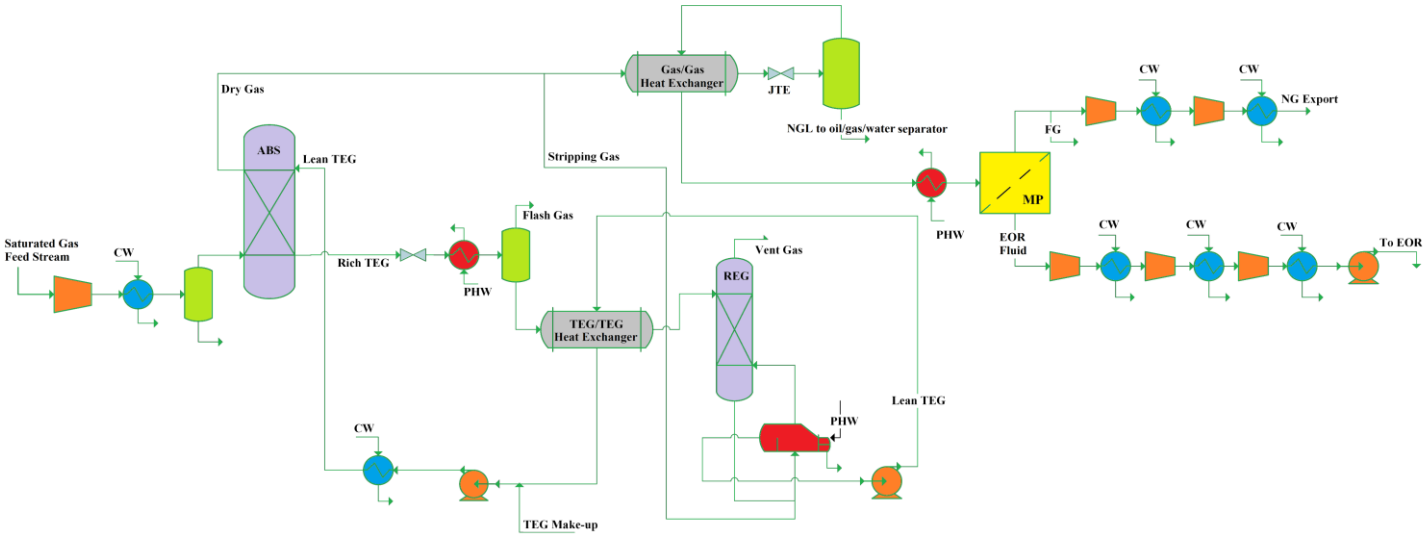

a)

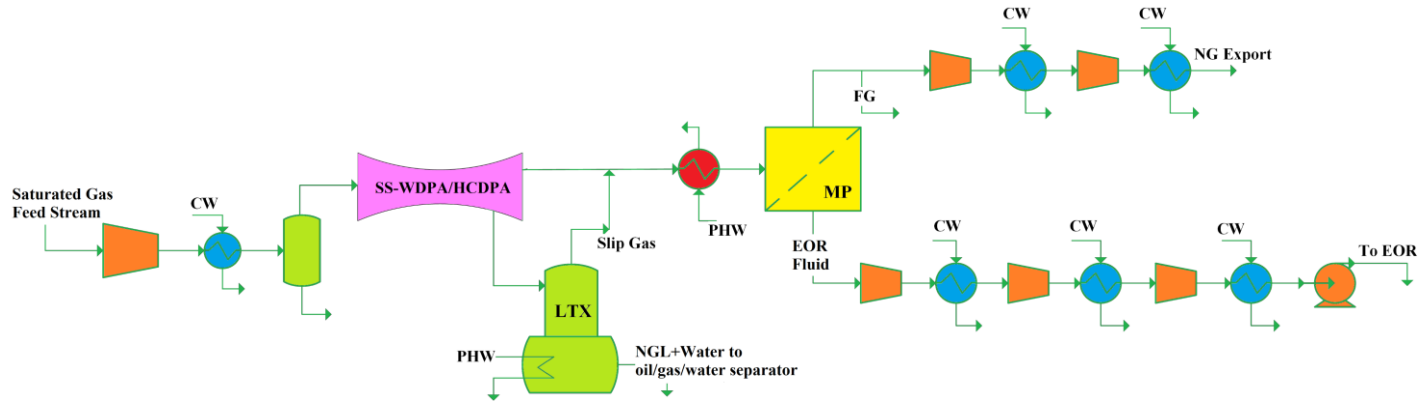

b)

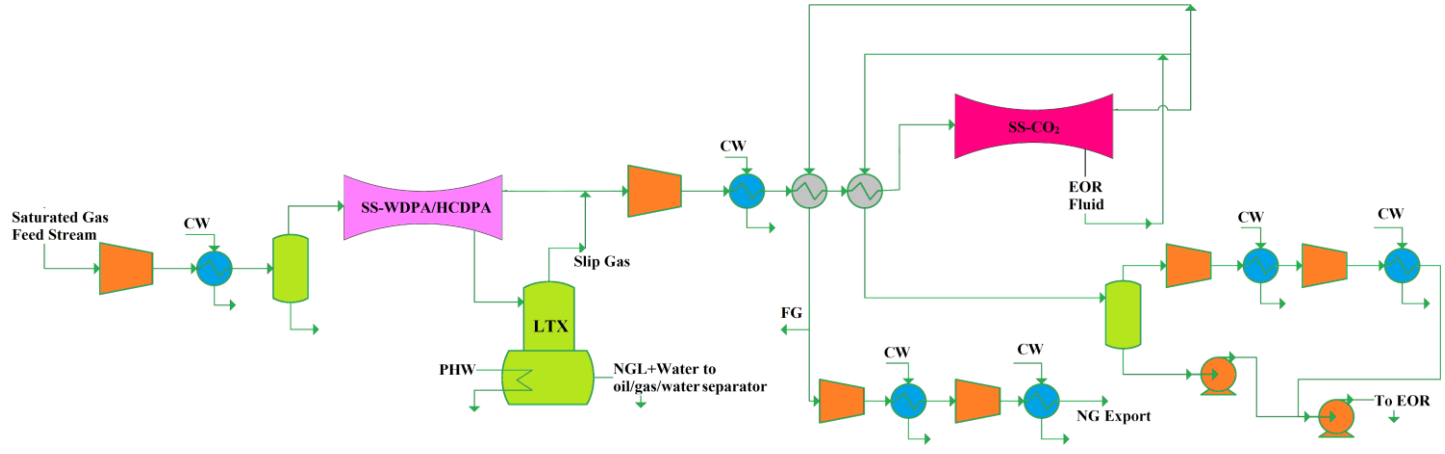

c)

Figure V.11. Process alternatives: a) Case 1 TEG absorption, JTE and MP; b) Case 2 SS-MP; and c) Case 3 SS-SS.

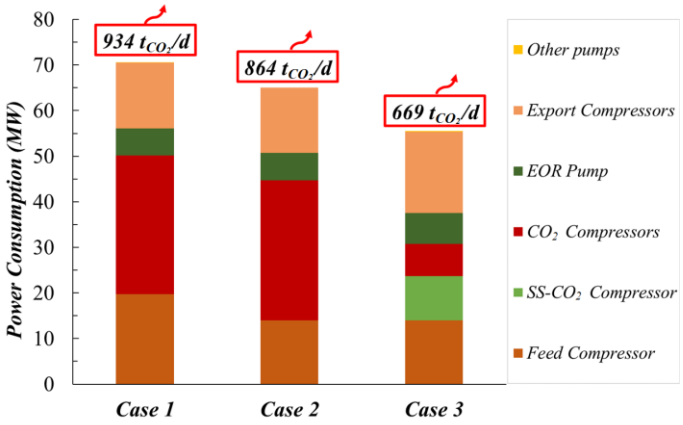

Figure V.12. Equipment power demand and CO_2 emissions: Cases 1, 2 and 3 (SS-CO_2 ≡ 2nd SS unit).

SS-MP entails great reduction of feed compression power leading to inferior power consumption and CO_2 emissions relatively to the conventional process (Fig. V.12). On the other hand, SS-SS deepens still more the reduction of power consumption, plant investment, manufacturing cost and CO_2 emissions because it produces CO_2-rich liquid appropriate for enhanced oil recovery (EOR) at higher pressure and lower temperature comparatively to the other alternatives, dramatically reducing the power compression necessary to send such CO_2-rich fluid to EOR. After such complete analysis contemplating power demand, CO_2 emissions and economic response (Fig. V.13), it is clear that the new proposed process with two consecutive SS units (the SS-SS alternative) can fully treat raw CO_2-rich NG and is shown the best and cleanest solution.

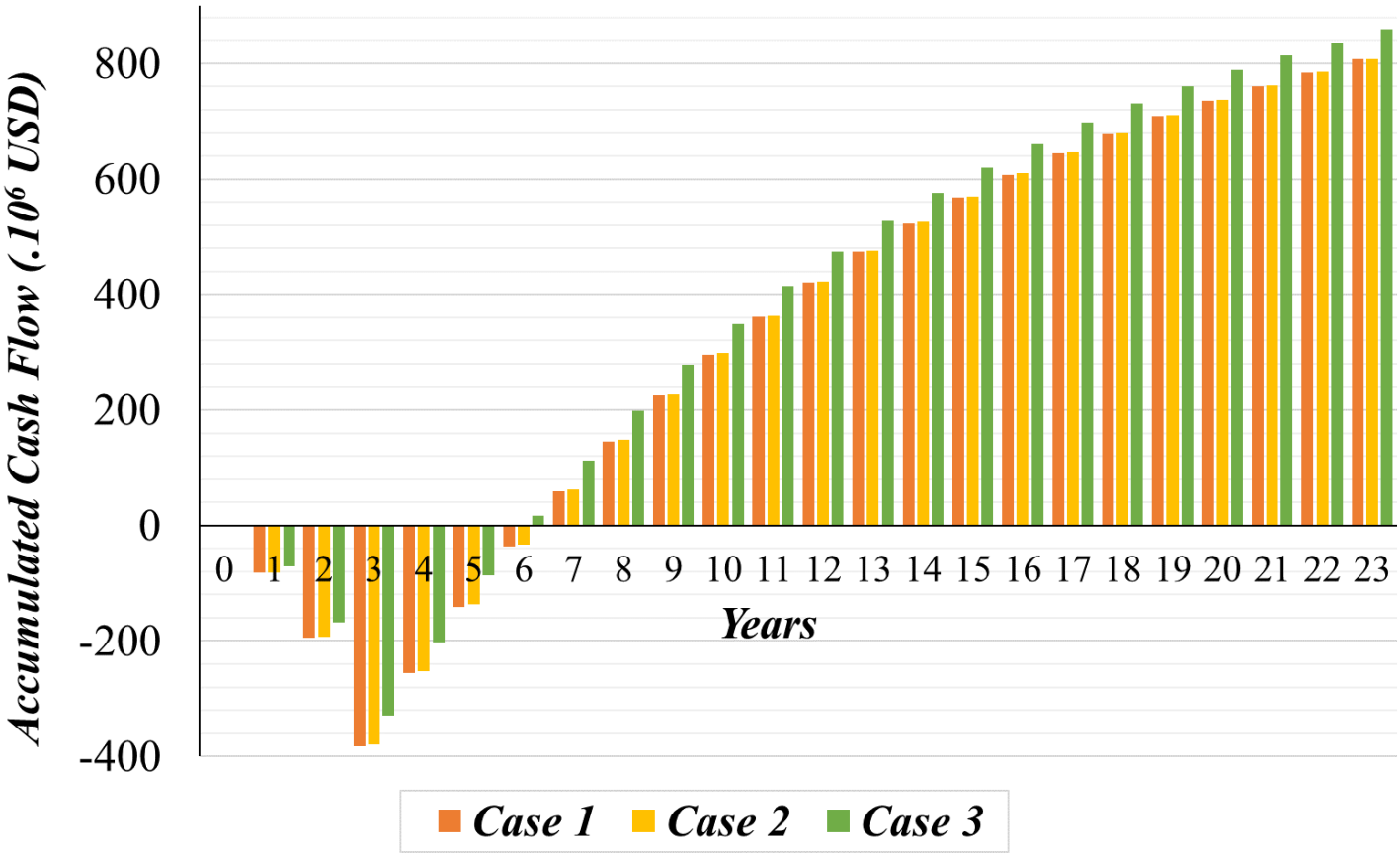

Figure V.13. ***NPV*** **(MMUSD) versus year: Cases 1, 2 and 3.**

V.4 - Carbon capture and high-capacity supercritical fluid processing with supersonic separator: Natural gas with ultra-high CO_2 content.

This work was published in Journal of Natural Gas Science and Engineering, Vol. 66, p. 265-283 (doi: 10.1016/j.jngse.2019.04.004) (Appendix E.15).

In this work, four process alternatives were investigated for processing high flow rates of CO_2 ultra-rich (*≈68%mol* CO_2) natural gas (NG) associated to good grade oil (37°API) in ultra-deepwaters offshore oil fields. The CO_2 ultra-rich NG is a low-grade fuel, but has to be processed in order to allow extraction of oil from the reservoir. Thus, this gas is available at huge flow rate (*≈50 MMsm^3/d*), besides being supercritical, highly dense, highly compressible and demanding attention in terms of thermodynamic modeling.

PFDs contemplate oil/gas/water separation, gas expansion, 1st SS unit for WDPA+HCDPA, 2nd SS unit and MP unit for CO_2 removal producing FG (*≈20%mol* CO_2) and compression for EOR.

WDPA+HCDPA is always done via 1st SS unit, obligating expansion of HPS Gas, since SS has issues with *≈68%mol* CO_2 gas above *85 bar* due to high compressibility and density that damp the speed of sound, entailing supersonic flow not rapid enough for cooling. In this sense, the inclusion of a turbo-expander was done as an attempt to reduce process power consumption.

Therefore, process alternatives differed in three ways: (i) recycling or not recycling condensate from 1st SS unit [RC or NR]; (ii) expansion of HPS Gas by JT (Joule-Thomson) or TX (Turbo-Expander) [JT or TX]; and (iii) CO_2 removal by 2nd SS unit or MP [SS or MP]. The Base-Case consists of JT expansion with recycle and SS-CO_2 removal and is denominated [RC-JT-SS]. Variant cases are [RC+TX+SS], [NR+JT+SS] and [RC+JT+MP].

The cases were compared by means of simulation results, power demands, and economic analysis via module costing technique. SS-UOE, MP-UOE and PEC-UOE were employed to represent the SS and MP operations in HYSYS PFDs of the gas processing plant.

Results show that despite the higher gas circulation rate promoted by recycling condensate from 1st SS unit, this decision is valid, since oil revenues increase leading to highest *NPV*, besides lowest *ppm* H_2O in EOR fluid, reducing risks of hydrates in EOR systems (Fig. V.14).

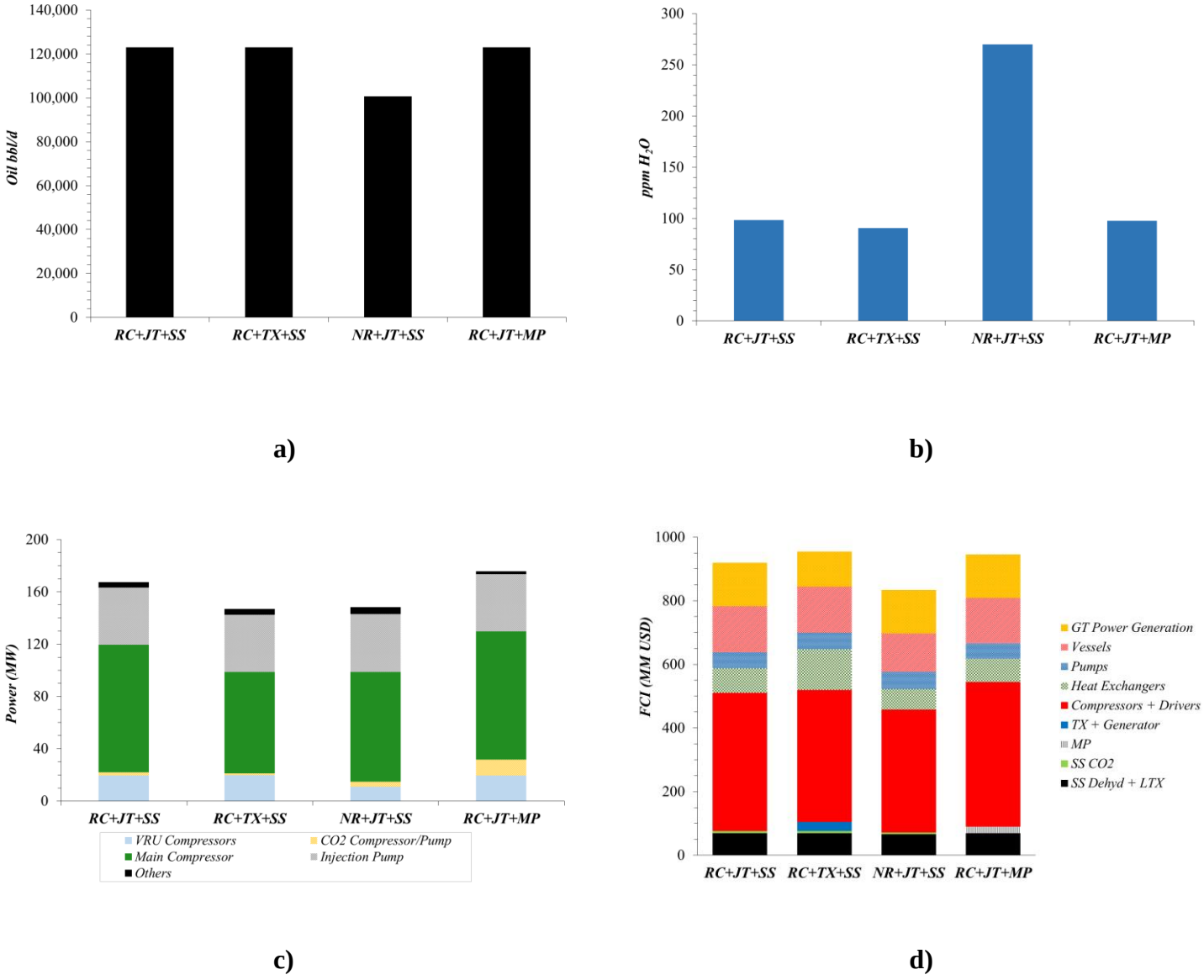

Figure V.14. Gas-hub alternatives: (a) oil (bbl/d); (b) EOR-Fluid *ppm*H_2O; (c) power-consumption (MW); (d) *FCI* (MMUSD)

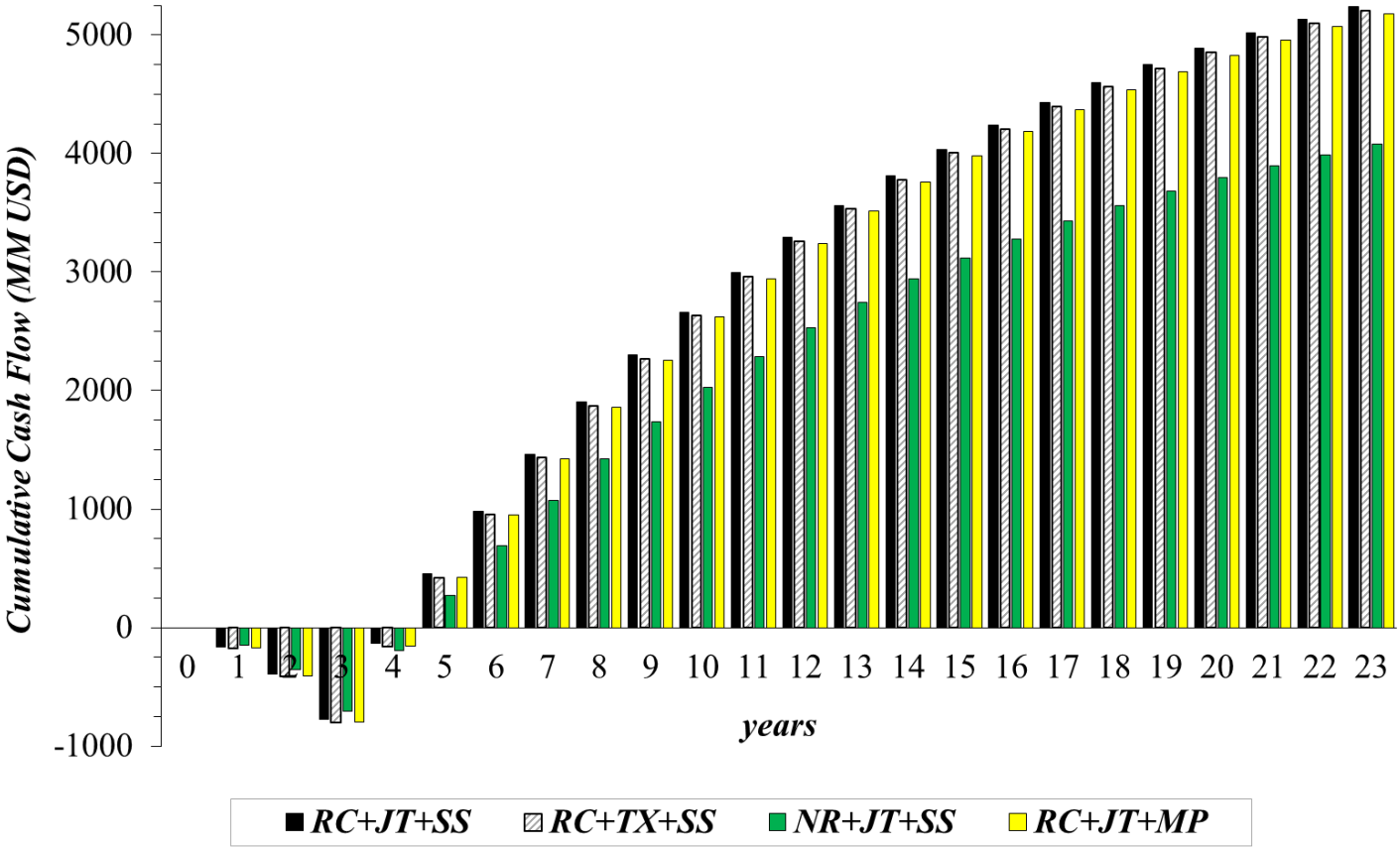

Figure V.15. *NPV* (MMUSD) of gas-hub alternatives for 20 operation-years.

The replacement of JT by TX to reduce power demand is not justified: despite the lowest power demand with TX, *FCI* is the highest due to expensive heat exchangers added with TX, entailing lower cash flow and *NPV*.

Regarding CO_2 capture, the proposed 2nd SS unit for CO_2 removal performed better than MP. Despite a more complex PFD using heat integration and CO_2 refrigeration cycle, the PFD with 2nd SS unit has lower *FCI* and less power demand than MP counterpart, both aspects explained by the CO_2 compressors demanded by MP low pressure CO_2 rich permeate.

Therefore, the best alternative for the studied scenario is the Base-Case, wherein two SS units are used to accomplish all separation targets, exhibiting the best performance both in terms of power consumption and profitability.

V.5 - Supersonic separator for cleaner offshore processing of supercritical fluid with ultra-high carbon dioxide content: Economic and environmental evaluation.

This work was published in Journal of Cleaner Production, Vol. 234, p. 1385-1398, 2019 (doi: 10.1016/j.jclepro.2019.06.304) (Appendix E.16).

In this work, two alternatives for large-capacity conditioning of CO_2 ultra-rich supercritical fluid in offshore plant with total fluid reinjection are investigated. The scenario is similar to the one presented in Section V.4 and comprehends the treatment of *≈56 MMSm³/d* of supercritical fluid with *≈68%mol* CO_2 for dehydration via Molecular-Sieves (MS) in MS-JT-MP alternative or via SS units in SS-SS alternative.

Results are compared in terms of power demands, CO_2 emissions, oil productions and economic metrics. In the case of employing MS, the required number of vessels for the required service is high, entailing high *FCI* costs. Further, SS-SS provides much greater oil production thanks to the recycle of C3+ condensate to the HPS from 1st SS unit. In terms of CO_2 capture, the proposed 2nd SS unit is comparatively better than MP, despite its greater complexity.

On the other hand, SS-SS produces *≈9.5%* more CO_2 emissions than the conventional MS-JT-MP, mainly due to the mandatory depressurization of the supercritical fluid to avoid compressibility shortcomings and enable the operation of the SS. Such depressurization imposes a downstream re-compression of this supercritical fluid, leading to higher power consumption and higher emissions. However, if an approach similar to the one presented in CHAPTER IV and Section V.1 of this Thesis of using the economic leverage provided by the SS-SS process to afford a post-combustion carbon capture plant for abating the excess relative *≈9.5%* CO_2 emissions, SS-SS can be considered the best alternative in environmental grounds as well, being potentially the cleaner process solution for this complex processing problem.

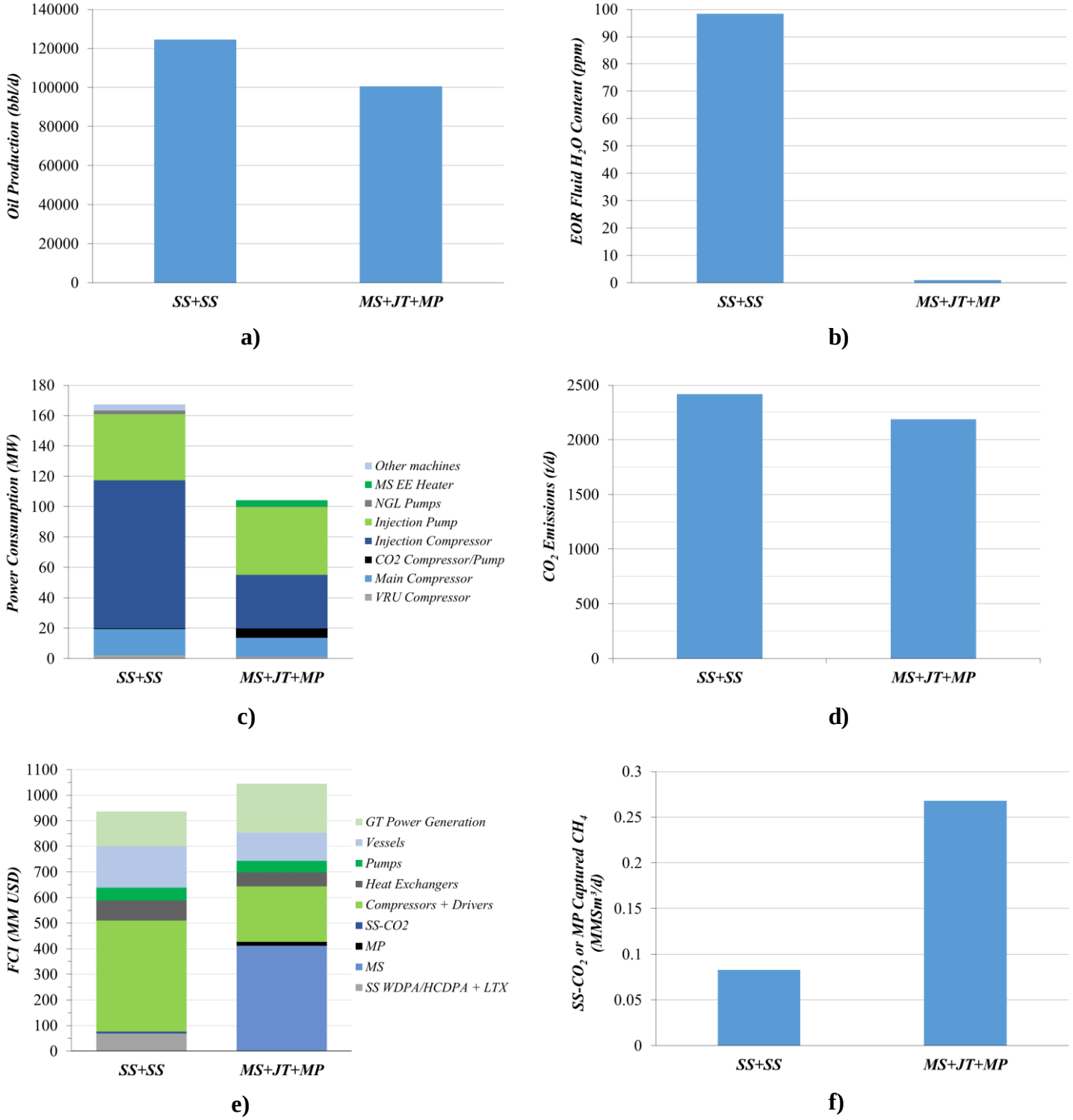

Figure V.16. SS-SS versus MS-JT-MP: (a) oil production; (b) ppmH_2O in EOR-Fluid; (c) power consumption; (d) CO_2 emissions; (e) *FCI*; (f) captured CH_4 in 2nd SS unit or in membrane-permeation (MP).

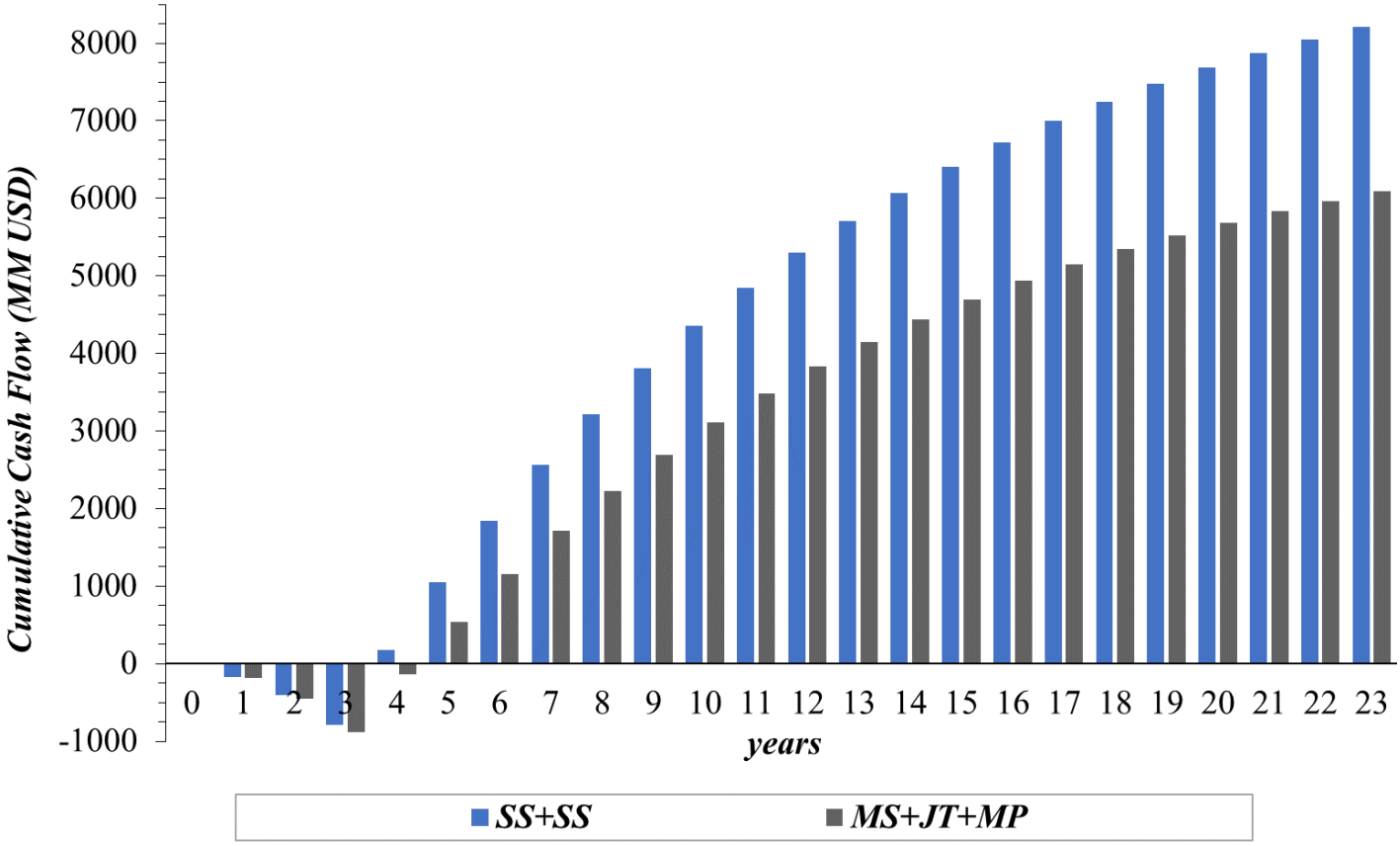

Figure V.17. Net present value (20 years of operation) for alternatives.

This work then quantitatively proves that it is possible to perform the conditioning of such supercritical fluid using only supersonic separators, achieving superior economic results, with greater oil production, lower *FCI*, lower footprint and potentially lower carbon emissions compared with the conventional processing.

V.6 – References

Arinelli L.O., Trotta T.A.F., Teixeira, A.M., de Medeiros, J.L., Araújo O.Q.F., 2017. Offshore Processing of CO2 Rich Natural Gas with Supersonic Separator versus Conventional Routes. Journal of Natural Gas Science and Engineering. Vol. 46, pp. 199-221. http://dx.doi.org/10.1016/j.jngse.2017.07.010.

Arinelli, L O; Teixeira, A M; De Medeiros, J L; Araújo, O Q F. Supersonic separator for cleaner offshore processing of natural gas with high carbon dioxide content: Environmental and economic assessments. Journal of Cleaner Production, v. 233, p. 510-521, 2019. doi:

Arinelli, L O; De Medeiros, JL; De Melo, DC; Teixeira, AM; Brigagão, GV; Passarelli, F M; Grava, W M; Araújo, O Q F. Carbon capture and high-capacity supercritical fluid processing with supersonic separator: Natural gas with ultra-high CO2 content. Journal of Natural Gas Science and Engineering, v. 66, p. 265-283, 2019.

De Melo, DC; Arinelli, L O; De Medeiros, J L; Teixeira, A M.; Brigagão, G V; Passarelli, F M; Grava, W M; Araujo, O Q F. Supersonic separator for cleaner offshore processing of supercritical fluid with ultra-high carbon dioxide content: Economic and environmental evaluation. Journal of Cleaner Production, v. 234, p. 1385-1398, 2019.

CHAPTER VI – CONCLUDING REMARKS

The need to avoid hydrate formation is undeniable in offshore natural gas fields, especially in deep-water environments, where favorable conditions for hydrate formation are typically found. In this context, the injection of Thermodynamic Hydrate Inhibitors (THIs) is an approved technology to successfully displace the hydrates equilibrium loci to lower temperatures in ultra-deep subsea gas production pipelines, therefore preventing hydrate formation.

After THI injection, production fluids reach the platform as a multiphase gas-dominated stream feeding the high-pressure three-phase separator (HPS). HPS splits the feed into: (i) bottom aqueous phase (comprised of water, THI and salts - Rich THI); (ii) hydrocarbon condensate phase, if present; and (iii) an upper gas phase. Offshore NG processing then consists of the treatment of the above mentioned 3 phases from HPS: (i) Rich THI solution has to be processed in recovery units (THI-RUs) in order to be recovered as a Lean THI solution to be pumped back to the wellhead; (ii) the condensate phase, if present, is sent to appropriate treatment; (iii) the gas phase must be conditioned in order to adjust water dew point (WDP) and hydrocarbon dew point (HCDP) for exportation.

Since THI-RUs are distillation-based technologies, they are very intensive in terms of heat consumption. Consequently, in offshore platforms, where space and energy resources are limited, besides determining energy requirements – Energy Performance – it is also of importance to perform a Thermodynamic Analysis to assess degradation of energy quality, which can be done by Exergy Analysis – Exergy Performance. Exergy Analysis was then conducted for MEG Recovery Units (MRUs).

Energy is related to properties that depend only on the present state of the material in the system at hand. On the other hand, Exergy is a property that depends both on the state of the material in the system and on the definition of the Reference Environment Reservoir (RER). Thus, two approaches for the definition of RER were investigated so as to perform Exergy

Analysis for three MRU technologies designed to operate on offshore NG production rigs: Traditional Process (TP), Full-Stream Process (FS) and Slip-Stream Process (SS).

The PFDs of the MRUs under consideration were solved within a professional simulation environment to obtain the Energy Performance of all MRUs – i.e. heat and power consumptions – and also all distributions of mass and energy flow rates along the MRUs. Formulae for exergy flows were derived from the application of 1st and 2nd Laws of Thermodynamics to a model of a steady-state open system interacting with a Reference Environmental Reservoir (RER), and then exergy analysis was conducted for MEG Recovery Processes via two RER Approaches:

- Usual RER Approach #1, a two-phase environment where the gas phase corresponds to the dry-basis standard atmosphere in VLE with pure liquid water at $25^{o}C$ and *1 atm* containing traces of MEG in the gas phase under oxidative chemical equilibrium with CO_2, H_2O and O_2; and

- Novel RER Approach #2, again a two-phase environment consisting of dry-basis atmospheric air in VLE with liquid water containing MEG at infinite dilution, but not in chemical equilibrium with air species.

RER Approach #1 provides a very negative value for RER chemical potential of MEG, therefore input and output MEG streams have very high positive values for exergy flows, which are close in absolute terms, since no reaction occurs with MEG along the processes. Then, irreversibilities represented a small relative fall relative to total exergy flow, which entailed exergy efficiencies close to 90%. On the other hand, RER Approach #2 included MEG in its own definition being infinitely diluted in water, thereby representing a scenario closer to the reality of MRU state of MEG, entailing a less negative value for RER chemical potential of MEG and consequently much lower values of exergy flows of streams.

Both approaches calculated the same rate of lost exergy for the same MRU and yielded consistent results. However, RER Approach #1 showed to be inappropriate because it leads to

too high values of exergy flow rates of streams, which are much higher than the corresponding values of rates of lost exergy. This masks results and hinders the discrimination of performances of units and processes in terms of exergy degradation. On the other hand, RER Approach #2 defines the RER condition of MEG as a liquid infinitely diluted in water, not in chemical equilibrium with air species. The corresponding exergy flow rates of streams are much lower now, with greater evidence of exergy losses and better discrimination of exergy efficiencies.

Hence, RER Approach #2 could clearly indicate the main points of exergy destruction, as originally intended by Exergy Analysis. Further, exergy efficiencies of MEG Recovery Units with RER Approach #2 presented values around 10%-11% which are very reasonable values for distillation-based processes as demonstrated in the distillation examples of Appendices A and B. RER Approach #1, although consistent and correct, failed to provide discrimination of Exergy Performances and realistic results, whereas the proposed novel RER Approach #2 was able to provide much more realistic and meaningful exergy efficiency values.

By means of Exergy Analysis with appropriate RER choice, commercial MEG Recovery Units were weighted with the respective main exergy sinks accurately identified and the respective exergy efficiencies correctly determined. Further, all results were validated by a consistency cross-check test, and this methodology can be extended to the analysis of any other chemical process, such as recovery processes of any other THI.

In addition, a critical issue when employing volatile THIs (such as methanol and ethanol) is related to the high THI losses to gas phase in HPS, which entail high THI make-up requirements and configure a major operating expense. In this sense, a novel process – “SS-THI-Recovery” – was developed in this thesis, which employs supersonic separators (SS) and is based on THI extraction at low temperatures using water as agent (a small water injection at the entrance of SS is a key aspect of this process).

SS-THI-Recovery process was successfully demonstrated to recover THIs methanol, ethanol and MEG from the gas phase leaving the three-phase high pressure separator in any gas

processing rig connected to offshore THI loops for natural gas production. SS-THI-Recovery can be installed as a simple appendix of THI-RU plants that traditionally recover THI from the THI-water phase from HPS bottoms. SS-THI-Recovery generates two revenue factors and one cost-reducing factor to the gas processing rig: (i) NG is produced with WDPA and HCDPA, ready for commercialization and/or exportation; (ii) Raw LPG is produced which can be refined producing commercial LPG and solvents; and (iii) THI is recovered from the HPS gas, reducing its losses from 79% to 99% depending on the THI.

Evidently, new SS-THI-Recovery could only be quantitatively demonstrated – without prototypes and experiments – if a competent and precise simulation resource is available for simulating SS nozzles and calculating with accuracy the three-phase VLWE thermodynamic sound speed property. In addition, such complex polar systems containing hydrocarbons (HCs), water and hydroxylated THIs require an appropriate EOS to handle multiphase equilibrium and multiphase properties. Therefore, SS-THI-Recovery process was simulated in Aspen Hysys v8.8 using SS-UOE, a thermodynamically rigorous model for simulating supersonic separators in the professional simulator in connection with PEC-UOE to correctly determine the speed of sound in multiphase flow (Arinelli et al., 2017, de Medeiros et al., 2017) and employing CPA-EOS, a widely recognized EOS to handle multiphase systems with water, hydroxylated THIs and HCs. The thermodynamic rigor of SS simulations involving three-phase VLWE supersonic flow was amply showed in the results of SS-THI-Recovery for Methanol, Ethanol and MEG, making the results of confidence.

The assessment of process performance shows that at least 79% of what would be lost to gas phase is recovered by this process, and such recovery factor could be further enhanced by increasing the flow rate of water injection in LLS. Such high recovery entails a very significant reduction of make-up costs, besides the lower costs related to storage and transportation of the chemical in the platform. In addition, the process is simple, presenting low footprint, and easy to be implemented, even in the case of less volatile THIs like MEG. Further, the produced NG is ready for export and sales, without the need for additional treatment steps, and raw LPG for exportation has commercial value.

The advantages of SS-based processes were investigated as a strategy for mitigating CO_2 emissions by means of investments in CO_2 capture technologies backed up by cost reduction and/or revenues increase via new processing technologies. Particularly, an economic analysis was conducted to quantifty the advantages of SS-THI-Recovery in comparison with the conventional gas processing. Therefore, two alternatives were considered: (i) conventional gas processing without carbon capture and (ii) SS-THI-Recovery coupled to a Carbon Capture and Storage (CCS) unit. A novel design of a CCS unit employing SS is also disclosed, which allows for the dehydration of the CO_2-rich stream with negligible pressure drop, requiring minimum compression power for exportation, and potentially improving process economics.

The economic analysis revealed that, despite lowering costs with utilities, raw materials, and CO_2 taxation, SS-THI-Recovery with CCS still presented a higher *COM* (Cost of Manufacturing) than the conventional gas plant because *COM* also depends on the fixed capital investment (*FCI*), which is *≈100%* higher for SS-THI-Recovery with CCS. On the other hand, SS-THI-Recovery with CCS achieved a deeper dew-point of final NG, transferring more C3+ to LPG increasing its yield and aggregating more value as noted in LPG revenues. Further, TEG dehydration drags C3+ from raw gas in the conventional gas plant, degrading its LPG revenues. Albeit the lower LHV (lower heating value) of final NG from conventional gas plant, its NG revenues were higher than the counterpart of SS-THI-Recovery with CCS thanks to higher NG production of the former. However, the high LPG revenues of SS-THI-Recovery with CCS overcame its higher *FCI*, *COM* and the higher NG revenues of conventional plant, leading to superior annual profit and *NPV* after 20 years of operation (*N=23*) when methanol is adopted as THI.

High oil prices strongly beneficiates SS-THI-Recovery with CCS because LPG is one of its important revenues and LPG price is proportional to oil price. The conventional gas plant is less beneficiated by rising oil prices because its LPG is residual and its major revenue is NG exportation, whose price does not correlate with oil price. Similarly, the higher the carbon taxes, the higher the *ΔNPV* of SS-THI-Recovery with CCS relative to the conventional plant because the former significantly reduced its CO_2 emissions. Finally, as NG prices rise, the difference of economic performances of both alternatives vanishes – with SS-THI-Recovery

with CCS always superior. Both processes have similar NG revenues, but with great difference in LPG revenues, which is more than *≈200%* higher for SS-THI-Recovery with CCS.

Therefore, SS-THI-Recovery in conjunction with THI-RU and a novel SS-based design of CCS plant in offshore environment is shown to produce sufficient economic benefits which can pay the costs of a CCS plant reducing CO_2 emissions (*≈43%*) while maintaining economic superiority relative to the conventional gas processing in several scenarios. Hence, the SS-based alternative is superior from both economic and environmental points of view, providing a cleaner production of natural gas and LPG and configuring a successful strategy for CO_2 management.

Finally, the economic analysis was extended to other THIs and similar conclusions are obtained. Whether employing any of methanol, ethanol or MEG as THIs, SS-THI-Recovery with carbon capture emits *≈43%* less CO_2 than the conventional gas plant, always with superior economic performance. Therefore, SS-THI-Recovery with carbon capture was shown to be highly competitive against the conventional gas processing.

Regarding the above discussed aspects, this Thesis achieved significant results, bringing insights and innovations for the literature and contributing to advance the scientific knowledge in the fields of THI recovery, natural gas processing and CO_2 mitigation. Suggestions for future works include:

- Investigation of the performance of a combination of different THIs (e.g. methanol and MEG, ethanol and MEG, etc.) for hydrate inhibition;
- Investigation of the effect of H_2S in the natural gas feed;
- Economic analysis of SS-THI-Recovery without carbon capture in comparison with conventional route;
- Search for alternative THIs (e.g. hydroxylated compounds) and the development of corresponding recovery technologies;
- Exergy Analysis of new THIs' recovery processes versus conventional processes.

VI.1 – References

Arinelli L.O., Trotta T.A.F., Teixeira, A.M., de Medeiros, J.L., Araújo O.Q.F., 2017. Offshore Processing of CO2 Rich Natural Gas with Supersonic Separator versus Conventional Routes. Journal of Natural Gas Science and Engineering. Vol. 46, pp. 199-221. doi: 10.1016/j.jngse.2017.07.010.

de Medeiros, J. L., Arinelli, L. O., Araújo, O. Q. F. Speed of Sound of Multiphase and Multi-Reactive Equilibrium Streams: A Numerical Approach for Natural Gas Applications. J. of Nat. Gas Sci. and Eng., 46, 222-241, 2017. doi: 10.1016/j.jngse.2017.08.006

APPENDIX A: THERMODYNAMIC EFFICIENCY OF A STEADY-STATE BINARY DISTILLATION COLUMN

In order to evaluate the magnitude of thermodynamic efficiencies of ordinary distillation columns, consider a simple steady-state binary distillation column at 1 bar operating with hypothetical species "1" and "2". To simplify the nomenclature, all molar fractions refer exclusively to component "1". Thus Z, X_D, X_B represent the molar fractions of component "1" in the feed stream (F mol/s), in the distillate product (D mol/s) and in the bottoms product (B mol/s), respectively. This binary distillation column with one feed and two product streams is shown in Fig. A-1. Consider the following Assumptions:

- Steady-state isobaric atmospheric distillation column at $P=1\ bar$ with perfect stages (A1)
- Column with total condenser and total reboiler at $P=1\ bar$ with bubble-point effluents (A2)
- Components "1"and "2" form liquid mixtures at $P=1\ bar$ with Ideal Solution behavior (A3)
- Vapor phase is considered Ideal Gas at $P= 1\ bar$ (A4)
- Feed F mol/s, distillate D mol/s and bottoms B mol/s as saturated liquids at $P=1\ bar$ (A5a)
- Feed flow rate of $F=100\ mol/s$ (A5b)
- Compositions of external streams: Feed $Z=0.5$; Distillate $X_D=0.95$; Bottoms $X_B=0.05$ (A6)
- Column is heated by an isothermal hot reservoir R_H at $T_H=200\ ^oC$ with duty $Q_H>0$ (A7)
- Column is cooled by an isothermal cold reservoir R_C at $T_C=50\ ^oC$ with duty $Q_C>0$ (A8)
- Enthalpy of saturated liquid at $P=1\ bar$ is a linear function of liquid composition

$$\overline{H}_L^{Sat}(X) = a + b.X \quad (kJ/mol) \tag{A9a}$$

- Enthalpy of saturated vapor at *P=1 bar* is a linear function of vapor composition, with constant distance to the curve of enthalpy of saturated liquids

$$\overline{H}_V^{Sat}(Y) = a + \lambda + b.Y \quad (kJ/mol) \tag{A9b}$$

- Enthalpy of vaporization at *P=1 bar* is independent of composition: $\lambda=30\ kJ/mol$

(A10)

- Relative volatility at *P=1 bar* is a constant independent of composition: $\alpha=2$

(A11)

- Column reflux ratio (*RR*) is *30%* above minimum reflux ratio: $RR=1.3*RR^{MIN}$

(A12)

- Approximately zero head losses $\Rightarrow$ column approximately isobaric $P_F \cong P_B \cong P_D \cong 1 \quad bar$

(A13)

The Vapor-Liquid Equilibrium (VLE) relationship, *Y*=g(X)*, at *P=1 bar* is obtained by Assumption (A11) as shown in Eq. (A14).

$$Y^* = \frac{\alpha.X}{1 - X + \alpha.X} \Rightarrow Y^* = \frac{2X}{1+X} \qquad \{Y^* = g(X) \tag{A14}$$

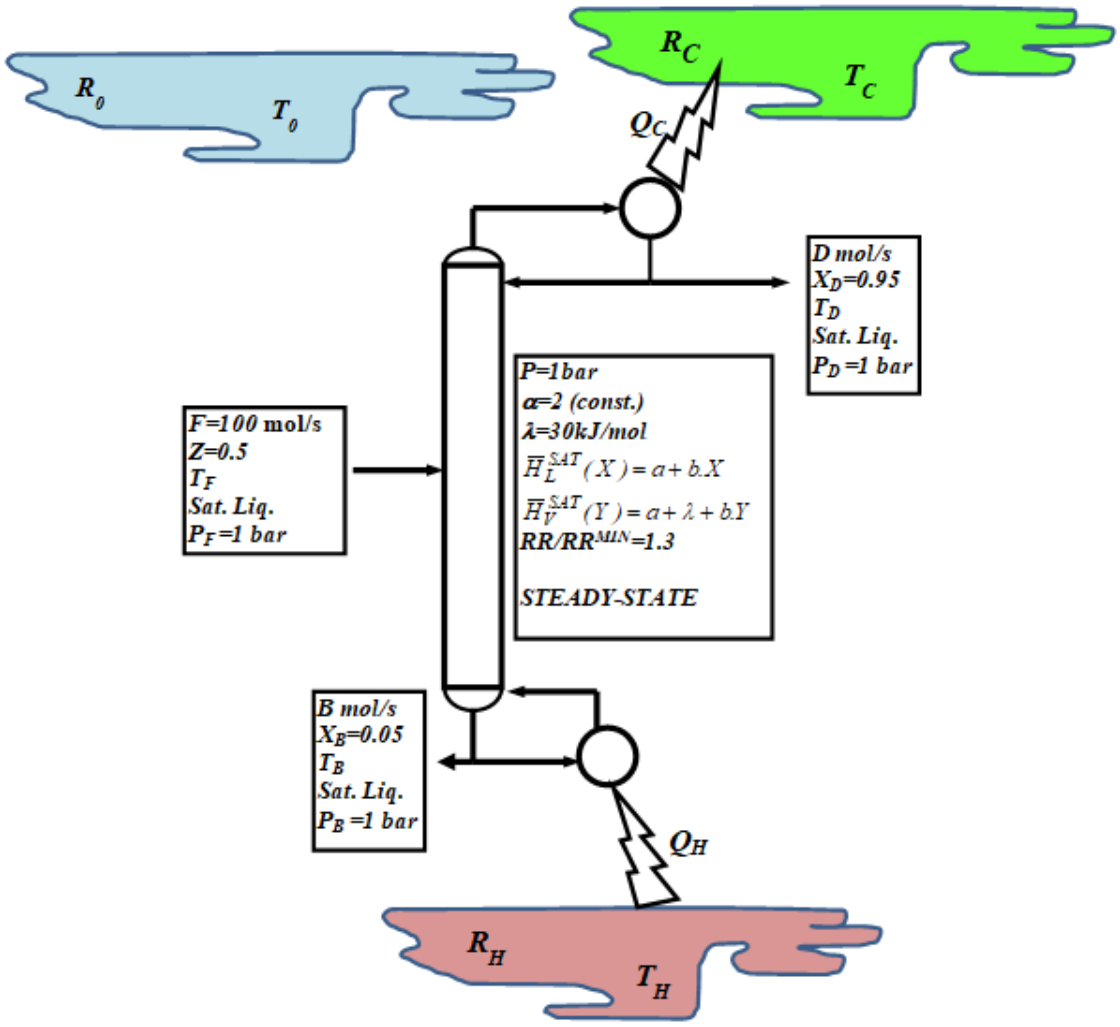

Figure A- 1. Binary Distillation Column: Feed and Product Streams as Saturated Liquids at 1 bar; Heating Duty Q_H from Hot Reservoir R_H (T_H=200 ^oC) to Reboiler; Cooling Duty Q_C from Condenser to Cold Reservoir R_C (T_C=50 ^oC); Reference Reservoir R_0 at T_0=25 ^oC is Idle (Not Interacting with Column)

A.1. Determination of Steady-State Operation Reflux Ratio and Corresponding Heat Duties

It can be shown that Eqs. (A9a) and (A9b) imply that the molar flow rates of liquid and vapor are constant in each column section. This is the well-known Constant Molar Overflow approximation (CMO) that is used in the McCabe-Thiele Method. This method can generate approximate designs of binary distillations. Calling the rectification section as section *0* and the stripping section as section *1*, the molar flow rates (mol/s) of liquid and vapor in these

sections are written by CMO according to Eqs. (A15) to (A18). By solving the column material balances, flow rates D and B are calculated as shown in Eqs. (A19) and (A20). From Eqs. (A9a) and (A9b), the enthalpy of vaporization λ is constant with the value of 30 kJ/mol by Assumption (A10). Also with V_0 and V_1, this gives the (positive) thermal duties Q_C and Q_H (kW) in Eqs. (A21) and (A22).

$$L_0 = D.RR \tag{A15}$$

$$L_1 = D.RR + F \tag{A16}$$

$$V_0 = D.(RR+1) \tag{A17}$$

$$V_1 = D.(RR+1) \tag{A18}$$

$$D = F.\left(\frac{Z - X_B}{X_D - X_B}\right) \Rightarrow D = 50\,mol/s \tag{A19}$$

$$B = F.\left(\frac{X_D - Z}{X_D - X_B}\right) \Rightarrow B = 50\,mol/s \tag{A20}$$

$$Q_C = D.(RR+1).\lambda = 1500.(RR+1) \quad kW \tag{A21}$$

$$Q_H = D.(RR+1).\lambda = 1500.(RR+1) \quad kW \tag{A22}$$

In the context of the McCabe-Thiele Method, sections *0* and *1* can be solved by a tray-to-tray calculation from top to bottom using the VLE relationship (Eq. (A14)) as in Eq. (A23) and the Operation Equations of sections *0* and *1* shown in Eqs. (A24) and (A25) respectively, where X_n and Y_n represent the compositions leaving stage n in VLE and X_n and Y_{n+1} represent a crossing pair of compositions (or inter-stage compositions) in those sections.

$$Y_n = g(X_n) \Rightarrow Y_n = \frac{2X_n}{1+X_n} \tag{A23}$$

$$Y_{n+1} = \left(\frac{L_0}{V_0}\right).X_n + \left(\frac{D.X_D}{V_0}\right) \qquad \Rightarrow Y_{n+1} = \left(\frac{RR}{RR+1}\right).X_n + \left(\frac{X_D}{RR+1}\right) \tag{A24}$$

$$Y_{n+1} = \left(\frac{L_1}{V_1}\right).X_n + \left(\frac{D.X_D - F.Z}{V_1}\right) \Rightarrow Y_{n+1} = \left(\frac{RR + F/D}{RR+1}\right).X_n + \left(\frac{X_D - Z.F/D}{RR+1}\right) \quad \text{(A25)}$$

It is easily shown that the Operating Equations (A24) and (A25) intersect in the *XY* plane at the point (X_{01}, Y_{01}) given in Eq. (A26).

$$X_{01} = Z \quad , \quad Y_{01} = \frac{X_D + Z.RR}{RR+1} \quad \text{(A26)}$$

At Minimum Reflux (RR^{MIN}) a pinch condition is attained at the feed zone, which is represented by the intersection point (X_{01},Y_{01}) in plane *XY*. This pinch condition is usually represented by $(X_{01}, Y_{01}^{\infty})$ meaning that the intersection point obeys Eq. (A26) simultaneously with the VLE relationship in Eq. (A14), as shown in Eq. (A27). Eq. (A27) then allows the Minimum Reflux Ratio to be determined via Eq. (A28). With $g(Z) = 2/3$ by Eq. (A14), results $RR^{MIN}=1.7$ for this simple example.

$$X_{01} = Z \quad , \quad Y_{01}^{\infty} = \frac{X_D + Z.RR^{MIN}}{RR^{MIN}+1} = g(Z) \quad \text{(A27)}$$

$$\frac{X_D + Z.RR^{MIN}}{RR^{MIN}+1} = g(Z) \Rightarrow RR^{MIN} = \frac{X_D - g(Z)}{g(Z) - Z} \xrightarrow{g(Z)=2/3} RR^{MIN} = 1.7 \quad \text{(A28)}$$

The design reflux ratio is obtained via Assumption (A12) in Eq. (A29). This determines the design values of the column heat duties via Eqs (A21) and (A22) as shown in Eqs. (A30).

$$RR = 1.3 * RR^{MIN} \Rightarrow RR = 2.21 \quad \text{(A29)}$$

$$Q_H = Q_C = 50 * 3.21 * 30 = 4815kW \quad \text{(A30)}$$

A.2. Minimum Power Required for Steady-State Separation at Constant *T & P*

The minimum power required ($\dot{W}^{REV}$) to produce the steady-state separation in Fig. A-1 can be obtained with the 1st and 2nd Laws of Thermodynamics assuming steady-state reversible operation of a reversible machine or open system executing the separation. This open system is shown in Fig. A-2.

In Fig. A-1 the respective bubble temperatures T_F , T_D , T_B of feed *F* and product streams *D* and *B* at *P=1 bar*, are evidently different, but they are not very distant from each other if the relative volatility is 2. For simplicity, it is assumed that these temperatures can be approximated by a certain value *T* (i.e. $T_F \cong T_D \cong T_B \cong T$), where *T* is of the order of $\approx 80\ ^oC$. Thus, the reversible separation requiring minimum work occurs at constant *T* and *P*, where $P_F \cong P_D \cong P_B \cong P=1\ bar$, as shown in Fig. A-2. The exact nature of the steady-state open system to undertake the separation is not relevant in principle, but it is not a distillation column. To guarantee its constant temperature *T* this open system is supposed in thermal equilibrium with a heat reservoir R_T at temperature *T*. As any reservoir, R_T has a very high heat capacity so that its temperature is constant at *T* independently of the heat exchange Q^{REV} between R_T and the open system. Q^{REV} and $\dot{W}^{REV}$ are defined according to the open system point of view; i.e. Q^{REV} is positive when the system receives heat and W^{REV} is positive when the system produces work.

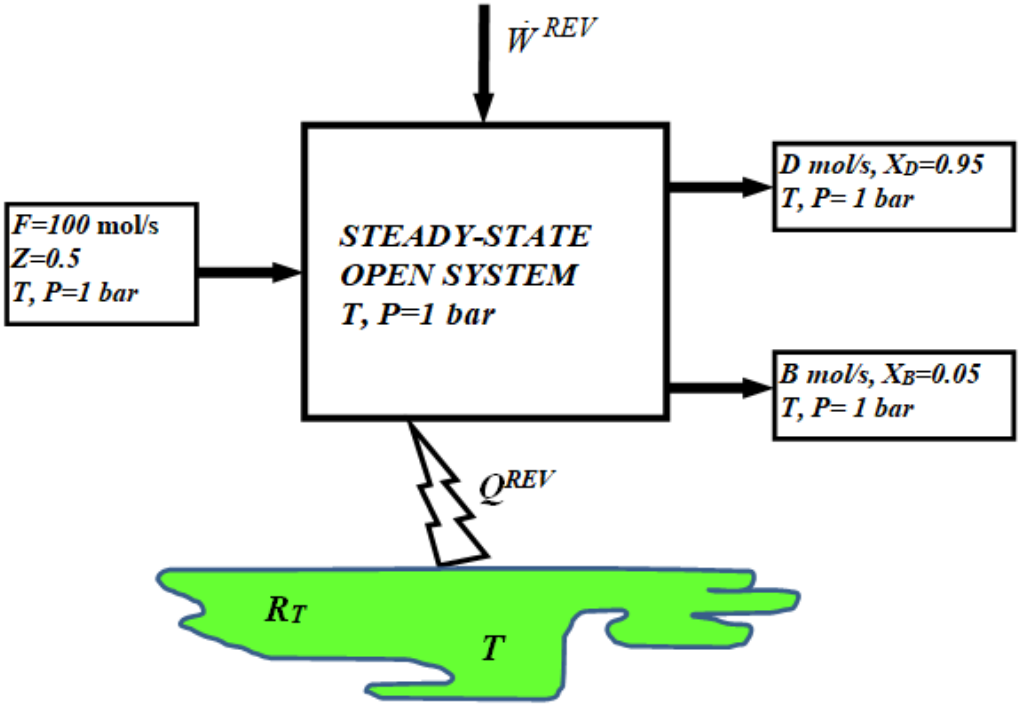

Figure A- 2. Open System for Minimum Power Separation at Constant *T* and *P* of Feed *F=100 mol/s* with Composition *Z=0.5* into Product Streams *D mol/s* and *B mol/s* respectively with Compositions X_D=0.95 and X_B=0.05

Applying the 1st Law of Thermodynamics to the steady-state open system in Fig. A-2, results Eq. (A31), where $\overline{H}_F$,$\overline{H}_D$, $\overline{H}_B$ represent the respective molar enthalpies of streams *F*, *D* and *B* in kJ/mol at *(T, P)*. Assuming reversible operation for $\dot{W}^{REV}$, the steady-state rate of creation of entropy in the Universe associated to this process is zero as shown in Eq. (A32), where $\overline{S}_F$,$\overline{S}_D$, $\overline{S}_B$ represent the respective molar entropies of streams *F, D* and *B* in kJ/mol.K at *(T, P)*. The second term in the left hand side of Eq. (A32) corresponds to the rate of change of entropy inside the isothermal reservoir R_T as consequence of the heat exchange Q^{REV} originally defined according to the point of view of the open system.

$$F.\overline{H}_F + Q^{REV} = \dot{W}^{REV} + D.\overline{H}_D + B.\overline{H}_B \qquad \text{(A31)}$$

$$-F.\overline{S}_F - \frac{Q^{REV}}{T} + D.\overline{S}_D + B.\overline{S}_B = 0 \qquad \text{(A32)}$$

Multiplying Eq. (A32) by *T* and adding it to Eq. (A31), results Eq. (A33) or (A34) for $\dot{W}^{REV}$, where $\overline{G}_F, \overline{G}_D, \overline{G}_B$ represent the respective molar Gibbs free energies of streams *F*, *D* and *B* (kJ/mol) at *(T, P)*.

$$\dot{W}^{REV} = -\left\{ D.(\overline{H}_D - T.\overline{S}_D) + B.(\overline{H}_B - T.\overline{S}_B) - F.(\overline{H}_F - T.\overline{S}_F) \right\} \quad \text{(A33)}$$

$$\dot{W}^{REV} = -\left\{ D.\overline{G}_D + B.\overline{G}_B - F.\overline{G}_F \right\} \quad \text{(A34)}$$

Eq. (A34) is a well-known result for the minimum power required (or maximum power produced) for a given steady-state transition of streams under constant (*T,P*). Eq. (A34) states that a steady-state transition with rate of Gibbs free energy (kW) assigned to product streams greater than the rate of Gibbs free energy (kW) assigned to the feed streams, the minimum requirement of power is the negative of the net rate of variation of Gibbs free energy (kW). For steady-state distillation separations, as the one in Fig. A-1, the output flow rate of Gibbs free energy is greater than the respective input rate at constant (*T,P*). This means that mechanical power have to be spent to support such separation ($\dot{W}^{REV} < 0$). Concerning the separation in Figs. A-1 and A-2, all streams *F, D, B* are liquids at *(T,P)* with Ideal Solution behavior. This allows to write Eqs. (A35a) to (A35c) below, where $\mu_1^L(T,P), \mu_2^L(T,P)$ are the chemical potentials of pure species "1" and "2" at (*T,P*); and $R=8.314*10^{-3}$ *kJ/mol.K* is the Ideal Gas constant.

$$\overline{G}_F = Z.\mu_1^L(T,P) + (1-Z).\mu_2^L(T,P) + R.T.\{Z.ln(Z) + (1-Z).ln(1-Z)\} \quad \text{(A35a)}$$

$$\overline{G}_D = X_D.\mu_1^L(T,P) + (1-X_D).\mu_2^L(T,P) + R.T.\{X_D.ln(X_D) + (1-X_D).ln(1-X_D)\} \quad \text{(A35b)}$$

$$\overline{G}_B = X_B.\mu_1^L(T,P) + (1-X_B).\mu_2^L(T,P) + R.T.\{X_B.ln(X_B) + (1-X_B).ln(1-X_B)\} \quad \text{(A35c)}$$

Since *D=B=F/2* by Eqs. (A19) and (A20), Eq. (36) follows.

$$\begin{aligned} D.\overline{G}_D + B.\overline{G}_B - F.\overline{G}_F = & \{D.X_D + B.X_B - F.Z\}.\mu_1^L(T,P) + \\ & \{D.(1-X_D) + B(1-X_B) - F(1-Z)\}.\mu_2^L(T,P) + \\ & \frac{FRT}{2}.\{X_D.ln(X_D) + (1-X_D).ln(1-X_D)\} + \\ & \frac{FRT}{2}.\{X_B.ln(X_B) + (1-X_B).ln(1-X_B)\} + \\ & - FRT.\{Z.ln(Z) + (1-Z).ln(1-Z)\} \end{aligned} \quad \text{(A36)}$$

The steady-state material balances of the column impose that $D.X_D + B.X_B - F.Z = 0$ and $D.(1-X_D) + B(1-X_B) - F(1-Z) = 0$, resulting Eq. (A37).

$$\begin{aligned} D.\overline{G}_D + B.\overline{G}_B - F.\overline{G}_F = & \frac{FRT}{2}.\{X_D.ln(X_D) + (1-X_D).ln(1-X_D)\} + \\ & \frac{FRT}{2}.\{X_B.ln(X_B) + (1-X_B).ln(1-X_B)\} + \\ & - FRT.\{Z.ln(Z) + (1-Z).ln(1-Z)\} \end{aligned} \quad \text{(A37)}$$

With $X_D = 0.95,\ X_B = 0.05,\ Z = 0.5,\ F = 100 mol/s,\ T \approx 80\,^oC\ (353.15 K)$, we have:

$$D.\overline{G}_D + B.\overline{G}_B - F.\overline{G}_F = 145.23\ kW \quad \text{(A38)}$$

Or

$$\dot{W}^{REV} = -145.23\ kW \quad \text{(A39)}$$

A.3. Actual Equivalent Power Consumption of a Steady-State Binary Distillation Column via the Method of Carnot Equivalent Cycles

The actual equivalent power ($\dot{W}$) consumed by the steady-state distillation column operating as discussed in Sec. A.1, producing the separation in Fig. A-1, is obtained from the reboiler and condenser heat duties in Eq. (A30), $Q_H = Q_C = 4815kW$. These duties have to be converted to equivalent positive mechanical powers – respectively, $\dot{W}_H > 0$ and $\dot{W}_C > 0$ – by means of two reversible Carnot cycles operating, respectively, with the reservoirs R_H (T_H=200^oC) and R_C (T_C=50^oC) as hot sinks, coupled to reservoir R_0 (T_0=25 ^oC) as cold sink (Fig. A-1). This arrangement, in Fig. A-3, imposes to reservoirs R_H and R_C the same steady-state transitions that are taking place in the steady-state distillation column. Carnot cycles are chosen because they are the machines with the best thermodynamic yield for conversion of heat into power (and vice-versa) given two heat reservoirs at different temperatures. The column heating duty Q_H =4815 kW absorbed from reservoir R_H is equivalent to a production of power $\dot{W}_H$ by a Carnot Engine coupled to reservoir R_0. Analogously, the column cooling duty Q_C =4815 kW is equivalent to a consumption of power $\dot{W}_C$ to drive a Carnot Heat Pump absorbing heat from reservoir R_0 and delivering Q_C to R_C. The net equivalent power consumed by the distillation column is $\dot{W}_H - \dot{W}_C$.

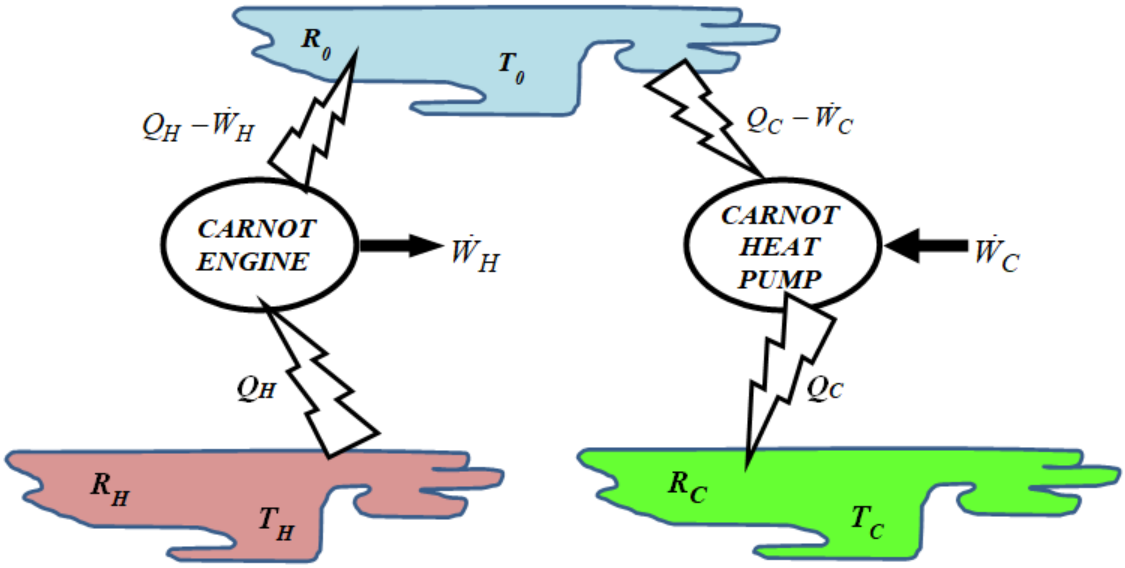

Figure A- 3. Converting the Heating and Cooling Duties Q_H and Q_C from the Steady-State Operation of the Distillation Column to Equivalent Production and Consumption of Powers $\dot{W}_H$ and $\dot{W}_C$ using Reservoirs R_H and R_C as Hot Sinks and the Reservoir R_0 as Cold Sink Coupled to a Carnot Engine and a Carnot Heat Pump

The rate of entropy creation associated with the arrangement in Fig. A-3 is zero because the two Carnot cycles are reversible machines. Thus, Eq. (A40a) and (A40b) represent, respectively, the conservation of entropy associated to the operation of the Carnot Engine and the Carnot Heat Pump. The final formulae in the right side of Eqs. (A40a) and (A40b) express the power production and power consumption equivalent to duties Q_H and Q_C.

With Eqs. (A40a) and (A40b), the absolute value of the net equivalent power consumption by the distillation column, $\left|\dot{W}^{EQUIV}\right| = \dot{W}_H - \dot{W}_C$, associated to a steady-state operation under the conditions of Fig. A-1, is shown in Eq. (A41). The numerical result is shown in Eq. (A42) after substituting operation values: Q_H = *4815 kW*, Q_C = *4815 kW*, T_H = *473.15 K*, T_C=*323.15 K* and T_0 = *298.15 K*.

$$-\frac{Q_H}{T_H} + \frac{Q_H - \dot{W}_H}{T_0} = 0 \Rightarrow \dot{W}_H = \left(1 - \frac{T_0}{T_H}\right).Q_H \qquad \text{(A40a)}$$

$$+\frac{Q_C}{T_C}-\frac{Q_C-\dot{W}_C}{T_0}=0\Rightarrow\dot{W}_C=\left(1-\frac{T_0}{T_C}\right).Q_C \qquad \text{(A40b)}$$

$$\left|\dot{W}^{EQUIV}\right|=\left(1-\frac{T_0}{T_H}\right).Q_H-\left(1-\frac{T_0}{T_C}\right).Q_C \qquad \text{(A41)}$$

$$\left|\dot{W}^{EQUIV}\right|=1408.38\,kW \qquad \text{(A42)}$$

A.4. Thermodynamic Efficiency of a Steady-State Binary Distillation Column

The Thermodynamic Efficiency of the steady-state binary distillation column in Fig. A-1 is simply calculated with the minimum required power for the separation $\left|\dot{W}^{REV}\right|$ from Eq. (A39) in Sec. A.2, and the actual equivalent consumption of power $\left|\dot{W}^{EQUIV}\right|$ from Eq. (A42) in Sec. A.3. This efficiency is given by Eq. (A43) as only $\eta = 10.31\ \%$.

$$\eta^{DISTILLATION} = \frac{\left|\dot{W}^{REV}\right|}{\left|\dot{W}^{EQUIV}\right|} * 100 = 10.31\ \% \qquad \text{(A43)}$$

Since the distillation column in the present demonstration operates a single – not too sharp – cut of the feed in terms of two distillation products, the result in Eq. (A43) can be generalized as a typical efficiency value for ordinary distillations successfully operating with a single ordinary cut and a narrow margin of reflux ratio above the respective minimum as in Fig. A-1. This result is a good representative efficiency even in the case of multicomponent distillation columns, provided there is only a single ordinary cut; i.e. the column has one feed and only two product streams which are ordinarily specified in terms of two key components.

If a similar multicomponent distillation column – operating a single ordinary cut with a narrow margin of reflux ratio above the respective minimum – is being modeled via rigorous simulation methods, the obtained Thermodynamic Efficiency would be of the same order of the value in Eq. (A43). In other words, the value in Eq. (A43) is a representative Thermodynamic Efficiency of a successful distillation column performing a single ordinary cut with a narrow margin of reflux ratio above minimum, despite it has been obtained via a binary distillation solved by a simplified McCabe-Thiele Method.

As the separation cut becomes sharper above the level in Fig. A-1, both $\left|\dot{W}^{REV}\right|$ and $\left|\dot{W}^{EQUIV}\right|$ increase with the former a little more rapidly. The result is that the Thermodynamic Efficiency of the column asymptotically increases above the value in Eq. (A43). For instance,

consider the same feed, pressure, VLE relationship, heat reservoirs, reflux ratio design criteria and thermodynamic modeling as in Fig. A-1, but with new distillate composition at X_D = *0.999* and new bottom composition at X_B = *0.001*. Then, the new values of *D, B,* RR^{MIN}, *RR*, Q_H, Q_C, $\dot{W}^{REV}$ $\left|\dot{W}^{EQUIV}\right|$ and $\eta^{DISTILLATION}$ will change as shown in Eqs. (A44a) to (A44i); evidencing a small increase of Thermodynamic Efficiency.

$$D = F.\left(\frac{Z - X_B}{X_D - X_B}\right) = 50\,mol/s \tag{A44a}$$

$$B = F.\left(\frac{X_D - Z}{X_D - X_B}\right) = 50\,mol/s \tag{A44b}$$

$$RR^{MIN} = \frac{X_D - g(Z)}{g(Z) - Z} \xrightarrow{g(Z)=2/3} RR^{MIN} = 1.994 \tag{A44c}$$

$$RR = 1.3 * RR^{MIN} \Rightarrow RR = 2.5922 \tag{A44d}$$

$$Q_H = Q_C = 50 * 3.5922 * 30 = 5388.3\,kW \tag{A44e}$$

$$\begin{aligned} D.\overline{G}_D + B.\overline{G}_B - F.\overline{G}_F = {} & \frac{FRT}{2}.\{X_D.ln(X_D) + (1 - X_D).ln(1 - X_D)\} + \\ & \frac{FRT}{2}.\{X_B.ln(X_B) + (1 - X_B).ln(1 - X_B)\} + \\ & - FRT.\{Z.ln(Z) + (1 - Z).ln(1 - Z)\} \\ = {} & 201.193\,kW \end{aligned} \tag{A44f}$$

$$\dot{W}^{REV} = -201.193\,kW \tag{A44g}$$

$$\left|\dot{W}^{EQUIV}\right| = \left(1 - \frac{T_0}{T_H}\right).Q_H - \left(1 - \frac{T_0}{T_C}\right).Q_C = 1576.1\,kW \tag{A44h}$$

$$\eta^{DISTILLATION} = \frac{\left|\dot{W}^{REV}\right|}{\left|\dot{W}^{EQUIV}\right|} * 100 = 12.77\,\% \tag{A44i}$$

The theoretical limit of a cut with pure components (X_D=*1*, X_B=*0*) at RR/RR^{MIN}=*1.3* can also be investigated. One obtains Eqs. (A45a) to (A45e):

$$RR^{MIN} = 2\ ,\ RR = 2.6 \tag{A45a}$$

$$Q_H = Q_C = 50 * 3.6 * 30 = 5400kW \tag{A45b}$$

$$\dot{W}^{REV} = -203.51\ kW\ ,\ \left|\dot{W}^{EQUIV}\right| = 1579.5\ kW \tag{A45d}$$

$$\eta^{DISTILLATION} = \frac{\left|\dot{W}^{REV}\right|}{\left|\dot{W}^{EQUIV}\right|} * 100 = 12.885\,\% \tag{A45e}$$

By last one can evaluate the impact of reflux ratio on the efficiency. Consider the theoretical limit of pure components used above giving $RR^{MIN}=2$ and $\dot{W}^{REV} = -203.51\,kW$ with $D=B=50\ mol/s$. The reflux ratio affects directly $\dot{W}^{EQUIV}$ via Eqs. (A41), (A21) and (A22), which were condensed in Eq. (A46). The final efficiency formula is in Eq. (A47). The behavior of the Thermodynamic Efficiency of this binary distillation column – with pure components cut – is shown in Fig. A-4 in terms of the reflux ratio. The best efficiency of 15.4618% corresponds to the minimum reflux operation, falling slowly towards zero at total reflux ($RR=\infty$).

$$\left|\dot{W}^{EQUIV}\right| = \left(\frac{T_0}{T_C} - \frac{T_0}{T_H}\right).\left(\left(\frac{RR}{RR^{MIN}}\right).RR^{MIN} + 1\right).D\lambda \tag{A46}$$

$$\eta^{DISTILLATION} = \frac{203.51}{\left(\frac{T_0}{T_C} - \frac{T_0}{T_H}\right).\left(\left(\frac{RR}{RR^{MIN}}\right).RR^{MIN} + 1\right).D\lambda} * 100 \tag{A47}$$

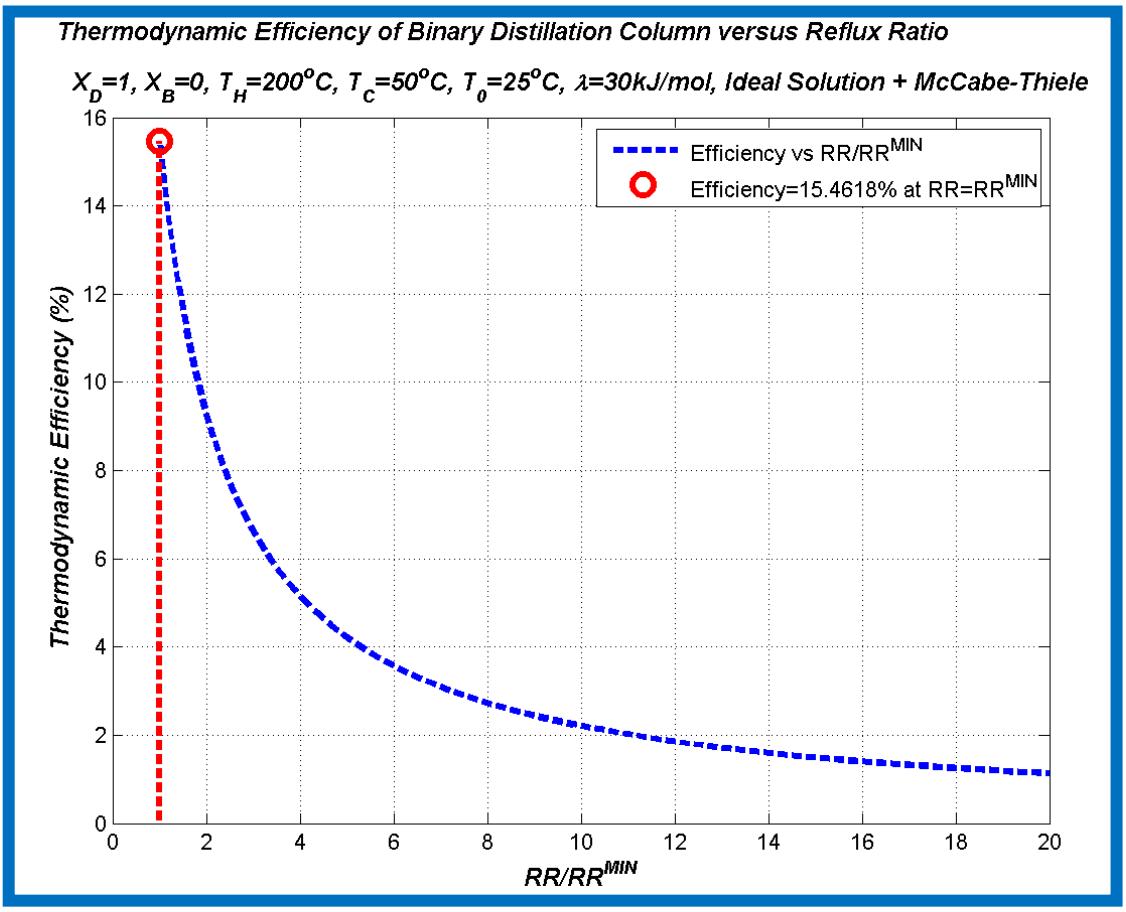

Figure A- 4. Thermodynamic Efficiency of Binary Distillation Column versus Reflux Ratio

APPENDIX B: THERMODYNAMIC EFFICIENCY OF A STEADY-STATE PROCESS WITH SEVERAL POWER CONSUMING OPERATIONS – THE CASE OF MEG RECOVERY UNIT

For a process composed exclusively by several steady-state equivalent power consuming operations – as a typical MEG Recovery Unit or MRU – the Thermodynamic Efficiency of the process can be written with the efficiencies of the constituent operations at a given steady-state condition of the entire process where the state of all streams are defined. Representing by η_k and $\left|\dot{W}_k^{EQUIV}\right|$ the efficiency and equivalent power consumption of operation k ($k=1...N$) in the steady-state operational point, which were calculated as shown in Secs. A.3 and A.4, the Overall Thermodynamic Efficiency is obtained by Eq. (B1), where the numerator and denominator respectively correspond to the minimum and actual power consumptions of the process.

$$\eta^{OVERALL} = \frac{\sum_{k=1}^{N} \eta_k . \left|\dot{W}_k^{EQUIV}\right|}{\sum_{k=1}^{N} \left|\dot{W}_k^{EQUIV}\right|} \qquad \text{(B1)}$$

Formula (B1) shows that the overall Thermodynamic Efficiency of a given steady-state operational condition of the process is a weighted average of the Thermodynamic Efficiencies of constituent units, where the weights correspond to the actual equivalent power consumption of units. Another consequence of Eq. (B1) is that the overall Thermodynamic Efficiency must be greater than or equal to the lowest Thermodynamic Efficiency of unit and also lower than or equal to the highest Thermodynamic Efficiency of unit. It must be recalled that Eq. (B1) refers specifically to Thermodynamic Efficiency and not to, for example, Exergy Efficiency.

Now consider a typical MRU case where there is a dominant sink of equivalent power consumption given by an ordinary distillation column, namely, the Atmospheric Distillation Column or ADC.

The dominant equivalent power term (kW) in Eq. (B1) can be written as shown in Eq. (B2), where Q_H^{ADC} ,.Q_C^{ADC} ,T_H^{ADC} , T_C^{ADC} represent the column heating and cooling duties (kW) and the temperatures (K) of isothermal heating and cooling media of a conceivable ADC. As commonly occurs, the heating and cooling duties are of the same order, allowing Eq. (B2) to be approximately reduced to Eq. (B3). Relaxing the denominator in Eq. (B1) by a lower bound defined by its dominant term in Eq. (B3), Eq. (B1) leads to an upper bound of the overall efficiency shown in Eq. (B4).

$$\left|\dot{W}_{ADC}^{EQUIV}\right| = \left(1 - \frac{T_0}{T_H^{ADC}}\right).Q_H^{ADC} - \left(1 - \frac{T_0}{T_C^{ADC}}\right).Q_C^{ADC} \tag{B2}$$

$$\left|\dot{W}_{ADC}^{EQUIV}\right| \cong \left(\frac{T_0}{T_C^{ADC}} - \frac{T_0}{T_H^{ADC}}\right).Q_H^{ADC} \tag{B3}$$

$$\eta^{OVERALL} \leq \eta^{ADC} + \sum_{k \neq ADC}^{N} \eta_k \cdot \frac{\left|\dot{W}_k^{EQUIV}\right|}{\left(\frac{T_0}{T_C^{ADC}} - \frac{T_0}{T_H^{ADC}}\right).Q_H^{ADC}} \tag{B4}$$

To impose a basis of calculation, assume that the three most common commercial MRU versions, TP (Traditional Process), FS (Full-Stream) and SS (Slip-Stream) process a Rich MEG feed of 100 t/d, 55% w/w H_2O + 45% w/w MEG at 25^oC, 1 bar. These MRUs have heating consumptions as shown in Table B1, which were extracted from the main paper *Exergy Analysis of Monoethylene Glycol Recovery Processes for Hydrate Inhibition in Offshore Natural Gas Fields*.

Since TP is constituted basically by a single ADC, and FS and SS also have similar ADCs with similar targets, besides other units, one can conclude that the heating duty of all ADCs,

considering the feed above, is approximately the heat consumption of TP, namely, $Q_H^{ADC} = 1734.1\ kW$. Also from Table B1 it can be seen that all the remaining operations of FS and SS have heating duty consumptions respectively totaling of the order of 555 kW and 150 kW. These duties are converted to the respective equivalent power consumptions by a typical factor of 1/3 according to the Method of Carnot Equivalent Cycles used in Sec. A.3 of Appendix A. This gives that the equivalent power consumptions of FS and SS operations, excluding ADC, correspond respectively to 185 kW and 50 kW. Since the Carnot term in the denominator of Eq. (B4) is also of the order of 1/3, one can reduce Eq. (B4) to the forms shown in Eqs. (B5a) to (B5c), respectively, for processes TP, FS and SS. In Eqs. (B5a) to (B5c) η^{OTHER} refers to the joint efficiency of other existing operations different from ADC. These formulae allow to estimate the Thermodynamic Efficiency of TP, FS and SS MRUs from the efficiency of ADC and the remaining operations.

$$\eta_{TP}^{OVERALL} \approx \eta^{ADC} \tag{B5a}$$

$$\eta_{FS}^{OVERALL} \approx \eta^{ADC} + 0.32 * \eta^{OTHER} \tag{B5b}$$

$$\eta_{SS}^{OVERALL} \approx \eta^{ADC} + 0.087 * \eta^{OTHER} \tag{B5c}$$

Table B- 1. Heat Consumptions and Lean MEG Compositions of MRU Processes

MRU	%w/w MEG of Lean MEG	Heat Consumption (kW)
TP	85.83	1734.1
FS	93.32	2289.8
SS	85.58	1889.9

APPENDIX C: RELATIONSHIPS FOR ECONOMIC ANALYSIS OF PROCESSES

Fixed Capital Investment (*FCI*, USD) is estimated via base bare module cost (C^0_{BM}) in a reference condition, corrected with design, pressure and material factors (F_{BM}) to give the bare module installed cost ($C_{BM}=C^0_{BM}*F_{BM}$). Contingency costs ($C_{CF}=C_{BM}*0.18$) and auxiliary facility costs are added to *FCI*, the former accounting for unexpected expenses and uncertainties, the latter regarding land purchase, off-sites and utility systems as *50%* of reference bare module costs. Thus, for onshore processes, *FCI* is obtained via Eq. (C.1), where N_{EQ} is number of equipment items and C^0_{BMi} is updated with Chemical Engineering Plant Cost Index of *550.3* (reference date Sept-2015, Chem. Eng. Magazine, Jan-2016). When capacity limits of cost predictors are below the required capacities, costs are extrapolated with the *Six-Tenth Rule*, Eq. (C.2a), where *CF* is a capacity factor (power, area or flow rate). Since installation and indirect costs of offshore systems are higher than onshore counterparts, an empirical *2.2* factor is used in Eq. (C.2b). Annual Cost of Manufacturing (*COM*, USD/y) is estimated with Eq. (C.3a), where *COL*, *CRM*, *CUT*, *CWT* are, respectively, annual costs (USD/y) of labor, raw materials, utilities and waste treatment. Gross Annual Profit (*GAP*, USD/y), Annual Profit (*AP*, USD/y) and Net Present Value (*NPV*, USD) follow in Eqs. (C.3b) to (C.3d), where *REV* (USD/y), *ITR* (%), *DEPR* (USD/y), *N* and *i* (%) refer, respectively, to revenues, income tax rate (*ITR=34%*.), annual depreciation (*10% FCI*), horizon (*N=20*) and annual interest rate (*i=10%*).

$$FCI^{ONSHORE} = 1.18 * \sum_{i=1}^{N_{EQ}} C_{BM\,i} + 0.5 * \sum_{i=1}^{N_{EQ}} C^{0}{}_{BM\,i} \quad \text{(C.1)}$$

$$FCI^{ONSHORE} = FCI^{ONSHORE^{LIMIT}} * \left(CF / CF^{LIMIT}\right)^{6/10} \quad \text{(C.2a)}$$

$$FCI^{OFFSHORE} = 2.2 * FCI^{ONSHORE} \quad \text{(C.2b)}$$

$$COM = 0.18 * FCI^{OFFSHORE} + 2.73 * COL + 1.23 * (CRM + CUT + CWT) \quad \text{(C.3a)}$$

$$GAP = REV - COM \quad \text{(C.3b)}$$

$$AP = GAP - (ITR/100) * (GAP - DEPR) \quad (GAP > DEPR) \quad or \quad AP = GAP \quad \text{(C.3c)}$$

$$NPV = -\left(0.2 + 0.3 * q^{-1} + 0.5 * q^{-2}\right) FCI^{OFFSHORE} + AP\left\{\sum_{k=3}^{N+3} q^{-k}\right\}, \; q \equiv (1 + i/100) \quad \text{(C.3d)}$$

APPENDIX D. SS-UOE VALIDATION

Yang et al. (2014) validated their CFD modeling by plotting SS pressure profile against the data from an older work of Arina in their Fig. 2 with good concordance. The work of Arina involves a SS expanding *3.071 kmol/h* of dry synthetic air (O_2*=21%mol,* N_2*=79%mol*) from P^{Inlet}*=100 kPa,* T^{Inlet}*=14.85°C* to P^{Outlet}*=83.049 kPa*. This is a low-pressure SS without phase-change as air is dry and supercritical. Arina's SS nozzle has non-linear diameter profiles in Eqs. (D.1) satisfying $\left(\frac{dA}{dx}\right)^{Throat} = 0$, with inlet, throat and outlet diameters respectively of D_I*=17.84mm,* D_T*=11.28mm* and D_O*=13.82mm,* and converging, diverging and total lengths respectively of L_C*=50mm,* L_D*=50mm* and *L=100mm*.

$$D(mm) = \sqrt{400 * \left(2.5 + (Z - 1.5) * 3Z^2\right) / \pi} \quad , \quad Z = x / L_C \quad , \quad 0 \le x \le L_C \tag{D.1a}$$

$$D(mm) = \sqrt{400 * \left(3.5 - (6 - 4.5Z + Z^2) * Z\right) / \pi} \quad , \quad Z = x / L_C \quad , \quad L_C \le x \le L \tag{D.1b}$$

Analogously, the thermodynamic SS framework of the present work – i.e. Unit Operation Extension SS-UOE – can also be validated by Arina's data (Yang et al., 2014). Firstly, Arina's diameter profiles where installed in SS-UOE (throat at $x=L_C=0.05m$). Arina's SS case was simulated by SS-UOE using PR-EOS with results in Fig. B.1. Fig. D-1 depicts the SS geometry match superposed by the axial pressure profiles respectively from SS-UOE and from Arina's data. As Eqs. (D.1a) and (D.1b) imply $\left(\frac{dA}{dx}\right)^{Throat} = 0$, there is no $dP/dx=-\infty$ singularity at sonic throat (as discussed in Sec. IV.4.1). Fig. D-1 shows that this condition was accomplished by both axial pressure profiles from SS-UOE and from Arina's data. Also, as phase-change effects are ruled out, the concordance of pressure profiles is everywhere perfect, except at normal shock where Arina's CFD profile exhibits a discreet, but perceptible, inclined linear trajectory across the shock front at $x \approx 70$ *mm,* which must be a true vertical discontinuity as reproduced by SS-UOE.

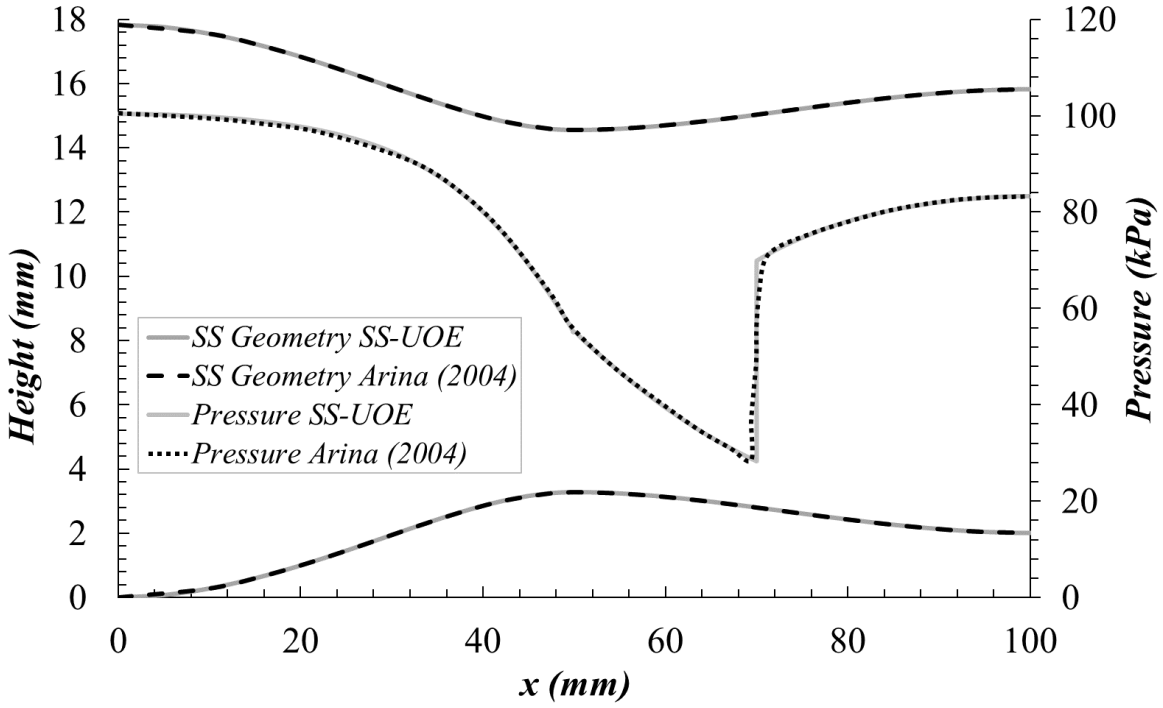

Figure D-1. SS with dry air (21%O_2+79%N_2): SS-UOE pressure profile versus Arina's counterpart

APPENDIX E. PUBLICATIONS

E.1. Exergy Analysis of Monoethylene glycol recovery processes for hydrate inhibition in offshore natural gas fields. Journal of Natural Gas Science and Engineering, Vol. 35, p. 798-813, 2016.

doi: 10.1016/j.jngse.2016.09.017

Journal of Natural Gas Science and Engineering 35 (2016) 798–813

Contents lists available at ScienceDirect

Journal of Natural Gas Science and Engineering

journal homepage: www.elsevier.com/locate/jngse

Exergy Analysis of Monoethylene glycol recovery processes for hydrate inhibition in offshore natural gas fields

Alexandre Mendonça Teixeira*, Lara de Oliveira Arinelli, José Luiz de Medeiros, Ofélia de Queiroz F. Araújo

Escola de Química, Federal University of Rio de Janeiro, Av. Horacio Macedo, 2030, Bl. E, 21949–900, Rio de Janeiro, RJ, Brazil

ARTICLE INFO

Article history:
Received 5 April 2016
Received in revised form
29 August 2016
Accepted 7 September 2016
Available online 13 September 2016

Keywords:
Exergy
Hydrate inhibition
MEG recovery
Exergy analysis

ABSTRACT

Gas hydrate formation is an issue in natural gas production. In offshore deepwater scenarios the situation is aggravated by the inaccessibility, salinity, low temperatures and high pressures. Monoethylene glycol (MEG) injection in well-heads is one of the used technologies for flow assurance in gas flowlines. Rich MEG is processed in MEG Recovery Units (MRU) to be recovered as Lean MEG returned to well-heads. In offshore rigs, besides determining energy requirements, the assessment of energy degradation is also important, which can be done by Exergy Analysis. In this work, an exergy formulation is developed and three technologies of offshore MRUs are assessed. Since exergy is a property that depends on the definition of a reference environment reservoir (RER), Exergy Analysis is performed via two RER approaches, both presenting consistent results. Approach #1 prescribes the usual standard atmosphere, with the addend that it is saturated by equilibrium with an infinite body of liquid water and MEG is in chemical equilibrium with air species. Since MEG is spontaneously oxidable, this entails very high exergy flows for MRU streams with MEG. As MEG is practically conserved, high exergy efficiencies result for all MRUs hindering their discrimination. Approach #2 prescribes also the standard atmosphere in equilibrium with liquid water containing MEG at infinite dilution, but not in chemical equilibrium with air. The MEG condition in MRU streams is now more akin with the MEG state in this RER, resulting that MEG streams have lower magnitude of exergy flow, leading to realistic exergy efficiencies that allow MRU discrimination. The underlying reason is that the input exergy flows now have magnitude comparable with

E.2 - Monoethylene Glycol as Hydrate Inhibitor in Offshore Natural Gas Processing: From Fundamentals to Exergy Analysis. SpringerBriefs in Petroleum Geoscience & Engineering, SPRINGER, 2018.

doi: 10.1007/978-3-319-66074-5 / ISBN: 978-3-319-66073-8

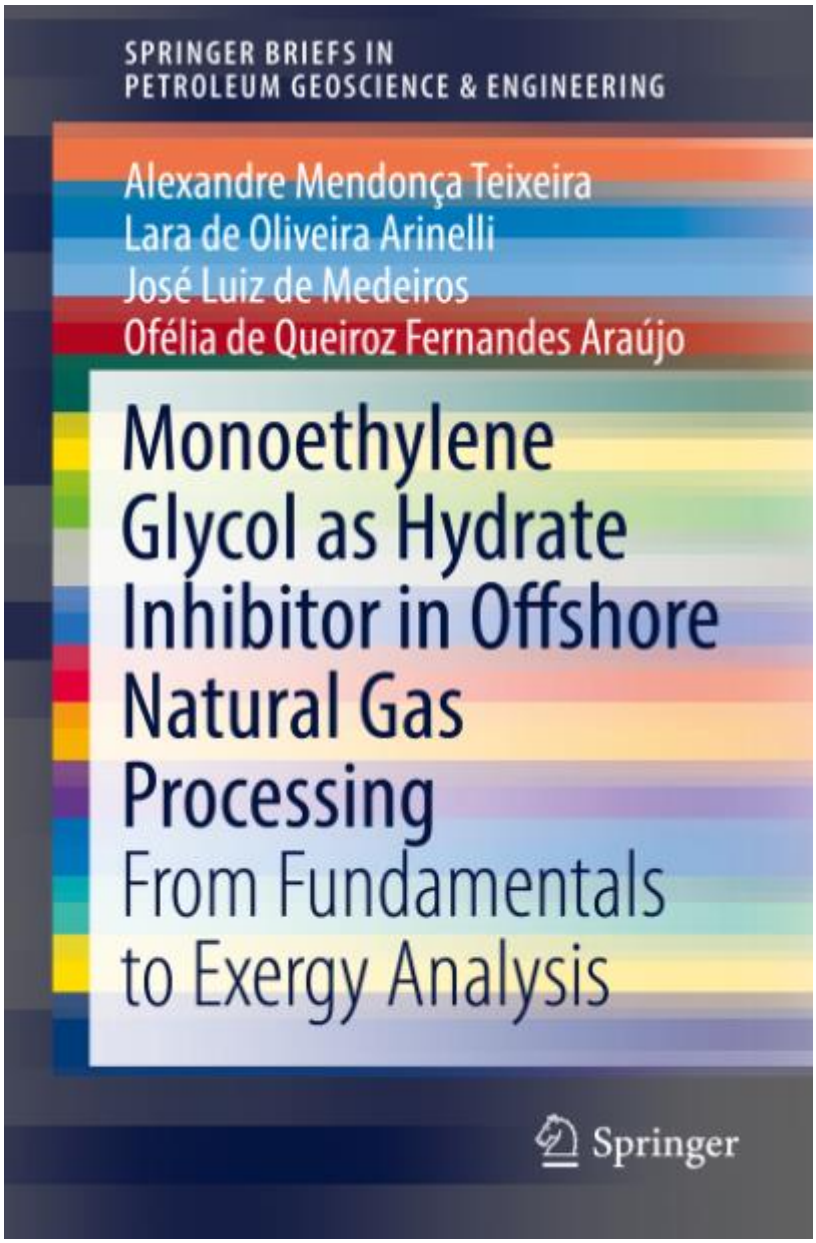

E.3 - Exergy Analysis of Monoethylene Glycol (MEG) Recovery Systems. Computer Aided Chemical Engineering. Proceedings of PSE-2015.

doi: 10.1016/B978-0-444-63578-5.50084-0

Krist V. Gernaey, Jakob K. Huusom and Rafiqul Gani (Eds.), 12th International Symposium on Process Systems Engineering and 25th European Symposium on Computer Aided Process Engineering. 31 May – 4 June 2015, Copenhagen, Denmark

Exergy Analysis of Monoethylene Glycol (MEG) Recovery Systems

Alexandre M. Teixeira[a], José Luiz de Medeiros[a], Ofélia Q. F. Araújo[a]

[a]*Escola de Química, Federal University of Rio de Janeiro (UFRJ), Av. Athos da Silveira Ramos, 149, Rio de Janeiro, 21941-909, Brazil*
alexandremtxr@gmail.com

Abstract

Hydrates are ice-like compounds comprised of water and light hydrocarbons whose formation in natural gas pipelines can lead to several problems such as pipeline blockage. To avoid these problems, the injection of Thermodynamic Hydrate Inhibitors (THI) in well-heads is widely employed. There are several options of THIs. In the present work, Monoethylene Glycol (MEG) was chosen due to its comparative advantages. As MEG can be reused, it must be re-concentrated and stripped of salts before recirculation through subsea pipelines. MEG Recovery Units (MRU) can be divided into three types: Traditional Process (TP), Full-Stream Process (FS) and Slip-Stream Process (SS). TP, FS and SS were discussed and compared via Energy and Exergy Analyses. The Exergy Analysis was based on two different approaches: firstly allocating the Reference Environmental Reservoir (RER) as the atmosphere at sea level; secondly allocating the RER as sea level atmospheric air saturated with water in equilibrium with liquid water containing MEG at infinite dilution. Those two

E.4 - Offshore Monoethylene Glycol Recovery Units: The Importance of Choice of MEG State in the Reference Environment for Effective Exergy Analysis. Proceedings of OTC Brasil, 2015.

doi: 10.4043/26135-MS

OTC-26135-MS

Offshore Monoethylene Glycol Recovery Units: The Importance of Choice of MEG State in the Reference Environment for Effective Exergy Analysis

A. M. Teixeira, J. L. Medeiros, and O. Q. F. Araújo, Federal University of Rio de Janeiro

This paper was prepared for presentation at the Offshore Technology Conference Brasil held in Rio de Janeiro, Brazil, 27–29 October 2015.

Abstract

Monoethylene glycol (MEG) injection is an approved technology to displace the hydrates equilibrium loci in ultra-deep subsea gas production pipelines. Further, rich MEG has to be processed in MEG Recovery Units (MRU) in order to be recovered as lean MEG to be pumped back. As distillation-based technologies, MRUs are very intensive in terms of heat consumption. In offshore platforms, where space and resources are limited, besides determining energy requirements, it is also of importance to perform a thermodynamic analysis to assess degradation of energy quality, which is done by Exergy Analysis (ExA). The exergy flow of a stream is the maximum amount of power obtainable when the stream is brought into equilibrium with a reference environmental reservoir (RER). In this regard, exergy is a property that depends both on the state of the stream and the definition of the RER. This work investigates how the choice of MEG state in the RER impacts the Exergy Analysis of MRUs. Specifically, two choices of MEG states in the RER are compared by performing ExA for three technologies of MRUs: Traditional, Full-Stream and Slip-Stream. Both approaches led to consistent results with the Traditional MRU having the highest exergy efficiency (if MEG is not supposed to be degraded), while the Full-Stream MRU presented the lowest exergy efficiency, and the Slip-Stream MRU occupied an intermediate position. However, Conception #1 allowed exergy flows to be too high, masking the exergy losses. As a consequence, all MRUs have very

E.5 – Exergy Analysis of Offshore Recovery Processes of Thermodynamic Hydrate Inhibitors. Proceedings of Rio Oil and Gas, 2016.

RIO OIL & GAS 2016 EXPO AND CONFERENCE
24-27 de outubro de 2016
Riocentro | Rio de Janeiro - Brasil

IBP1186_16

EXERGY ANALYSIS OF OFFSHORE RECOVERY PROCESSES OF THERMODYNAMIC HYDRATE INHIBITORS

Alexandre M. Teixeira[1], José Luiz de Medeiros[2], Ofélia Q. F. Araújo[3]

Abstract

In offshore natural gas (NG) production, hydrate formation is a big concern that can impact the production and even stop the entire NG flow. In this context, the injection of Thermodynamic Hydrate Inhibitors (THI) in well-heads is widely employed in order to avoid these undesirable problems. After injection, the Rich THI solution has to be processed in recovery units in order to be recovered as a Lean THI solution to be pumped back. In the present work, Monoethylene Glycol (MEG), Methanol and Ethanol were chosen as THIs and their recovery processes were comparatively evaluated. Considering the same NG field, i.e., certain natural gas composition and well-head conditions, hydrate formation temperature was evaluated, and the corresponding required temperature suppression was determined, which was used as criteria for comparing the three THIs. For MEG, three processes were assessed: Traditional Process (TP), Full-Stream Process (FS) and Slip-Stream Process (SS). For Methanol and Ethanol, the atmospheric distillation processes were evaluated. In offshore rigs, where space and resources are limited, besides determining energy requirements, assessing degradation of energy quality is also important, which is done by Exergy Analysis. All those processes were compared via Energy and Exergy Analyses, and the latter was performed by defining the Reference Environmental Reservoir (RER) as sea level atmospheric air saturated with water in equilibrium with liquid water containing the THI at infinite dilution. In general, the use of low molecular weight THI like methanol and ethanol benefits the energy consumption of recovery processes, whereas MEG presents higher energy consumption. However, THI losses for methanol and ethanol are very significant due to their high volatility. On the other hand, MEG losses are negligible. Further, this choice of RER for MEG processes is appropriate and they exhibit exergy efficiencies close to what is expected for distillation trains, with TP having the highest exergy efficiency, FS exhibiting the lowest exergy efficiency and SS occupying an intermediate position. However, such RER conception leads to efficiencies higher than expected for methanol and ethanol recovery processes, and much higher than for MEG processes, indicating that the search for a new definition of RER is needed for those cases in order to achieve more realistic exergy efficiencies.

E.6 - Recovery of thermodynamic hydrate inhibitors methanol, ethanol and MEG with supersonic separators in offshore natural gas processing. Journal of Natural Gas Science and Engineering, Vol. 52, p. 166-186, 2018.

doi: 10.1016/j.jngse.2018.01.038

Journal of Natural Gas Science and Engineering 52 (2018) 166–186

Contents lists available at ScienceDirect

Journal of Natural Gas Science and Engineering

journal homepage: www.elsevier.com/locate/jngse

Recovery of thermodynamic hydrate inhibitors methanol, ethanol and MEG with supersonic separators in offshore natural gas processing

Alexandre Mendonça Teixeira, Lara de Oliveira Arinelli, José Luiz de Medeiros*, Ofélia de Queiroz F. Araújo

Escola de Química, Federal University of Rio de Janeiro, Av. Horacio Macedo, 2030, BL E, 21949–900, Rio de Janeiro, RJ, Brazil

ARTICLE INFO

Keywords:
Thermodynamic hydrate inhibitor
THI recovery
Supersonic separator
Three-phase supersonic flow
Multiphase sound speed
HYSYS Unit Operation Extension

ABSTRACT

In offshore natural gas (NG) production, hydrate formation is a big concern that can impact the production and even stop NG flow. In this context, the injection of Thermodynamic Hydrate Inhibitors (THIs) in wellheads is widely employed in order to avoid these undesirable problems on subsea flowlines to gas processing rigs. However, in the main three-phase high-pressure separator in the gas rig, THI losses for gas phase are significant, particularly when the adopted THI is volatile like methanol and ethanol. This work discloses a new supersonic separator (SS) THI recovery process – SS-THI-Recovery – that treats the gas effluent from three-phase high-pressure separator achieving four simultaneous results: (i) gas water dew-point adjustment (WDPA); (ii) gas hydrocarbon dew-point adjustment (HCDPA); (iii) production of C3+ (propane and heavier) liquids as LPG; and (iv) recovery of almost all THI which would be lost in the gas otherwise. The proposition employs a supersonic separator (SS) battery followed by an anti-hydrates separator (LTX), a liquid-liquid THI extraction step and auxiliary THI distillation. SS-THI-Recovery was evaluated with HYSYS 8.8 simulator using methanol, ethanol and monoethylene glycol (MEG) as THIs. Supposing that the THI in the gas phase would be totally lost along with the exported gas otherwise, with SS-THI-Recovery the losses of methanol, ethanol and MEG were reduced by 91.9%, 79.3% and 99.2%, respectively, and such recovery factors could be further improved by increasing water flow rate in liquid-liquid THI extraction. Such high THI recovery entails reduction of THI costs with make-up, storage and transportation. Additionally, SS-THI-Recovery process is simple, with low footprint, and of easy implementation even for non-volatile THIs like MEG. Furthermore, the produced NG is ready for commercia-

E.7 - Processo para Recuperar Inibidores Termodinâmicos de Hidratos de Cargas de Gás Natural Utilizando Separador Supersônico Simultaneamente Ajustando Ponto de Orvalho de Hidrocarbonetos e Ponto de Orvalho de Água do Gás Final. Brazilian Patent Application BR 10 2017 015092 5, Filed in 13/07/2017.

República Federativa do Brasil
Ministério da Economia
Instituto Nacional da Propriedade Industrial

(21) BR 102017015092-5 A2

(22) Data do Depósito: 13/07/2017

(43) Data da Publicação Nacional: 29/01/2019

(54) Título: PROCESSO PARA RECUPERAR INIBIDORES TERMODINÂMICOS DE HIDRATOS DE GÁS DE CARGAS DE GÁS NATURAL UTILIZANDO SEPARADOR SUPERSÔNICO SIMULTANEAMENTE AJUSTANDO PONTO DE ORVALHO DE HIDROCARBONETOS E PONTO DE ORVALHO DE ÁGUA DO GÁS FINAL

(51) Int. Cl.: C10L 3/10.

(52) CPC: C10L 3/107; C10L 3/108; C10L 2290/08; C10L 2290/545.

(71) Depositante(es): UNIVERSIDADE FEDERAL DO RIO DE JANEIRO.

(72) Inventor(es): ALEXANDRE MENDONÇA TEIXEIRA; LARA DE OLIVEIRA ARINELLI; OFÉLIA DE QUEIROZ FERNANDES ARAÚJO.

(57) Resumo: A presente invenção define um novo processo para recuperar inibidores termodinâmicos de hidratos de gás (ITH) de cargas de gás natural utilizando separador supersônico, com injeção ou não de água líquida, de modo a extrair o ITH dos hidrocarbonetos pela formação de duas fases líquidas no condensado produzido no separador supersônico, simultaneamente ajustando o ponto de orvalho de hidrocarbonetos e o ponto de orvalho de água do gás final tratado pelo processo.

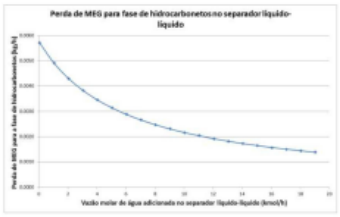

E.8 - Offshore Processing of CO2-Rich Natural Gas with Supersonic Separator. Multiphase Sound Speed, CO2 Freeze-Out and HYSYS Implementation, SPRINGER, 2019.

doi: 10.1007/978-3-030-04006-2 / ISBN: 978-3-030-04005-5

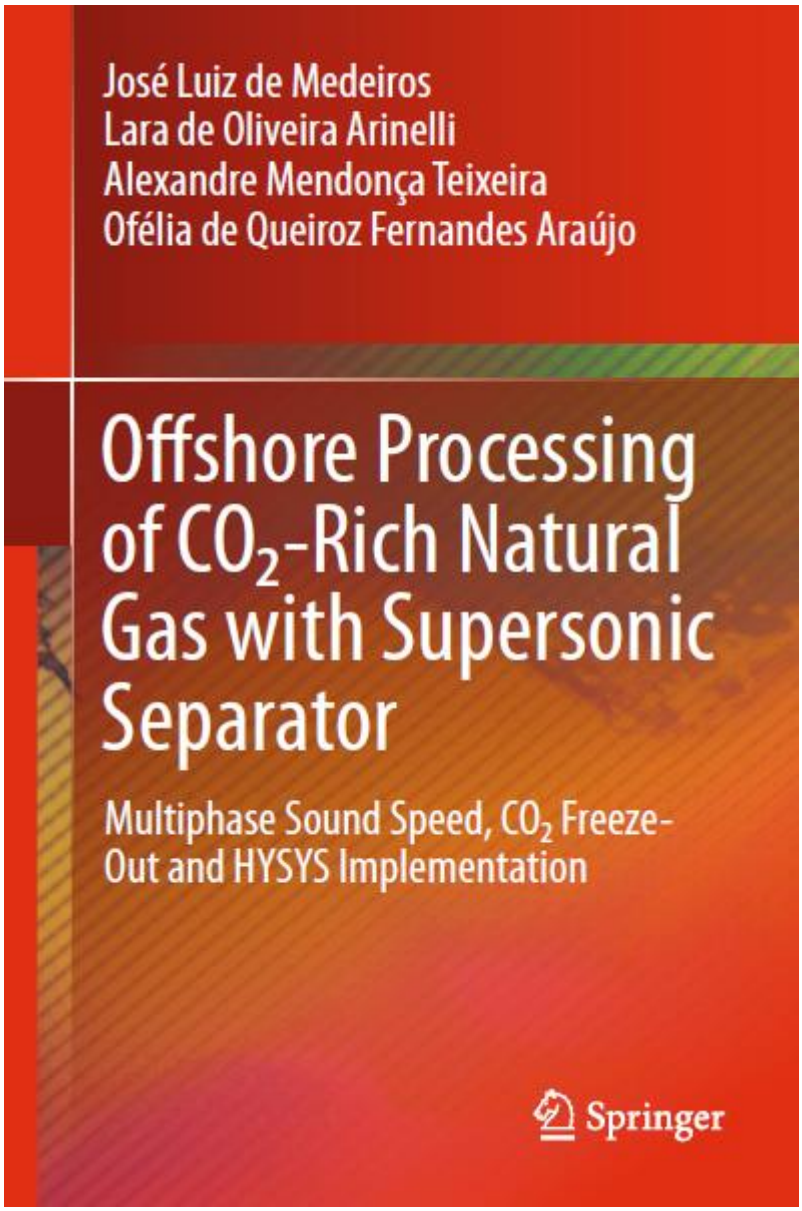

E.9 - Offshore Natural Gas Conditioning and Recovery of Methanol as Hydrate Inhibitor with Supersonic Separators: Increasing Energy Efficiency with Lower CO_2 Emissions. Materials Science Forum, Vol. 965, pp 97-105, 2019.

doi: 10.4028/www.scientific.net/MSF.965.97

Materials Science Forum
ISSN: 1662-9752, Vol. 965, pp 97-105
doi:10.4028/www.scientific.net/MSF.965.97

Submitted: 2018-12-19
Revised: 2019-05-14
Accepted: 2019-05-14
Online: 2019-08-08

Offshore Natural Gas Conditioning and Recovery of Methanol as Hydrate Inhibitor with Supersonic Separators: Increasing Energy Efficiency with Lower CO_2 Emissions

Alexandre Mendonça Teixeira[1,a*], Lara de Oliveira Arinelli[1,b], José Luiz de Medeiros[1,c] and Ofélia de Queiroz Fernandes Araújo[1,d]

[1]Escola de Química, Federal University of Rio de Janeiro (UFRJ), Av. Athos da Silveira Ramos, 149, Centro de Tecnologia, Cidade Universitária, 21941-972, Rio de Janeiro, RJ, Brazil

[a]alexandremtxr@gmail.com, [b]lara.arinelli@gmail.com, [c]jlm@eq.ufrj.br, [d]ofelia@eq.ufrj.br

* corresponding author: alexandremtxr@gmail.com

Keywords: supersonic separator; thermodynamic hydrate inhibitor; natural gas; CO2 emissions.

Abstract. The oil and gas industry represents an important contributor to CO_2 emissions as offshore platforms are power intensive for producing, processing and transporting hydrocarbons. In offshore rigs CO_2 emissions mainly come from on-site gas-fired power generation for heat and electricity production. The accumulation of atmospheric CO_2 is one of the main causes of the planetary greenhouse effect, thus CO_2 emissions should be minimized. To achieve that, more energy efficient processes for natural gas (NG) conditioning are needed in order to minimize platform power consumption and thus lowering the associated generation of CO_2. In addition, in offshore scenarios gas-hydrate obstructions are a major concern in flow assurance strategies, since thermodynamic conditions favoring hydrate formation are present, such as high pressure, low external temperature and gas contact with free water. To avoid hydrate issues, hydrate inhibition is carried out by the injection of a thermodynamic hydrate inhibitor (THI) in well-heads such that it flows along with production fluids, thus removing the thermodynamic conditions for hydrate formation and ensuring unimpeded flow. Therefore, the three-phase high-pressure separator (HPS) is fed with production fluids, where the HPS splits the feed into: (i) an upper gas phase, (ii) hydrocarbon condensate, and (iii) a bottom aqueous phase. The gas phase goes to NG conditioning for hydrocarbon dew point adjustment (HCDPA) and water dew point adjustment (WDPA) so as to make NG exportable. The hydrocarbon condensate (if present) is collected for stabilization and the bottom aqueous phase consisting of water, salts and THI is sent to a THI recovery unit (THI-RU) for THI re-concentration and reinjection. In conventional plants, WDPA and HCDPA are done by glycol absorption and Joule-Thomson expansion respectively. Moreover, the HPS gas carries some THI such as methanol

E.10 – Economic Leverage of Thermodynamic Hydrate Inhibitor Recovery from Raw Natural Gas with Supersonic Separator: Post-combustion capture of 43% of CO2 emissions preserving offshore gas plant profitability. Proceedings of SDEWES-2018.

Conference on Sustainable Development of Energy, Water and Environment Systems, Palermo, 30.9.-4.10.2018

SDEWES2018.0107

Economic Leverage of Thermodynamic Hydrate Inhibitor Recovery from Raw Natural Gas with Supersonic Separator: Post-Combustion Capture of 43% of CO2 Emissions Preserving Offshore Gas Plant Profitability

A. Teixeira*, L. De Oliveira Arinelli, J.L. De Medeiros, O. Araujo

Federal University of Rio de Janeiro, Brazil (*alexandremtxr@gmail.com)

Abstract

Offshore oil and gas production is a major CO_2 emitter as gas processing is highly power intensive for conditioning and transporting natural gas (NG). In offshore rigs CO_2 emissions mainly come from gas-fired power generation. In order to make room for economically sustained post-combustion carbon capture, new more efficient NG processing is needed. Offshore NG fields requiring injection of thermodynamic hydrate inhibitor (THI) must have a THI recovery unit (THI-RU) for re-concentration of THI in the bottom water phase from the high-pressure separator (HPS) fed with incoming raw NG, while the HPS gas goes to NG conditioning for hydrocarbon dew point adjustment (HCDPA) and water dew point adjustment (WDPA) so as to make NG exportable. In conventional plants, WDPA and HCDPA are done by glycol absorption and Joule-Thomson expansion respectively. Moreover, the HPS gas carries some THI (e.g. methanol) that is lost in the processing. This work analyses a new process – SS-THI-Recovery – where HPS gas feeds a supersonic separator (SS) with injected water. As a result, SS ejects a cold two-phase condensate with almost all water, THI and C3+ hydrocarbons, discharging exportable NG with enough HCDPA and WDPA grades, while the condensate gives aqueous THI returned to the THI-RU and tradable LPG. Thus, SS-THI-Recovery not only avoids THI losses as well as exports NG and LPG, improving dramatically the gas plant profitability. It is shown that such leverage for methanol as THI can pay a post-combustion mono-ethanolamine (MEA) plant capturing about 43% of the gas plant CO_2 emissions, assuming 80MW of power generation. Both conventional gas plant and SS-THI-Recovery alternative (both coupled to respective THI-RUs and the latter also coupled to a post-combustion MEA plant) were simulated in HYSYS v8.8 with subsequent equipment design and economic analysis. Despite the higher capital investment of SS-THI-Recovery alternative, it has several advantages: (i) superior revenues due to higher

E.11 – Economic Leverage Affords Post-Combustion Capture of 43% of Carbon Emissions: Supersonic Separators for Methanol Hydrate Inhibitor Recovery from Raw Natural Gas and CO_2 Drying. Journal of Environmental Management, Vol. 236, pp. 534-550, 2019.

doi: 10.1016/j.jenvman.2019.02.008

Journal of Environmental Management 236 (2019) 534–550

Contents lists available at ScienceDirect

Journal of Environmental Management

journal homepage: www.elsevier.com/locate/jenvman

Research article

Economic leverage affords post-combustion capture of 43% of carbon emissions: Supersonic separators for methanol hydrate inhibitor recovery from raw natural gas and CO_2 drying

Alexandre Mendonça Teixeira, Lara de Oliveira Arinelli, José Luiz de Medeiros*, Ofélia de Queiroz F. Araújo

Escola de Química, Federal University of Rio de Janeiro, Av. Horacio Macedo, 2030, Bl. E, 21949–900, Rio de Janeiro, RJ, Brazil

ARTICLE INFO

Keywords:
Supersonic separator
Methanol hydrate inhibitor
CO_2 capture and storage
Post-combustion capture
Supersonic separator CO_2 drying

ABSTRACT

Offshore oil/gas productions are power intensive and CO_2 emitters from gas-fired power generation. This work investigates supersonic separator as a strategy for affording post-combustion capture backed up by cost reductions. Conventional offshore gas processing usually loses thermodynamic hydrate inhibitor methanol in processing and exported gas. This work analyses a supersonic separator variant gas processing simultaneously reducing methanol losses. Such process dramatically improves gas-plant profitability via cost-reduction of methanol make-up and power-consumption, simultaneously increasing revenues from liquefied-petroleum-gas by-product. This economic leverage affords post-combustion carbon capture, including subsequent CO_2 dehydration and compression for exportation of high-pressure liquid CO_2. This corresponds to abate 43% of CO_2 emissions boosting revenues via enhanced oil recovery. Moreover, CO_2 is dehydrated via another supersonic separator operating with minimum head-loss, minimizing compression costs. Despite its much higher investment, the new process with carbon capture presents higher net value (865.63 MMUSD) than the conventional processing without carbon capture (829.31 MMUSD), being economically feasible and more environmentally adequate with cleaner natural gas production and successful CO_2 management. The new process is superior in several scenarios

E.12 – Offshore processing of CO_2 rich natural gas with supersonic separator versus conventional routes. Journal of Natural Gas Science and Engineering, Vol. 46, p. 199-221, 2017.

doi: 10.1016/j.jngse.2017.07.010

Journal of Natural Gas Science and Engineering 46 (2017) 199–221

Contents lists available at ScienceDirect

Journal of Natural Gas Science and Engineering

journal homepage: www.elsevier.com/locate/jngse

Offshore processing of CO_2 rich natural gas with supersonic separator versus conventional routes

Lara de Oliveira Arinelli*, Thiago Affonso F. Trotta, Alexandre Mendonça Teixeira, José Luiz de Medeiros, Ofélia de Queiroz F. Araújo

Escola de Química, Federal University of Rio de Janeiro, P.O. Box 68.594, 21941-972, Rio de Janeiro, RJ, Brazil

ARTICLE INFO

Article history:
Received 20 February 2017
Received in revised form
8 July 2017
Accepted 16 July 2017
Available online 12 August 2017

Keywords:
Natural gas conditioning
Supersonic separator
Membrane permeation
CO_2 removal
Unit operation extension

ABSTRACT

The supersonic separator (SS) was investigated for treating humid natural gas with *44%mol* CO_2 in offshore rigs and compared to the conventional Water Dew Point Adjustment (WDPA) via TEG Absorption, Hydrocarbon Dew Point Adjustment (HCDPA) via Joule-Thomson Expansion (JTE) and CO_2 removal via Membrane Permeation (MP). SS was tested as a single-step operation for WDPA + HCDPA. To simulate SS and MP, two Unit Operation Extensions (UOE) were developed for simulator HYSYS 8.8 (AspenTech). MP-UOE uses an empirical approach calibrated with operation data, whereas SS-UOE is entirely funded on thermodynamics, not demanding calibration. MP-UOE and SS-UOE use the thermodynamic infrastructure of HYSYS: property packages and several proved multiphase flash algorithms. MP-UOE and SS-UOE performed accordingly the expected characteristics of the respective operations and were critical to accomplish this analysis as SS and MP are not available in simulators. In terms of final gas quality (WDP $\leq$ *-45°C @1.01 bar*, HCDP $\leq$ *0°C @45 bar*, *%CO_2* $\leq$ *15%mol*) the best process configuration was found to be a hybrid one: SS WDPA + HDPA and MP CO_2 removal, with low footprint and low power demand (*-6.9%*) relative to conventional 3-step way. If used for CO_2 removal, SS could abate CO_2 from *44%* to *21.85%mol*. Albeit less effective than MP, SS CO_2 removal is a noticeable option that produces fuel gas for power generation with *%CO_2* $\approx$ *20%* as required by new turbo-shafts. Moreover, CO_2 is withdrawn from SS as a pumpable liquid allowing a cut of *44%* in the power demanded for CO_2 separation and injection as EOR agent.

E.13 – Supersonic separator for cleaner offshore processing of natural gas with high carbon dioxide content: Environmental and economic assessments. Journal of Cleaner Production, Vol. 233, p. 510-521, 2019.

doi: 10.1016/j.jclepro.2019.06.115

Journal of Cleaner Production 233 (2019) 510–521

Contents lists available at ScienceDirect

Journal of Cleaner Production

journal homepage: www.elsevier.com/locate/jclepro

Supersonic separator for cleaner offshore processing of natural gas with high carbon dioxide content: Environmental and economic assessments

Lara de Oliveira Arinelli, Alexandre Mendonça Teixeira, José Luiz de Medeiros*, Ofélia de Queiroz F. Araújo

Escola de Química, Federal University of Rio de Janeiro, Rio de Janeiro, RJ, Brazil

ARTICLE INFO

Article history:
Received 23 February 2019
Received in revised form
13 May 2019
Accepted 11 June 2019
Available online 12 June 2019

Keywords:
CO_2-Rich natural gas processing
Supersonic separator
CO_2 capture
Membrane permeation
Environmental assessment
Economic assessment

ABSTRACT

Supersonic separators offer a cleaner offshore processing of natural gas with carbon dioxide content from deep-water oil-gas fields. Conventional offshore gas processing comprises water dew-point adjustment via glycol-absorption, hydrocarbon dew-point adjustment via Joule-Thomson expansion, and carbon dioxide removal via membrane-permeation. Alternative processing contemplates the use of supersonic separators for adjusting gas dew-points followed by carbon dioxide capture via membrane-permeation (so-called SS-MP scheme); or for adjusting gas dew-points and also accomplishing carbon dioxide abatement (so-called SS-SS scheme). The conventional process is environmentally and economically compared with SS-MP and SS-SS for application in offshore rigs treating raw gas (44%mol carbon dioxide) to produce exportable fuel-gas (≈20%mol carbon dioxide), while dispatching carbon dioxide rich fluid (≈75%mol carbon dioxide) for enhanced oil recovery in the oil-gas field. Results show that SS-MP requires 7.8% less power than the conventional process. Moreover, implementing SS-SS deepens the advantage against the conventional operation because SS-SS produces carbon dioxide rich fluid at high-pressure, requiring much less compression power for enhanced oil recovery than the low-pressure permeate from membrane-permeation. SS-SS has lowest carbon emission (−28.3%), lowest power consumption (−21.3%) and best economic performance: lowest manufacturing cost and lowest

E.14 - CO_2 Rich Natural Gas Processing: Technical, Power Consumption and Emission Comparisons of Conventional and Supersonic Technologies. Materials Science Forum, Vol. 965, pp 79-86, 2019.

doi: 10.4028/www.scientific.net/MSF.965.79

Materials Science Forum
ISSN: 1662-9752, Vol. 965, pp 79-86
doi:10.4028/www.scientific.net/MSF.965.79

Submitted: 2018-12-18
Revised: 2019-05-14
Accepted: 2019-05-14
Online: 2019-08-08

CO_2 Rich Natural Gas Processing: Technical, Power Consumption and Emission Comparisons of Conventional and Supersonic Technologies

Lara de Oliveira Arinelli[1,a*], Alexandre Mendonça Teixeira[1,b], José Luiz de Medeiros[1,c] and Ofélia de Queiroz Fernandes Araújo[1,d]

[1]Escola de Química, Federal University of Rio de Janeiro (UFRJ), Av. Athos da Silveira Ramos, 149, Centro de Tecnologia, Cidade Universitária, 21941-972, Rio de Janeiro, RJ, Brazil

[a]lara.arinelli@gmail.com, [b]alexandremtxr@gmail.com, [c]jlm@eq.ufrj.br, [d]ofelia@eq.ufrj.br

*corresponding author: lara.arinelli@gmail.com

Keywords: Rich CO_2 Natural Gas Processing, Supersonic Separator, CO_2 Capture, Membranes, Energy Analysis, CO_2 Emissions, Process Engineering, Enhanced Oil Recovery

Abstract. Supersonic separator is investigated via process simulation for treating CO_2 rich (>40%) natural gas in terms of dew-points adjustment and CO_2 removal for enhanced oil recovery. These applications are compared in terms of technical and energetic performances with conventional technologies, also comparing CO_2 emissions by power generation. The context is that of an offshore platform to treat raw gas with 45%mol of CO_2, producing a lean gas stream with maximum CO_2 composition of ≈20%mol, suitable for use as fuel gas, and a CO_2 rich stream that is compressed and injected to the oil and gas fields. The conventional process comprises dehydration by chemical absorption in TEG, Joule-Thomson expansion for C3+ removal, and membrane permeation for CO_2 capture. The other alternatives use supersonic separation for dew-points adjustment, and membranes or another supersonic separation unit for CO_2 capture. Simulations are carried out in

E.15 – Carbon capture and high-capacity supercritical fluid processing with supersonic separator: Natural gas with ultra-high CO_2 content. Journal of Natural Gas Science and Engineering, Vol. 66, p. 265-283, 2019.

doi: 10.1016/j.jngse.2019.04.004

Journal of Natural Gas Science and Engineering 66 (2019) 265–283

Contents lists available at ScienceDirect

Journal of Natural Gas Science and Engineering

journal homepage: www.elsevier.com/locate/jngse

Carbon capture and high-capacity supercritical fluid processing with supersonic separator: Natural gas with ultra-high CO_2 content

Lara de Oliveira Arinelli[a], José Luiz de Medeiros[a,*], Darley Carrijo de Melo[b], Alexandre Mendonça Teixeira[a], George Victor Brigagão[a], Fabio Menezes Passarelli[b], Wilson Mantovani Grava[b], Ofélia de Queiroz F. Araújo[a]

[a] Escola de Química, Federal University of Rio de Janeiro, CT, E, Ilha do Fundão, Rio de Janeiro, RJ, 21941-909, Brazil
[b] CENPES, PETROBRAS S.A., Ilha do Fundão, Rio de Janeiro, RJ, 21941-970, Brazil

ARTICLE INFO

Keywords:
Supersonic separator
Supercritical fluid processing
Ultra-high CO_2 content
Natural gas conditioning
CO_2 removal
CO_2 freeze-out

ABSTRACT

Some deep-water offshore fields produce oil with high gas/oil ratios and ultra-high %CO_2 (> *60%mol*) with the onus of processing low-grade gas simultaneously handling huge CO_2 dispatch goals. Thus, processing solutions are needed to make feasible such high-capacity gas rigs hundreds of kilometers offshore. Feasibility relies on the choices for CO_2 capture and adjustment of water and hydrocarbon dew-points of such high flow rate gas. This problem was approached adopting supersonic separators for dew-point adjustments and for CO_2 capture on a floating-hub processing 50 MMsm^3/*d* of CO_2 ultra-rich gas, reinjecting *96%* of treated CO_2-rich gas for enhanced oil recovery, while reserving *4%* as fuel-gas after CO_2 abatement to *20%mol* for power production. Process alternatives were assessed in terms of power demand and profitability comparing supersonic separator with membrane-permeation for CO_2 removal. Results show that 1st supersonic separator for dew-point adjustments of raw gas recycling condensate to the oil-gas-water separator and 2nd supersonic separator for CO_2 removal avoiding CO_2 freeze-out, give optimum net present value and minimum CO_2 emissions. On one hand, these facts are consequences of less compressor investment as 2nd supersonic separator ejects pressurized CO_2 condensate requiring *5%* less compression power for enhanced oil recovery relatively to the power required by the low-pressure CO_2-rich permeate from the membrane-permeation alternative. On the other hand, the best net value of

E.16 – Supersonic separator for cleaner offshore processing of supercritical fluid with ultra-high carbon dioxide content: Economic and environmental evaluation. Journal of Cleaner Production, Vol. 234, p. 1385-1398, 2019.

doi: 10.1016/j.jclepro.2019.06.304

Journal of Cleaner Production 234 (2019) 1385–1398

Contents lists available at ScienceDirect

Journal of Cleaner Production

journal homepage: www.elsevier.com/locate/jclepro

Supersonic separator for cleaner offshore processing of supercritical fluid with ultra-high carbon dioxide content: Economic and environmental evaluation

Darley C. de Melo [b], Lara de O. Arinelli [a], José Luiz de Medeiros [a, *], Alexandre M. Teixeira [a], George Victor Brigagão [a], Fabio M. Passarelli [b], Wilson M. Grava [b], Ofélia de Q.F. Araujo [a]

[a] Escola de Química, Federal University of Rio de Janeiro, CT, E, Ilha do Fundão, Rio de Janeiro, RJ, 21941-909, Brazil
[b] CENPES, PETROBRAS S.A., Ilha do Fundão, Rio de Janeiro, RJ, 21941-970, Brazil

ARTICLE INFO

Article history:
Received 2 March 2019
Received in revised form
29 May 2019
Accepted 27 June 2019
Available online 28 June 2019

Handling editor: Prof. Jiri Jaromir Klemeš

Keywords:
Natural gas
Supercritical fluid
CO_2
Supersonic separator
Offshore processing
Environmental analysis

ABSTRACT

Offshore gas processing presents challenges, especially when high flow rates, high-pressure and high carbon dioxide contents are involved. The present scenario comprehends offshore processing of high flow rate of high-pressure natural gas with 68%mol carbon dioxide, which results from oil production and behaves as a dense supercritical fluid. The processing goals with this fluid comprise: [A] water dew-point adjustment; [B] hydrocarbon dew-point adjustment; [C] decarbonation of a small part to 20%mol carbon dioxide fuel-gas for power production; and [D] compression/pumping of the remaining fluid enriched with carbon dioxide from decarbonation for enhanced oil recovery. For these tasks the industry considers traditional well established processes such as molecular-sieves adsorption for water dew-point adjustment, Joule-Thompson expansion for hydrocarbon dew-point adjustment and membrane-permeation for carbon dioxide removal. However, conventional technologies can become cumbersome in such awkward conditions. Thus, unconventional solutions are sought for reliability, lower equipment size/weight, and better power consumption, emissions and environmental sustainability. Recently, supersonic separators have been analyzed in proof-of-concept researches for natural gas processing. In this regard, this work quantitatively proves that goals [A],[B],[C] are achievable using only supersonic sep-